

Severity Estimation for Risk-based Motion Planning

Dem Fachbereich
Elektrotechnik und Informationstechnik
der Technischen Universität Darmstadt
zur Erlangung des akademischen Grades
eines Doktor-Ingenieurs (Dr.-Ing.)
genehmigte Dissertation

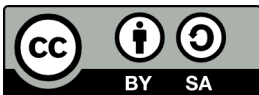
von

M. Sc. Fabian Müller

Referent: Prof. Dr.-Ing. J. Adamy
Korreferent: Prof. Dr. rer. nat. Bernhard Sendhoff

D17
Darmstadt 2022

Müller, Fabian: Severity Estimation for Risk-based Motion Planning
Darmstadt, Technische Universität Darmstadt,
Jahr der Veröffentlichung der Dissertation auf TUprints: 2023
URN: urn:nbn:de:tuda-tuprints-233259
Tag der Einreichung am Fachbereich: 23.09.2022
Tag der mündlichen Prüfung: 16.12.2022



Veröffentlicht unter CC BY-SA 4.0 International
<https://creativecommons.org/licenses/>

“A life without risk is like no life at all”
Indecent Proposal (Movie from 1993)

Preface

This thesis is a result of a cooperation between the Control Methods and Robotic Labs at Technische Universität Darmstadt and the Honda Research Institute in Offenbach. At first, I want to thank Mr. Prof. Jürgen Adamy for the chance to work at his institute and that he provides a scientific, collegial and trustful work atmosphere. He gives me freedom to follow my own ideas, gives back cover for my decisions and external affairs.

I also want to thank Mr. Bernhard Sendhoff for letting me participate at this project and the opportunity to develop scientifically at Honda. A special thank goes to Julian Eggert, which whom I had the most fruitful, detailed and deepest discussions during the four years of my project time. His content advices and critics requested my full potential. I also want to thank Sebastian Schmitt, who gives me important positive critics to cheer me up in times, where I struggled a lot.

I want to thank my colleagues Moritz Bühler, Karsten Kreutz and Valentina Ansel and all the others who teared me out to do breaks in the coffee kitchen which mostly ends up in hilarious or deep conversations. Additionally, I'd like to thank Birgit Heid and Volker Willert for their never-ending altruistic supports. I also want to thank all students and project teams I had the pleasure to work with, especially for the open discussions, for sharing their ideas, for questioning and for giving me feedback to improve myself.

I want to thank my family and my friends, who accompany me throughout times of studies and this project - never giving me a hint or a feeling that I couldn't make it. Last but not least, I want to thank my girlfriend Lilly who always had a watching eye on me, soaked up my problems and turned them into little firecracker peas. I love you.

Contents

Index Register	I
Abbreviations and Symbols	XI
Kurzfassung	XXII
Abstract	XXIV
1 Introduction	1
1.1 Problem Formulation	2
1.2 Contributions	4
1.3 Thesis Outline	5
2 Risk-Based Motion Planning Framework	8
2.1 Traffic Environment	8
2.2 Autonomous Driving	12
2.3 The Risk Concept	14
2.4 Event-Based Motion Planning Framework	19
2.4.1 Related Work	19
2.4.2 Components of Behavior Planner	25
2.4.3 Prediction Model	28
2.4.4 Cost Evaluation of Scene States	36
2.4.5 Decision Model	42
2.5 Conclusion	44
3 Survival Theory	46
3.1 Related Work	47
3.2 Problem Statement	50
3.3 Approach	50
3.4 Quantities of Survival Theory	51
3.4.1 Event vs. Event-Free	52
3.4.2 Time-Course Sensitivity	57
3.4.3 Total Scene Prediction Measures	60
3.5 Multiple Events	61

3.6	Rate Formulation for Continuous Time	64
3.7	Conclusion	66
4	Collision Event	68
4.1	Related Work	68
4.2	Problem Statement	70
4.3	Approach	71
4.3.1	Collided Trajectories	71
4.3.2	Structure	72
4.4	Collision Region	73
4.4.1	Static Collision Region	77
4.4.2	Dynamic Collision Region	78
4.5	Collided States	81
4.5.1	Probability Density Function Shape Truncation . .	82
4.5.2	Evaluation of Collision State Probability Density Function	87
4.6	Non-Collided States	92
4.6.1	Unimodal Gaussian	92
4.6.2	Evaluation of Using Unimodal Gaussians for Sur- vived State Probability Density Function	93
4.6.3	Gaussian Mixture	95
4.7	Collision Event Rate	104
4.8	Evaluation of Collision Probability Models	106
4.8.1	Multi-Vehicle Overtaking Scenario	106
4.8.2	Two-Vehicle Intersection Scenario	110
4.8.3	Two-Vehicle Overtaking Scenario	113
4.8.4	Sampling Time Dependency	115
4.9	Conclusion	116
5	Other Events	118
5.1	Distributed Events	118
5.1.1	Approach	118
5.1.2	Evaluation	120
5.2	Dynamical State Restriction	122
5.2.1	Adaptation of State Probability Density Function	122
5.2.2	Evaluation	126
5.3	Escape Event	127
5.3.1	Evaluation	130
5.4	Conclusion	130

6	Design of Severity Model	132
6.1	Related Work	133
6.2	Problem Definition	136
6.3	Modeling Scheme for Multiple Events	137
6.3.1	Prediction of Crash Events and A Posteriori Scene Evolutions	137
6.3.2	Collision Evaluation	140
6.4	Components of Severity	144
6.4.1	Physical Crash Model	145
6.4.2	Coping Model	149
6.4.3	Injury Model	151
6.4.4	Ethical Model	153
6.5	Severity Models	157
6.5.1	Constant Severity	157
6.5.2	Wall-Impact Severity	158
6.5.3	Vehicle-to-Vehicle Impact Severity	159
6.5.4	Multi-Collision Event Severity	160
6.6	Comparison of Severity Models	162
6.7	Conclusion	164
7	Severity's Influence on Motion Behavior	166
7.1	Scenario Overview	167
7.2	Same Lane Scenarios	169
7.2.1	Following and Being Tailgated	169
7.2.2	Frontal Approaching	172
7.3	Parallel Lane Scenarios	173
7.3.1	Overtaking	174
7.3.2	Being Passed	175
7.3.3	Frontal Passing	176
7.3.4	Behavior Overview	177
7.4	Influence of Vehicles Mass-Ratio	180
7.5	Distributed Collision Areas	181
7.6	Conclusion	182
8	Summary and Outlook	183
8.1	Summary	183
8.2	Published Contributions	185
8.3	Outlook	187

A Attachment	189
A.1 Hyperplanes Simplification over Time	189
A.2 Simplifying Dynamic Collision Region	191
A.3 Transition of Dynamic Collision Region to Flux Calculation	192
A.4 Accuracy of Instantaneous Survival Probability	194
A.5 Simulation Parameters	196
A.5.1 Time vs. Accuracy	196
A.5.2 Parameters of Collision Probability Models	196
A.5.3 Parameters of Severity Models	197
A.5.4 Parameters of Behavior Planner	197
A.5.5 Multi-Object Overtaking Scenarios	198
A.5.6 Intersection Scenario	199
A.5.7 Overtaking Scenario	200
A.5.8 Overtaking Scenario with variable Sampling Time	201
A.5.9 Scenario with distributed Events	202
A.5.10 Scenario with Restriction Event	202
A.5.11 Scenario with Escaping Event	203
A.6 Probability Distributions	204
A.6.1 Probability Density Function	205
A.6.2 Stochastic Moments	208
A.6.3 Truncated Gaussian Probability Density Functions	209
A.6.4 Distance Measures	211
A.7 Bayesian Theory	212
A.7.1 Sum and Product Rule	212
A.7.2 Bayesian Theorem	213
A.7.3 Statistical Independence	213
A.7.4 Bayesian Network	214
Bibliography	217

Abbreviations and Symbols

Abbreviations

AIS	Abbreviated Injury Scale
ADAS	Advanced Driver Assistance Systems
ANFIS	Adaptive Neuro-Fuzzy Interface System
AV	Autonomous Vehicle
BTN	Break Threat Number
CA	Constant Acceleration
CDF	Cumulative Distribution Function
CTRV	Constant Turn Rate and constant Velocity
CTRA	Constant Turn Rate and constant Acceleration
CV	Constant Velocity
DC	Collision Model with Dynamic Collision Region, Truncation and Splitting
EDR	Event Data Recorder
EKF	Extended Kalman Filter
ER	Event Rate Model
FDM	Foresighted Driver Model
FEM	Finite Element Method
GIDAS	German In-Depth Accident Study
GMM	Gaussian Mixture Model
HD	High Definition
HIC	Head Impact Criterion
ICS	Inevitable Collision State
IDM	Intelligent Driver Model
ISS	Injury Severity Score
MAIS	Maximum Abbreviated Injury Scale
MAIS _n +	Minimum injury MAIS level n
MCS	Monte Carlo Simulation
MPC	Model Predictive Control
NASS/CDS	National Automotive Sampling System/ Crashworthiness Data System
NHTSA	National Highway Traffic Safety Administration
OLC	Occupant Load Criterion
PDF	Probability Density Function
RRT	Rapidly Random Tree

SC	Collision Model with Static Collision Region and Truncation
TE	Traffic Environment
tcs.	time-course sensitive
TP	Traffic Participant
TTB	Time-to-Brake
TTC	Time-to-Collision
TTK	Time-to-Kickdown
TTM	Time-to-Maneuver
TTPMD	Time-to-Minimum-Distance
TTS	Time-to-Steer
TTX	Time-to-X
UK	United Kingdom
UKF	Unscented Kalman Filter
US(A)	United States of America
V2X	Vehicle to X
WTTC	Worst TTC

Symbols

Notationen

x	Scalar
x^i	Quantity belonging to TP i
\hat{x}	Mean quantity
\mathbf{x}	Column vector
\mathbf{x}^T	Row vector
\mathbf{x}_k	Column vector at time step k
$\mathbf{x}_{0:k}$	Time-discrete trajectory of \mathbf{x} starting in 0 and ending at time step k
\mathbf{X}	Matrix
\mathbf{X}_k	Matrix at time step k
\mathbb{S}	Set
$\partial\mathbb{S}$	Margin of a subset \mathbb{S}
\mathbb{S}^c	Complement Set of a subset \mathbb{S}
\mathbb{S}_k	Set at time step k
\mathbf{X}^T	Transpose of matrix \mathbf{X}
\mathbf{X}^{-1}	Inverse of matrix \mathbf{X}
$ \mathbf{X} $	Determinant of matrix \mathbf{X}
$Tr(\mathbf{X})$	Trace of matrix \mathbf{X}
$\mathbf{x}\mathbf{y}^T$	Dyadic product of \mathbf{x} and \mathbf{y}
$\mathbf{0}$	zero vector
\mathbf{E}^n	Identity matrix $n \times n$
\mathcal{X}	Random variable
$f(\cdot)$	Scalar function
$\mathbf{f}(\cdot)$	Vector function
$\mathbb{E}(\cdot)$	Expectation operator
$\int_{\mathbb{S}} d\mathbf{x}$	Integration over $\mathbf{x} \in \mathbb{S} \subseteq \mathbb{R}^n$
\oplus	Minkowski sum operator
$p(x)$	PDF of a continuous random variable x
$P(x)$	CDF of a continuous random variable x
$p(\mathbf{x})$	PDF of a continuous random vector \mathbf{x}
$p(\mathbf{x}, \mathbf{y})$	Joint PDF of two \mathbf{x} and \mathbf{y}
$p(\mathbf{x} \mathbf{y})$	Conditional PDF of two \mathbf{x} and \mathbf{y}

Latin Capital Letters

\mathbf{A}^i	Time-continuous system matrix of one TP i
$\mathbf{A}_{\Delta t}^i$	Time-discrete system matrix of one TP i depending on time interval Δt
$\tilde{\mathbf{A}}$	Adaptation matrix for affine Transformation
\mathbf{B}^i	Time-continuous input matrix of one TP i
$\mathbf{B}_{\Delta t}^i$	Time-discrete input matrix of one TP i depending on time interval Δt
\mathbf{C}^i	Positional extraction matrix
\mathbf{C}^{ij}	Relative positional extraction matrix
D_{hell}	Hellinger Distance of two PDF's
D_{meha}	Mahalanobis Distance
D_{prox}	Proximity value for splitting a Gaussian PDF
$D_{\text{prox}}^{\text{lim}}$	Proximity threshold for splitting a Gaussian PDF
D_{alloc}	Allocation value for splitting a Gaussian PDF
$D_{\text{alloc}}^{\text{lim}}$	Allocation threshold for splitting a Gaussian PDF
H	Predicted time step horizon
\mathbb{H}^l	Subset defined by two hyperplanes in scene state space \mathbb{R}^n
\mathbb{H}_{sp}^l	Subset defined by one hyperplane in scene state space \mathbb{R}^n
I	Intention variable
\mathbf{I}	Intention vector
I_{safe}	Intention while safe state
I_{ctrl}	Intention while controlling vehicle
I_{nonctrl}	Intention while non-controlling vehicle
\mathbb{M}	Shape in two-dimensional positional space
\mathbb{M}_{OCC}	Occupied area in two-dimensional positional space
$\mathbb{M}_{\text{OCC}}^{ij}$	Geometrical overlap in two-dimensional relative positional space of two TP's i and j
\mathbb{M}_{COLL}	Collision region in scene state space \mathbb{R}^n
$\mathbb{M}_{\text{COLL},k}^{\text{stat}}$	Collision region representing overlap of two TP's at time step k
$\mathbb{M}_{\text{COLL},k}^{\text{dyn}}$	Collision region representing overlap of two TP's between two subsequent time steps $k - 1$ and k
$\hat{\mathbb{M}}_{\text{COLL}}^{\text{dyn}}$	Approximating set of $\mathbb{M}_{\text{COLL}}^{\text{dyn}}$
$\mathbb{M}_{\text{COLL},\text{poly}}$	Polygonal collision region \mathbb{M}_{COLL}
$\mathbb{M}_{\text{COLL}}^{\infty}$	Swath collision region over infinite time

N_e	Number of events
N_o	Number of TP's
N_{hard}	Number of hard constraints
N_{OC}	Number of occupants
N_{COLL}	Number of crashes
$P_{\text{inst, ev}}$	Instantaneous event probability
$P_{\text{inst, COLL}, k}^{\text{dyn}}$	Instantaneous collision event probability determined by $\widehat{M}_{\text{COLL}}^{\text{dyn}}$
$P_{\text{inst, COLL}, k}^{\text{stat}}$	Instantaneous collision event probability determined by $M_{\text{COLL}}^{\text{stat}}$
$P_{\text{tcs, ev}}$	Time-course sensitive event probability
$P_{\text{tot}}(e)$	Total event probability over predicted time horizon
$P_{\text{inst, surv}}$	Instantaneous survival probability
$P_{\text{tcs, surv}}$	Time-course sensitive survival probability
P_{ov}	Overlap probability between two axis-oriented, rectangular shaped TP's
$\mathbf{Q}_{\Delta t}^i$	Time-discrete noise covariance matrix of one TP i depending on time interval Δt
$\mathbf{R}_{\text{rot}}^2(\alpha)$	Rotation matrix depending on angle in 2-dimensional space
$\mathbf{R}_{\text{rot}}^{90}$	Rotational matrix for 90°
\mathbb{R}^n	State space
T	Predicted time horizon
T^h	Time interval between two subsequent time steps $k - 1$ and k
T_{mult}	Representative term for product of two different event rates
\mathbf{W}_u	Cost weight matrix for comfort
$\mathbb{X}_{\text{hard}, h}^i$	Non-reachable sub state space for one TP i given by h 'th restriction
$\mathbb{X}_{\text{free}}^i$	Reachable sub state space for one TP i
\mathbb{X}_{des}	Desired/targeted sub state space

Latin Lowercase Letters

a_x	Acceleration in global x-direction
a_y	Acceleration in global y-direction
a_{brake}	Acceleration after collision
\mathbf{a}_{orth}	Normalized vector which is orthogonal to relative velocity vector
\mathbf{a}	Two-dimensional normal vector of hyperplane
\mathbf{a}^l	Two-dimensional normal vector of $\mathbb{M}_{\text{OCC}}^{ij}$ edge l
$\mathbf{a}_{\text{split}}$	Normal vector of hyperplane splitting non-collided PDF
b	Shift of hyperplane
$\tilde{\mathbf{b}}$	Shift vector for affine transformation
b^l	Shift of $\mathbb{M}_{\text{OCC}}^{ij}$ edge l
b_{split}	Shift of hyperplane splitting non-collided PDF
b^-	Lower boundary shift of $\mathbb{M}_{\text{COLL}}^\infty$
b^+	Upper boundary shift of $\mathbb{M}_{\text{COLL}}^\infty$
c_{ESC}	Escaping event severity
c_{CONST}	Severity offset
\hat{c}_{COLL}	Mean collision risk
\hat{c}_{comf}	Instantaneous mean comfort costs
$\hat{c}_{\text{tes,comf}}$	Tcs. mean comfort costs
\hat{c}_{risk}	Instantaneous mean risk costs
$\hat{c}_{\text{tsc,risk}}$	Tcs. mean risk costs
\hat{c}_{util}	Instantaneous mean utility
$\hat{c}_{\text{tes,util}}$	Tcs. mean utility
Δd	Lateral distance difference between vehicle and reference position
Δd_{th}	Threshold value for lateral distance in coping model
Δd_{sl}	Slope value for Lateral distance in coping model
e	Event variable
e_{COLL}	Collision event between two TP's
e_{ESC}	Escape event
e_{NON}	No event
e_{OCC}	Collision event in object distributed area
e_{SR}	Raising state restriction event
g	Gravitation constant

inj^q	Injury level of occupant q after one collision
inj_{tot}^q	Injury level of occupant q regarding whole prediction horizon
k	Time step
m	Mass of one TP
\tilde{m}	Mass ratio between two TP's
n	State dimension of traffic scene
n_i	State dimension of TP i
p	Input space dimension of scene
p_i	Input space dimension of TP i
\mathbf{n}	Input noise vector
\mathbf{n}_{flow}	Flux vector for distributed events
\mathbf{n}_{force}	Crash force direction vector
p_x	Position in global x-direction
p_y	Position in global y-direction
$p_{x,ev,k}(\mathbf{x}_k)$	Event PDF
$p_{x,COLL,k}^{stat}(\mathbf{x}_k)$	Collision event PDF determined by \mathbb{M}_{COLL}^{stat}
$p_{x,COLL,k}^{dyn}(\mathbf{x}_k)$	Collision event PDF determined by $\widehat{\mathbb{M}}_{COLL}^{dyn}$
$p_{x,surv,k}(\mathbf{x}_k)$	Survival PDF
\mathbf{r}^i	Positional vector of TP i
\mathbf{r}_{COLL}^i	Positional vector after collision
\mathbf{r}_{CON}^i	Positional vector at contact time
\mathbf{s}^i	Moving direction of TP i
t	time
\mathbf{u}^i	Input vector into motion model of TP i
v_{lim}	Allowed or limited driving velocity on road
v_x	Velocity in global x-direction
v_y	Velocity in global y-direction
\mathbf{v}^i	Velocity vector of TP i
\mathbf{v}_{COLL}^i	Velocity vector after collision
\mathbf{v}_{CON}^i	Velocity vector at time of contact
\mathbf{v}^l	Hyperplane normal vector in scene state space of edge l from $\mathbb{M}_{COLL,poly}$
\mathbf{v}_{sp}^l	Normal vector of splitting hyperplane
w^l	Hyperplane shift in scene state space of edge l from polygonal collision region $\mathbb{M}_{COLL,poly}$
w_{sp}^l	Normal vector of splitting hyperplane
w_{comf}	Cost weight for comfort
w_{inj}	Cost weight of injury probability
w_{lim}	Cost weight for raising speed limitation

w_{prog}	Utility weight for progressing/traveling
w_{veh}	Width of ego vehicle
\mathbf{x}	Scene state
\mathbf{x}_{CON}	Scene state at contact time
\mathbf{x}_{COLL}	Scene state after collision
\mathbf{z}	Normalized path direction

Greek Letters

α_{COLL}	Angle between path and after crash orientation
β_0	Slope value for collision event rate τ_{COLL}^{-1}
γ^i	Yaw angle or orientation of TP i
$\Delta \mathbf{r}$	Relative position of two TP's
Δt	Time difference between time step k and $k + 1$
Δt_{crash}	Crash duration
$\tilde{\Delta t}_{\text{CON}}$	Time to contact
$\Delta \mathbf{v}$	Relative velocity vector of two TP's
μ_f	Road-to-wheel friction
ρ_{DISTR}	Occupation density of static objects
Σ_u^i	Covariance matrix for input noise of TP i
Σ_x^i	Covariance matrix for time-discrete state of TP i
τ_e^{-1}	Event rate
τ_{AGG}^{-1}	Cumulative rate of different event types
τ_{COLL}^{-1}	Rate for collision event e_{COLL}
τ_{ESC}^{-1}	Rate for escape event e_{ESC}
τ_{max}^{-1}	Maximum rate for collision event rate τ_{COLL}^{-1}
τ_{OCC}^{-1}	Rate for collision in object distributed area event e_{OCC}

Special Functions and Transformations

$c_{\text{trav}}(\mathbf{r}_k, \mathbf{v}_k)$	Utility function
$c_{\text{lim}}(\mathbf{r}_k, \mathbf{v}_k)$	Cost function for raising allowed or desired speed
$c_{\text{comf}}(\mathbf{u}_k)$	Cost function for comfort
$c_{\text{agg}}(\mathbf{x}, \mathbf{u}, I)$	Cost aggregation for one specific point in time
$C_{\text{tot}}(\mathbf{u}_{0:H}^1, \mathbf{x}_0)$	Cumulated costs over predicted time points
$\delta(\cdot)$	Dirac delta function
$l(\cdot; \mu, m)$	Logistic PDF with mean μ and scale parameter m
$L(\cdot; \mu, m)$	CDF of logistic PDF
$\sigma(\cdot)$	Step function
$\mathcal{N}(\cdot; \mu, \Sigma)$	Gaussian PDF with mean μ and covariance Σ^2
$\Phi(\cdot; \mu, \Sigma)$	CDF of Gaussian PDF $\mathcal{N}(\cdot; \mu, \Sigma^2)$
$\mathcal{G}(\mathbf{x})$	Gaussian Mixture Model
$p(\mathbf{u}_k \mathbf{I}_k)$	Behavior model
$p(\mathbf{I}_{k+1} \mathbf{I}_k, \mathbf{e}_k)$	Intention transition model
$p(e_k \mathbf{x}_k)$	Event detection model
$p^{\text{stat}}(e_k = e_{\text{COLL}} \mathbf{x}_k)$	Collision event detection model with static collision region $\mathbb{M}_{\text{COLL}}^{\text{stat}}$
$p^{\text{dyn}}(e_k = e_{\text{COLL}} \mathbf{x}_k)$	Collision event detection model with dynamic collision region $\mathbb{M}_{\text{COLL}}^{\text{dyn}}$
$p(\mathbf{x}_{k+1} \mathbf{x}_k, \mathbf{u}_k)$	Motion model
$p(\mathbf{x}_{k+1} \mathbf{x}_k, \mathbf{u}_k, \mathbf{e}_k)$	State transition model
$c_{\text{risk}}(\mathbf{x}_k, e_k)$	Risk/ Cost event function
$c_{\text{sev}}(\mathbf{x}_k, e_k)$	Severity function
$c_{\text{sev,ext}}(\mathbf{x}_k, e_k)$	Extended severity function including after-event costs
$c_{\text{COLL}}^{\text{const}}(\mathbf{x}_k)$	Constant severity model
$c_{\text{COLL}}^{\text{wall}}(\mathbf{x}_k)$	Wall impact severity model
$c_{\text{COLL}}^{\text{v2v}}(\mathbf{x}_k)$	Multiple events severity model
$c_{\text{COLL}}^{\text{multi}}(\mathbf{x}_k)$	Inter-vehicles impact severity model
$p(\mathbf{I}_{k+1} = I_{\text{safe}} \mathbf{x}_k, \mathbf{x}_{\text{COLL},k})$	Crash coping model

$p(\mathbf{x}_{\text{COLL},k} e_k = e_{\text{COLL}}, \mathbf{x}_k)$	Physical crash model
$p^{\text{wall}}(\mathbf{x}_{\text{COLL}} e_k = e_{\text{COLL}}, \mathbf{x}_k)$	Physical crash model between vehicle and wall
$p(\text{inj}_k^q \mathbf{x}_{\text{COLL},k}, \mathbf{x}_k)$	Injury model of one occupant at one predicted time point k
f_{eth}	Ethical model
$f_{\text{eth}}^{\text{agg}}$	Ethical model taking cumulating occupant injury probabilities
$f_{\text{eth}}^{\text{max}}$	Ethical model taking maximum occupant injury probability
$f_{\text{eth}}^{\text{as}}$	Ethical model taking probability of at least one occupant injury probability

Kurzfassung

Das Ziel autonomen Fahrens ist die Erhöhung von Sicherheit, Nutzen und Komfort für alle Straßenteilnehmer. Vor allem der Bereich der Risikowahrnehmung ist von zentraler Bedeutung, um kritischen Situationen vorzubeugen bzw. um möglichen Schaden abzuwenden. Faktoren wie die Messunsicherheiten in der Umfeldwahrnehmung, Unsicherheiten über das zukünftige Verhalten der Verkehrsteilnehmer ändern die Wahrscheinlichkeit des Eintretens kritischer Ereignisse, wie einer Kollisionen zwischen Verkehrsteilnehmern, und damit das Risiko geplanter Fahrmanöver.

In dieser Arbeit wird basierend auf einer Umweltrepräsentation und gegebenen Bewegungsmodellen eine Risikobewertung für eine zeit-diskrete Ereignisvorhersage mit Fokus auf Kollisionen zwischen zwei Fahrzeugen vorgestellt, die als Teil eines Kosten-basierten Planers ist, welcher zusätzlich auch den Nutzen und Komfort entlang einer geplanten Trajektorie hinzuzieht. Eine Risikobewertung beinhaltet neben der oft modellierten Wahrscheinlichkeit des Eintretens kritischer Ereignisse auch deren Schäden wie Verletzungen der Insassen oder Wertverluste am Fahrzeug. Klassische Metriken betrachten entweder die Unfallwahrscheinlichkeit oder die Unfallschwere. In dieser Arbeit werden beide Komponenten des Risikos zusammen betrachtet, dessen Auswirkung auf das Fahrverhalten in mittelkritischen Szenarien wie beim Überholen oder Vorbeifahren in Engstellen sichtbar werden.

Die Modellierung des Kollisionsereignisses betrachtet zwei polygonalgeformte Objekte aus der Vogelperspektive - vorzugsweise Rechtecke - unterschiedlicher Größe. Zustände wie Positionen und Geschwindigkeiten der Objekte unterliegen Unsicherheiten, die durch Gauß'sche Verteilung angenähert werden. Um alle Kollisionen auch bei hochdynamischen Objekten zu erkennen, erfolgt die Detektion quasi zeit-kontinuierlich. Das heißt, dass neben der Überprüfung an den diskreten Abtastzeitpunkten auch Kollisionskonstellationen betrachtet werden, die sich zwischen zwei aufeinander folgenden Zeitpunkten befinden. Des Weiteren werden analytische Methoden zur Bestimmung der Kollisionswahrscheinlichkeit und aller Zustandsverteilungen vorgestellt, die entweder Zustände mit kollidierten Verkehrsteilnehmern abbilden oder nur Kollisionsfreie Trajektorien beinhalten. Im

Vergleich zu einer klassischen Monte Carlo Simulationen mit 1000 Samples wird die Rechenzeit bei gleich bleibender Genauigkeit deutlich verringert. Zur weiteren Erhöhung der Genauigkeit wird die Zustandsverteilung der nicht-kollidierten Trajektorien mithilfe mehrdimensionaler Gauß'schen Mischverteilungen (GMM) im Zustandsraum repräsentiert, dessen Anzahl an Komponenten von den möglichen Ausweichszenarien abhängt.

Für die Schwere einer Kollision wird eine Modellierung vorgestellt, die neben der Verletzungsschwere des ersten Kontakts auch den Schaden nachfolgender Kollisionsereignisse berücksichtigt. Insgesamt beinhaltet das Unfallschwermodell folgende Komponenten: a posteriori Zustände nach der Kollision durch Anwendung der Impulserhaltungsgleichungen, die Kontrollfähigkeit der Fahrzeuge nach der Kollision, die Verletzung der Fahrzeuginsassen durch die Kollision sowie eine ethische Abwägungen zwischen den Verletzungswahrscheinlichkeiten aller beteiligter Insassen. Zur Evaluierung des vorgestellten Modells wird dieses im Anschluss mit drei, weniger detaillierten Modellen, welche stark an die Literatur angelehnt sind, verglichen.

In den Simulationen kritischer Fahrscenarien zeigt sich unter anderem, dass bei einer Verwendung von Unfallschwermodellen sich durch das Zusammenspiel mit der Unfallwahrscheinlichkeit, sich zwischen einfachen Folgeszenarien und nahen Überholmanövern ein Geschwindigkeits-adaptiver Übergangsbereich einstellt. Hier bildet sich eine Geschwindigkeitsdifferenz heraus, die ein minimales Risiko während des Überholvorgangs kreiert und in erster Linie vom seitlichen Abstand abhängig ist. Zusätzlich führt die Anwendung der Impulserhaltungsgleichung mit seinen Massen und die Verletzungsmodellierung aller Insassen dazu, dass der schwächere Kollisionspartner zwischen ungleichen Fahrzeugen, wie bspw. ein PKW gegenüber einem Lastkraftwagen, geschützt wird, was sich unter anderem durch eine deutliche Reduktion der Überholgeschwindigkeiten ausdrückt.

Abstract

The goal of autonomous driving is to increase safety, benefit and comfort for all road users. Above all, the area of risk perception is of central importance in preventing critical situations or averting possible harm. Factors such as measurement uncertainties in environment perception, uncertainties about the future behavior of road users change the probability of occurrence of critical events, such as a collision between road users, and thus the risk of planned driving maneuvers.

In this work, based on an environmental representation and given motion models, a risk assessment for a discrete-time event prediction with focus on collisions between two vehicles is presented as part of a cost-based planner, which additionally adds utility and comfort along a planned trajectory. A risk assessment includes not only the often modeled probability of occurring critical events, but also their damages such as injuries to occupants or loss of value of the vehicle. Classical metrics consider either accident probability or severity. In this work, both components of risk are considered together, whose impact on driving behavior becomes visible in medium-critical scenarios such as overtaking or passing in narrow scenarios.

The modeling of a collision event considers two polygonal-shaped objects from the bird's eye view - preferably rectangles - of different sizes. States like positions and velocities of the objects are subject to uncertainties which are approximated by a Gaussian distribution. In order to detect all collisions even with highly dynamic objects, the detection is quasi time-continuous. This means that in addition to checking at discrete sampling time points, collision constellations located between two consecutive time points are also considered. Furthermore, analytical methods for the determination of the collision probability and of all state distributions are presented, which either represent states with collided traffic participants or include only collision-free trajectories. Compared to a classical Monte Carlo simulation with 1000 samples, the computation time is significantly reduced while maintaining the same accuracy. To further increase the accuracy, the state distribution of the non-collided trajectories is represented using multidimensional Gaussian Mixture Models in state space, whose

number of combined unimodal components depends on possible avoidance scenarios.

A modeling approach is presented for the severity of a collision that considers the injuries of subsequent collision events in addition to the injury severity of the initial contact. Overall, the accident severity model includes the following components: a posteriori states after the collision by applying the momentum conservation equations, the control capability of the vehicles after the collision, the injury of the vehicle occupants during the collision, and an ethical trade-off between the injury probabilities of all involved occupants. To evaluate the presented model, it is subsequently compared with three less detailed models, which are strongly based on the literature.

In the simulations of critical driving scenarios, it is shown, among other things, that when accident severity models are used, a speed-adaptive transition range is established between simple following scenarios and narrow overtaking maneuvers due to the interaction between severity and collision probability evaluations. Here, a speed difference is formed that creates a minimum risk during the overtaking maneuver and is primarily dependent on the lateral distance. In addition, the application of the momentum conservation equation with its masses and the injury modeling of all occupants leads to the protection of the weaker collision partner between dissimilar vehicles, such as a car versus a truck, which is expressed by a significant reduction in overtaking speeds.

1 Introduction

According to the World Health Organization (WHO) the number of fatal traffic accidents reaches more than 1,3 million per year, so a road user dies in average every 24 seconds [117]. Due to the rising world population and new costumers through growing wealth, the global trend is not slowing down: the number of accidents with fatal outcomes and the number of vehicles increase continuously (see Fig. 1.1).

But there are also good news. In some countries the absolute and relative number of fatal accidents is decreasing. E.g, in Germany, in 2015 only 0,4% of all deaths are caused to road accidents [43] and only 4 fatalities per one billion km occurred in 2020 [140]. On the one side, this progress is a consequence of traffic regulations for passive protection systems like a mandatory seat belt wearing, speed limitations in urban areas and decreasing maximum blood alcohol concentration limitations. On the other hand, also technical achievements like the anti-blocking system (ABS), automotive cruise control (ACC), lane keeping and lane changing assists, brake assists or collision warning system play a major role for the reduction of fatal accident outcomes [174] .

Nevertheless, around 90% of accidents with injuries are related to human errors [42]. So the **Vision Zero**, which aims to reach a traffic without any fatal or severe injuries, is only possible if human errors could be avoided or compensated by monitoring or taking over the control from the driver by autonomously working system like advanced driver assistance systems (ADAS) or autonomous vehicles (AV), respectively. Due to a recent user acceptance study, the anticipated improved safety is also a main reason for choosing an autonomous vehicle instead of driving by their own [65].

But with the rise of autonomous vehicles, the decisions of the driver are shifted to the designer or programmer of that system, who affectively become the new drivers. Debates about ethical standards arise and dilemma situations like the trolley problem get more scientific investigation: a train is moving into a group of people and a switchman that can intervene but has only the options to let kill one person to safe the lives of group members [15] or vice versa. To question reasons for the moving train in that dilemma scene, e.g. transporting goods or other persons, brings up more

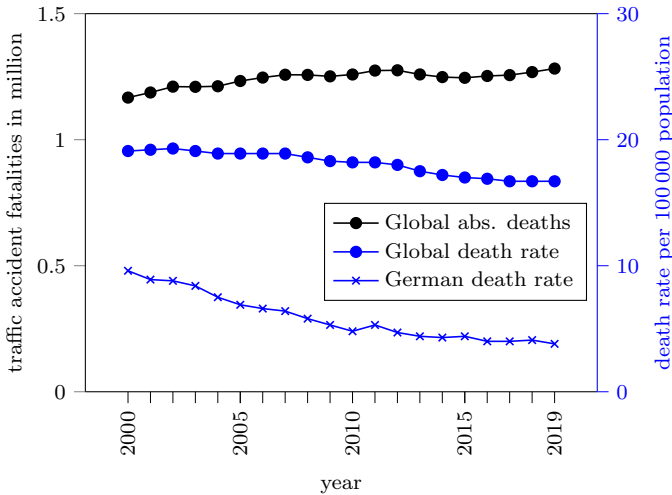


Figure 1.1: Estimated fatal road accidents in absolute numbers and in relation to population per year [116].

extravagant scenarios, where utility is weighted against human life.

This example shows that there is a public interest in the functionality of an artificial system including the decision making process and a desired public-designer feedback-loop to take control at least on the trade-off between comfort, economical utility and human integrity [78].

1.1 Problem Formulation

An autonomous system needs a core set of components to work appropriately. One is an environmental model, given by a perceptual system composed of external sensors like cameras, radar or ultrasonic sensors and a post-processing to extract traffic scene components like other traffic participants, lanes, signs and road boundaries. The decision making system - another component - takes these often uncertain elements from the perception module to choose actions according to a sufficient behavior like avoiding critical situations, operating to fulfill traffic laws, recommended driving behavior and satisfying occupants comfort requirements. Such a system is represented in Fig. 1.2.

For validating the criticality produced by technical systems, the ISO

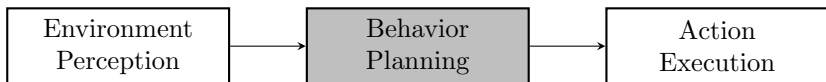


Figure 1.2: Connection of the behavior planning system to other autonomous system’s modules. Arrows show the flow of information stream.

norm 31000 [82] of the International Organization for Standardisation (ISO) has defined the risk concept as a basic approach to evaluate critical events such as e.g. collisions with other traffic participants. The risk itself is a quantifier which consists of an event probability, which determines how likely an event will occur, and the associated event severity, which represents the kind of costs associated to damage of the vehicle or injuries of occupants. If this risk concept is incorporated into the behavior planner in an on-line and foreseeable manner, the autonomous system could produce safe behavior.

Mostly, both risk components, probability and severity, are treated separately in planning systems. Either the collision probability is calculated and any contact between vehicles is treated as fatal [45, 133, 141] or only the severity is determined in detail like in crash mitigation maneuvers [74, 91, 145], where the collision cannot be avoided anymore. For example, [109] shows that different speed levels influence the outcome of a crash and lead to higher injuries of the occupants. Only considering the collision probability would neglect that some traffic participants are more dangerous than others. Therefore the autonomous vehicle could misinterpret situations, which could lead to fatal consequences instead of producing less harmful outcomes or it could lead to overcautious behavior in harmless situations. On the other side, cases, where a crash cannot be avoided anymore and only the severity impacts the decision process, are very rare and are mostly a consequence of previous (bad) decisions.

In this thesis, the collision severity and probability are treated equally as two quantifiers for calculating risk in a maneuver planning process. This approach shifts the severity calculation from highly critical further into less critical scenarios, so that more danger-appropriate decisions will be made and the autonomous vehicle will produce more plausible behavior. To investigate this severity shift, the following three main questions arises:

1. How can the evaluation of different (critical) events and a priority between events be incorporated into an overall decision making framework?

This framework should also include the ability to handle multiple traffic participants, sensor/ motion uncertainties and multiple events. After clarifying, how the decision model is structured and designed, the following question addresses the risk components:

2. How can event probability models and severity models being determined for different critical event types, especially for collision events?

For this, different existing probability and severity calculations models have to be analyzed for weaknesses and representation errors for different critical scenarios in context of a prediction framework of future time points.

The last and main question considers the closed feedback-loop behavior and addresses the impact of crash consequences:

3. How do severity models affect motion behavior in risky scenarios?

This includes an investigation of naive severity models, where only collision probability is the crucial part and the more advanced severity models with a more complex structure.

The design and the investigation of the probability model is necessary to analyze the severity model impact on the motion behavior appropriately, because both models influence in a different manner, the motion behavior. An inaccurate and not properly designed probability model does not allow concrete findings for the severity model investigation.

1.2 Contributions

By tackling these questions, the following main contributions play a part:

- A novel prioritizing event-based motion framework considering critical events, law violations and utility parts in one predicted time point.
- A novel time-course-sensitive probability model as extension of state-of-the-art survival considerations for prediction of multiple critical events with multiple traffic participants over the overall predicted time horizon.
- A novel, effectively computable event probability calculation for inter-vehicle collisions, which incorporates vehicle shapes. It imitates state-of-the-art flux calculations so that it drastically reduces

probability calculation deficiencies caused by time-sampling issues of time-discrete frameworks.

- A novel distribution adaptation method considering different crash avoidance opportunities in the prediction process.
- A novel distribution adaptation method to keep using simple unrestricted motion models for state predictions by outsourcing internal state restrictions.
- A novel event probability calculation for collisions with groups of quasi-homogeneous distributed collision partners.
- A novel severity design framework incorporating multiple crash events by modeling explicitly the crash process, after-crash behavior and after-first-event crashes, injury probabilities and ethical concatenation of different occupants.
- Three novel severity models with a different level of detail impacts the motion planner in a way that different behaviors in moderate risky scenarios and in scenarios with different massed vehicles occur.

The presented models are investigated in a simulation framework for motion planning to investigate their properties and functionalities.

1.3 Thesis Outline

The structure of this thesis is depicted in Fig. 1.3. The thesis starts with an introduction into traffic environments and basic concepts for autonomous vehicle at the beginning of Ch. 2. Based on this, the definition of risk is discussed in more detail to get a better idea of the main components of this thesis. At the end of this chapter, the framework for the used motion planning system with its prediction model, cost evaluation and behavior priorities is outlined. It contains simplifications to better focus on the influence of the risk assessment like probability and severity on the behavior.

In dealing with the massive number of possible scene evolutions and multiple traffic participants, Ch. 3 presents simplifications based on state-of-the-art approaches. Further findings of this chapter give structure for adding new event types to the overall motion planning framework.

The first and most important event of this thesis is the collision event. The collision event probability with other traffic participants, especially

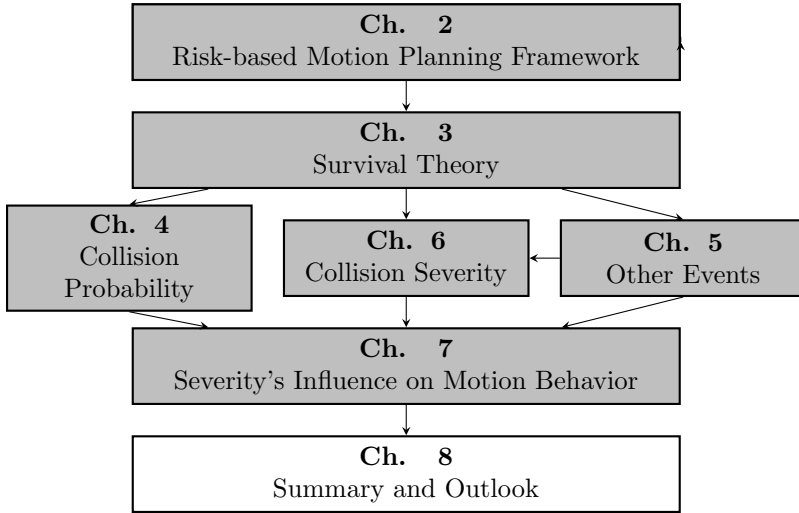


Figure 1.3: Thesis structure with chapter dependencies.

with some other vehicles, is outlined in Ch. 4. Here, the basics of a collision event detection is outlined, which provide basics to the concept of shape-based collision probability calculation, where the magnitudes and distributions of the collided states are separated from the non-collided states. In addition, new calculation methods are presented and are compared in some selected scenarios to show their prediction accuracy.

In Ch. 5, other event types are introduced dealing with distributed objects, internal state restrictions, law violating events like breaching speed limitations and the escape event. Some of these events are a prerequisite to understand models of subsequent chapters.

The Ch. 6 introduces to the second main component of an risk evaluation, the severity. Here, sub-models and their relationships are presented to gain an ethical assessment of collisions. Furthermore, four severity models, three of them inspired by state-of-the-art approaches are discussed. The influence of the severity models on the driving behavior are investigated in Ch. 7. This chapter also includes the impact of vehicle masses asymmetries on the behavior which is shown intensively.

The related works is presented within the respective chapters. The summary and outlook are given in the last chapter Ch. 8.

Readers, not familiar with probability theory or those who want to

refresh important parts used in this thesis are invited to read the corresponding chapters in attachment Sec. A.6 for probability distributions and Sec. A.7 for Bayesian Theory.

2 Risk-Based Motion Planning Framework

This chapter introduces the motion planning framework, used as a basis for integrating risk assessment and behavior planning. For a smooth introduction, the first two sections discuss the main terms of traffic environments to get familiar with the surrounding conditions, the representation and the general algorithm structure of an autonomous vehicle (AV). They also provide first notations and assumptions for vehicles and drivers behavior. Based on this, the risk concept is presented, discussed in general and is applied for motion planning in the subsequent section, together with related work, basic components, extensions and first simplifications. The chapter ends with a conclusion and a summary of the novelties of the introduced framework.

2.1 Traffic Environment

The traffic environment (TE), in which the autonomous vehicles need to operate, can be very diverse and confusing due to many road users and complex road paths (see Fig. 2.1). Not all environments can clearly be described like a speed limited highway or a unidirectional, one lane bounded tunnel. For humans more confusing or stressing environments are non-regulated parking areas, where many different traffic participants (TP's) like hidden pedestrians and vehicles meet each other. Reactions of an on-coming vehicle with high speed to a suddenly crossing child could also be manifold. Will the child keep running or will it stop? Should the vehicle driver stop, steer or brake and steer simultaneously? Should the driver steer to the left or to the right? What if it's not a car, but a smaller motorcycle? The situation could become less dangerous, because it is easier to avoid smaller sized objects. These examples and open questions show that traffic environments could have different evolutions depending on the current scene and often, there is not only one unique solution for everyone to achieve their goals.

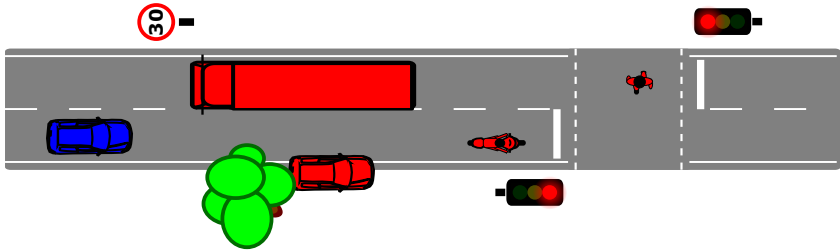


Figure 2.1: Traffic environment with road users like an ego vehicle (blue), a motorcycle, a truck, a passenger car, a pedestrian, static objects like trees and signs with speed limitations or traffic lights and lane boundaries.

To handle these complex, partially observable and stochastic surroundings, the traffic environment is structured in the following as a basis for the algorithms in the subsequent sections. The physical environment is given by all static objects, e.g., road boundaries, walls or parked vehicles, and the dynamic objects like pedestrians, vehicles or trains. All objects including their types, properties, current states and the geometry of the road or lanes is called a traffic **scene**.

Exemplary properties of, e.g., a motorcycle is its dynamic capability of fast accelerating and its small dimension compared to a truck, which for example allows a motorcycle driver to pass easily through two queues of standing vehicles sticking in a traffic jam. Firstly, the subject object like the motorcycle is called ego vehicle with index $i = 1$ and all other traffic participants are called **others** or other vehicles with $i > 1$. These vehicles could be trucks, bicycles, passenger cars and other motorcycles and they have their own shape $\mathbb{M}^i \subset \mathbb{R}^2$, kinematic limitations, masses m^i and dynamical behavior.

The **physical states** $\mathbf{x}^i \in \mathbb{X}^i \subseteq \mathbb{X}^i$ of a vehicle i contain directly measured quantities from sensor systems like positions p_x^i, p_y^i , velocities v_x^i, v_y^i of the mass center point on a two-dimensional “top-view” road surface, described in an orthogonal x and y coordinate basis. Additionally, the orientation of vehicles γ^i is needed to feed **motion models**, the kinematic relationship between successive states and inherently determines kinematic restrictions. Different types of road users have different motion models. Nevertheless, in this thesis they are all represented by the same minimal set of states \mathbf{x}^i for simplicity.

The concatenation of all N_o object related physical states \mathbf{x}^i to one

overall state vector $\mathbf{x} \in \mathbb{X}^{\sum_{N_o} n_i}$, is called **scene state** vector:

$$\mathbf{x} = [(\mathbf{x}^1)^T, \dots, (\mathbf{x}^i)^T, \dots, (\mathbf{x}^{N_o})^T]^T .$$

Based on that concatenation of individual object states \mathbf{x}^i , the scene can be fully described by on vector \mathbf{x} at one specific point in time t .

Another concept is that sequence of states in a limited time interval $t \in [t_1, t_2]$ is called trajectory. Trajectories of scene states $\mathbf{x}_{t_1:t_2}$ are called **scene evolution**, which describes a sequence of a scene with all dynamic objects:

$$\mathbf{x}_{t_1:t_2} = \{\mathbf{x}(t) \in \mathbb{R}^n | t \in [t_1, t_2]\} .$$

A prototypical scene evolution is called **scenario**. The corresponding state evolution in single-object related trajectories $\mathbf{x}_{t_1:t_2}^i$ is called maneuver [103]. Small differences in a stop and go maneuver, e.g. the time length of having zero velocity, would not lead to a completely new maneuver, only to a slightly different parametrization. Therefore, maneuvers and scenarios are representatives of trajectory clusters.

Not every physical state of an object is reachable or allowed. Typical hard **restrictions** of physical states are often due to physical limitations like e.g. maximum speeds, which depend on the motor engine capabilities or physical constitution of pedestrians. Examples are also stiff road boundaries or house walls, which in most cases cannot be removed. Restrictions between object form collision areas. For each restriction type h the corresponding subset of state space represents a non-reachable region $\mathbb{X}_{\text{hard},h}^i \subset \mathbb{X}^i$. With the help of these subsets, the free space $\mathbb{X}_{\text{free}}^i$ can be determined, where the object is able to move inside, not violating any of the existing N_{hard} hard constraints:

$$\mathbb{X}_{\text{free}}^i \subset \mathbb{X}^i \setminus \bigcup_{h \in \{1, \dots, N_{\text{hard}}^i\}} \mathbb{X}_{\text{hard},h}^i .$$

In contrast to these hard, intrinsic constraints, there exist also soft or extrinsic constraints. They consider more abstract restrictions which would not hinder objects to get into a specific position or onto a specific velocity level, but rather declare some non-allowed states, which should force desired behavior to regulate traffic. These often country-specific rules are for example: speed limitations, not crossing solid road lines, one-way streets and so on. Some rules depend on other objects like: stopping at red light, left yields to right or no overtaking on the right. In some emergency cases, it is necessary to leave, e.g., designated lanes to avoid crashes. Therefore,

breaching an extrinsic restriction should rather be treated as undesirable and punished by costs than as never being reachable. In other words, regulations cannot totally prevent any misbehavior of objects.

Another kind of states next to physical states are hidden or physically not explainable, but are often helpful: the **internal states**. The most famous internal states are **intentions** I^i of the vehicle driver or pedestrian, considering motion targets like turning left, right or driving straight on an intersection, switching to a neighbor lane or driving into a specific parking slot. Most maneuvers are connected to these intentions so that one or more maneuvers can be concatenated to achieve a specific physical target.

These targets are described by a set of desired states $\mathbb{X}_{\text{des}} \subset \mathbb{R}^n$, e.g. a parked car i is expressed by a range of possible orientation γ^i , nearly parallel to the neighbor cars or pedestrian walk, an area around the center position p_x^i, p_y^i of the parking slot and zero velocities $v_x^i = v_y^i = 0$. For target lanes during a lane change maneuver the positional states are inside a hull around the associated lane path. If these spatial intentions I^i vary in time, they become spatio-temporal intentions I_t^i . Let us regard an intersection, where two vehicles approach nearly at the same time. To avoid a collision one could brake to yield and the other one could accelerate to drive first or vice versa. These spatio-temporal intentions change over time until they match and are robust, otherwise the conflict could not be solved, if for example both insist to yield.

Other internal states are, e.g., parameters describing object motion or driving style like reaction times, safety distances, visibility or consideration of other traffic participants, rule awareness and so on.

Furthermore, the physical and internal states of all objects forms a **situation** i.e., a traffic scene with all internal states. For example two vehicles intent to enter the same side road from a main-road. The scene without intentions would not present any conflict, but adding the internal goals, which in this case are similar, leads to a potential conflict in the future. The situation can be solved in multiple ways depending on the spatio-temporal intentions. A typical solution ends up in a scenario, which become a prototype or representative of a cluster of similar scene evolutions.

After clarifying terms like physical states, internal states, scenes, situations, maneuvers, scenarios, intrinsic and extrinsic restrictions, the components of an autonomous vehicle can be introduced.

2.2 Autonomous Driving

In the previous chapter, the properties and restrictions were shown describing the traffic environment. The author of [166] mentions three general aspects, which should be provided by an autonomous vehicle: a goal, safety and rules. This means, that the system has to act according to its own preferences in a way that all the presented restrictions related to traffic rules, other vehicles, road geometries and motion dynamics are considered and not violated. A typical rough system architecture of an AV consists of three main parts on the software side: the sensory system, the world modeling and the behavior planner system. The sensors and actuators are the provider of current environmental information and manipulators of the outer world [2].

The first system, the sensory system, processes the input sensor signals from Laser Imaging Detection and Ranging (LiDAR), camera or ultrasonic sensors, needed for creating an internal representation of the world. The world consists of static objects like road boundaries, standing vehicles or construction site barriers, dynamic objects like pedestrians, other vehicles and bicycle drivers, and also signals like the traffic light or static traffic signs for limiting velocity or give-away limitations. Point clouds with depth information given by LiDAR sensors for far distant objects or ultrasonic sensors for near-distant objects are fused with monocular or stereo-camera pictures. Because of the limited number, accuracy and field of view of sensor systems, the scene information of a traffic scene is not complete and often very noisy. With “Vehicle to X” (V2X)- technology additional information can be exchanged. Between vehicles (V2V) intentions like desired paths or maneuvers can be transmitted. But also hidden objects, not observable by all traffic participants can be shared. Traffic light states can be send to the cars to enable moving traffic.

With the raw sensor data collected over time, the environment could not be described sufficiently. This data has to be interpreted to gain a usable representation. Static objects or free spaces can be detected via occupation maps, where filters are implemented to determine whether a specific area is occupied by an object or is free to drive through [141]. Sometimes it is useful to take prior knowledge into account, e.g. high definition (HD) Maps provide a detailed road and lane description given by geographical measurements. Combined with the self perceived scene, this could help to increase the accuracy of the ego’s and other’s position [34] or understand the road semantics. To detect dynamic objects a scene has to be observed for a small period of time. Sometimes the detection is very challenging

because of the moving sensor system on the vehicle. To robustly infer kinematic quantities like positions, velocities or orientations tracking filter techniques for dynamical objects are applied. They use underlying motion model and observations of the same detected traffic participants with aid of subsequent snapshots in a period of time. Common filters are Extended Kalman Filter (EKF) and Unscented Kalman Filter (UKF) which use a Gaussian state distribution to model the uncertainty of the kinetic states. By usage of interacting multiple model filters, also the probability of executed maneuvers out of a set of possible maneuvers representing, e.g. spatial-temporal intentions or special escaping maneuvers, can be detected [141]. Through redundant information obtained by the V2X communication, the current scene state could be measured more accurately and the prediction of the scene becomes more precisely. Transmitted information between vehicles regarding the critical components has to be checked and verified for plausibility with regards to the own measurement to detect external attacks and misinformation, to avoid blind trust, which could lead to fatal crashes. The internal representation of the current world scene state with all its elements is feed into the behavior planner or generator and is assumed to be given with some state noise.

The last system belonging to an autonomous vehicle is the behavior planner. Given the internal world state representation with all its elements and a preset navigation goal like a parking slot in front of one's house, the next action could be planned. For this, the system takes assumptions of other driver's future actions and intentions to consider internal and external state restrictions like collisions with other traffic participants or road boundaries and traffic rule limitations. To plan robustly, the behavior planner deals with uncertain information like an initial state distribution, different possible driving maneuvers of traffic participants, unknown intentions or driving styles. Furthermore, to ensure that planned actions of maneuvers will be executed in the correct way, the behavior planner incorporates possible action limitations related to engine power or wheel frictions to not overstress the system and to guarantee expected behavior. Because each executed action, like braking at the middle of an intersection, will not change only its own state, but also provoke actions of some others, which will change their future actions and so on. This reaction chain or dependency between traffic participants is called interaction.

There is also an dependency between the three presented sub systems. For example, the more accurate the sensor processing is, the more accurate are the world state representations and the semantic classifications, the more the vehicle could focus on the true conflicting vehicles and thus

the vehicle acts less overcautious and more efficiently. There exists another cause-effect chain starting at the behavior planning system and going through the real world state to the sensory processing system to the world model. This means, that the behavior planner could influence the quality of the model world representation by adapting the driving behavior. For example, a vehicle overtakes a school bus, where the bus blocks the view on the space in front of the bus, where children could cross the street. If the vehicle approaches that space, the field of view will become wider and more hidden children could be detected. Longer observation times and less motion disturbances caused by small speed maneuvers increases the accuracy of measurements.

The whole software system of an autonomous vehicle should be applicable in real world, which means that the subsystems should process and calculate needed information in real-time, so without big time latency. This requirement is often a bottleneck when designing algorithms.

In this thesis, a behavior planner is designed which is at least expandable to the concepts like interaction or hidden world parts. For simplification, it is assumed that the sensory processing and the internal world representation are given. Furthermore, the external world with actuators and sensor systems is not explicitly modeled and are only part of a simulation. Nevertheless, to investigate the capabilities of the motion planner and its produced behavior, simulations can be used, which are applied to a lot of different critical scenarios, which cannot be performed in real world due to high costs in case of failures.

2.3 The Risk Concept

There are different terms like risk, criticality or threat often used in the context of autonomous driving. But what do these terms mean? What are the differences or similarities compared to “risk” and how can they be determined?

The Risk itself is a metric **risk** [82, 103] and is defined as:

$$\text{Risk} = \text{Probability} \times \text{Severity} \quad .$$

The risk includes the overall danger of an event or an undesired state by its consequence or severity and its likelihood [108]. In Fig. 2.2, one can see that the risk is a combination of severity and probability and that it can represent two extrema, the collision mitigation with severity reduction

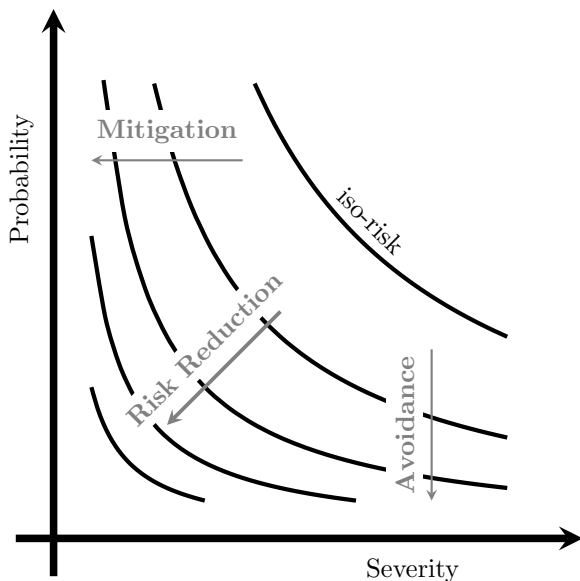


Figure 2.2: Diagram with constant risk curves (iso-risk's), where the risk is increasing from the bottom left to the upper right. At its margins, the risk reduction concept includes impact mitigation for severity reduction and avoidance strategies for likelihood reduction. Both strategies approximately represent a gradient descent on a risk potential and are special cases of the more general risk reduction strategy. The general risk reduction can also cope sufficiently in regions, where both the severity and the probability are moderate. For events, which do not have any severe outcome or cannot occur, the risk becomes zero.

and the collision avoidance with probability reduction. In-between these extrema, both factors will be reduced by considering the risk.

To distinguish the risk term to threat, the following example explain it in more detail. Considering a vehicle in an flat and open field, like the Black Rock Desert, Nevada (USA), where some of the fastest vehicles, the “trust SSC” was tested. At this desert, there exist nothing which can disturb the vehicle of freely driving forward. There is no threat in the scene, because nothing serious can happen: no crashes, no loss of control through bumps with undesired roll-overs. If this rocket vehicle would drive in New York, Berlin or Shanghai, there will be the potential of collisions with other participants. So **threat** or **danger** describes the existence of

a possible event with serious outcome. In other words, it is the absence of safety. Threat is independent of the consideration whether the event will happen or not and is more describing that the event can happen. So it is rather a binary state than a continuous quantity.

The existence of a fatal event does not mean that the vehicle is not able to avoid crashes and that it has the capability to cope with the threat within the traffic environment. As long as the vehicle is not in an Inevitable Collision State (ICS) [60], meaning that a collision is certain, the collision can be avoided at least with an optimal maneuver. But optimality is mostly far from reality. The driver has to act before an inevitable collision state becomes certain. The urgency to avoid a fatal outcome with the limited action sets a vehicle can execute for collision avoidance, is described by the term **criticality**. In the literature there are many measures defining a criticality to warn drivers about collisions or to find the point in time, where an autonomous system should take the control to execute avoidance maneuvers. Four classes for criticality measures can be found:

- **Evaluation by experts:** The criticality is quantified by traffic psychologists like in [146], where a scale from 0 to 100 is used to describe its criticality level. An adaptive neuro-fuzzy interface system (ANFIS) at T-intersections is implemented depending on gap sizes and vehicle type, which at the end was validated by expert data [137]. The authors of [105] use an ANFIS system to find out decision probabilities in non-signalized crossing scenes and validate their model by playing a zero sum non-cooperative game.
- **Heuristic functions:** In [35], the authors introduce a criticality index function as a product of severity and urgency, which represents a needed momentum change of the ego vehicle to avoid a crash with another traffic participants in left-turn-conflicts. A warning system for near crashes is presented in [165], where an oncoming vehicle is detected by its increasing occupied field of vision angle.
- **Input-based:** The authors of [50] define a Brake Threat Number (BTN) for signaling dangerous lane departures. It bases on a constant acceleration for an avoidance maneuver relative to the gravity constant g .
- **Time-based:** This class is motivated by the idea that with decreasing time to an event or a scene state the criticality is increasing. These measures are known as “Time to X” (TTX). The X can stand

for different events like a collision (TTC) [170] or a general maneuver (TTM), braking (TTB) [88], kickdown (TTK) or steering (TTS) [76] to avoid a collision. These different maneuvers can be merged into one representative Time to React (TTR) [76, 150] which informs the driver, how much time remains until the collision is inevitable [60]. In contrast to the TTR measure, the Worst Time To Collision (WTTC) calculates the time until the first collision can occur [159] by considering those action sequences leading to the collision in the minimum of time. According to the authors, this concept raises many false positives, so the WTTC measure monitoring is too conservative. Other time-based metrics are the Time Headway (TH) for highway scenarios or Post Encroachment Time (PET) [130] for merge-in scenarios. They determine the duration, the following or merging vehicle would use to reach the position or intersection center after the other car has left it. Another measure for arbitrary predicted trajectories is the Time To Predicted Minimum Distance (TTPMD) which is used in the EUCLIDE project for collision warnings [126].

Often, these metrics assume perfect knowledge about the ego vehicle and other traffic participants. Motion and sensor uncertainties or inaccurate assumptions about future motion patterns like e.g. constant velocity or acceleration in curves, motivates to take a probabilistic view on time- and input-based measures to not oversee potential conflicts. A probabilistic calculation with motion and sensor uncertainties of the Brake Threat Number (BTN) is given in [148]. A similar measure like the BTN without gravity normalization is presented in [12]. For time-based measures, probabilistic TTC [18, 21–23, 77, 95, 96, 104, 133, 141], TTR [161] or TTPMD [151] are introduced as robust criticality metrics. In addition, the concept of inevitable collision states is extended to a probabilistic view [20], so that all states are avoided which have a probability to end up in a collision, not those states which already will have a collision.

Next to measures whose only aim is to avoid crashes, there are metrics considering the outcome of a potential collision e.g., with increasing warning levels. In [9], the authors take the geometrical overlap and the penetration duration of two vehicles into account to adapt the warning levels, the higher both feature values are, the higher the warning level. In [171], the internal energy of the crash and in [71] the kinetic energy of the ego vehicle are influencing the level of criticality. The authors of [164] define a safety energy for each object in the scene whose virtual masses

have an underlying statistical origin in fatality data. As a consequence, objects will appear as more dangerous if their speed level is higher. In works [162, 163] a severity index was implemented with additive components for distinguishing between different relative heading angles and mass ratios.

As one can see, many criticality measures consider vehicle dynamics, the probability and the outcome or severity of a crash. In case of more than one source of threat or critical event type, the risk framework can concatenate different hazards to one final value, where a decision can rely on.

In [82], some principles for a proper risk management are defined, among others, the risk should be part of the decision making, explicitly addressing uncertainty, being systematic and structured, transparent and taking human and cultural factors into account. The author of [166] applies this risk concept on robots with a decision making system that should consist of four components: 1. identification of possible actions for a given situation, 2. forecast of probable changes in the environment and actions of others, 3. prediction of possible future situations and 4. risk assessment for predicted scenarios. A survey on motion prediction and risk assessment techniques is presented in [103].

All in all, the risk is a continuous quantification which extends the binary concept of threat. It is an essential part of decision making in uncertain environments for predicted scenarios.

Furthermore, a macroscopic view on traffic shows that 10^{-6} fatalities per driving hour occur. In [143], the author states that a robot or autonomous systems should reduce the fatality rate by a factor of 1000 to 10^{-9} . This small number is very challenging to test the system on-line, because of the needed high amount of scenarios to obtain significant results and to validate off-line, because of the missing interaction with real traffic participants. Therefore, the underlying models for severity and probability should be as accurate as possible to prevent the occupants from dangerous outcomes. The prediction of risk can help to quantify the total driven risk of autonomous vehicles and thus validating the driven trajectories of autonomous vehicles without applying another metric.

2.4 Event-Based Motion Planning Framework

The main focus of this thesis is the risk calculation with its severity and event probability models. In the previous section it was discussed that the risk concept should be part of the decision process in autonomous vehicles. It can handle uncertain traffic environments and can evaluate the expected severity of critical events. To investigate the driving behavior depending on the risk assessment of critical events, a simple motion planner is designed which is served as a basic framework for incorporating all traffic participants in the scene, is handling different risk sources and is expandable for using more sophisticated driving strategies and detailed prediction models. The presented motion planner is complex enough to represent motion behavior of other more sophisticated planners, but at the same time it is simple enough to investigate severity models, probability models and their effects in detail.

2.4.1 Related Work

A motion planners main target is to “prevent the autonomous vehicle from entering the unsafe area” [166]. In [166], the author names further objectives like accomplishing the mission or long-term navigation goal and complying with the traffic regulations. The authors of [59] add some safety requirements for autonomous systems, like taking own dynamics and input limitations into account, taking other traffic participant’s behavior into account and considering an infinite time horizon. The last statement of an infinite prediction horizon ensures that independent of the vehicle’s dynamic and internal restrictions like brake forces, a collision can be avoided.

Works like [27, 80, 84] identify different stages for motion driving depending on the current task: normal driving, collision avoidance, collision mitigation and post-crash behavior. In Fig. 2.3 these stages can be more or less strictly separated. A five staged version instead of four staged version is described by an accident model, which categorizes its hierarchic levels according to the risk levels with a final “Loss” state and general strategies to leave one state to reach the previous one with lower risk [166].

In the following, an overview of these crash stages will be presented, where the focus is on the strategies, models and limitations. To better

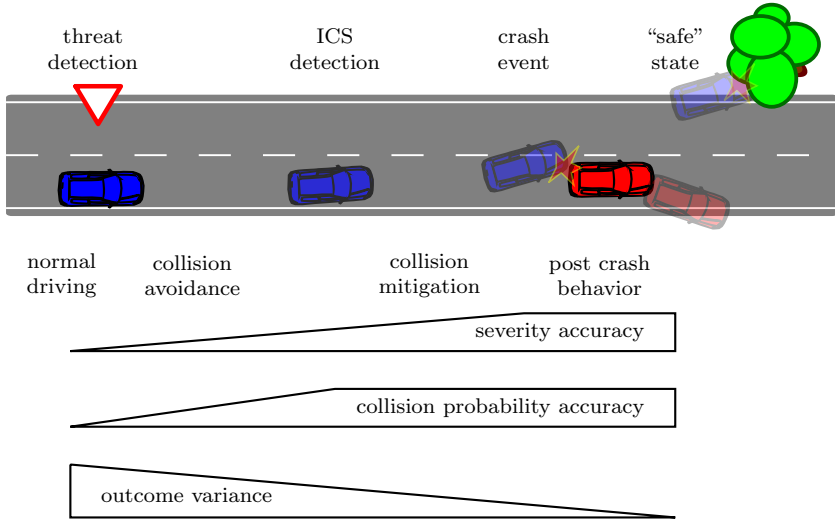


Figure 2.3: Stages of motion planning with increasing risk [27], needed level of detail for severity model and collision probability model and declining range of predicted outcome. The threat detection describes the transition from normal driving to collision avoidance. The Inevitable Collision State (ICS) detection represents the discrete transition from collision avoidance to collision mitigation. After the crash event, the vehicle can have subsequent crashes or can end up in a “safe” state, depending on the post crash motion.

describe these stages, the mitigation phase is split into three sub-phases: the mitigation phase, the pre-crash phase or accident preparation and the crash event itself. The explanation starts with the last stage i.e. after the first crash was happened.

Post Crash Phases

The post crash phase starts right after the first collision, when two crash partners move apart from each other. Regarding data for the US [44] and Germany/ United Kingdom [57] in the turn of the millennium, one of four collisions have at least one subsequent crash. In these multi-collisions, the injury rate is four times higher than for single crashes. Additionally, the injury level for these multiple collisions is also increased [57]. Post-collision braking assists tries to minimize the number and severity of post-crashes

by braking autonomously as fast as possible [106].

Crash Phase and Accident

During the accident, the motion planner has no influence on the outcome of the crash anymore. Only passive systems like belts, a fired airbag or energy absorbing vehicle designs can reduce the harm of the passengers. Injuries of the occupants and the damages are mainly determined at the point in time, when the collision is happening. The crash constellation like frontal, side or rear-end crashes [56], speed levels [109] and masses [56] influences the crash outcome significantly. In [51], a multi-degree of freedom mass-spring-damper system for vehicle and occupants was designed to model crash dynamics during the impacts in head-on crashes. It can help to simulate the vehicle-passenger interaction like intrusions into the passenger compartment, which can lead to bruises, and acceleration changes, which can lead to contacts with interior parts [16]. An overview of some injury prediction techniques is given in [147]. In [144], the authors present economical costs depending on the level of injury in a crash. This prediction of harms and outcome is given by a severity model, which predict cost taking vehicle states before and after the crash. These state changes can be predicted by a physical crash model.

Accident Preparation or Pre-Crash Phase

This stage is right at the moment before the crash will happen. The decision, whether to fire airbags for reducing the passenger harms are tackled by [112–114]. An airbag system which is firing too often or at the wrong moment could increase the harm, because drivers are not able to see anything or cannot be protected for subsequent, more serious crashes. In [112–114], the hitting forces with interior parts are calculated using simple crash mechanic models. The model and its parameters are validated and trained by a more accurate mechanical simulation database, created by Finite Element Methods (FEM's). Another context-aware pre-triggering system uses a crash severity database system, which includes physical crash model predictions and real crash database. According to a support vector machine, the systems can activate a downstream safety system in case of frontal crashes by taking parameter distributions like masses or compartment stiffnesses into account [27].

Mitigation Phase

After the point of no return was passed and a collision seems to be inevitable, the motion planner has the chance to reduce the severity of a critical event by a well chosen action sequence. In [97] and [84], a braking system based on a (probabilistic) Time To Collision (TTC) prediction was implemented. A more sophisticated system based on the detection of inevitable states was introduced in [31] and for multiple objects in [32] with consideration of slip and brake system dynamics. All the works are motivated by the idea that the kinetic energy has to be reduced as effectively as possible to decrease the level of harm. The effectiveness of such braking assists was validated in [66], where the authors concluded that 3 of 4 severe crashes were avoidable. But there are more motion opportunities to mitigate crashes than strict braking maneuvers. In [91], a local planner searches for a motion strategy to reduce the virtual overlap area between the vehicles along predicted trajectories. It takes also dynamical limitations for steering and braking into account. In [74], the wheel base of the other vehicle in a side-crash is targeted by the autonomous vehicle. These crash points at the exterior are stiffer than the compartment zone and therefore safer for occupants, which sit in the vehicle hit from the side. Another approach is a deformation map, a two dimensional potential field, based on a Finite Elements Method (FEM) database, which calculates the vehicles curvature of a potential path to produce less intrusions for both vehicles [145]. The drawback of this approach is, that for one thing the approach is not considering braking and steering maneuvers and for the other thing the deformation map is very noisy, so that a global minimum is hard to find. If there is more than one object in a dense scene, which can not be avoided, a decision can be based on its ego vehicle kinetic energy [67]. In [162, 163], a Model Predictive Controller (MPC) optimizes a strategy based on a potential field which includes heuristically a crash severity measure depending on mass ratios and different heading angles. Summarized, a mitigation system needs a detailed model for own and other vehicle dynamics, as well as a target like the frontal wheelbase or a severity surrogate.

Collision Avoidance Phase

To protect the occupants from a collision, trigger systems have to warn or intervene before a collision cannot be avoided anymore, so far before an inevitable collision state occurs [60]. Collision-free maneuvers can be

determined analytically [139] or with a model predictive controller [172] in a deterministic world. For stochastic environments, [20] provides a complete introduction into probabilistic inevitable states. But mostly, there exist avoidance systems, which predict and let execute simple maneuvers e.g. brakings based on a required acceleration [92] or on Time-to-React (TTR) measures [76]. The authors of [169] introduce a safety distance to not crash into a leading vehicle. In [102], twelve different trajectory candidates are predicted and checked for collision in an occupancy map in relative state space. An advanced time to occupancy measure for all trajectory candidates identifies the point in time, when to activate the avoidance system and follow the trajectory with the smallest criticality measure. In the aforementioned collision avoidances systems, the severity plays only a minor role. Motion models with limitations are very simple e.g. they base on constant velocity, constant steering and constant acceleration models.

There are some works, which include a severity and collision probability according to the risk measure, mentioned in the previous section 2.3. These works blur discrete boundaries between mitigation, where the collision probability becomes one anyway and the severity plays the important assessment factor, and the collision avoidance, where the collision probability is crucial but will not be the only factor anymore. One example is introduced in [30], where severe injuries of pedestrians from a vehicle impact as well as motion uncertainties are considered. Another example is described in [28], where predicted acceleration impulses for an uncertain predicted crash works as an identifier for severity. The author of [5] evaluates and plans trajectories according to their maximal crash probability with different other dynamic objects and calculates the internal crash energy as outcome. In [99], a simple motion planner acts according to a preset risk level. This approach shows that a vehicle would reduce its speed level to decrease the severity in a predicted crash if the probability is not decreasing.

Normal driving Phase

If collisions have very low probability or very low risk, the motion planner can focus on additional tasks like approaching navigation goals, comfortable driving, obeying traffic rules or decreasing energy consumption. An overview of different real-time-planning techniques like Rapidly-Exploring-Random-Trees (RRT's), model predictive controller and Lattice planners is given in [93] and [69]. Often, these different objective are evaluated

according to associated costs for violation and are summed up to obtain overall representative cost value for one predicted motion strategy. In [33] and [49], yaw angle velocities and distances to a desired lane provide an initial input strategy distribution, which works as a prior to obtain conflict-free trajectories after collision checks. In [73], a cost function based on evaluating collisions with static and dynamic objects as well as ego dynamics like accelerations are considered. The authors of [101] creates a motion optimizer, penalizing on the one hand the motion model input in a quadratic fashion and on the other hand variances of the state distribution. Non-allowed collision-states are represented by linear state restrictions and are modeled as hard constraints. Similarly, in the work of [25], a maximum collision probability is modeled as a hard constraint for a linear program which includes distances to waypoints and travel costs. These motion planners ensure safe strategies according to predicted state uncertainties.

Recently, global motion planners evaluate crash severities next to others cost terms like utility and comfort e.g. in a potential field [85, 131], in a two-ramp maneuver-based optimization with uncertainty considerations [129], in a model predictive controller as soft constraints [79, 80, 173] or in Rapidly Random Tree (RRT)-based optimizations [36, 38, 39]. There are also some local planners like an Euler-Lagrange optimization [135] based on a holistic framework [134] and the Foresighted Driver Model (FDM) [46]. The work of [46] combines a heuristic risk map framework [37] for arbitrary risk sources, like losing control in curves, and with utility-based components of the Intelligent Driver Model (IDM) [156]. The Foresighted Driver Model can handle multiple scenarios like following and intersections and shows a speed reduction in frontal passing. The severity models and the probability models have often strong assumptions to simplify the calculation process, because they will be evaluated multiple times during the prediction-based optimization process to find the one with the minimal costs. Local planners can reduce the optimization effort, but with drawback of finding mostly local optima.

The phases of normal driving, collision avoidance and mitigation can often not be separated accurately. Triggers rely on different concepts so that the boundaries between these phases seems to be fuzzy. Furthermore driving strategies differs from one phase to another, so that they have to be tuned sufficiently to not end up in oscillating behavior strategies. Nevertheless, some properties can be summed up. The range in expected outcome, described by the minimum and maximum possible risk of all

scene evolutions, is decreasing with the time to a critical event. For example, an inevitable crash can be mitigated in a way that the maximum severity is reduced, but there will still be a minimum severity left, because the crash cannot be avoided anymore. Otherwise, a planning system for normal driving can increase the maximum severity by speeding up in dangerous scenes. Until here, it can be noted that a consideration of severity in each phase seems to be inevitable and advantageous. Whereas, the level of model detail changes depending on the existence of remaining traffic environment uncertainties or in other words: the models do not have to be precisely modeled, if there are many scene evolution alternatives are left. An overview about the levels of detail for a severity model and the event probability model as well as the range of expected outcome is sketched in Fig. 2.3.

Nevertheless, as far as the author knows, there is no framework considering multiple events in one scene evolution like road boundary crashes after an inter-vehicle collision. State-of-the-art severity models are only taking the first event into account. They often heuristically weights the outcome by internal crash energy or kinetic energy of the ego vehicle, fatality rates or others. A comparison between these models by investigating their effects on the motion planner behavior was not yet investigated. Furthermore, the corresponding collision probability models differ in their properties. Therefore, a holistic framework for evaluating different risk evaluations is needed. This framework should also incorporate navigation goals, dynamic and static objects, dynamical restrictions and law violations along the whole predicted trajectories.

2.4.2 Components of Behavior Planner

The framework for behavior planning applied in this thesis is very similar to existing approaches mentioned in the previous section and therefore is part of an overall autonomous driving system framework. The focus in this thesis is on the behavior planning module and its components like risk assessment to investigate critical scenes with other traffic participants. The performance of this component is depending on the input e.g. objects, boundaries, lanes, traffic signals extracted by sensor signals. Furthermore, some additional information about the objects like goals and motion restrictions are needed to enrich the motion planner with information. The requirements or assumptions defined on the provide internal world representation, especially on the dynamical objects, are as follows:

- Multiple traffic participants
- Different object types: bicycles, trucks/ trains or passenger cars and pedestrians with different masses
- Polygonal (rectangular) object shapes
- Known motion models with probabilistic positions and velocities in x and y coordinate from a bird's eye view
- Known guiding lanes as navigation constraints for each object
- Probabilistic inputs caused by disturbances and motion noises
- Tangential object orientations to the driving paths

Given these (uncertain) information and assumptions, the behavior planner copes with other traffic participants in a way that critical scenarios will not arise or get mitigated. For that the behavior planner consists of three main components, which are also shown in Fig. 2.4, which enables a criticality assessment of future scenes to choose the least critical actions to avoid any kind of harmful events:

1. A prediction process for future states, events and intentions.
2. An evaluation process to quantify the overall risk and utility of the predicted trajectories with pre- and post-event behavior.
3. A decision model, which determines an optimal strategy based on the plan evaluation and behavior preferences.

The prediction process is necessary to deal with dynamical restrictions formulated by the given motion models, where e.g. states cannot immediately change to arbitrary desired (safe) scene states, because of dynamical limitations e.g. maximum steering angle or maximal braking forces. Having hypothetically infinite fast state change, it would not be guaranteed that other traffic participants want to share the same space in the next time step, because they could have other plans about how the scene should evolve. The prediction process usually includes assumed or learned assumptions about other traffic participants. Another part of the prediction process is the detection of critical or undesired events, which will be evaluated in the subsequent components. This enables to quantify the possible future scene evolution as a scalar value. Because the ego vehicle can change the future evolution with its planned action, it needs a quantification for

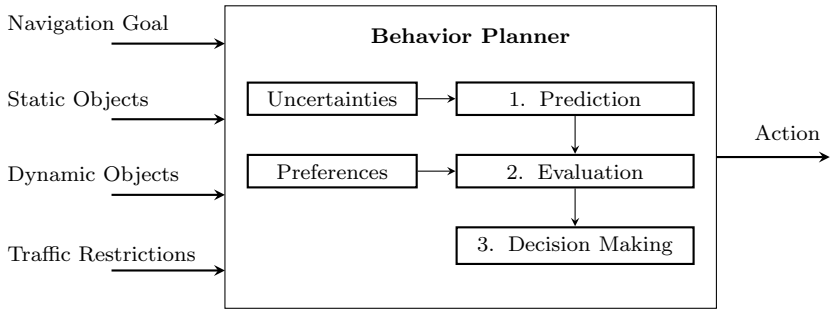


Figure 2.4: Behavior planner module with its input information, its main components and its output to the action execution system.

each predicted event to create a potential field of what is wrong and what is good. The decision model takes these event costs and other utility factors to create one final cost value according to an importance list for behavior preferences so that avoiding crashes will be more important than comfortable driving. Based on that cost value through prediction and evaluation, the planner optimizes its future actions according to the valley of a cost potential field.

The prediction, the evaluation and the decision making are working strongly together. If the prediction is wrong, events cannot be detected, which could lead to underestimated cost and to an engagement into critical scenarios. Similar would happen, if the prediction is correct but the event costs are underestimated. In contrast, overestimated costs lead to very cautious and passive behavior, in worst cases to dead-locks. In case of a non-optimal planner, the information of the precedent prediction and evaluation module is not fully exhausted and could become redundant. Each of the components should be designed carefully to satisfy the requirements for autonomous vehicles.

Nevertheless, these three components of the behavior planner ensure an early adaptation of the ego vehicle's behavior depending on predicted risks or law violations to reach the desired navigation goal as fast and comfortably as possible. In the following section, the three components are explained in more detail.

2.4.3 Prediction Model

The prediction model propagates current scene states into the future by using assumptions about the dynamics and behavior of other traffic participants, e.g., a motorcycle acts more dynamically than a truck with a trailer.

Each traffic participant limits the set of possible future states, because of the reduced free space through additional collision states. The scene gets more threats. If any behavior is assumed to be possible, this will lead to an overcautious and obstructing behavior, because also destructive behavior like from crash forcing traffic participants is incorporated. On the other side, a too conservative limitation of possible behavior and very restrictive motion models would take a smaller set of possible evolutions into account but could miss detection of critical events, which in turn could drastically underestimate the potential risk of planned actions. As a consequence, the autonomous vehicle behaves more aggressively and the vehicle has a higher chance to end up in a crash. A proper choice of the prediction model and its variables is necessary to avoid overcautious or careless predictions.

Obviously, the traffic participant and its state \mathbf{x}^i should stay inside the free space $\mathbb{X}_{\text{free}}^i$, where no event will ever happen. But, if the entity touches boundaries of non-reachable state set $\partial\mathbb{X}_{\text{hard}}^i$ defined for example by robust walls or shapes of other traffic participants, the entities would immediately stop or bounce back through the impact forces. In case of slight touches on a highway between two vehicles, it is possible that the first bounce effect leads to uncontrolled motion behavior and forces subsequent crashes with other objects like road limitations. The first and subsequent event produces more harm for the occupants than the first touching event. Therefore, to estimate the full consequences of traffic scenes, the propagation should not stop even if the first hard constraint is violated.

In the following, these short-termed touches to hard constraints are treated as **events**. These events can be of multiple types like collision to another traffic participant or collisions with a crowd of pedestrians, where it is difficult to distinguish between single entities. Events can also be of symbolic nature e.g. an escaping from the current scene or reaching impossible states which are not explicit modeled in the dynamics. These events have in common that scene states change in a short period of time and in a different way than the normally assumed motion dynamics.

Sometimes, these sudden state changes conclude to situations where vehicles get out of control. A crash scenario on a highway shows, that

the danger often arises not only from the first slight touch, but more from the uncontrolled motion behavior afterwards. The vehicle could crash into other boundaries or could do a rollover. Commonly, the goals of both involved vehicle drivers change from following their overall navigation goal to the target that the vehicles are moved to a safe state. Both attitudes are the **intention** I^i and describe long-lasting behavior patterns and goals. These stable intentions between events will help to categorize behavior patterns and simplify the prediction process.

To sum up, the following main time-depending variables will help to predict motion in free spaces and to model interactions with hard constraints to also incorporate after-event scene evolutions:

- Physical scene states $\mathbf{x} \in \mathbb{R}^n$: This is a combination of all N_o entity states $\mathbf{x}^i \in \mathbb{X}^i$, where $\mathbb{R}^n = \mathbb{R}^{n_1} \times \dots \times \mathbb{R}^{n_{N_o}}$ with dimension $n = \sum_{i=1}^{N_o} n_i$.
- Scene inputs $\mathbf{u} \in \mathbb{R}^p$: This is a combination of all N_o entity inputs $\mathbf{u}^i \in \mathbb{R}^{p_i}$ specifying the behavior, where $\mathbf{u} \in \mathbb{R}^p = \mathbb{R}^{p_1} \times \dots \times \mathbb{R}^{p_{N_o}}$ with dimension $p = \sum_{i=1}^{N_o} p_i$.
- Events $\mathbf{e} \in \mathbb{E}$: This represents any kind of events in a vector with binary elements $e \in \{0, 1\}$, where each element symbolizes one specific type of event (and with a specific partner). In this thesis the following event types are presented:
 - e_{COLL} : Each crash between ego and another traffic participant j (critical)
 - e_{OCC} : Collisions with crowded entities (critical)
 - e_{ESC} : Escaping from the current plan until reaching a safe state
 - e_{SR} : Non-reachable states or dynamic restrictions
 - e_{NON} : A symbolic representation for state changes, where none of the aforementioned events were happened
- Intention $\mathbf{I} \in \mathbb{I}$: This is a combination of all N_o entity states intention vectors $I^i \in \{0, 1\}$: $\mathbf{I} \in \mathbb{I} = I^1 \times \dots \times I^{N_o}$. Each entity i associated intention I^i describes abstract goals, affects maneuvers and determines the cost structure. Three different main intentions are defined:
 1. Controlled mode I_{ctrl} : The entity moves according to a general motion assumption or can plan freely in case of the ego vehicle.

2. Non-controlled mode I_{nonctrl} : Emergency behavior like braking or regaining control
3. Safe mode I_{safe} : Nothing can happen anymore. It symbolizes the end of the prediction process. These intentions can only be changed in a hierarchic way, so that the I_{ctrl} of one entity can change to I_{safe} , but not the other way round.

In continuous time, the aforementioned variables have to be determined at each future time point $s+t$, where t is the current time point and s the time parameter for future time points between $s=0$ and the maximum time horizon of $s=T$. For a time-discrete calculation, the time is split into time intervals of length Δt and the time step k with $s=k\Delta t$, where the prediction process is broken down to a fixed number of time point $H=T/\Delta t$. In this thesis, both descriptions are used, but the models will be introduced in a time-discrete manner and sometimes extended into a time-continuous case where the time interval between two subsequent discrete time steps $[k\Delta t, (k+1)\Delta t]$ is needed for increasing precision.

With the above definitions, the aforementioned variables can describe the scene at one predicted time point k . The transitions of intentions and states from one time point k to a subsequent time point $k+1$ will be discussed in the following. The conditional dependencies between variables over time are modeled by a Markov Model. The relationships between these variables are shown in a Bayesian network exemplary for two subsequent time steps in Fig. 2.5.

The full Bayesian model, gained by the Bayesian network, for a finite time step horizon H is mathematically described as follows:

$$\begin{aligned}
 p(\mathbf{x}_{0:H}, \mathbf{u}_{0:H-1}, \mathbf{I}_{0:H-1}) &= \dots \\
 \dots &= p(\mathbf{x}_0) p(\mathbf{I}_0) \prod_{k=0}^{H-1} p(\mathbf{I}_{k+1} | \mathbf{I}_k, \mathbf{e}_k) p(\mathbf{x}_{k+1} | \mathbf{x}_k, \mathbf{u}_k, \mathbf{e}_k) p(\mathbf{u}_k | \mathbf{I}_k) p(\mathbf{e}_k | \mathbf{x}_k) \cdot
 \end{aligned}$$

Here, the initial probability density function's (PDF's) for state $p(\mathbf{x}_0)$ and intention $p(\mathbf{I}_0)$ are measured or assumed and the transition models allow the computation of subsequent states, intentions and events. On the one side, the transition model enables the possibility for the detection of events, on the other side it also models the impact of events on the physical states \mathbf{x}_k and on some long-lasting states like the intentions \mathbf{I}_k , so that the vehicle's behavior after an event can be modeled separately.

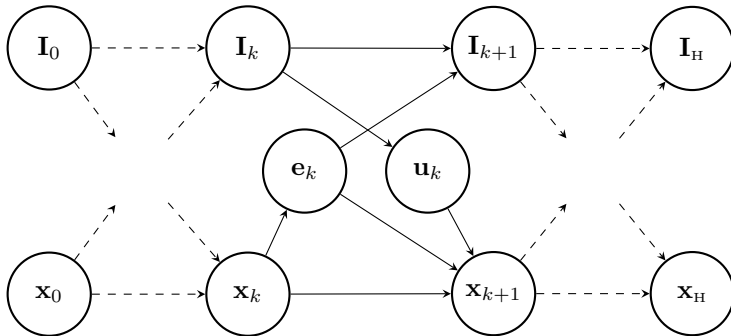


Figure 2.5: Bayesian network of the prediction model starting with the initial state $p(\mathbf{x}_0)$ and intention distributions $p(\mathbf{I}_0)$. Two further intermediate probabilistic variables for each discrete time step k describe the event \mathbf{e} and input \mathbf{u} variables. The network propagates all variables in a forward manner until the prediction horizon H is reached. The solid arrows show the conditional dependencies between all variables.

In the following, the sub models for clarifying the dependencies between these variables are presented in more detail.

Event Detection Model

The event detection model $p(\mathbf{e}_k | \mathbf{x}_k)$ is mostly an indicator, which detects whether an event in the current state \mathbf{x}_k is happening or not. The collision event e_{COLL} (Ch. 4) and non-reachable states e_{SR} (see Sec. 5.2) are part of this binary categorization. Some events like collisions with a crowded entity e_{OCC} (see Sec. 5.1) or escaping events e_{ESC} (see Sec. 5.3) are non-binary, because it is not certain if these events are happening in the considered state or not. The artificial event e_{NON} represents the case, if none of the aforementioned events is happening. So each event has its own detection model with different properties and will be introduced in the associated sections.

Intention Transition model

The intention transition model $p(\mathbf{I}_{k+1} | \mathbf{I}_k, \mathbf{e}_k)$ describes how events \mathbf{e}_k change the attitudes of the drivers or entities. Starting with a controlled behavior I_{ctrl} , where the ego vehicle and other traffic participants are moving according to their overall navigation goals, the initial distribution $p(\mathbf{I}_0)$

is described by the following product of single intentions I^i :

$$p(\mathbf{I}_0) = \prod_{i=1}^{N_o} \delta(I_0^i - I_{\text{ctrl}}^i) = \delta(\mathbf{I}_0 - I_{\text{ctrl}}) .$$

If an event occurs, which is normally very short-termed, this can impact longer lasting intentions of all traffic participants. Intentions won't change or change only very slowly if no events e_{NON} is happening so that $p(\mathbf{I}_{k+1}|\mathbf{I}_k, \mathbf{e}_k = e_{\text{NON}}) = \delta(\mathbf{I}_{k+1} - \mathbf{I}_k)$ holds approximately.

As aforementioned, the intentions change through events. For events with heavy bounces or friction losses like a collision between two vehicles e_{COLL} the intentions switch to the non-controlled mode I_{nonctrl} , where the vehicle is not able to control itself and execute an emergency maneuver. The safe mode I_{safe} is kind of a protected state: Once the vehicle reaches this state by escaping e_{ESC} the current scene, the traffic participants are immune against any further event. The safe mode symbolizes the end of the prediction process for a single scene evolution.

All in all, given the initial intention distribution $p(\mathbf{I}_0)$, the intentions \mathbf{I}_{k+1} at the next time step $k + 1$ are changed according to:

$$p(\mathbf{I}_{k+1}) = \sum_{\mathbb{I}} p(\mathbf{I}_{k+1}|\mathbf{I}_k, \mathbf{e}_k = e_{\text{NON}}) p(\mathbf{I}_k) p(e_{\text{NON}}) + \dots \\ \dots + \sum_{\mathbb{E}} p(\mathbf{I}_{k+1}|\mathbf{I}_k, \mathbf{e}_k = e_k) p(\mathbf{I}_k) p(e_k) .$$

The event provoking intentions $p(\mathbf{I}_e|e_k)$ for each event are discussed in the associated chapters Ch. 4, Ch. 5 and Ch. 6.

Behavior Model

The behavior model $p(\mathbf{u}_k|\mathbf{I}_k)$ determines the inputs \mathbf{u}_k for the next time interval related to the current intentions \mathbf{I}_k of the traffic participant. Each entity i has its own inputs \mathbf{u}_k^i according to their own motion models and independent of the other entities. So the inputs are chosen according to their own corresponding intention I_k^i :

$$p(\mathbf{u}_k|\mathbf{I}_k) = \prod_{i=1}^{N_o} p(\mathbf{u}_k^i|I_k^i) .$$

Here, the intentions I_k^i produce the following inputs of each entity:

- I_{ctrl} : For ego vehicle the input \mathbf{u}_k^1 is predefined by the current strategy given by the decision model 2.4.5, explained later in more detail. The input for all other traffic participants is assumed to be $\mathbf{u}_k^{>1} = \mathbf{0}$, so that they will move with constant input according to their motion model along their paths.
- I_{nonctrl} : In case of non-controlled intention, the traffic participant aims to reach a safe state by braking with a high deceleration $\mathbf{u}_k^i = -|a_{\text{brake}}| \mathbf{v}_k^i / \|\mathbf{v}_k^i\|$ against the motion direction. This roughly depicts the behavior after a collision, to slow down as fast as possible to zero velocity. This intention is used in Sec. 6.3.1. Once the non-control mode arises, the entity cannot come back to the I_{ctrl} , meaning that at least shock situations and crash management hinder the occupants to move back immediately to their original navigation goals.
- I_{safe} : The input can be arbitrary because this intention state indicates the end of the prediction, so that nothing can happen anymore.

The input \mathbf{u}_k is independent of the current state \mathbf{x} and the intentions \mathbf{I}_k only changes through events so that this framework can only represent intention-forced behavior and cannot represent state-based interactions between traffic participants.

Motion Model

The motion model $p(\mathbf{x}_{k+1}|\mathbf{x}_k, \mathbf{u}_k, \mathbf{e}_k)$ describes the transition model for scene states \mathbf{x}_k of time point k into the next time step $k+1$. The resulting scene \mathbf{x}_{k+1} depends first of all on the current \mathbf{x}_k and the scene input \mathbf{u}_k of all the scene entities. In case of some event type \mathbf{e}_k the state will drastically change e.g. through impact force during a collision. The scene motion model $p(\mathbf{x}_{k+1}|\mathbf{x}_k, \mathbf{u}_k, \mathbf{e}_k)$ describes the physical scene evolution by taking all single entities states \mathbf{x}_{k+1}^i , inputs \mathbf{u}_k^i and motion models $p(\mathbf{x}_{k+1}^i|\mathbf{x}_k^i, \mathbf{u}_k^i, \mathbf{e}_k)$ to obtain the next scene state \mathbf{x}_k :

$$p(\mathbf{x}_{k+1}|\mathbf{x}_k, \mathbf{u}_k, \mathbf{e}_k) = \prod_{i=1}^{N_o} p(\mathbf{x}_{k+1}^i|\mathbf{x}_k^i, \mathbf{u}_k^i, \mathbf{e}_k) .$$

Because of the missing dependency between the states of other traffic participants, interaction is not incorporated. This would unreasonably increase the complexity for investigating only risk model effects.

In this framework a two-directional double integrator system with positions p_x^i, p_y^i and velocities v_x^i, v_y^i in a frenet coordinate system is used as a motion model for non-event transitions [167]. The frenet system's first coordinate is oriented parallel to the lane or path direction and the second coordinate is orthogonal to the left. The inputs $\mathbf{u}^i = [a_x^i, a_y^i]$ are accelerations along the frenet-coordinates. The dynamics of each entity i can be described by the following linear state space model with $\mathbf{x}^i = [p_x^i, p_y^i, v_x^i, v_y^i]$:

$$\dot{\mathbf{x}}^i = \mathbf{A}^i \mathbf{x}^i + \mathbf{B}^i \mathbf{u}^i + \mathbf{B}^i \mathbf{n}^i, \quad (2.1)$$

with system matrix $\mathbf{A}^i \in \mathbb{R}^{n_i \times n_i}$, input matrix $\mathbf{B}^i \in \mathbb{R}^{n_i \times p_i}$, input $\mathbf{u}^i \in \mathbb{R}^{p_i}$ given by the behavior model and an acceleration noise $\mathbf{n}^i \sim \mathcal{N}(\mathbf{0}, \boldsymbol{\Sigma}_u^i)$, representing different driving styles, small differences in maneuvers and motion model inaccuracies. The frenet states are transformed back into the world coordinate system according to their projection on the path. The paths orientation is equal to the vehicle's orientation γ^i of one entity.

The transformation of the time-continuous system (Eq. (2.1)) to a time-discrete system in Frenet space is given by:

$$\mathbf{x}_{k+1}^i = \mathbf{A}_{\Delta t}^i \mathbf{x}_k^i + \mathbf{B}_{\Delta t}^i \mathbf{u}_k^i + \mathbf{n}_k^i,$$

where the input \mathbf{u}^i is assumed to be constant during the time interval $\tau \in [0, \Delta t]$ between two subsequent time steps. The corresponding time-discrete matrices $\mathbf{A}_{\Delta t}^i$ and $\mathbf{B}_{\Delta t}^i$ and the noise $\mathcal{N}(\mathbf{n}_k^i; \mathbf{0}, \mathbf{Q}_{\Delta t}^i)$ are calculated according to the following formula set [149, 157]:

$$\mathbf{A}_{\Delta t}^i = \exp(\mathbf{A}^i \Delta t) = \begin{bmatrix} 1 & 0 & \Delta t & 0 \\ 0 & 1 & 0 & \Delta t \\ 0 & 0 & 1 & 0 \\ 0 & 0 & 0 & 1 \end{bmatrix} \quad (2.2)$$

$$\mathbf{B}_{\Delta t}^i = \int_0^{\Delta t} \exp(\mathbf{A}^i \tau) d\tau \mathbf{B} = \begin{bmatrix} \frac{\Delta t^2}{2} & 0 \\ 0 & \frac{\Delta t^2}{2} \\ \Delta t & 0 \\ 0 & \Delta t \end{bmatrix}$$

$$\begin{aligned} \mathbf{Q}_{\Delta t}^i &= \int_0^{\Delta t} \exp(\mathbf{A}^i \tau) \mathbf{B}^i \Sigma_u^i (\mathbf{B}^i)^T \exp(\mathbf{A}^i \tau) d\tau \\ &= \begin{bmatrix} \frac{\Delta t^3}{3} \sigma_{u,x}^2 & 0 & \frac{\Delta t^2}{2} \sigma_{u,x}^2 & 0 \\ 0 & \frac{\Delta t^3}{3} \sigma_{u,y}^2 & 0 & \frac{\Delta t^2}{2} \sigma_{u,y}^2 \\ \frac{\Delta t^2}{2} \sigma_{u,x}^2 & 0 & \Delta t \sigma_{u,x}^2 & 0 \\ 0 & \frac{\Delta t^2}{2} \sigma_{u,y}^2 & 0 & \Delta t \sigma_{u,y}^2 \end{bmatrix}. \end{aligned}$$

Alternatives to the above used double integrator system in frenet space are constant velocity (CV), constant acceleration (CA), constant turning rate (CTRV) and constant turning rate acceleration (CTRA) motion models [142].

If no event happens e_{NON} , the motion model will be given by the linear time-discrete system with process noise, described in Eq. (2.2):

$$\begin{aligned} p(\mathbf{x}_{k+1}^i | \mathbf{x}_k^i, \mathbf{u}_k^i, \mathbf{e}_k = e_{\text{NON}}) &= \dots \\ \dots &= \int_{\mathbb{R}^{p_i}} \delta(\mathbf{x}_{k+1}^i - \mathbf{A}_{\Delta t}^i \mathbf{x}_k^i - \mathbf{B}_{\Delta t}^i \mathbf{u}_k^i - \mathbf{n}_k^i) \mathcal{N}(\mathbf{n}_k^i; \mathbf{0}, \mathbf{Q}_{\Delta t}^i) d\mathbf{n}_k^i \end{aligned}$$

Assuming a Gaussian state probability density function (PDF) written as $p(\mathbf{x}_k^i) = \mathcal{N}(\mathbf{x}_k^i; \hat{\mathbf{x}}_k^i, \Sigma_{x,k}^i)$ and a deterministic input distribution or dirac impulse $p(\mathbf{u}_k^i) = \delta(\mathbf{u}^i - \hat{\mathbf{u}}_k^i)$ of the behavior model, the resulting state PDF $p(\mathbf{x}_{k+1}^i)$ of the subsequent time step $k+1$ will also be normal distributed with a new mean state $\hat{\mathbf{x}}_{k+1}^i$ and a new covariance matrix $\Sigma_{x,k+1}^i$:

$$\begin{aligned} \hat{\mathbf{x}}_{k+1}^i &= \mathbf{A}_{\Delta t}^i \hat{\mathbf{x}}_k^i + \mathbf{B}_{\Delta t}^i \hat{\mathbf{u}}_k^i \\ \Sigma_{x,k+1}^i &= \mathbf{A}_{\Delta t}^i \Sigma_{x,k}^i (\mathbf{A}_{\Delta t}^i)^T + \mathbf{Q}_{\Delta t}^i. \end{aligned} \quad (2.3)$$

For non-linear time-discrete motion models, there exists some techniques to obtain the a posteriori state PDF. Non-linear systems can be linearized around the current mean state $\hat{\mathbf{x}}_k^i$, so that the equation system of Eq. (2.3) holds for a short time interval [138]. Another option is the unscented transformation, where representative points are picked from an a priori distribution to calculate the mean and variance of an a posteriori Gaussian distribution [138]. In case of an expected multiple modality distribution, a swarm of particles drawn from the a priori state and input distributions are transformed individually with the non-linear system to obtain the a posteriori distribution. The obtained state distribution by the so called Monte Carlo Simulation (MCS) can be depicted via histograms. However,

in this thesis, the linear double integrator according to Eq. (2.2) in Frenet space is used in every simulation of the prediction process like in Ch. 4 or in Ch. 7.

The motion models for other events, except the artificial non-event, are targeted in the associated sections.

2.4.4 Cost Evaluation of Scene States

After forecasting the future states of all entities, the second component of the autonomous system evaluates the scene evolution at each time step [36, 46, 79, 80, 85, 129, 131], which includes two tasks: penalize bad and reward good states or behaviors. The involvement into critical events like crashes or losing control as well as violating traffic rules are predestined candidates for penalization. These non-desired scene states could cost at least money if a critical event is happening. In contrast, the predicted plan will be rewarded if the autonomous vehicle gets closer to the goal state or ensures comfortable driving maneuvers. The reward is very similar to a penalization except of the sign.

The evaluation of future plans is strongly depending on the intentions, the autonomous vehicle will have at this moment in time. Critical events change the goals of the autonomous vehicle and some aspects like comfortable driving or achieving a navigation goal become irrelevant. The most ignoring intention is the safe mode I_{safe} , where all critical events and utility components are neglected. But also the intention in case of non-controlled vehicles I_{nonctrl} does not have any focus on utility or comfort. In case of a controlled vehicle I_{ctrl} , all critical events, utility and comfort are considered. As one can see, the intentions influence the cost evaluation, and therefore the perception of the current time phase within the prediction process.

In the following, the applied, general calculations of utility, breaching speed limitation punishments, comfort and risk are presented for the deterministic case and in case of Gaussian scene state probability density functions.

Utility Costs

The utility of an agent evaluates specific states, which are rewarded. One type is the progress utility, which deals with the motivation of the ego vehicle of moving as fast as possible along a given path to reduce the travel time and reaching its navigation goal. Each minute of traveling is

waste of time and can be substituted to do something meaningful instead. In a way, it translates the phrase "time is money" into a mathematical expression. The vehicle obtains the ambition to move and not to stand still, which belongs to the overall motivation I_{ctrl} in case of controllable vehicles. The corresponding utility function c_{trav} for progressing quickly along the road in each predicted time interval Δt is as follows:

$$c_{\text{trav}}(\mathbf{r}_k, \mathbf{v}_k, \mathbf{I}_k) := -w_{\text{prog}}(I_k^1) \mathbf{z}(\mathbf{r}_k^1)^T \mathbf{v}_k^1 \Delta t \quad , \quad (2.4)$$

where $\mathbf{z}(\mathbf{r}^1)$ is the normalized direction of a projected point on the path belonging to the ego vehicle and $w_{\text{prog}} > 0$ is the utility specific weight. Motions with high longitudinal velocity are highly rewarded. The mean traveling utility \hat{c}_{trav} is calculated in the following way:

$$\hat{c}_{\text{trav}}(I_k^1) = \int_{\mathbb{R}^n} c_{\text{trav}}(\mathbf{r}_k, \mathbf{v}_k, \mathbf{I}_k) p(\mathbf{x}_k | \mathbf{I}_k) d\mathbf{x}_k \quad .$$

In case of straight paths/ lanes, or very low curvature along the path compared to the dimension of the normal distribution parallel to the lane, the path orientation $\mathbf{z}(\mathbf{r}_k) = \mathbf{z}(\hat{\mathbf{r}}_k) = \hat{\mathbf{z}}_k$ is assumed to be constant for all positions in state PDF $p(\mathbf{x}_k | I_k^1)$, so that the mean travel utility simplifies to :

$$\begin{aligned} \hat{c}_{\text{trav}}(I_k^1) &= -w_{\text{prog}}(I_k^1) \Delta t \hat{\mathbf{z}}_k^T \int_{\mathbb{R}^n} \mathbf{v}_k p(\mathbf{r}_k, \mathbf{v}_k | I_k^1) d\mathbf{r}_k d\mathbf{v}_k \\ &= -w_{\text{prog}}(I_k^1) \Delta t \hat{\mathbf{z}}_k^T \hat{\mathbf{v}}_k \quad . \end{aligned} \quad (2.5)$$

Costs for Violation of Traffic Rules

Traveling as fast as possible is not always desired, because increasing speed would increase over-proportionally needed driving power to hold the velocity level due to resistance forces. In addition, in most countries, there are some speed limitations set to the roads. Therefore it makes sense to punish states above a certain desired speed level v_{lim} , which are undesired.

To counteract the progressing costs according to Eq. (2.4), the velocity difference to the speed limitation has to be at least increasing linearly:

$$c_{\text{lim}}(\mathbf{r}_k, \mathbf{v}_k, \mathbf{I}_k) := \begin{cases} w_{\text{lim}}(I_k^1) (\langle \hat{\mathbf{z}}_k, \mathbf{v}_k \rangle - v_{\text{lim}}(\mathbf{r}_k)) \Delta t & \text{if } \hat{\mathbf{z}}_k^T \mathbf{v}_k > v_{\text{lim}}(\mathbf{r}_k) \\ 0 & \text{else.} \end{cases} \quad (2.6)$$

In Eq. (2.6), the cost weight has to be $w_{\text{lim}} = 2|w_{\text{prog}}|$ in case of a symmetric state PDF around their mean states to compensate the traveling utility and to create a local minimum at $\hat{\mathbf{v}}_k = v_{\text{lim}}(\hat{\mathbf{r}}_k)$.

Assuming low curvatures paths like it is was applied for the progress utility and path stable desired velocities $v_{\text{lim}}(\mathbf{r}) \approx v_{\text{lim}}(\hat{\mathbf{r}}_k) = \hat{v}_{\text{lim}}$, the integration over a Gaussian distributed state PDF $p(\mathbf{r}_k, \mathbf{v}_k | \mathbf{I}_k)$ reformulates to:

$$\hat{c}_{\text{lim}}(I_k^1) = w_{\text{lim}}(I_k^1) \Delta t \int_{\mathbb{R}^n} \sigma(\hat{\mathbf{z}}_k^T \mathbf{v}_k - \hat{v}_{\text{lim}}) (\hat{\mathbf{z}}_k^T \mathbf{v}_k - \hat{v}_{\text{lim}}) p(\mathbf{r}_k, \mathbf{v}_k | \mathbf{I}_k) d\mathbf{r}_k d\mathbf{v}_k$$

$$\stackrel{\text{A.6.3}}{=} w_{\text{lim}}(I_k^1) \Delta t \hat{\mathbf{z}}_k^T \mathbf{v}_k^t K^t . \quad (2.7)$$

For the transition from the first to the second row, a linear truncation of normal distribution was applied according to Sec. A.6.3 of the attachment, where the truncated Gaussian PDF is approximated by another Gaussian PDF, where the parameter K^t is the normalization factor and \mathbf{v}_k^t is the corresponding mean velocity for the PDF part above the speed limitation \hat{v}_{lim} .

Comfort Costs

The second type of costs focuses on the input values. The higher the input values, the more uncomfortable the travel appears to the occupants or the more energy is needed. According to other works [38, 80, 129, 173] the input accelerations are punished by a quadratic function c_{comf} with weight matrix $\mathbf{W}_u \in \mathbb{R}^{p \times p}$ for distinguishing between different comfort feeling effects depending on input channels and input channel combinations:

$$c_{\text{comf}}(\mathbf{u}_k, \mathbf{I}_k) := w_{\text{comf}}(I_k^1) \|\mathbf{W}_u \mathbf{u}_k^1\|^2 \Delta t ,$$

where w_{comf} is the intention specific comfort weight.

The mean comfort costs \hat{c}_{comf} of a Gaussian distributed, non-limited input $p(\mathbf{u}_k | I_k^1) = \mathcal{N}(\mathbf{u}_k^1; \hat{\mathbf{u}}_k, \Sigma_{u,k})$ is given by:

$$\hat{c}_{\text{comf}}(I_k^1) = w_{\text{comf}}(I_k^1) \Delta t \int_{\mathbb{R}^p} \|\mathbf{W}_u \mathbf{u}_k^1\|^2 p(\mathbf{u}_k^1 | I_k^1) d\mathbf{u}_k$$

$$= w_{\text{comf}}(I_k^1) \Delta t (\|\mathbf{W}_u \hat{\mathbf{u}}_k\|^2 + \text{Tr}(\mathbf{W}_u \Sigma_{u,k} \mathbf{W}_u^T)) \quad (2.8)$$

Other types of costs like motor energy consumption for ecological and economical considerations or traffic violations can be modeled in a similar way.

Event Costs

The event costs quantify the occurrence of an event e_k and determines how much will this event cost. The events includes collision events with other vehicles e_{COLL} or crowded entities e_{OCC} . The event probability $p(e_k|\mathbf{x}_k)$ multiplied by the related severity $c_{\text{sev}}(\mathbf{x}_k, e_k)$ results in the event risk $c_{\text{risk}}(\mathbf{x}_k, e_k)$ of a predicted state \mathbf{x}_k :

$$c_{\text{risk}}(\mathbf{x}_k, e_k) = c_{\text{sev}}(\mathbf{x}_k, e_k) p(e_k|\mathbf{x}_k) \ .$$

Like in the case of utility and comfort, it is of interest, how big the mean risk $\hat{c}_{\text{risk}}(e_k)$ of a scene state PDF is. Therefore, the mean risk is the average risk of a distributed state with PDF $p(\mathbf{x}_k)$ and is calculated as follows:

$$\hat{c}_{\text{risk}}(e_k) = \int_{\mathbb{R}^n} c_{\text{sev}}(\mathbf{x}_k, e_k) p(e_k|\mathbf{x}_k) p(\mathbf{x}_k) d\mathbf{x}_k \ .$$

In Ch. 4, the collision event probability and especially the mean risk between two vehicles is discussed in more detail by assuming a constant severity $c_{\text{sev}}(\mathbf{x}, e) = c_{\text{COLL}} = 1$. More advanced severity models are presented in Ch. 6. Other events like dynamical state restrictions e_{SR} , escape events e_{ESC} or collisions with distributed static objects e_{OCC} are outlined in Ch. 5.

Event Priorities

In many scenes, instead of one event, many different events can appear. Each one, has its own after-event-evolution and own outcome. Based on the costs, the motion planner will adapt its own action sequence in a way that the costs become minimal, which means that if the planner has to choose between two possible maneuvers, it will select the one with the lowest costs. Therefore the outcome of the events guides the vehicle to produce low costs behavior in future.

Some of the events and costs are more important than others, which should be implemented by aggregating different predicted outcomes. Consider two exemplary maneuvers: one maneuver is very comfortable with small accelerations magnitudes, but will lead to a scratch on the vehicles exterior and another maneuver where traffic laws are violated to avoid the crash with a heavy uncomfortable action sequence. In this case, it is very clear to choose the second maneuver and take the traffic penalty into account to avoid a potential crash. According to several similar comparisons

of these scenarios creates a priority list with decreasing importance for motion behaviors:

1. Avoiding severe crashes to mitigate passenger injuries
2. Avoiding any kind of critical events like crashes
3. Avoiding any violation of traffic rules like raising speed limitations
4. Making progress along a given route and avoiding uncomfortable or high energy consuming actions

This preference list starts with the most important fact of not having heavy crashes with severe outcomes for the occupants, which should be ensured through autonomous driving [143]. If the first item of the priority list is fulfilled, the second principle is obligatory, so that those trajectories are preferred which don't exhibit any critical event like crashes, scratches or touches [107]. If this is guaranteed, the traffic rules have to be considered like yielding in a minor-priority road, stopping in front of a red traffic light or keeping speed limitations. Only in case of not violating any of the above priorities, the focus is on the utility to progress and a comfortable driving style. Both will be balanced to create a satisfactorily motion behavior.

The order given by the above priority list can also be derived by an economical consideration. Crashes with long-lasting consequences like handicaps through injuries create the most economical costs and harm, whereas comfort and utility should be weighted least of all, because their economical costs are the lowest. To integrate all costs into one overall cost function, there exist two strategies:

- I. Take the costs of the state related to the highest ranked item in the priority list. This implicitly neglect all other costs of minor stages.
- II. All costs of the priority list are part of an overall cost evaluation at one scene state, but the cost weight are increasing by their priority.

Utility and comfort costs sharing the same priority stage, so they are weighted against each other by having similar weight dimensions.

As it can be seen in Fig. 2.6 on the left, in the deterministic case for one predicted time point only one item of the priority list (here: collision avoidance) can be active, so that according to the cost structure inside these regions, the states are adapted into the direction of smaller costs. In contrast to one single state at a predicted time point, the states can be distributed according to their PDF (see Fig. 2.6 on the right). Many

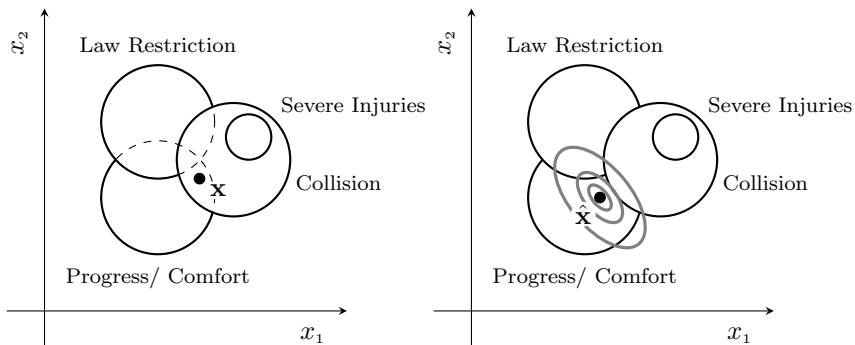


Figure 2.6: Cost hierarchy in state space. Left: A deterministic state \mathbf{x} or trajectory parameter (black dot) is inside regions of collision and utility with progress and comfort. Because the utility is lower prioritized than the collision events, the weights for the collision severity has to be much higher than the utility weight to ensure avoiding maneuvers which are not disturbed by issues of an uncomfortable driving style. Right: A distributed state with mean vector $\hat{\mathbf{x}}$ is located in the utility region, but some parts of the state PDF are laying inside the collision and law restriction region. Each PDF part contributes costs according to their region, so that the aggregated costs can consists of multiple parts. Depending on the extension of the PDF multiple components impact the evaluation, which is in contrast to the deterministic case.

regions are simultaneously active, so that the costs at one time point has many components. As a consequence, the motion planner adapts its PDF in a way that only some of the distant states with low PDF value are exposed to high cost regions. All in all, an inter-region outweigh of events determines the behavior and lead to targeted scene state evolutions which are far distinct to critical events and therefore create a cautious behavior.

The cost parts corresponding to the events or utilities within one predicted time step are aggregated for simplicity according to the II. strategy, so that the cost parts for one scene state \mathbf{x} and input \mathbf{u}^1 are summed up to one quantity $c_{\text{agg}}(\mathbf{x}, \mathbf{u}^1, I^1)$:

$$c_{\text{agg}}(\mathbf{x}, \mathbf{u}^1, I^1) = c_{\text{util}}(\mathbf{x}^1, I^1) + c_{\text{comf}}(\mathbf{u}^1, I^1) + \sum_{\mathbb{E}} c_{\text{sev}}(\mathbf{x}, e) p(e|\mathbf{x}) \quad (2.9)$$

The mean costs \hat{c}_{agg} are gained from the integration of Eq. (2.9) over all predicted scene states and inputs by weighting them with their correspond-

ing PDF values $p(\mathbf{x}_k | \mathbf{u}_{0:k-1}^1, \mathbf{x}_0)$ and $p(\mathbf{u}_k^1)$:

$$\begin{aligned} \hat{c}_{\text{agg}} = & \int_{\mathbb{R}^n} \left(\sum_{\mathbb{I}} c_{\text{util}}(\mathbf{x}^1, I^1) p(I^1, \mathbf{x}) + \sum_{\mathbb{E}} c_{\text{sev}}(\mathbf{x}, e) p(e|\mathbf{x}) p(\mathbf{x}) \right) d\mathbf{x} + \dots \\ & \dots + \sum_{\mathbb{I}} \int_{\mathbb{R}^{p_i}} c_{\text{comf}}(\mathbf{u}^1, I^1) p(I^1, \mathbf{u}^1) d\mathbf{u}^1 . \end{aligned} \quad (2.10)$$

The total costs of one strategy with an action sequence along the full time horizon $\mathbf{u}_{0:H}^1$ and all possible future scene evolutions including all events aggregates to an overall cost value $C_{\text{tot}}(\mathbf{u}_{0:H}^1, \mathbf{x}_0)$:

$$\begin{aligned} C_{\text{tot}}(\mathbf{u}_{0:H}^1, \mathbf{x}_0) = & \sum_{k=0}^H \sum_{\mathbb{I}} \int_{\mathbb{R}^{p_i}} c_{\text{comf}}(\mathbf{u}_k^1, I_k^1 = I_{\text{ctrl}}) p(\mathbf{u}_k^1, I_k^1 | \mathbf{x}_0, I_0^1, \mathbf{u}_{0:k-1}^1) d\mathbf{u}_k^1 \\ & \dots + \sum_{k=1}^H \sum_{\mathbb{I}} \int_{\mathbb{R}^n} c_{\text{util}}(\mathbf{x}_k^1, I_k^1) p(I_k^1, \mathbf{x}_k | \mathbf{x}_0, I_0^1, \mathbf{u}_{0:k-1}^1) d\mathbf{x}_k + \dots \\ & \dots + \sum_{k=1}^H \sum_{\mathbb{I}} \sum_{\mathbb{E}} \int_{\mathbb{R}^n} c_{\text{sev}}(\mathbf{x}_k, e_k) p(e_k | \mathbf{x}_k) p(\mathbf{x}_k | \mathbf{x}_0, I_0^1, \mathbf{u}_{0:k-1}^1) d\mathbf{x}_k . \end{aligned} \quad (2.11)$$

Because of the summation in Eq. (2.10), the integrals over each cost type can be considered separately.

The event priority fuses warnings for multiple and different risk sources as well as uncomfortable transitions and progress utility into one predicted measure. For very low risk critical event probabilities, the associated costs for critical events are balanced with the utility and comfort term. In case of high critical event probabilities the critical event costs are much higher than the rest and dominates the cost evaluation.

2.4.5 Decision Model

The obtained overall costs of the whole scene evolution guides the planner to choose the next executable action to handle the traffic situation sufficiently and navigate through the cost potential field. This cost measure consists of a separate evaluation of utility $c_{\text{util}}(\mathbf{x}^1, I^1)$ like progressing, maximum velocities, comfort $c_{\text{comf}}(\mathbf{u}^1, I^1)$ and event risk $c_{\text{sev}}(\mathbf{x}, e) \cdot p(e|\mathbf{x})$ including collisions and other state restrictions. The choice of one final

strategy according to this measure is the last step of the behavior planner, where the first action of the strategy is executed.

To guarantee safety, collision events should outweigh other events and utilities like mentioned in the previous section. But there is another consideration regarding the time horizon. In [59], the author states that the time horizon $H \rightarrow \infty$ has to be infinite to not oversee events which are far in the future but could not avoid crashes because of their slow internal dynamics. In the work of [5] the time horizon is set to a maximum limit, where in the last time step of the time horizon is calculated, how likely the vehicle is within an inevitable collision state. Many works for motion planning [36, 46, 79, 80, 85, 131] only consider a fixed time horizon to avoid non-converging integrals, with a time horizon that is high enough to forecast early any potential conflicts and let all traffic participants being stopped. In [129], the authors use a decreasing exponential function to weight costs caused earlier in time higher than those later in time by introducing an escape rate, so that far events are considered but not neglected. This approach shows safe behavior with a smooth importance increase of predicted events, so that this concept is also followed in this thesis. The related escape event e_{ESC} is discussed in Ch. 5.

As aforementioned, the total costs of Eq. (2.11) evaluate the predicted scene depending on the ego vehicle's maneuver $\mathbf{u}_{0:H}$ and the current scene state \mathbf{x}_0 . The minimal predicted mean trajectory costs take the uncertain measured state of the initial time point $k = 0$ into account, which is represented by the scene state PDF $p(\mathbf{x}_0)$. The overall strategy is minimizing the mean costs, which is mathematically expressed by:

$$\mathbf{u}_{0:T}^* = \underset{\mathbf{u}_{0:T} \in \mathbb{U}}{\operatorname{argmin}} \int_{\mathbb{R}^n} C_{\text{tot}}(\mathbf{u}_{0:H}^1, \mathbf{x}_0) p(\mathbf{x}_0) d\mathbf{x}_0 \quad (2.12)$$

$$\mathbf{u}_k^1 \in \mathbb{U} \quad \forall k \in \{0, \dots, H\} .$$

In this work, the focus is on the collision probability calculation and severity design. That's why a simple planner is implemented, which does not have the high complexity of a multidimensional optimization, but is forced to reduce the predicted costs as much as possible. The idea is to find one robust speed level which the ego vehicle should be able to keep in future time points. For this, only the first action or acceleration value \mathbf{u}_0 is taken as a variable and the rest of the trajectory $\mathbf{u}_1^1, \dots, \mathbf{u}_H^1$ has constant zero acceleration to simulate constant speed in future (see Fig. 2.7). Therefore the optimization process in Eq. (2.12) is simplified to

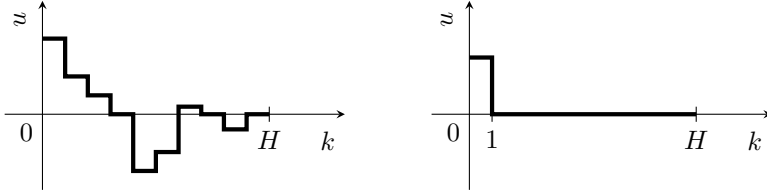


Figure 2.7: Planned input curves depending on predicted time steps with maximum time step horizon H (left) and a simplified optimization based on varying only the constant input value(s) of the first time interval (right).

the following expression:

$$\mathbf{u}_0^* = \underset{\mathbf{u}_0^1 \in \mathbb{U}}{\operatorname{argmin}} \int_{\mathbb{R}^n} C_{\text{tot}}(\mathbf{x}_0, \mathbf{u}_0^1) p(\mathbf{x}_0) \ . \quad (2.13)$$

The authors of [129] show that in some scenarios like merging into a dense traffic priority road a more complex planner with concatenated ramps should be used. So the underlying assumption is that events producing effects on a simple planner would also influence more complex planners which also can handle more complex situations but showing the same qualitative phenomena. For later simulations, this simplification of minimizing the degree of freedom to one shows sufficient behavior.

2.5 Conclusion

In this chapter, the following contributions for the risk-based motion planner are achieved:

- A novel prediction process for uncertain sensor measurements and motion prediction which includes explicitly different types of events and event-caused intention changes for a detailed representation of future traffic scene evolutions.
- An evaluation method based on prioritizing behavior strategies like mitigation, collision avoidance and in-between strategies depending on cost components like risk, utility and comfort.
- A simplified cost-based decision model based on a constant velocity prediction with first-time-step acceleration ramp for investigating behaviors of different event types.

The next chapter formulates a general framework for prediction and cost evaluation based on the presented risk-based motion planner. The so called Survival Theory provides a scheme for incorporating easily different event types and handling multiple events which take place at the same predicted time point. Furthermore, the risk-based motion planner with its prediction, evaluation and decision model is used to investigate the impact of the collision severity (described in Ch. 6) on the driving behavior, outlined in Ch. 7.

3 Survival Theory

In the previous chapter (Ch. 2), the behavior planning framework with three main components was introduced. Except of the decision model which takes the solutions of the prediction and evaluation model, the components were outlined in a very general way. In this chapter, the target is to reduce the complexity of the prediction and evaluation process by systematically calculating intermediate variables along the prediction time to determine the mean total cost value for one predicted trajectory.

The calculation of the optimal action depends on the current scene and on the variety of possible scene evolutions. These multiple evolution alternatives have the following multiple reasons. Firstly, possible events and their associated changes of driver intentions drastically influence the scene evolution. Next to that, the uncertain environment perception leads to a distributed initial state, so that different starting points of scene evolutions have to be assumed. Last but not least, the prediction itself is noisy through the uncertain behavior or input choice of other traffic participants, known as driving style (see Fig. 3.1). To calculate and evaluate all alternatives a high amount of scene evolutions has to be determined, so that a lot of computational effort is needed for simulations like memory occupation or calculation time. Some of these evolutions branch out from single shared states through time, so that they can be represented by a tree with scene states as nodes and uncertain, probabilistic transitions as edges. One can imagine, that with predicted time, the size of this tree would increase exponentially.

To overcome these drawback of tree expansion, several questions have to be answered:

1. How can this expanding tree be reduced? Which branches can be combined, truncated or neglected?
2. How can the events along the predicted time points be evaluated? What happens if multiple events occur?

The following sections starts by presenting the related work already done to tackle this drawback. Subsequently, the concept of survival theory

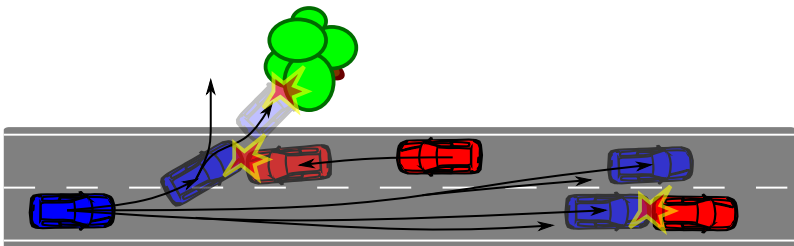


Figure 3.1: Six different scene evolutions (black arcs) on a country road for an ego vehicle (blue). Two scenarios end up in a crash with another vehicle (red cars), where one crash is followed by another collision with a tree. In another scenario a crash is successfully avoided by either braking down to zero velocity or steering to the left.

is introduced and the approach is extended including the derivation of important quantities to determine the overall maneuver costs. The concept can also handle multiple events at the same time (Sec. 3.5) and is also formulated to a time-continuous consideration based on rates (Sec. 3.6).

3.1 Related Work

In the literature, the prediction process is treated diversely. They couple or decouple the event detection and evaluation with or from each other, so that intentions and states depending on events would change or not. First, consider the case, where the motion prediction is given by a conditional relationship according to $p(\mathbf{x}_{k+1}|\mathbf{x}_k, \mathbf{u}_k, \mathbf{e}_k) = p(\mathbf{x}_{k+1}|\mathbf{x}_{k+1}, \mathbf{u}_k, \mathbf{e}_k = e_{\text{NON}})$, where the events do not interrupt the state transition process. After the state prediction process is completed, the event detection $p(\mathbf{e}_k|\mathbf{x}_k)$ is only needed for evaluating the trajectory costs. The occurred events itself do not change the intentions or states. This can lead to multiple detections and evaluations of the same event type which is producing subsequent collisions with the same traffic participant j . To overcome this and not overestimate the collision probability, only the **maximum** event probability over the whole prediction horizon is taken as representative costs [46, 77, 83, 95, 99, 121, 154, 171]. This approach for determining event probabilities is fast to evaluate and is a good approximation in cases, where uncertainties are small. But for highly distributed states, single events will be detected over a long period of time, where in each time point the

event probability is very small. Taking only the maximum costs of the corresponding single predicted time point underestimates drastically the collision probability, because all the other time points before and after this time point of maximum costs are neglected.

A second method, which separates the prediction and evaluation process, is the assumption of having independent events over the prediction time process. Instead of using the maximum, a survival probability is formulated, which reduces the probability of events further in time by the probabilities of previous time points, so that an aggregation over all predicted time points is possible. So each event along the scene prediction is part of the overall costs. This approach is followed by [20] with its inevitable collision state probability calculation and in the event rate approach from [45, 129]. Other work assumes that the events cannot happen a second time, the probabilities over all time points are simply summed up [26, 136, 173]. Commonly, the assumption of independent events over time does not hold, because of events that can hinder or raise another event in later time points. In general, it leads to many overestimations and misinterpretations e.g. in static traffic scenes with high sensor noise, where the same collision is counted more than once over the prediction time. In contrast, the flux calculation of [125] can exactly calculate the collision probability in an analytic way, but does not consider severity or other events. In [80], an heuristic mixture of maximum risk and summed incremental risk was calculated. The potential field-based planners of [131, 173] use a sum over quadratic risk for guiding the planner to safe behavior.

Approaches, which are assumed to be the most accurate, couple the prediction process and the event occurrence with the **conditional** motion model $p(\mathbf{x}_{k+1}|\mathbf{x}_k, \mathbf{u}_k, \mathbf{e}_k)$. To solve the complex prediction process of these interacting variables, mostly Monte Carlo Simulation (MCS) techniques are used [28, 33, 49, 58, 141], at least for evaluating other calculation methods. In a Monte Carlo Simulation, a high amount of sampled trajectories from the initial state probability density function (PDF) is propagated into the future and checked for collision events, that's why it makes the stochastic numerical integration method very time-consuming. Some works [21–23] approximate the Monte Carlo Simulation output by using an Unscented Transformation, which reduces the calculation time by a factor of 1000 with 2% mean accuracy. The drawback is that it does not provide event state distributions so that state dependent severities cannot be calculated. Furthermore other event types cannot be included. Another method is to remove already collided parts during the prediction process by e.g. truncating analytically Gaussian PDF's [122] or by executing a

state space discretization for a Markov chain calculation [7, 8]. In [7], the discretization for satisfying real-time applicability is $2.5 m$ for longitudinal and $0.5 m$ for lateral direction, which is very large, when it comes to moderate probability scenarios. But these discretization approaches do not integrate the impact of events on the state changes. In the work of [122] with an analytic Gaussian PDF truncation, an accuracy of around 5% can be achieved, if the state space for non collided states stays quasi-convex in each predicted time point, which unfortunately does not hold for small objects and very enlarged state PDF's. A virtual removal of already collided PDF parts is presented in [133], where enlarging circles are predicted and circle regions are marked depending on the fact whether the region was already collided in previous predicted time points or are now non-reachable. The area of these regions is considered in the final collision probability calculation. An aggregation of state space regions over an infinitive time horizon is implemented in [119] and [3] where the total collision probability of linear relative motions and Gaussian PDF is calculated, but without considering enlarging or changing PDF distributions. In [100], a technique for motions approximated by fifth order polynomials is introduced, which needs only algebraic checks so that a Monte Carlo Simulation can be speed up. The drawback is that it cannot consider other event types.

A similar categorization like the connection between prediction and evaluation can be done for different event types, risk sources or vehicles respectively. A first class treats each event prediction over the complete time horizon separately and takes the maximum probability of all events [36, 102, 121]. A second class considers approaches which assume that two events cannot happen at the same time, so that the probabilities can easily be summed up [25, 28, 80, 80, 136, 171, 173]. In the third class, each event is treated independently, so that the order of events occurrence does not matter. Here, the total collision probability is equal to the counter probability of the survival probability of each subsequently executed collision event [5, 6, 20, 45, 96]. The last class explicitly considers shared state spaces of multiple different events and can predict those PDF parts which are not part of any event [7, 8, 23, 33, 122, 141].

The last difference in frameworks used in the literature is about the number of different risk sources. E.g. in [22, 125] the authors describe very fast calculation methods but can only handle one collision with another object, whereas [23, 26, 141] can take multiple static or dynamic objects into account. Different event types like losing control in curves and collisions are handled in one overall framework in [45, 129].

Until here, there is no fast calculating method for trajectory predic-

tion, which can treat different event types over time with their conditional dependencies as well as the possibility to calculate the severity for an expected outcome. Based on the scheme in [129], a more detailed calculation is introduced.

3.2 Problem Statement

The target of this chapter is to create a calculation scheme for risk, utility and comfort evaluations based on the event-intention planning framework of the previous chapter. For this, the following properties have to be fulfilled:

- Simple integration of time-discrete motion models which consider uncertainties in sensor measurement and behavior.
- Simple incorporation of different event types and cost parts according to a fixed modeling scheme.
- The time dependency in the prediction process, where states and events impacts the scene evolution.
- An explicit representation of states and times when events happen to determine state-dependent severities and other costs.
- A calculation of probabilities for multiple events happening within the same time interval **and** in the same state.

Considering all these items makes the framework adaptable to various scenarios with different traffic participants, law restrictions and cost types.

3.3 Approach

To drastically reduce the expanding tree of scene evolutions or to avoid a full Monte Carlo Simulation with scenes as particles, the idea is to find representative state PDF's in each predicted time point which share the same event or intention history. So each PDF distinguishes from the others by having a different event or intention history. The noisy states provided by the uncertain sensor measurements and the uncertain behavior are fused to one parametrized distribution like a Gaussian PDF or one representative mean state. So the prediction tree would only create new branches if an event is happening.

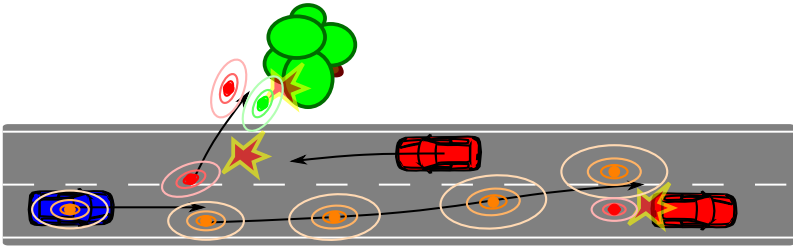


Figure 3.2: Traffic scene of Fig. 3.1 simplified by the survival theory consideration, concatenating all predicted probability density function with equal event history: controlled intention where no event is happening (orange), uncontrolled braking after crashing into one vehicle (red), second crash after first crash (green).

A further consideration (and this is where the name of this chapter comes from) is to focus only on states, which are not involved in any critical event until the predicted time point or in other words “have survived”. In these survived states, the autonomous vehicle is still having full control, so the intention is equal to I_{ctrl} . In contrast, scene evolutions, where the behavior of the ego vehicle will change, are reduced into simple predefined representative motion patterns like deceleration with maximum braking force after a crash according to $I_{nonctrl}$. Depending on the state, when the critical event was happened, these non-changeable, non-survived motion patterns produce specific costs until the end of the scene evolution, when I_{safe} will appear. The differentiation between manipulatable survived states with I_{ctrl} and state PDF parts involved in an event at predicted time points is the core consideration of the survival theory and bases mainly on the idea of [45]. According to that, costs of all future evolutions in Eq. (2.13) can be imagined as costs along one survived scenario prediction, see Fig. 3.2.

In the following sections, terms and quantities are introduced to present this idea of simplifying the framework of Ch. 2 in a structured way.

3.4 Quantities of Survival Theory

The survival theory needs a small number of quantities to describe the calculation process in a comprehensive way. First of all, a distinction of the state PDF with its shape according to its parametrization and the magnitude of quantities like event probability has to be formulated in an

explicit manner. The PDF shape will clearly impact events happening at later predicted time points and so it has to be accurate to depict the prediction process well enough. In contrast, the magnitudes for event probabilities, utilities and others are needed for the cost calculation and therefore for the assessment of the predicted scene evolutions, but won't influence the prediction of the states or events themselves.

The second principle for specifying quantities is related to the time-scale belonging to the magnitudes, e.g. an event and its probability at one predicted time step can either be seen at the current predicted time point k or from the point of view of the initial time point t , the starting time of the prediction. The first one is an **instantaneous** view (inst.) on a specific predicted time point k whereas the second view takes also the event probabilities of earlier predicted time points between the time point t and k into account. That's why it is called **time-course sensitive** view (tcs). So time-course sensitive quantities are mostly smaller than instantaneous probabilities, because other events in earlier predicted time points interfere the state PDF predictions and reduce the probability of reaching the specific predicted point in time k . The one factor separating both quantities from each other, the instantaneous and time-course sensitive view, is the survival probability, which expresses the likelihood of not being engaged in any event before.

The last category regarding the time evolution are the **total** quantities, which aggregate all time step related values over the full predicted time horizon H to one representative value e.g. total costs for a full scene evolution. Example curves for all quantities are presented in Fig. 3.3.

In the following sections, the quantities, categorized as aforementioned, are defined and the relations between them are shown to obtain a straightforward calculation of the overall scene costs.

3.4.1 Event vs. Event-Free

The focus of the survival theory is mainly on the survived trajectories or in non-deterministic case survived scene state PDF evolution. In case of only one possible event e in a scenario, a state distribution $p(\mathbf{x})$ can be marginalized over the hidden variable according to the discrete version of Eq. (A.11) so that an event-involved $p(\mathbf{x}|e)$ and an event-free distribution part $p(\mathbf{x}|e_{\text{NON}})$ is created:

$$\begin{aligned} p(\mathbf{x}) &= p(\mathbf{x}, e_{\text{NON}}) + p(\mathbf{x}, e) \\ &= p(\mathbf{x}|e_{\text{NON}})p(e_{\text{NON}}) + p(\mathbf{x}|e)p(e) \quad . \end{aligned} \tag{3.1}$$

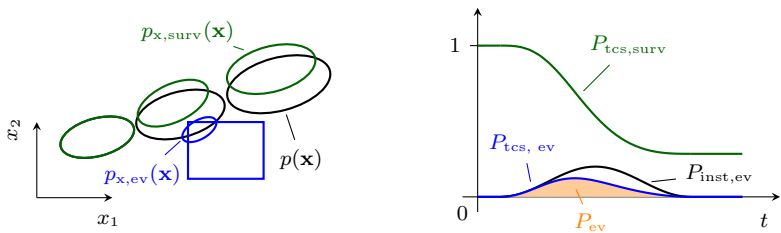


Figure 3.3: Time-course sensitive prediction model with magnitude and PDF shape adaptation over predicted time. Left: Gaussian PDF propagation with shape adaptation (green) through a rectangular obstacle (blue) and without time-course sensitivity (black). The blue ellipse represents the collided state PDF. Right: The corresponding total event probability calculation with a given instantaneous collision event probability curve (black), time-course sensitive survival probability (green), time-course sensitive event probability (blue) and total event probability (orange).

The scalar factors $p(e)$ and $p(e_{\text{NON}})$ are the event probability and the event-free or survival probability, respectively. Here, one can see that these magnitudes are also separated from the state distributions. This is the main extension to the survival theory originally formulated in [45], where only the magnitude was explicitly described.

Given an event detection model for one event $p(e|\mathbf{x})$, similarly to the event detection model for multiple events introduced in Ch. 2, its counter probability $p(e_{\text{NON}}|\mathbf{x}) = 1 - p(e|\mathbf{x})$ and a state PDF $p(\mathbf{x})$, one can calculate the quantities by marginalizing over the hidden variables and reformulating according to the Bayesian theorem outlined in Eq. (A.13):

$$\begin{aligned}
 p(e) &= \int_{\mathbb{R}^n} p(e|\mathbf{x}) p(\mathbf{x}) d\mathbf{x} & (3.2) \\
 p(e_{\text{NON}}) &= \int_{\mathbb{R}^n} p(e_{\text{NON}}|\mathbf{x}) p(\mathbf{x}) d\mathbf{x} = 1 - p(e) \\
 p(\mathbf{x}|e) &= \frac{p(e|\mathbf{x}) p(\mathbf{x})}{p(e)} \\
 p(\mathbf{x}|e_{\text{NON}}) &= \frac{(1 - p(e|\mathbf{x})) p(\mathbf{x})}{p(e_{\text{NON}})} .
 \end{aligned}$$

Note, that the PDF's $p(\mathbf{x})$, $p(\mathbf{x}|e)$ and $p(\mathbf{x}|e_{\text{NON}})$ are normalized, so that their integration over scene state \mathbf{x} equals one.

The equation set of (3.2) shows that the event detection model $p(e|\mathbf{x})$ plays an important role in determining event-engaged and event-free PDF's and its corresponding probabilities.

Event-Depending Intentions

The intention transition model is depending on the last intention I_{k-1} and the current event e_k . If no event $e_k = e_{\text{NON}}$ happens at predicted time step k , the intentions of each vehicle keep unchanged:

$$p(I_k|e_k = e_{\text{NON}}, I_{k-1}) = \delta(I_k - I_{k-1}) \quad , \quad (3.3)$$

where the starting distribution for each traffic participant assumed to be $p(I_0) = \delta(I_{\text{ctrl}})$. Therefore, as long as no event happens all vehicles drive in a controlled way. Next to this, there exist also events, which do not change intentions like the state restriction event e_{SR} introduced in Ch. 5. For them, a similar transition holds like in Eq. (3.3). If once the intention is changed to I_{nonctrl} or I_{safe} due to events, the intention of the autonomous vehicle cannot switch back to the controlled intention I_{ctrl} or in case of I_{safe} to I_{nonctrl} . The intention I_{ctrl} is a substitute for scene evolutions without any critical events, which is similar to the event-free formulation in [45]. The advantage of controlled-intention-based scene evolution compared to event-free is that events without change of intentions are part of the main prediction path of collision-free events.

Instantaneous Event and Survival Probabilities

Now, consider a state distribution at one specific predicted time point k . To reach a time point in a controlled way, all previous time points have to be considered. But instead of identifying any combination of events which won't change the drivers intention in time point k , the definition of the instantaneous event and survival probability are directly dependent on the controlled intention I_{ctrl} in the previous time point $k-1$:

$$\begin{aligned} P_{\text{inst, ev, } k} &:= p(e_k | I_{k-1} = I_{\text{ctrl}}) \\ &= \int_{\mathbb{R}^n} p(e_k | \mathbf{x}_k) p(\mathbf{x}_k | I_{k-1} = I_{\text{ctrl}}) d\mathbf{x}_k \end{aligned} \quad (3.4)$$

$$\begin{aligned} p_{\mathbf{x}, \text{ ev, } k}(\mathbf{x}_k) &:= p(\mathbf{x}_k | e_k, I_{k-1} = I_{\text{ctrl}}) \\ &= \frac{p(e_k | \mathbf{x}_k) p(\mathbf{x}_k | I_{k-1} = I_{\text{ctrl}})}{p(e_k | I_{k-1} = I_{\text{ctrl}})} \quad , \end{aligned} \quad (3.5)$$

where $P_{\text{inst, ev}, k}$ is the **instantaneous event probability** and $p_{\text{x, ev}, k}(\mathbf{x}_k)$ is the **event-engaged state PDF**.

The **instantaneous survival probability** $P_{\text{inst, surv}, k}$ and the **survived state PDF** $p_{\text{x, surv}, k}(\mathbf{x}_k)$ of the current predicted time point k is defined as follows:

$$\begin{aligned}
 P_{\text{inst, surv}, k} &:= p(I_k = I_{\text{ctrl}} | I_{k-1} = I_{\text{ctrl}}) \\
 &= \sum_{\mathbb{E}} \int_{\mathbb{R}^n} p(I_k = I_{\text{ctrl}} | e_k, I_{k-1} = I_{\text{ctrl}}) p(e_k | \mathbf{x}_k) \cdots \\
 &\quad \cdots p(\mathbf{x}_k | I_{k-1} = I_{\text{ctrl}}) d\mathbf{x}_k \\
 p_{\text{x, surv}, k}(\mathbf{x}_k) &:= p(\mathbf{x}_k | I_k = I_{\text{ctrl}}) \\
 &= \sum_{\mathbb{E}} \frac{p(I_k = I_{\text{ctrl}} | e_k, I_{k-1} = I_{\text{ctrl}}) p(e_k | \mathbf{x}_k) p(\mathbf{x}_k | I_{k-1} = I_{\text{ctrl}})}{p(I_k = I_{\text{ctrl}} | I_{k-1} = I_{\text{ctrl}})} .
 \end{aligned}$$

Instantaneous Utility and Comfort

The evaluation of utility and comfort helps to create trajectories which let the ego vehicle progress smoothly with small jerks. Both cost components are only being assessed for scene trajectories not involved in any crash or other critical events. Considering these scene evolutions $p_{\text{x, surv}, k}(\mathbf{x}_k)$ which are controllable at only one predicted time point k , the **instantaneous mean utility** $\hat{c}_{\text{util}, k}$ is calculated by integration of costs over the survived scene states at the current predicted time point k :

$$\hat{c}_{\text{util}, k} = \int_{\mathbb{R}^n} c_{\text{util}}(\mathbf{x}_k^1, I_k^1 = I_{\text{ctrl}}) p_{\text{x, surv}, k}(\mathbf{x}_k) d\mathbf{x}_k . \quad (3.6)$$

The instantaneous mean comfort $\hat{c}_{\text{comf}, k}$ is calculated depending on the applied input for controlled intentions according to:

$$\hat{c}_{\text{comf}, k} = \int_{\mathbb{R}^P} c_{\text{comf}}(\mathbf{u}_k^1, I_k^1 = I_{\text{ctrl}}) p(\mathbf{u}_k^1 | I_k = I_{\text{ctrl}}) d\mathbf{u}_k . \quad (3.7)$$

Here, the equations (2.5), (2.7) and (2.8) derived in the previous chapter can be applied in case of Gaussian PDF states and PDF inputs.

Instantaneous Risk

To calculate the mean instantaneous costs of a scene prediction starting with an event includes two parts. First, there are costs produced by the event e_k itself like uncomfortable accelerations through crashes or injuries of participants to name only two. The other cost part is the aggregation of all predicted costs after the event e_k was happened. Therefore, subsequent crashes can be taken into account e.g. damage costs of a second crash into boundaries after a first crash has happened or a friction loss in curve. Both parts are represented in the **instantaneous mean risk** $\hat{c}_{\text{risk},k}$:

$$\begin{aligned} \hat{c}_{\text{risk},k}(e_k) &= \int_{\mathbb{R}^n} c_{\text{sev}}(\mathbf{x}_k, e_k) p(e_k|\mathbf{x}_k) p(\mathbf{x}_k|I_{k-1} = I_{\text{ctrl}}) d\mathbf{x}_k + \dots & (3.8) \\ &\dots + \int_{\mathbb{R}^n} \int_{\mathbb{R}^p} C_{\text{tot}}(\mathbf{x}_{k+1}, \mathbf{I}_{k+1}) p(\mathbf{I}_{k+1}|e_k, I_k) p(\mathbf{x}_{k+1}|\mathbf{x}_k, \mathbf{u}_k, e_k) \cdot \dots \\ &\dots \cdot p(\mathbf{e}_k|\mathbf{x}_k) p(\mathbf{x}_k|I_{k-1} = I_{\text{ctrl}}) d\mathbf{u}_k d\mathbf{x}_k \ . \end{aligned}$$

The first term on the right side of this equation describes the current costs through that event e_k and the second term in the last two rows represent the predicted costs after a specific event has happened. Note, that the last term is dependent on the previous planned actions $\mathbf{u}_{0:k}$, but independent on the further planned actions $\mathbf{u}_{k+1:H}$, because the behavior has changed after the event according to \mathbf{I}_{k+1} to either I_{nonctrl} or I_{safe} . The total costs $C_{\text{tot}}(\mathbf{x}_{k+1}, \mathbf{I}_{k+1})$ include the prediction and evaluation process starting in the next predicted time step $k+1$. To get into the new scene states \mathbf{x}_{k+1} , the transition model $p(\mathbf{x}_{k+1}|\mathbf{x}_k, \mathbf{u}_k, e_k)$ for all event-engaged states has to be used.

However, if a predefined behavior according to the new intention \mathbf{I}_{k+1} is assumed, an extended severity function $c_{\text{sev,ext}}(\mathbf{x}_k, e_k)$ will replace the sum of the current event costs $c_{\text{sev}}(\mathbf{x}_k, e_k)$ and the after-event consequences depending on the considered state \mathbf{x}_k . In other words, the total costs of the after-event scene evolution are projected into the severity of the predicted time k when the first event e_k was happened. According to Bayesian theorems of Eq. (A.13), Eq. (3.8) is reformulated with the definitions of event engaged state PDF $p_{\text{x,ev},k}(\mathbf{x}_k)$ and the instantaneous event

probability $P_{\text{inst, ev, } k}$:

$$\hat{c}_{\text{risk, } k}(e_k) = \int_{\mathbb{R}^n} c_{\text{sev, ext}}(\mathbf{x}_k, e_k) p_{\text{x, ev, } k}(\mathbf{x}_k) d\mathbf{x}_k \cdot P_{\text{inst, ev, } k} \quad , \quad (3.9)$$

where the extended severity function $c_{\text{sev, ext}}(\mathbf{x}_k, e_k)$ is expressed by using the definitions of the Bayesian network for prediction of \mathbf{x}_{k+1} and \mathbf{I}_{k+1} and marginalize over the hidden action \mathbf{u}_k :

$$\begin{aligned} c_{\text{sev, ext}}(\mathbf{x}_k, e_k) &= c_{\text{sev}}(\mathbf{x}_k, e_k) + \dots \\ &\dots + \int_{\mathbb{R}^p} C_{\text{tot}}(\mathbf{x}_{k+1}, \mathbf{I}_e) p(\mathbf{I}_{k+1} | e_k, I_k) p(\mathbf{x}_{k+1} | \mathbf{x}_k, \mathbf{u}_k, \mathbf{e}_k) d\mathbf{u}_k \quad . \end{aligned} \quad (3.10)$$

Furthermore it is possible to split the mean risk $\hat{c}_{\text{risk, } k}$ of Eq. (3.9) into a two factor product of mean severity $\hat{c}_{\text{sev, ext}}(e_k)$ and the event probability $P_{\text{inst, ev, } k}$:

$$\hat{c}_{\text{risk}}(e_k) = \hat{c}_{\text{sev, ext}}(e_k) \cdot P_{\text{inst, ev, } k} \quad , \quad (3.11)$$

where the mean severity $\hat{c}_{\text{sev, ext}}(e_k)$ is given by:

$$\hat{c}_{\text{sev, ext}}(e_k) = \int_{\mathbb{R}^n} c_{\text{sev, ext}}(\mathbf{x}_k, e_k) p_{\text{x, ev, } k}(\mathbf{x}_k) d\mathbf{x}_k \quad . \quad (3.12)$$

In Ch. 6, several severity functions $\hat{c}_{\text{sev, ext}}(e_k)$ with and without predictive cost term are presented and investigated.

3.4.2 Time-Course Sensitivity

The term ‘‘time-course sensitivity’’ means that the survival probability and the survived state PDF are adapted over the predicted time. Depending on previous predicted events, the magnitude of the survival probability is reduced and the state PDF shape has shrunk according to the distribution parts engaged in events. Given the instantaneous adaptations of the state PDF of Eq. (3.5) and the instantaneous survival probability according to Eq. (3.4), the transition into the next time point $k+1$ has to be determined and is outlined in the following.

Propagation of Survived State Probability Density Function

The event-free state PDF's $p_{\mathbf{x},\text{surv},k}(\mathbf{x}_k)$ and $p(\mathbf{x}_{k+1}|\neg\mathbf{e}_{0:k})$ in case of one type of event can also be written into a two-step recursive manner. The first step is the calculation of the survived state PDF after applying the event in the current time step k :

$$p_{\mathbf{x},\text{surv},k}(\mathbf{x}_k) = \sum_{\mathbb{E}} \frac{p(I_k = I_{\text{ctrl}}|e_k, I_{k-1} = I_{\text{ctrl}})p(e_k|\mathbf{x}_k)}{P_{\text{inst},\text{surv},k}} p(\mathbf{x}_k|I_{k-1} = I_{\text{ctrl}}) .$$

The second step is the transition of the survived state PDF $p_{\mathbf{x},\text{surv},k}(\mathbf{x}_k)$ into the next time step $k + 1$, so that the events at the new time step can be applied:

$$\begin{aligned} p(\mathbf{x}_{k+1}|I_k = I_{\text{ctrl}}) &= \dots \\ &= \int_{\mathbb{R}^n} \int_{\mathbb{R}^p} p(\mathbf{x}_{k+1}|\mathbf{x}_k, \mathbf{u}_k, e_k = e_{\text{NON}}) p(\mathbf{u}_k|I_k = I_{\text{ctrl}}) p_{\mathbf{x},\text{surv},k}(\mathbf{x}_k) d\mathbf{u}_k d\mathbf{x}_k . \end{aligned} \quad (3.13)$$

Starting with the initial state PDF at the current time point $k = 0$ with $p(\mathbf{x}_0|I_{-1}) = p(\mathbf{x}_0)$, the two-step recursive algorithm can be executed. In case of a Gaussian Mixture state PDF, the transition model $p(\mathbf{x}_{k+1}|\mathbf{x}_k, \mathbf{u}_k, e_k = e_{\text{NON}})$ is implemented using the linear model in Frenet space according to Eq. (2.3). The actions \mathbf{u} of the behavior model $p(\mathbf{u}_k|\mathbf{x}_k, I_k = I_{\text{ctrl}})$ are chosen based on the spatial intentions and are zero for a constant velocity prediction.

Propagation of Survival Probability

The **time-course sensitive survival probability** $P_{\text{tcs},\text{surv},k}$ is the probability of reaching the predicted time point without any engagement into an event and is defined as the probability to be in a controlled mode I_{ctrl} at a predicted time point k from the perspective of the actual time point $k = 0$:

$$P_{\text{tcs},\text{surv},k} := p(I_k = I_{\text{ctrl}}) .$$

For the recursive formulation, the definition of the instantaneous sur-

vival probability $P_{\text{inst,surv},k}$ and the Markov chain property are used:

$$\begin{aligned}
 P_{\text{tcs,surv},k+1} &= p(I_{k+1} = I_{\text{ctrl}}) = \prod_{h=0}^{k+1} p(I_h = I_{\text{ctrl}} | I_{h-1} = I_{\text{ctrl}}) \\
 &= p(I_{k+1} = I_{\text{ctrl}} | I_k = I_{\text{ctrl}}) \prod_{h=0}^k p(I_h = I_{\text{ctrl}} | I_{h-1} = I_{\text{ctrl}}) \\
 &= P_{\text{inst,surv},k+1} \cdot P_{\text{tcs,surv},k} \quad , \quad (3.14)
 \end{aligned}$$

where the pre-initial time-course sensitive survival probability $P_{\text{tcs,surv},-1} = 1$. With $P_{\text{inst,surv},k} \in [0, 1]$, one can see that the time-course sensitive survival probability is monotonically decreasing over the predicted time and will be zero for all predicted time points $h > k$ if $P_{\text{inst,surv},k} = 0$.

Time-Course Sensitive Event Probability

The **time-course sensitive event probability** $P_{\text{tcs, ev},k}$ is defined in a similar way as the time-course sensitive survival probability $P_{\text{tcs,surv},k}$:

$$\begin{aligned}
 P_{\text{tcs, ev},k+1} &:= p(e_{k+1}, I_k = I_{\text{ctrl}}) \\
 &= \underbrace{p(e_{k+1} | I_k = I_{\text{ctrl}})} \cdot \underbrace{p(I_k = I_{\text{ctrl}})} \\
 &= P_{\text{inst,ev},k+1} \quad \cdot \quad P_{\text{tcs,surv},k} \quad . \quad (3.15)
 \end{aligned}$$

According to Eq. (3.15), the instantaneous event probability $P_{\text{inst,ev},k}$ is reduced by the time-course sensitive survival probability, which includes the probabilities of not being engaged in any event before. Therefore the time-course sensitive event probability $P_{\text{tcs,surv},k}$ represents the “true” predicted event likelihood in the view of the initial time point $k = 0$ by considering all predicted events until $k \neq 0$. Without the time-course sensitive survival probability, the event probability will always be systematically overestimated.

Time-Course Sensitive Costs

The example of the time-course sensitive event probability shows that the true predicted event likelihoods are decreased by the time-course sensitive survival probability of the predicted time point k . This principle holds also for instantaneous mean costs quantities like utility (see Eq. (3.6)), comfort

(see Eq. (3.7)) and risk costs (see Eq. (3.11)). Thus, the true cost portion to the total scene evolution costs is given by the following equations:

$$\begin{aligned}\hat{c}_{\text{tcs,util},k+1} &:= \hat{c}_{\text{util},k+1} \cdot P_{\text{tcs,surv},k} \\ \hat{c}_{\text{tcs,conf},k+1} &:= \hat{c}_{\text{conf},k+1} \cdot P_{\text{tcs,surv},k} \\ \hat{c}_{\text{tsc,risk},k+1}(e_k) &:= \hat{c}_{\text{risk},k+1}(e_k) \cdot P_{\text{tcs,surv},k} \quad .\end{aligned}\tag{3.16}$$

Eq.'s (3.16) show that time-course sensitive quantities can be calculated for all costs along the survived scene evolution, only by taking the corresponding instantaneous costs and multiplying them by the time-course sensitive survival probability $P_{\text{tcs,surv},k}$.

3.4.3 Total Scene Prediction Measures

The costs and probabilities in each time point, no matter if there are modulated by the time-course sensitive survival probability or not, do not describe a whole scene evolution. For this two representative integral measures are presented in the following, which assess the future in terms of an event probability or comfort, utility and costs.

Total Event Probability

The **total event probability** $P_{\text{tot}}(e)$ is often used as a risk indicator [133, 141] where the severity is fixed to one. It quantifies, how likely a crash with another traffic participant is in future. In this thesis, this quantity is only used as a helping indicator to verify and compare different distribution representations for specific event detection models. Examples for different event types are provided in the subsequent Ch. 4 and Ch. 5. However, instead of comparing the full instantaneous or time-course sensitive values by e.g. mean square error, a complete scene evolution is expressed by one integral measure, summing up the time-course sensitive event probabilities starting in the current state $k = 0$ until the predefined time horizon H as follows:

$$\begin{aligned}P_{\text{tot}}(e) &= \sum_{k=0}^H P_{\text{tcs, ev},k} \\ &= P_{\text{inst, ev},0} + \sum_{k=0}^{H-1} P_{\text{inst, ev},k+1} \cdot P_{\text{tcs,surv},k} \quad .\end{aligned}\tag{3.17}$$

In case of only one event in the scene, one can take the instantaneous event probability $P_{\text{inst, ev}, k}$ from the recursive definition of the survival probability Eq. (3.14) and inserted it into Eq. (3.17). This leads to the finding that the total event probability $P_{\text{tot}}(e)$ equals the counter probability of the last predicted survival probability: $P_{\text{tot}}(e) = 1 - P_{\text{tcs, surv}, H}$.

Total Predicted Costs

The example of the total event probability of the previous section shows, that the instantaneous event probability has to be multiplied with the survival probability to get the time-course sensitive quantity, which subsequently is summed up to one scalar value representing a whole scene evolution. This method also works with other instantaneous quantities like the instantaneous comfort and utility costs $\hat{c}_{\text{conf}, k}$ and $\hat{c}_{\text{util}, k}$, defined in Eq. (3.6), Eq. (3.7), and the instantaneous risk $\hat{c}_{\text{risk}, k}$ of Eq. (3.11). Therefore, to obtain the **overall scene evolution costs** $C_{\text{tot}}(\mathbf{u}_{0:H}^1, \mathbf{x}_0)$, the time-course sensitive quantities are summed up according to (3.16) over the full time horizon $k \in \{0, \dots, H\}$ as follows:

$$C_{\text{tot}}(\mathbf{u}_{0:H}^1, \mathbf{x}_0) = \sum_{k=0}^H (\hat{c}_{\text{tcs, util}, k} + \hat{c}_{\text{tcs, conf}, k} + \hat{c}_{\text{tsc, risk}, k}(e_k)) \quad . \quad (3.18)$$

Eq. (3.18) is the simplified cost evaluation comparing to Eq. (2.11) for a predicted scene along the main path of a survived, time sensitive scene evolution. All predictions after an event has happened are projected onto the associated starting event, so that a representative instantaneous extended mean severity $\hat{c}_{\text{sev, ext}}(e_k)$ includes all costs and subsequent costs of that prediction branch.

Nevertheless, all the equations are derived by having only one event type in the scene evolution. In the next section, it is shown how the aforementioned equations are adapted in case of multiple events happening at the same predicted time point e.g. crashes with different traffic participants.

3.5 Multiple Events

In this section, it is shown how the aforementioned quantities are calculated for multiple events taking place in a same time interval $[k\Delta t, k\Delta t + \Delta t]$ and/or in the same states. In a time continuous consideration, where a point in time is real and it is nearly improbable, that

two events take place at the same point in time. In a time-discrete case, although the time interval Δt is very small, it is greater than zero. For longer time intervals, it is probable that within this interval more than one event happens, like crashes from left **and** right or between different vehicles. Therefore single scene states can have multiple events, which are not independent from another. Similar holds for distributed states, where the events-related PDF parts should be removed from the survived state PDF by considering the non-independence of these events.

Now consider, an event vector $\mathbf{e} = [e_{\text{NON}}, e^1, \dots, e^{N_e}]$ with binary elements instead of a single event e . Given a state PDF $p(\mathbf{x})$ and marginalize over all hidden events \mathbf{e} , the state PDF can be split into the event-free case PDF and in a PDF where at least one event is taking place (notated as $\mathbf{e}^{\geq 1}$)- like it was applied for only one event like in Eq. (3.1):

$$p(\mathbf{x}) = p(\mathbf{x}, e_{\text{NON}}) + p(\mathbf{x}, \mathbf{e}^{\geq 1}) \quad . \quad (3.19)$$

In the following, the calculation of both summands is presented. Starting by the event-free summand $p(\mathbf{x}, e_{\text{NON}})$ of Eq. (3.19), which can be rewritten as the absence of all other events and using the product rule of Eq. (A.12) for independent variables :

$$\begin{aligned} p(\mathbf{x}, e_{\text{NON}}) &= p(\mathbf{x}) \prod_{h=1}^{N_e} p(\neg e^h | \mathbf{x}) \\ &= p(\mathbf{x} | \neg e^1) p(\neg e^1) \prod_{h=2}^{N_e} p(\neg e^h | \mathbf{x}) \\ &= p(\mathbf{x} | \neg e^1, \neg e^2) p(\neg e^2 | \neg e^1) p(\neg e^1) \prod_{h=3}^{N_e} p(\neg e^h | \mathbf{x}) \\ &= p(\mathbf{x} | \neg e^1, \dots, \neg e^{N_e}) \prod_{h=1}^{N_e} p(\neg e^h | \neg e^1, \dots, \neg e^{h-1}) \\ &= p(\mathbf{x} | e_{\text{NON}}) p(e_{\text{NON}}) \quad . \end{aligned}$$

The intermediate distributions and probabilities are given by:

$$\begin{aligned} p(\neg e^h | \neg e^1, \dots, \neg e^{h-1}) &= \int_{\mathbb{R}^n} p(\neg e^h | \mathbf{x}) p(\mathbf{x} | \neg e^1, \dots, \neg e^h) d\mathbf{x} \quad (3.20) \\ p(\mathbf{x} | \neg e^1, \dots, \neg e^h) &= \frac{p(\neg e^h | \mathbf{x})}{p(\neg e^h | \neg e^1, \dots, \neg e^h)} p(\mathbf{x} | \neg e^1, \dots, \neg e^{h-1}) \quad , \end{aligned}$$

where the initial distribution $p(\mathbf{x})$ and event-free probability are adapted according to a predefined order of each single event e . This order of events can be chosen randomly, with increasing or decreasing associated event probability. After applying the whole event vector \mathbf{e} of one time step, the proper survival probability and distribution is gained. This is important because the survived state PDF will be predicted into subsequent time steps. Approximations with errors implemented at this point would force errors at later time points, so that these errors will be passed until the end of the prediction horizon.

The right summand $p(\mathbf{x}, \mathbf{e}^{\geq 1})$ of Eq. (3.19), representing the distribution in case that at least one event has happened, is estimated by the right term of the following inequality term:

$$\begin{aligned} p(\mathbf{x}, \mathbf{e}^{\geq 1}) &\leq \sum_{h=1}^{N_e} p(\mathbf{x}|e^h) p(e^h) \\ &= \sum_{h=1}^{N_e} p(e^h|\mathbf{x}) p(\mathbf{x}) . \end{aligned} \quad (3.21)$$

Here, overlaps of different events and their dependence are neglected, which has several advantages. First, it will reduce the calculation time, if not any combination has to be determined, so that it results in a linear time complexity instead of a quadratic one. Second, events occurring in the same time interval do not exclude each other e.g. the vehicle could crash with another vehicle and lose additionally control in a curve. The combined event, where both take place, is not treated as a separate case. And the last benefit is the order independence in the calculation procedure, because for each single event the initial distribution $p(\mathbf{x})$ is taken instead of conditional distributions $p(\mathbf{x}|e^1)$ like in Eq. (3.20). However, with the right side of Eq. (3.21), event probabilities and thus the costs at one predicted time point are never being underestimated in cases where the costs of a combined event is always lower than the summation of each individual event cost by neglecting other events.

According to the introduced notations in the previous section 3.4 for instantaneous survived and event-engaged PDF's, the total costs $C_{\text{tot}}(\mathbf{u}_{0:H}^1, \mathbf{x}_0)$ of Eq. (3.18) for multiple events are simply extended as follows:

$$C_{\text{tot}}(\mathbf{u}_{0:H}^1, \mathbf{x}_0) = \sum_{k=0}^H \left(\hat{c}_{\text{util},k} + \hat{c}_{\text{comf},k} + \sum_{h=1}^{N_e} \hat{c}_{\text{risk},k}(e_k^h) \right) P_{\text{tcs,surv},k-1} ,$$

where $P_{\text{tcs,surv,-1}} = 1$ like above and costs of each event are summed up over all events. Here, one can see that cost calculation errors at one predicted time interval do not impact the cost calculation of later time steps.

3.6 Rate Formulation for Continuous Time

As it was shortly discussed in the previous section, events can be easier formulated in continuous time, because events happen subsequently and mostly not “simultaneously” within a time interval. For that, the author of [45] derives an event probability calculation based on Poisson processes and obtains an analytical description for survival and total event probability. Applications of this concept for autonomous vehicles are presented in [128, 129].

The main assumption of this approach is that an instantaneous event probability $P_{\text{inst,ev}}$ can be represented as rate τ_e^{-1} in the following way:

$$P_{\text{inst,ev}} = \tau_e^{-1} \cdot \Delta t \ .$$

According to the reference [45] only the magnitude is considered, so changes of PDF’s are not explicitly incorporated.

The instantaneous survival probability $P_{\text{inst,surv}}$ in (3.2) was defined as the counter probability of an event probability, which includes an event detection model and the survived state PDF. Because of the missing concurrency of events, the instantaneous survival probability of one point in time - not a time interval - is calculated assuming independent event probabilities:

$$\begin{aligned} P_{\text{inst,surv}} &= \prod_{\mathbb{E}} (1 - \tau_e^{-1} \Delta t) \\ &= 1 - \sum_{\mathbb{E}} \tau_e^{-1} \Delta t + T_{\text{mult}} \cdot \Delta t^2 + \dots \\ &\approx 1 - \sum_{\mathbb{E}} \tau_e^{-1} \Delta t \ , \end{aligned}$$

where the term T_{mult} considers the sum of combinatorial product of two event rates τ_e^{-1} . For very small rates $\tau_e^{-1} \ll 1$ and time intervals $\Delta t \approx 0$, terms with exponents higher than one can be neglected. One can see that the instantaneous survival probability is depending on the sum of the individual event rates which is represented as the aggregated event rate

τ_{AGG}^{-1} as it is defined as follows:

$$\tau_{\text{AGG}}^{-1} := \sum_{\mathbb{E}} \tau_e^{-1} . \quad (3.22)$$

With the obtained first order description of the instantaneous survival probability, the aggregated event rate τ_{AGG}^{-1} , the time continuous survival probability $P_{\text{surv}}(s)$ is derived by taking two subsequent time points s and $s + \Delta t$ into account. The time-course sensitive survival probability of the later time point $P_{\text{surv}}(s + \Delta t)$ is reduced by the instantaneous survival probability between these two time points like in Eq. (3.15):

$$P_{\text{surv}}(s + \Delta t) = (1 - \tau_{\text{AGG}}^{-1} \Delta t) P_{\text{surv}}(s) .$$

After bringing the survival probability on one side, it follows:

$$\frac{P_{\text{surv}}(s + \Delta t) - P_{\text{surv}}(s)}{P_{\text{surv}}(s)} = -\tau_{\text{AGG}}^{-1} \Delta t .$$

Now, letting $\Delta t \rightarrow dt$ and $P_{\text{surv}}(s + dt) - P_{\text{surv}}(s) = dS$ and integrating both sides one obtains an analytical formula for calculating the survival probability:

$$P_{\text{surv}}(s) = \exp \left(- \int_0^s \tau_{\text{AGG}}^{-1}(t) dt \right) , \quad (3.23)$$

where $P_{\text{surv}}(s = 0) = 1$.

With the definition of Eq. (3.17), the total probability $P_{\text{tot}}(e)$ of a time interval $s \in [0, H\Delta t]$ for one specific event is the integration of the instantaneous event probability multiplied by the survival probability and is in time-continuous manner given by:

$$P_{\text{tot}}(e) = \int_0^{H\Delta t} \tau_e^{-1}(s) \exp \left(- \int_0^s \tau_{\text{AGG}}^{-1}(t) dt \right) ds . \quad (3.24)$$

With Eq. (3.24) it is also possible to obtain time discrete instantaneous probabilities by taking the event related rate and integrate over the time interval $s \in [0, \Delta t]$. For example, assuming a constant event rate τ_e^{-1} it follows:

$$\begin{aligned} P_{\text{inst, ev, k}} &= \int_0^{\Delta t} \tau_e^{-1} \exp \left(- \int_0^s \tau_e^{-1} dt \right) ds \\ &= 1 - \exp(-\tau_e^{-1} \Delta t) . \end{aligned} \quad (3.25)$$

This makes clear, that the instantaneous probabilities in discrete time are rather a consideration over an associated time interval than of a specific time point. In time-continuous case, the label instantaneous is properly used and meaning one point in time. Nevertheless, in this thesis, the term instantaneous probability stands for the time-discrete case, where short intervals of size Δt are used. If a time-continuous case arises, an event rate will be used as the correct representation of collision events.

Inferring from the instantaneous probability to the time continuous way is also possible, but not always feasible. Given a time-discrete instantaneous probability $P_{\text{inst, ev, } k}$ a constant event rate can be determined:

$$\tau_e^{-1} = -\frac{1}{\Delta t} \ln(1 - P_{\text{inst, ev, } k}) \quad . \quad (3.26)$$

In case of $P_{\text{inst, ev, } k} = 1$, the rate τ_e^{-1} becomes infinity.

The big advantage of the time-continuous approach is the simple addition of further event rates to the aggregated rate τ_{AGG}^{-1} of Eq. (3.22), which let the model be extended in a very simple manner. The drawback of this rate-based framework is the modeling of the event rate itself. The rates combines the event detection modeling and the distributed states which makes the models physically hard to derive, so that they are often derived in a heuristic fashion.

3.7 Conclusion

This chapter provides a general concept of simplifying the prediction and evaluation process calculation by focusing on the prediction evolutions, where the ego vehicle keeps the control without having any events. All other branches of the prediction process, starting with critical events, are summed up to a representative severity functions. This idea is a time-discrete extension of the survival theory framework. Contributions to the survival theory are as follows:

- A simplifying framework for time-discrete cost calculation for a motion-planner's prediction process to avoid exponential tree expansions over time through occurring events and caused intention changes, where the framework distinguish explicitly between magnitude and state PDF prediction for considering conditional dependencies over time, like it is already published by the author in [110] and as coauthor in [47].

-
- A general scheme for different event types and their outcome to incorporate them into the motion-planner's prediction process.
 - A new method for handling multiple events and their evaluation at one time step of the prediction process which considers conditional dependencies between events.
 - The transition from time-discrete to a rate-based approach of [45] and vice versa.

In the following chapters, different event types according to the presented scheme are introduced with a main focus on the collision event between two vehicles.

4 Collision Event

The collision event between two vehicles is crucial for handling complex scenarios with different other traffic participants (TP's). So the ego vehicle has to evaluate the likelihood of future crashes as accurate as needed in a variety of different scenes. Especially, multiple vehicles in risky scenarios have to be evaluated accurately to reduce the chance of severe crashes. This chapter starts with the related work in Sec. 4.1 and shows drawbacks of current approaches. The formulation of the problem and the needed quantities are presented in Sec. 4.2. Based on a general consideration of collided trajectories, the idea of the novel algorithm is presented in Sec. 4.3, where a collision region is defined in Sec. 4.4 to calculate collided state Probability Distributions Functions (PDF's), introduced in Sec. 4.5 and survived state PDF's (see Sec. 4.6). An alternative approach is presented in Sec. 4.7 based on collision rates. In the last section (Sec. 4.8), the probability calculation methods, gained in this chapter are compared in different scenarios.

4.1 Related Work

The probability calculation for collision events between two vehicle is often considered in uncertain motion planning and it often takes a lot of computational power to get satisfying accuracies. In many works, a general indicator function determines overlaps in 2D between two vehicles [121, 141, 154, 171], which can be represented as a collision region in positional space through a Minkowski region [20, 52, 120, 125]. The volume of the positional PDF inside the Minkowski region represents the collision probability. The determination of this integral is often very difficult and it can only calculates traffic scenes with only one type of event or one pair of collision partners. Nevertheless, an overview of different techniques is done by [104]. The author identifies three main classes as follows:

1. **Particle-based approaches:** Typically Monte Carlo simulations (MCS) draw samples from an initial PDF and check each sample for

a collision by detecting shape overlaps [10, 28, 36, 49, 77, 95, 98, 99]. This method belongs to the stochastic integration methods, so that each calculation with a set of new randomly drawn samples or particles provides a new result. The accuracy and variance of the outcome can be reduced by taking a high amount of samples, mostly more than 10.000. The high particle number often takes a lot of computational effort, because each sample represents an own scenario. Furthermore, regions with low probability density are only sparsely represented. That's why some speed enhancements techniques are implemented by using conservative pre-checks, which enlarges conservatively the conflict space by simple axis-oriented bounding boxes [58] or bounding circles [58, 141] and are far faster to check. Another approach clusters collided states with a Gaussian Mixture Model (GMM) to obtain an efficient representation of collided regions, so that for example a Rapidly-Exploring-Random Tree expansion for motion planning gets more efficient [81].

2. **State space discretization:** This approach decomposes the state space into a grid, where its occupancy can be checked very easily. In the works [6–8], this technique shows good accuracy compared to a Monte-Carlo Simulation and provides a deterministic outcome. In [102] and [136], the authors use occupancy maps for filters in 2D-positional space based on the same principle. A three dimensional voxel representation in relative space was presented in [3]. The general problem of this approach is the exponential increasing number of grid cells in case of higher state dimensions, which can drastically reduce the accuracy if online-applicability is required.
3. **Normal distributions:** In this class of approaches, the state distribution is assumed to be Gaussian, which stays in contrast to the previous two classes, where any initial PDF can be used. This assumption allows to make some simplification in motion prediction like the usage of Kalman filters or unscented transformations and also some simplification in the calculation of probability value itself [73, 84, 120, 121, 127, 154]. In the works of Berthelot et al. [21–23], a Monte Carlo method for obtaining minimum object distances was approximated by an unscented transformation with another, approximating Gaussian. A technique which aggregates collided regions over an infinite time horizon are introduced in [4, 83, 119]. Extensions for nonlinear motion with tubes [3] or sigma hulls [101] are also based on a fusion of collided regions over time. Another approach

of this category provides a very fast and accurate calculation of flux through collision boundaries, where a Gaussian state PDF is penetrating the Minkowski region [125]. This method has the advantage that it is not prone to time sampling issues, because of its time-continuous nature. Nevertheless, these aforementioned Gaussian-based methods can only calculate probability values for one collision event and not determine any collided state PDF representations, which is needed for latter severity calculation. An analytic Gaussian truncation technique combined with a Kalman filter prediction was implemented in [122], which provides satisfying results for quasi-convex free space/non-occupied regions and determines non-collided state PDF's for each predicted time point. But this technique is not suited for convex obstacles, where the PDF is much larger than the objects themselves.

4. **Other Approaches:** There are different approaches trying to represent heuristically the collision probability in a predicted point like distance-based rates combined with the event rate model [45, 129], already presented in Sec. 3.6, with dynamic potential fields [96, 173], by circular-approximated shapes and overlap counts [9] or occupied circle areas [133].

All in all, there is no fast collision probability method for low and high probable events, which can be implemented for arbitrary motion models with positional and speed-including normal PDF's with sufficient accuracy. Furthermore, collided and non-collided states have often to be calculated separately, which increases calculation effort.

4.2 Problem Statement

The task is to create a collision risk calculation for representing a crash between two vehicles which also fits into the presented framework of Ch. 2 and which was simplified in Ch. 3. For this, several components have to be modeled. First, the instantaneous risk for a collision event has to be determined, which is now called the instantaneous collision risk \hat{c}_{COLL} , which is defined as a product according to Eq. (3.11):

$$\hat{c}_{\text{COLL}}(e_k = e_{\text{COLL}}) = \hat{c}_{\text{sev}}(e_k = e_{\text{COLL}}) \cdot P_{\text{inst,COLL},k} \quad , \quad (4.1)$$

where $\hat{c}_{\text{sev}}(e_k = e_{\text{COLL}})$ is the severity of a collision and $P_{\text{inst,COLL},k}$ the instantaneous collision probability. For the calculation of the severity,

the collision event-engaged state PDF $p(\mathbf{x}_k | e_k = e_{\text{COLL}}, I_{k-1} = I_{\text{ctrl}})$ has to be determined. Its complement, the non-event/survived state PDF $p(\mathbf{x}_k | e_k = \neg e_{\text{COLL}}, I_{k-1} = I_{\text{ctrl}})$ and the corresponding instantaneous non-event probability $p(e_k = \neg e_{\text{COLL}} | I_{k-1} = I_{\text{ctrl}})$ for the instantaneous survival probability are needed to calculate subsequent time steps in the prediction process. This adaptation of the PDF guarantees that a collision happening once, cannot happen a second time in subsequent time steps.

All in all, the current chapter presents the following models and approximations for the collision event, except the severity (see Ch. 6), in the following order:

1. The collision event detection model $p(e_k = e_{\text{COLL}} | \mathbf{x}_k)$ and its transition to a collision region for two polygonally shaped vehicles as a basis for determining the collision event related quantities and PDF's
2. An analytic approximation for determining the collided state PDF $p(\mathbf{x}_k | e_k = e_{\text{COLL}}, I_{k-1} = I_{\text{ctrl}})$ and the corresponding instantaneous collision probability $P_{\text{inst, COLL}, k}$ for calculating the instantaneous risk according to Eq. (4.1)
3. Two analytical approximations for the non-collided state PDF $p(\mathbf{x}_k | e_k = \neg e_{\text{COLL}}, I_{k-1} = I_{\text{ctrl}})$ and $p(e_k = \neg e_{\text{COLL}} | I_{k-1} = I_{\text{ctrl}})$ to predict the critical-event-free distributions for subsequent predicted time points like in Eq. (3.13)

The PDF's for collided and non-collided states are Gaussian's or Gaussian Mixtures for their simplicity of further scene state transitions.

4.3 Approach

The presented approach is a modification and extension of the truncation process for Gaussian PDF's introduced in [122], which works also for convex obstacles and high collision probabilities. The new presented approach solves Monte Carlo Simulation's sampling issues and multimodal PDF representations. It approximates state of the art Monte Carlo Simulation, but is much faster and applicable to a variety of time-discrete predictions.

4.3.1 Collided Trajectories

The approach starts from a very general point of view. In Fig. 4.1, one can see three different trajectories in positional space with one common start

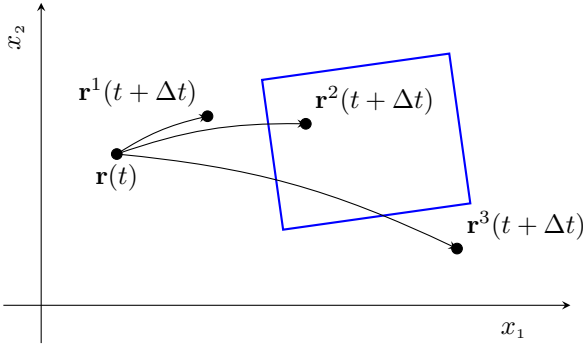


Figure 4.1: Collided and non-collided trajectories in two-dimensional space with one obstacle (blue). Three trajectories starting in $\mathbf{r}(t)$ and ending in three different points: The first trajectory ends in $\mathbf{r}^1(t + \Delta t)$ representing the case where no collision occurs (case 1). A collision occur for the second end position vector $\mathbf{r}^2(t + \Delta t)$, where a simple collision check uses only the end time point $t + \Delta t$ for detection (case 2). In case 3, a collision for the third trajectory with end point $\mathbf{r}^3(t + \Delta t)$ can only be detected if the full trajectory is considered.

position $\mathbf{r}(t)$ and three different end positions $\mathbf{r}(t + \Delta t)$. The trajectories between two points can intersect an obstacle. Depending on the time sampling width or motion speed compared to the obstacle region dimension, the collision can be detected or not. So the task is to identify all collided trajectories independent of the time-discrete sampling. For this, the first step is to determine the so called **static collision region** based on the vehicle's shape and orientation, which detects whether a point is located inside an obstacle or whether two vehicles are overlapping, which works well for case 2. If only the end points are checked by the static collision region, it cannot distinguish between case 1 without collisions and case 3 with a collision in between. Therefore, the static collision region has to be enlarged to a **dynamic collision region**, which is able to detect transitions of trajectories through an obstacle (case 3) and can fix the problem of time-discrete sampled trajectories.

4.3.2 Structure

Regardless of the used type of collision region, static or dynamic, which are presented in Sec. 4.4, the determination of the associated PDF's describing the collided and survived parts based on an initial PDF are tackled in

Sec. 4.5 and in Sec. 4.6. The general six-step-approach considering both types is shown in Fig. 4.2. It starts by transforming the uncertain states and the deterministic vehicle shapes into the relative space (steps 1-2). Then, the edges of geometrical representation of the vehicle overlap is used to iteratively truncate the initial Gaussian PDF in relative space to gain a Gaussian representation for the collided state PDF (steps 2-4). In step 5, the non-collided PDF representation (orange) is determined based on the collided state Gaussian PDF (red) and the initial Gaussian PDF (black) like a subtraction. Because the approach takes the initial, full multivariate Gaussian scene state PDF through all the steps, it is possible to infer the individual PDF's of each vehicle (step 6). The following sections present the approach step by step and derive all necessary quantities. An extension of this approach by varying step (step 5) is discussed in Sec. 4.6.3, where a multi-modal Gaussian Mixture Model is used to represent the survived or non-collided PDF in a more accurate way.

4.4 Collision Region

The detection, whether two vehicles are collided or sharing the same space depends on the vehicle shapes \mathbb{M}^i , their orientation γ^i and their positions p_x^i, p_y^i in global positional space. The vehicle positions p_x^i, p_y^i are part of the world scene state, so that the center position vector $\mathbf{r}^i = [p_x^i, p_y^i]$ can be picked by a positional extraction matrix $\mathbf{C}^i \in \mathbb{R}^{2 \times n}$ by multiplying the matrix with the world scene state \mathbf{x} :

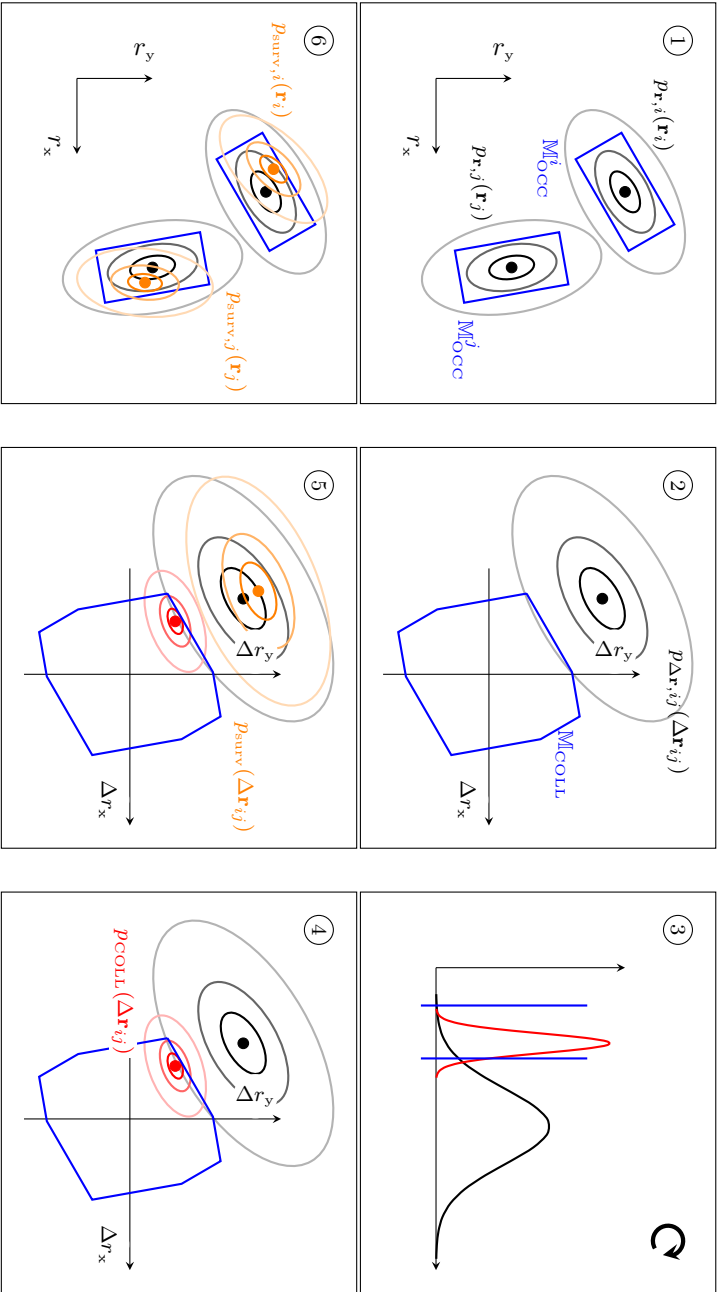
$$\mathbf{r}^i = \mathbf{C}^i \mathbf{x} \ .$$

The regions $\mathbb{M}_{\text{OCC}}^i$ in the positional space \mathbb{R}^2 occupied by each vehicle are defined by an oriented shape \mathbb{M}^i , the orientation γ^i and the center location \mathbf{r}^i :

$$\mathbb{M}_{\text{OCC}}^i(\mathbf{r}^i, \gamma^i) = \{\mathbf{r}^i + \mathbf{R}_{\text{rot}}^2(\gamma^i) \mathbf{m}^i \mid \mathbf{m}^i \in \mathbb{M}^i\} \ ,$$

where $\mathbf{R}_{\text{rot}}(\gamma^i)$ is the rotation matrix in two-dimensional space and \mathbf{m}^i is a positional vector inside the oriented shape \mathbb{M}^i . According to [120, 141, 154, 171], the detection model is an indicator function with a binary output, symbolizing whether an overlap between two shapes exists or not:

$$p(e = e_{\text{COLL}} | \mathbf{x}) = \begin{cases} 1 & \text{if } \mathbb{M}_{\text{OCC}}^i(\mathbf{C}^i \mathbf{x}, \gamma^i) \cap \mathbb{M}_{\text{OCC}}^j(\mathbf{C}^j \mathbf{x}, \gamma^j) \neq \emptyset \\ 0 & \text{else.} \end{cases} \quad (4.2)$$



With the indicator function of Eq. (4.2), a **collision region** in state space \mathbb{R}^n can be defined. States, where the detection models become one belong to the collision region \mathbb{M}_{COLL} and states, where the occupied areas $\mathbb{M}_{\text{OCC}}^i$, $\mathbb{M}_{\text{OCC}}^j$ do not intersect, are not part of the collision region. The collision region \mathbb{M}_{COLL} is defined as follows:

$$\mathbb{M}_{\text{COLL}} = \{\mathbf{x} \in \mathbb{R}^n \mid \mathbb{M}_{\text{OCC}}^i(\mathbf{C}^i \mathbf{x}, \gamma^i) \cap \mathbb{M}_{\text{OCC}}^j(\mathbf{C}^j \mathbf{x}, \gamma^j) \neq \emptyset\} \quad (4.3)$$

It represents all scene states $\mathbf{x} \in \mathbb{R}^n$, where vehicle i and j are collided.

Similar to the derivation shown in [120], the definition of the collision region in Eq. (4.3) can be rewritten as:

$$\begin{aligned} & \mathbb{M}_{\text{OCC}}^i(\mathbf{C}^i \mathbf{x}, \gamma^i) \cap \mathbb{M}_{\text{OCC}}^j(\mathbf{C}^j \mathbf{x}, \gamma^j) \neq \emptyset \\ \Leftrightarrow & \exists \mathbf{m}^i \in \mathbb{M}_{\text{OCC}}^i(\mathbf{C}^i \mathbf{x}, \gamma^i), \mathbf{m}^j \in \mathbb{M}_{\text{OCC}}^j(\mathbf{C}^j \mathbf{x}, \gamma^j) \text{ s.t. } \mathbf{m}^i = \mathbf{m}^j \\ \Leftrightarrow & \exists \tilde{\mathbf{m}}^i \in \mathbb{M}_{\text{OCC}}^i(\mathbf{0}, \gamma^i), \tilde{\mathbf{m}}^j \in \mathbb{M}_{\text{OCC}}^j(\mathbf{0}, \gamma^j) \text{ s.t. } \tilde{\mathbf{m}}^i - \mathbf{C}^i \mathbf{x} = \tilde{\mathbf{m}}^j - \mathbf{C}^j \mathbf{x} \\ \Leftrightarrow & \exists \tilde{\mathbf{m}}^i \in \mathbb{M}_{\text{OCC}}^i(\mathbf{0}, \gamma^i), \tilde{\mathbf{m}}^j \in \mathbb{M}_{\text{OCC}}^j(\mathbf{0}, \gamma^j) \text{ s.t. } \mathbf{C}^j \mathbf{x} - \mathbf{C}^i \mathbf{x} = \tilde{\mathbf{m}}^j - \tilde{\mathbf{m}}^i \\ \Leftrightarrow & (\mathbf{C}^j - \mathbf{C}^i) \mathbf{x} \in \mathbb{M}_{\text{OCC}}^j(\mathbf{0}, \gamma^j) \oplus (-\mathbb{M}_{\text{OCC}}^i(\mathbf{0}, \gamma^i)) \quad . \end{aligned}$$

The term $\mathbb{M}_{\text{OCC}}^j(\mathbf{0}, \gamma^j) \oplus (-\mathbb{M}_{\text{OCC}}^i(\mathbf{0}, \gamma^i))$ in the last row is the Minkowski addition of both oriented shapes [52] in relative positional space, where the rotated shape of vehicle i is mirrored by both axes (depicted by the negative sign) and added to the other oriented vehicle's shape. Defining the difference positional extraction matrix \mathbf{C}^{ij} and the Minkowski region $\mathbb{M}_{\text{OCC}}^{ij}(\gamma^i, \gamma^j)$ according to

$$\mathbf{C}^{ij} = \mathbf{C}^j - \mathbf{C}^i \quad (4.4)$$

$$\mathbb{M}_{\text{OCC}}^{ij}(\gamma^i, \gamma^j) = \mathbb{M}_{\text{OCC}}^j(\mathbf{0}, \gamma^j) \oplus (-\mathbb{M}_{\text{OCC}}^i(\mathbf{0}, \gamma^i)) \quad (4.5)$$

provides a more compact definition of the collision region:

$$\mathbb{M}_{\text{COLL}} = \{\mathbf{x} \in \mathbb{R}^n \mid \mathbf{C}^{ij} \mathbf{x} \in \mathbb{M}_{\text{OCC}}^{ij}(\gamma^i, \gamma^j)\} \quad ,$$

where $\mathbb{M}_{\text{OCC}}^{ij}(\gamma^i, \gamma^j)$ represents the occupied region in the relative positional space and \mathbb{M}_{COLL} the collision region in the scene state space. An exemplary Minkowski addition $\mathbb{M}_{\text{OCC}}^{ij}(\gamma^i, \gamma^j)$ of two rectangular shaped vehicles is shown in Fig. 4.3.

Furthermore, the Minkowski addition has several useful properties [41]. The Minkowski sum of ...

- ... two convex sets result in a convex Minkowski set.

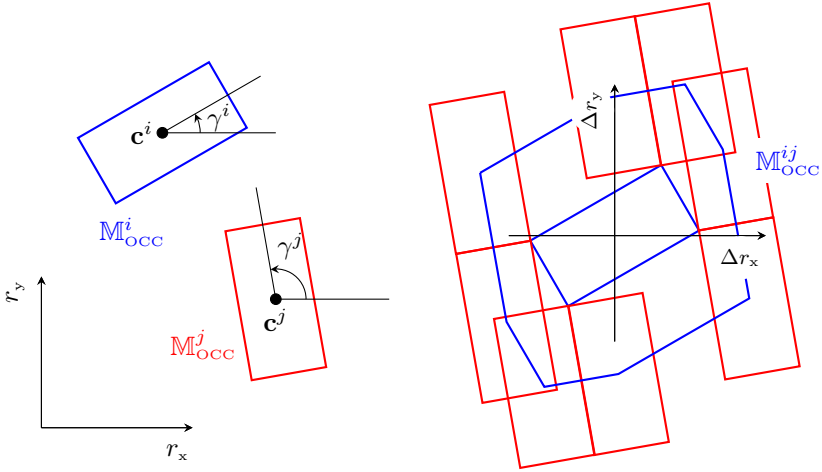


Figure 4.3: Schema of a geometrical convolution of two vehicle shapes M_{OCC}^i and M_{OCC}^j . Left: Initial scene with two oriented vehicle shapes. Right: Minkowski Addition to obtain collision region in relative positional space M_{OCC}^{ij} .

- ... two polygonal sets result in a polygonal Minkowski set.
- ... two point symmetric sets result in a point symmetric Minkowski set.

Because of this, the Minkowski region of two rectangular shaped vehicles rotated around their center point is a polygonal, point symmetric, convex set with maximally eight corner points and edges, like in Fig. 4.3. A simple algorithm for polygonal Minkowski additions is presented in [41].

Using the knowledge of a polygonally shaped Minkowski region, an edge l of the Minkowski region $M_{\text{OCC}}^{ij}(\gamma^i, \gamma^j)$ can be described by hyperplanes with normal vectors $\mathbf{a}^l \in \mathbb{R}^2$, heading into inner points of the Minkowski region and a shift $b^l \in \mathbb{R}$. So a polygonal and convex collision region is the intersected subset of eight different sets limited by eight hyperplanes (\mathbf{a}^l, b^l) representing the edges of the collision region:

$$M_{\text{COLL,poly}} = \bigcap_{l=1}^8 \{ \mathbf{x}_k \in \mathbb{R}^n | (\mathbf{a}^l)^T (\mathbf{C}^{ij} \mathbf{x}) \geq b^l \} . \quad (4.6)$$

The normal vector of the hyperplane (\mathbf{v}^l, w^l) defined in scene state space is a reformulation of the hyperplanes (\mathbf{a}^l, b^l) in positional space according

to the difference positional extraction matrix \mathbf{C}^{ij} :

$$\begin{aligned}\mathbf{v}^l &= (\mathbf{C}^{ij})^T \mathbf{a}^l \\ w^l &= b^l \quad .\end{aligned}$$

In case of point symmetry, one edge of the Minkowski region is anti-parallel to another edge on the other side of the polygon: $\mathbf{v}_k^l = -\mathbf{v}_k^{l+4}$. The intersection set for a polygonal and point symmetric Minkowski region $\mathbb{M}_{\text{COLL,poly}}$ gets reduced to the following formulation:

$$\begin{aligned}\mathbb{M}_{\text{COLL,poly}} &= \bigcap_{l=1}^4 \{ \mathbf{x} \in \mathbb{R}^n \mid -w^{l+4} \geq (\mathbf{v}^l)^T \mathbf{x} \geq w^l \} \\ &:= \bigcap_{l=1}^4 \mathbb{H}^l \quad ,\end{aligned}$$

where the shifts hold the following condition $-w_k^{l+4} \geq w^l$. Note that the shifts w and edge normal vectors \mathbf{v} of the hyperplane restricted sets $\mathbb{H}^l \subset \mathbb{R}^n$ are depending on the vehicle's shape $\mathbb{M}^i, \mathbb{M}^j$ and their current orientation γ^i, γ^j in the two-dimensional positional space.

In the following, the definition of a collision region represented by hyperplanes is used to get the static collision region, which only considers the current predicted time step k , and the dynamic collision region, which also considers penetrations of the collision region within a time interval between two subsequent time steps $k-1$ and k .

4.4.1 Static Collision Region

The collision region $\mathbb{M}_{\text{COLL},k}^{\text{stat}}$ for the collision event detection model only focuses on the current states \mathbf{x}_k in the predicted time point k and is defined as:

$$\mathbb{M}_{\text{COLL},k}^{\text{stat}} = \bigcap_{l=1}^4 \{ \mathbf{x}_k \in \mathbb{R}^n \mid -w_k^{l+4} \geq (\mathbf{v}_k^l)^T \mathbf{x}_k \geq w_k^l \} \quad . \quad (4.7)$$

As aforementioned, each hyperplane (\mathbf{v}_k^l, w_k^l) points into the direction of the collided states, so that for these states $\mathbf{x}_k \in \mathbb{M}_{\text{COLL,poly}}$ the plane equation becomes positive $\mathbf{v}_k^l \mathbf{x}_k - w_k^l \geq 0$ and for non-collided states negative. Thus, the event detection model from Eq. (4.2) can be represented by a

product of indicator step-functions σ , which equals one in case of positive plane distances and zero for non-collided states. These sub-indicators frame the collided region. In case of four hyperplane restricted sets \mathbb{H}_k^l , the event detection model with static collision region is represented as follows:

$$p^{\text{stat}}(e_k = e_{\text{COLL}} | \mathbf{x}_k) = \begin{cases} 1 & \text{if } \mathbf{x}_k \in \mathbb{M}_{\text{COLL},k}^{\text{stat}} \\ 0 & \text{else.} \end{cases} \quad (4.8)$$

$$= \prod_{l=1}^4 \sigma((\mathbf{v}_k^l)^T \mathbf{x}_k - w_k^l) \cdot \sigma(-(\mathbf{v}_k^l)^T \mathbf{x}_k - w_k^{l+4}) \ .$$

The step function based sub-indicator representation of Eq. (4.8) will help to simplify calculation in previous sections, especially for the determination of the collided state PDF.

4.4.2 Dynamic Collision Region

The static collision region $\mathbb{M}_{\text{COLL}}^{\text{stat}}$ of Eq. (4.7) imposes the state restrictions at one moment in time. In many cases, states start from outside at one time point $(k-1)\Delta t$ and will end up inside this static collision region at time point $k\Delta t$ (case 2 of Fig. 4.1). But for discrete time-steps of length Δt , trajectories with high velocities move through the positional state space, therefore the end point could also lay behind the collision region and a collision won't be detected anymore. This time-sampling issue can lead to overseen vehicles and underestimated collision probabilities and reduces the prediction accuracy.

To overcome the time-sampling issue, the region inside the complete time interval $\tilde{\Delta}t \in \mathbb{T}^h = [-\Delta t, 0]$ between start and end point is considered; for this purpose a representative history state \mathbf{x}^h is introduced. To calculate the history state \mathbf{x}^h , the inverse linear motion model is taken from Eq. (2.3) with time interval dependent system matrix $\mathbf{A}_{\tilde{\Delta}t}$, input matrix $\mathbf{B}_{\tilde{\Delta}t}$ and with neglected process noise:

$$\mathbf{x}_k = \mathbf{A}_{\tilde{\Delta}t} \mathbf{x}^h(\tilde{\Delta}t) + \mathbf{B}_{\tilde{\Delta}t} \mathbf{u}_{k-1} \quad (4.9)$$

$$\Leftrightarrow \mathbf{x}^h(\tilde{\Delta}t) = (\mathbf{A}_{\tilde{\Delta}t})^{-1}(\mathbf{x}_k - \mathbf{B}_{\tilde{\Delta}t} \mathbf{u}_{k-1}) \ .$$

The dynamic collision region is defined as the union of static collision regions (see Eq. (4.6)) over time interval \mathbb{T}^h , which is now depending on

the scene state history \mathbf{x}^h :

$$\mathbb{M}_{\text{COLL},k}^{\text{dyn}} = \bigcup_{\tilde{\Delta}t \in \mathbb{T}^h} \bigcap_{l=1}^8 \{ \mathbf{x}^h \in \mathbb{R}^n \mid (\mathbf{a}_k^l)^T (\mathbf{C}^{ij} \mathbf{x}^h(\tilde{\Delta}t)) \geq b_k^l \} .$$

Substituting the history scene state \mathbf{x}^h by taking Eq. (4.9) results in the following equation:

$$\begin{aligned} \mathbb{M}_{\text{COLL},k}^{\text{dyn}} &= \bigcup_{\tilde{\Delta}t \in \mathbb{T}^h} \bigcap_{l=1}^8 \{ \mathbf{x}_k \in \mathbb{R}^n \mid (\mathbf{v}_k^l(\Delta t))^T \mathbf{x}_k \geq w_k^l(\Delta t) \} \\ &:= \bigcup_{\tilde{\Delta}t \in \mathbb{T}^h} \bigcap_{l=1}^8 \mathbb{H}_k^l(\tilde{\Delta}t) , \end{aligned} \quad (4.10)$$

where the parameters of the time dependent hyperplane restricted set $\mathbb{H}_k^l(\tilde{\Delta}t)$ are as follows:

$$\begin{aligned} \mathbf{v}_k^l(\tilde{\Delta}t) &= (\mathbf{C}^{ij} (\mathbf{A}_{\tilde{\Delta}t})^{-1})^T \mathbf{a}_k^l \\ w_k^l(\tilde{\Delta}t) &= b_k^l + (\mathbf{a}_k^l)^T (\mathbf{C}^{ij} (\mathbf{A}_{\tilde{\Delta}t})^{-1} \mathbf{B}_{\tilde{\Delta}t} \mathbf{u}_{k-1}) . \end{aligned} \quad (4.11)$$

The set union in Eq. (4.10) is difficult to determine, that's why an approximation of the collision region $\widehat{\mathbb{M}}_{\text{COLL}}^{\text{dyn}}$ limits the number of considered subsets to a finite value:

$$\widehat{\mathbb{M}}_{\text{COLL},k}^{\text{dyn}} = \bigcap_{l=1}^8 (\mathbb{H}_k^l(-\Delta t) \cup \mathbb{H}_k^l(0)) \approx \mathbb{M}_{\text{COLL},k}^{\text{dyn}} . \quad (4.12)$$

A detailed way, why the collision region $\widehat{\mathbb{M}}_{\text{COLL}}^{\text{dyn}}$ is only an approximation for a double integrator system in case of non zero acceleration is outlined in attachment A.1.

The drawback of this approach is that the region described by the two hyperplanes $\mathbb{H}_k^l(-\Delta t)$ and $\mathbb{H}_k^l(0)$ is not convex. This issue is circumvented by splitting the collision region into two convex pieces. For this, another truncation plane which is placed in the intersection line of $\mathbb{H}_k^l(-\Delta t)$ and $\mathbb{H}_k^l(0)$ is introduced. The structure of the linear system and input matrix $\mathbf{A}_{\Delta t}$, $\mathbf{B}_{\Delta t}$ according to Eq. (2.2) allows to do a simple subtraction of both hyperplanes parameters according to Eq. (4.11) to obtain the desired splitting plane region $\mathbb{H}_{\text{sp},k}^l$ with $(\mathbf{v}_{\text{sp},k}^l)^T \mathbf{x}_k \geq w_{\text{sp},k}^l$:

$$\begin{aligned} \mathbf{v}_{\text{sp},k}^l &= \mathbf{v}_k^l(-\Delta t) - \mathbf{v}_k^l(0) \\ w_{\text{sp},k}^l &= \mathbf{v}_k^l(-\Delta t)^T \mathbf{B}_{\Delta t} \mathbf{u}_{k-1} . \end{aligned}$$

The independence of b_k^l as part of the shift $w_{sp,k}^l$ is beneficial for reusing the splitting set $\mathbb{H}_{sp,k}^l$ for each element of parallel hyperplanes with normal vectors \mathbf{a}_k^l or $-\mathbf{a}_k^l$, respectively. This reduces the number of splitting sets.

Using the splitting sets, the approximated collision region $\widehat{\mathbb{M}}_{COLL,k}^{dyn}$ can be rewritten. Because $(\mathbf{v}_{sp,k}^l)^T \mathbf{v}_k^l(-\Delta t) > 0$ and $(\mathbf{v}_{sp,k}^l)^T \mathbf{v}_k^l(0) < 0$ holds, the splitting hyperplane set $\mathbb{H}_{sp,k}^l$ and its complement $\mathbb{H}_{sp,k}^{l,c}$ shrink both boundary sets $\mathbb{H}_k^l(-\Delta t)$ and $\mathbb{H}_k^l(0)$ in a way that the intersected regions become convex and can be reunified:

$$\begin{aligned} \widehat{\mathbb{M}}_{COLL,k}^{dyn} &= \bigcap_{l=1}^8 (\mathbb{H}_k^l(-\Delta t) \cup \mathbb{H}_k^l(0)) \\ &= \bigcap_{l=1}^4 [\mathbb{H}_{sp,k}^l \cap \mathbb{H}_k^l(-\Delta t) \cap \mathbb{H}_k^{l+4}(0)] \cup \dots \\ &\quad \dots \cup [\mathbb{H}_{sp,k}^{l,c} \cap \mathbb{H}_k^l(0) \cap \mathbb{H}_k^{l+4}(-\Delta t)] , \end{aligned} \quad (4.13)$$

where $\mathbb{H}_{sp,k}^l \cap \mathbb{H}_k^l(-\Delta t) \cap \mathbb{H}_k^{l+4}(0)$ and $\mathbb{H}_{sp,k}^{l,c} \cap \mathbb{H}_k^l(0) \cap \mathbb{H}_k^{l+4}(-\Delta t)$ are the resulting convex regions. The detailed derivation of Eq. (4.13) is shown in attachment A.2. Comparing to the static collision region with only four needed intersection operations (see Eq. (4.7)), the dynamic collision region $\widehat{\mathbb{M}}_{COLL,k}^{dyn}$ takes 28 set operations, which is 6.5 times higher, so the calculation time is expected to be higher. As it will be seen later, this formulation will increase the computational calculation performance significantly, because all collided states are elements of this compact representation of the Minkowski region.

The event detection model $p^{dyn}(e_k = e_{COLL} | \mathbf{x}_k)$ of Eq. (4.2) for the approximated dynamic collision region $\widehat{\mathbb{M}}_{COLL}^{dyn}$ is reformulated to:

$$p^{dyn}(e_k = e_{COLL} | \mathbf{x}_k) = \begin{cases} 1 & \text{if } \mathbf{x}_k \in \widehat{\mathbb{M}}_{COLL,k}^{dyn} \\ 0 & \text{else} \end{cases} , \quad (4.14)$$

which can also be represented using sub indicators, similarly to Eq. (4.8), where a set union is equal to an addition and a set intersection is equal to a multiplication of the hyperplane associated step functions.

The dynamic event detection model of Eq. (4.14) can detect collisions within the transitions from one time point to a subsequent time step, which is similar to a flux approach, where the PDF volume is counted, which enters the collision region [125]. The transformation from Eq. (4.14) to

a flux calculation is exemplarily shown in attachment A.3 along one axis with position x and velocity v .

All in all, collision probability detection models for one time point and for a time interval, the corresponding collision regions in scene state and their representation via hyperplane areas were derived in this section. In the following, the introduced models, sets and reformulations will be used to simplify the calculations of the instantaneous collision probability, the collided and the non-collided PDF's.

4.5 Collided States

After the derivation of two collision event models, which indicate whether an arbitrary scene state $\mathbf{x} \in \mathbb{R}^n$ lays inside or passes through a collision region, the associated instantaneous collision probability value $P_{\text{inst,COLL},k}$ and the collided state PDF parameters have to be determined given the initial state PDF.

The instantaneous collision event probability $P_{\text{inst,COLL},k}$ represents the likelihood of being involved in a collision of two vehicles i and j at one predicted time step k . The formulation of the general definition according to Eq. (3.4) for arbitrary events is adapted to the specific collision event $e_k = e_{\text{COLL}}$, so that the desired instantaneous collision probability $P_{\text{inst,COLL},k}$ of static and dynamic collision region is calculated in the following way:

$$\begin{aligned} P_{\text{inst,COLL},k}^{\text{stat/dyn}} &= p(e_k = e_{\text{COLL}} | I_{k-1} = I_{\text{ctrl}}) \\ &= \int_{\mathbb{R}^n} p^{\text{stat/dyn}}(e_k = e_{\text{COLL}} | \mathbf{x}_k) p(\mathbf{x}_k | I_{k-1} = I_{\text{ctrl}}) d\mathbf{x}_k \quad . \end{aligned} \quad (4.15)$$

Generally, the integral of the instantaneous collision probability $P_{\text{inst,COLL},k}^{\text{stat/dyn}}$ in Eq. (4.15) does not have any analytic solution. Numerical methods are used e.g. Simpson's rule, Riemann sum [40] or Monte Carlo Simulation, where the particles are drawn from a distribution and the number of collided particles approximates the integral solution. The Monte Carlo Simulation can be implemented very easily but produce stochastic output values where the resulting variance can be decreased by taking a higher number of particles, which on the other hand increases the computational effort [98].

The collided state PDF's $p^{\text{stat/dyn}}(\mathbf{x}_k | e_k = e_{\text{COLL}}, I_{k-1} = I_{\text{ctrl}})$ are determined according to the general formulation of Eq. (3.5) using Eq. (4.15)

resulting in:

$$\begin{aligned}
 p^{\text{stat/dyn}}(\mathbf{x}_k | e_k = e_{\text{COLL}}, I_{k-1} = I_{\text{ctrl}}) &= \dots \\
 \dots &= \frac{p^{\text{stat/dyn}}(e_k = e_{\text{COLL}} | \mathbf{x}_k) p(\mathbf{x}_k | I_{k-1} = I_{\text{ctrl}})}{P_{\text{inst, COLL}, k}^{\text{stat/dyn}}} .
 \end{aligned} \tag{4.16}$$

The state PDF's of Eq. (4.16) represent the part of the initial PDF $p(\mathbf{x}_k | I_{k-1} = I_{\text{ctrl}})$ which are inside the collided region of the current predicted time (static) or which states were collided between the previous and current time point (dynamic). Non-parametric PDF estimators are multidimensional histograms, where the amount of Monte Carlo Simulation particles are allocated to predefined state sections, called bins, and counted. Increasing the amount of particles, the size of bins in a histogram can be downscaled, which increases the accuracy of the PDF. Nevertheless, the Monte Carlo Simulation needs a lot of computational resources and time, that's why an alternative is desired.

4.5.1 Probability Density Function Shape Truncation

In the following, an analytic technique is presented, which calculates both - the magnitude and the shape - of the collided state PDF simultaneously by approximating the PDF with another Gaussian PDF. This method assumes polygonally shaped, convex and point-symmetric vehicle shapes like introduced in the previous section and needs a Gaussian state PDF as initial distribution.

The idea bases on iterative truncations, which is similar to slicing a cake. The edges of the collision polygon equal the cuts of a knife. After executing all cuts and removals, the remaining piece is the wanted collided state PDF. Furthermore, its non-normalized volume is taken for the instantaneous collision probability. The authors of [122] already implement a similar principle, but are executing each cut as if it were an uncut cake, so that some pieces of the cake could be removed multiple times. Afterwards, the removed volumes are subtracted by the full volume, which will cause in the second case a lower non-collided volume value than in the first case, because of the neglected overlaps between the removed regions. Sometimes, these removals lead to negative collision probabilities and could create negative definite covariance matrices, which lead to other numerical problems. Furthermore it only considers boundaries where the paled region outside boundaries stays convex. In contrast to the method

of [122], the new presented method overcomes the required convexity for this free-event region and calculates only non-negative probabilities.

To determine the collision probability value and PDF in combination, the product of the collision event detection model $p(e_k = e_{\text{COLL}}|\mathbf{x}_k)$ and the initial free-event distribution $p(\mathbf{x}_k|I_{k-1} = I_{\text{ctrl}})$ will be reformulated in a similar way like in Eq. (4.16), where the two desired quantities dropped out:

$$p(e_k|\mathbf{x}_k) \cdot p(\mathbf{x}_k|I_{k-1} = I_{\text{ctrl}}) = p(\mathbf{x}_k|e_k = e_{\text{COLL}}, I_{k-1} = I_{\text{ctrl}}) \cdot P_{\text{inst,COLL}} \cdot$$

Assume an initial Gaussian PDF $p(\mathbf{x}_k|I_{k-1} = I_{\text{ctrl}}) = \mathcal{N}(\mathbf{x}_k; \hat{\mathbf{x}}_k, \Sigma_{\mathbf{x},k})$ and a static collision region $\mathbb{M}_{\text{COLL},k}^{\text{stat}}$ with four parallel edges $N_{\text{pe}} = 4$ according to Eq. (4.7), where the collision detection is represented by one function $E_{N_1}(\mathbf{x}_k)$ consisting of the product of N_1 step functions, each representing one linear edge of the collision region. The difference to the collision event detection model is that it starts by an arbitrary edge number N_1 and ends at the total number of parallel edge pairs N_{pe} :

$$\begin{aligned} E_{N_1}(\mathbf{x}_k) &= \prod_{l=N_1}^{2N_{\text{pe}}} \sigma((\mathbf{v}_k^l)^T \mathbf{x}_k - w_k^l) \\ &= \prod_{l=N_1}^{N_{\text{pe}}} \sigma((\mathbf{v}_k^l)^T \mathbf{x}_k - w_k^l) \cdot \sigma(-(\mathbf{v}_k^l)^T \mathbf{x}_k - w_k^{l+N_{\text{pe}}}) \quad . \end{aligned}$$

With the help of the function definition $E_{N_1}(\mathbf{x}_k)$, the collision event detection model of Eq. (4.8) can be applied as follows by using iteratively the Gaussian two-sided truncation according to Eq. (A.10):

$$\begin{aligned} p(e_k|\mathbf{x}_k) p(\mathbf{x}_k|I_{k-1} = I_{\text{ctrl}}) &= \mathcal{N}(\mathbf{x}_k; \hat{\mathbf{x}}_k, \Sigma_{\mathbf{x},k}) E_{N_1=1}(\mathbf{x}_k) \\ &\stackrel{\text{(A.10)}}{\approx} \mathcal{N}(\mathbf{x}_{k+1}; \hat{\mathbf{x}}_k^1, \Sigma_{\mathbf{x},k}^1) K_{\text{trunc},k}^1 E_{N_1=2}(\mathbf{x}_k) \\ &\quad \vdots \\ &\stackrel{\text{(A.10)}}{\approx} \mathcal{N}(\mathbf{x}_k; \hat{\mathbf{x}}_k^{N_{\text{pe}}}, \Sigma_{\mathbf{x},k}^{N_{\text{pe}}}) \prod_{h=1}^{N_{\text{pe}}} K_{\text{trunc},k}^h \\ &= p_{\mathbf{x},\text{COLL},k}(\mathbf{x}_k) P_{\text{inst,COLL},k}^{\text{stat}} \quad . \end{aligned}$$

This iterative implementation of Eq. (A.10) for approximating a truncated Gaussian PDF by another Gaussian PDF provides at one hand the collision

probability $P_{\text{inst,COLL},k}^{\text{stat}}$ and on the other hand the collision event state PDF $p^{\text{stat}}(\mathbf{x}_k | e_k = e_{\text{COLL}}, I_{k-1} = I_{\text{ctrl}})$, where the indices N_{pe} for the mean and covariance matrix are substituted by a “c”, meaning “collided”:

$$P_{\text{inst,COLL},k}^{\text{stat}} = p^{\text{stat}}(e_k = e_{\text{COLL}} | I_{k-1} = I_{\text{ctrl}}) := \prod_{h=1}^{N_{\text{pe}}} K_{\text{trunc},k}^h$$

$$p_{\mathbf{x},\text{COLL},k}^{\text{stat}}(\mathbf{x}_k) = p^{\text{stat}}(\mathbf{x}_k | e_k = e_{\text{COLL}}, I_{k-1} = I_{\text{ctrl}}) := \mathcal{N}(\mathbf{x}; \hat{\mathbf{x}}_k^c, \Sigma_{\mathbf{x},k}^c)$$

This procedure is shown for parallel edges in Fig. 4.4 or described by the following algorithm in short:

1. Start with initial PDF $p(\mathbf{x}_k | I_{k-1} = I_{\text{ctrl}}) = \mathcal{N}(\mathbf{x}; \hat{\mathbf{x}}_k, \Sigma_{\mathbf{x},k})$
2. Set $\mathcal{N}(\mathbf{x}_k; \hat{\mathbf{x}}_k^0, \Sigma_{\mathbf{x},k}^0) = \mathcal{N}(\mathbf{x}; \hat{\mathbf{x}}_k, \Sigma_{\mathbf{x},k})$, $l = 1$ and $g = 0$.
3. Apply \mathbb{H}_k^l and \mathbb{H}_k^{l+4} on the new Gaussian $\mathcal{N}(\mathbf{x}_k; \hat{\mathbf{x}}_k^g, \Sigma_{\mathbf{x},k}^g)$ via Eq. (A.10).
4. Set $g = g + 1$ and $l = l + 1$.
5. Repeat step 3 and 4 for all edge pairs to obtain the final value $P_{\text{inst,COLL},k}^{\text{dyn}}$ and PDF $p_{\mathbf{x},\text{COLL},k}^{\text{dyn}}(\mathbf{x}_k)$.

Each analytic truncation guarantees non-negative scaling factors so that the whole iterative truncation method produces non-negative collision probabilities. A disadvantage is that these approximations for the collision probability magnitude as well as the PDF depends on the order of the implemented edge pairs, which causes different values and shapes respectively. This effect is emphasized by using only one edge of the collision region instead of a pair of parallel edges, because each truncation and approximation combination would push the point of maximum likelihood away from the edge. By the usage of two parallel edges like in the aforementioned case, this effect is decreased. So it leads to less variance in the mean position during the iterative truncation process and stabilizes the truncation in a way.

A special case appears, if the initial Gaussian shaped survived state PDF $p(\mathbf{x}_k | I_{k-1} = I_{\text{ctrl}}) = \mathcal{N}(\mathbf{x}; \hat{\mathbf{x}}_k, \Sigma_{\mathbf{x},k})$ will have main axes which are parallel to all edges of the collision region. In this case, the Minkowski region is rectangular instead of polygonal and is oriented according to the main axis of the corresponding positional covariance matrix. A truncation and approximation along one axis does not impact the PDF shape along

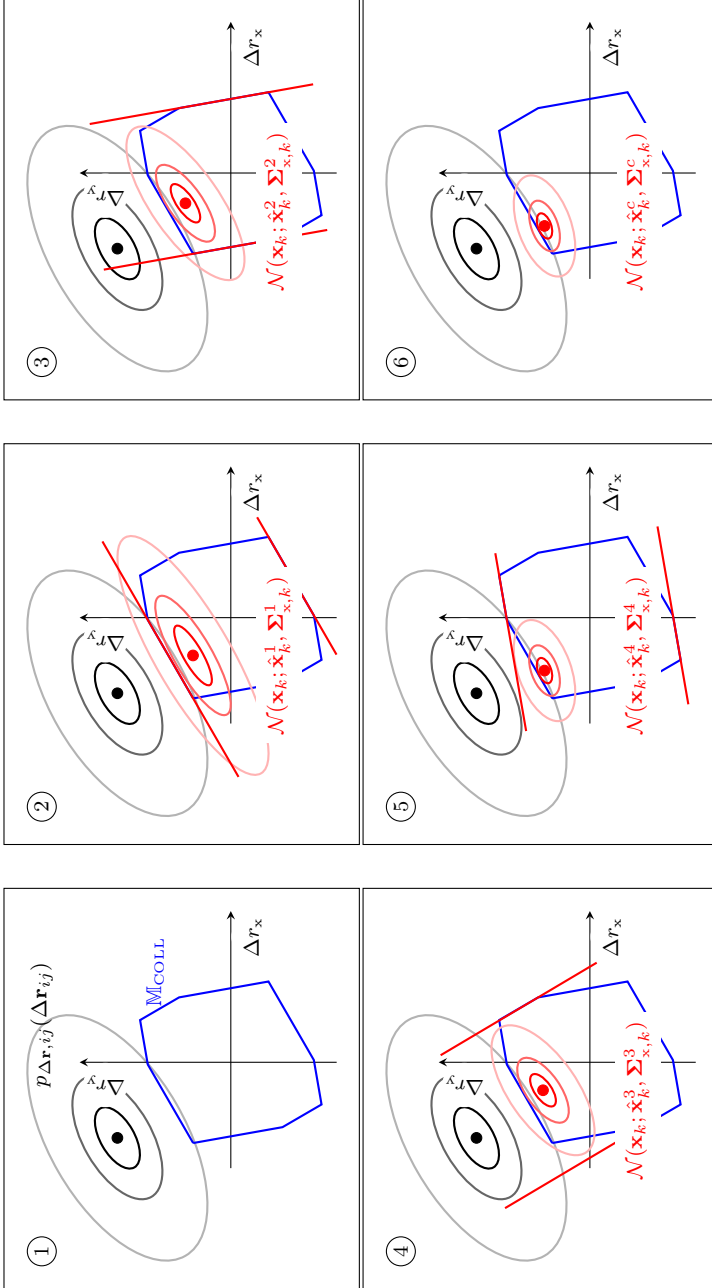


Figure 4.4: Schema of the iterative truncation algorithm for determining the collided state PDF $p_{x, \text{COLL}, k}^{\text{stat}}(\mathbf{x}_k) = \mathcal{N}(\mathbf{x}; \hat{\mathbf{x}}_k^c, \Sigma_{x,k}^c)$ given the collision region $M_{\text{COLL}, k}^{\text{stat}}$ with four parallel edges pairs N_{pe} and the initial state PDF $p(\mathbf{x}_k | I_{k-1}) = \mathcal{I}_{\text{eff}(1)} = \mathcal{N}(\mathbf{x}_k; \hat{\mathbf{x}}_k, \Sigma_{x,k})$. The red parallel lines represent the truncation planes. Not seen here is the projection of the Gaussian PDF's onto the normal vectors $\hat{\mathbf{v}}_k$ into the one-dimensional space. There, the one-dimensional Gaussian is truncated according to the projected plane boundaries. In the end, the truncated Gaussian PDF will be expanded to the full state dimension, where a projection into the positional space is seen in this schema

the other axis, because they are mutually orthogonal. Therefore, the two parallel edges truncation and approximations provides an exact solution and it is not depending on the order.

For the dynamical collision probability, a similar procedure is applied, which due to the higher number of sets and set operations is more complex than the calculation of the case of using a static collision region (see Eq.'s (4.13)). The implementation of a set intersection with a hyperplane restricted set \mathbb{H}_k^l is done by using the formulas for one-sided truncated Gaussian (see Eq.'s (A.9)). For parallel edges, the Eq.'s (A.10) for two-sided truncated Gaussian are applied. The union of two PDF's is applied according to the laws of conservation of stochastic momentum according to Eq. (A.8). The algorithm to obtain the dynamical collision probability magnitude $P_{\text{inst,COLL},k}^{\text{dyn}}$ and PDF shape $p_{\text{x,COLL},k}^{\text{dyn}}(\mathbf{x}_k)$ is given by:

1. Start with initial PDF $p(\mathbf{x}_k | I_{k-1} = I_{\text{ctrl}}) = \mathcal{N}(\mathbf{x}; \hat{\mathbf{x}}_k, \Sigma_{\mathbf{x},k})$.
2. Set $\mathcal{N}(\mathbf{x}_k; \hat{\mathbf{x}}_k^0, \Sigma_{\mathbf{x},k}^0) = \mathcal{N}(\mathbf{x}; \hat{\mathbf{x}}_k, \Sigma_{\mathbf{x},k})$, $l = 1$ and $g = 0$.
3. For edge pair l and $l + 4$ apply the splitting hyperplane restricted set $\mathbb{H}_{\text{sp},k}^l$ to truncate the current Gaussian $\mathcal{N}(\mathbf{x}_k; \hat{\mathbf{x}}_k^g, \Sigma_{\mathbf{x},k}^g)$ via Eq. (A.9).
4. Apply $\mathbb{H}_k^l(-\Delta t)$ and $\mathbb{H}_k^{l+4}(0)$ on the obtained Gaussian from step 3 via Eq. (A.9).
5. For edge pair l and $l + 4$ apply the complement splitting hyperplane restricted set $\mathbb{H}_{\text{sp},k}^{l,c}$ to truncate the current Gaussian $\mathcal{N}(\mathbf{x}_k; \hat{\mathbf{x}}_k^g, \Sigma_{\mathbf{x},k}^g)$ via Eq. (A.9).
6. Apply $\mathbb{H}_k^l(0)$ and $\mathbb{H}_k^{l+4}(-\Delta t)$ to the obtained Gaussian from step 5 via Eq. (A.9).
7. Merge both Gaussian PDF's from steps 4 and 6 with Eq. (A.8) to obtain $\mathcal{N}(\mathbf{x}_k; \hat{\mathbf{x}}_k^{g+1}, \Sigma_{\mathbf{x},k}^{g+1})$.
8. Set $g = g + 1$ and $l = l + 1$.
9. Repeat Step 3 to 8 for all edge pairs to obtain the final value $P_{\text{inst,COLL},k}^{\text{dyn}}$ and PDF $p_{\text{x,COLL},k}^{\text{dyn}}(\mathbf{x}_k) = \mathcal{N}(\mathbf{x}_k; \hat{\mathbf{x}}_k^{N_{\text{pe}}}, \Sigma_{\mathbf{x},k}^{N_{\text{pe}}})$

The main difference between the previous algorithm for static collision regions is that this algorithm executes additional truncations by the splitting hyperplanes $\mathbb{H}_{\text{sp},k}^l$ and its complement, the non-parallel truncation planes $\mathbb{H}_k^l(0)$ and $\mathbb{H}_k^{l+4}(-\Delta t)$ and a merging procedure between the two

left-over truncated PDF's produced by the splitting hyperplane and its complement.

In this section, new methods for the static and dynamic collision region were introduced, making use of only analytical formulas. In the oncoming section, the new analytical truncation method is investigated by its accuracy and time consumption compared to Monte Carlo Simulation.

4.5.2 Evaluation of Collision State Probability Density Function

In the previous sections, static and dynamic collision regions were introduced which can calculate the desired instantaneous collision probability and the collided PDF. The following experiments investigate the iterative truncation methods in terms of accuracy and computational time comparing to a naive Monte Carlo Simulation with different amount of particles. The last experiment of this section shows the significant difference in the event detection between the static and dynamic collision region.

Calculation Time vs. Accuracy for Static Collision Region

In the first experiment, the accuracy of instantaneous collision probability approximations with static collision according to Eq. (4.15) is determined for 1000 different constellations. The numerical integration library quad of the Python Scipy package [158], which uses a Clenshaw–Curtis method with Chebyshev polynomials, was used as reference. These constellations are uniformly sampled for the following states: positions in polar coordinate space, vehicle orientation angles, variance along x-axis and a relative variance value to obtain the y-axis variance (see Sec. A.5.1 for variables and ranges). The relative error of collision probability magnitudes for the analytic method and the Monte Carlo Simulation are summarized in boxplots depending on the reference magnitude (see Fig. 4.5).

One can see that the accuracy of the Monte Carlo Simulation is always the highest for regions with high magnitude and it becomes less accurate for small probabilities. This is due to the small number of particles which are drawn in small density regions. There, the accuracy is limited due to the discrete set of particles and can reach e.g. $1/100.000 = 10^{-5}$ for the MC with $100k$ particles. The intervals without boxplots represent magnitude intervals without any collision because of missing particles. The calculation with Monte Carlo Simulation oversees possible low probable collision events.

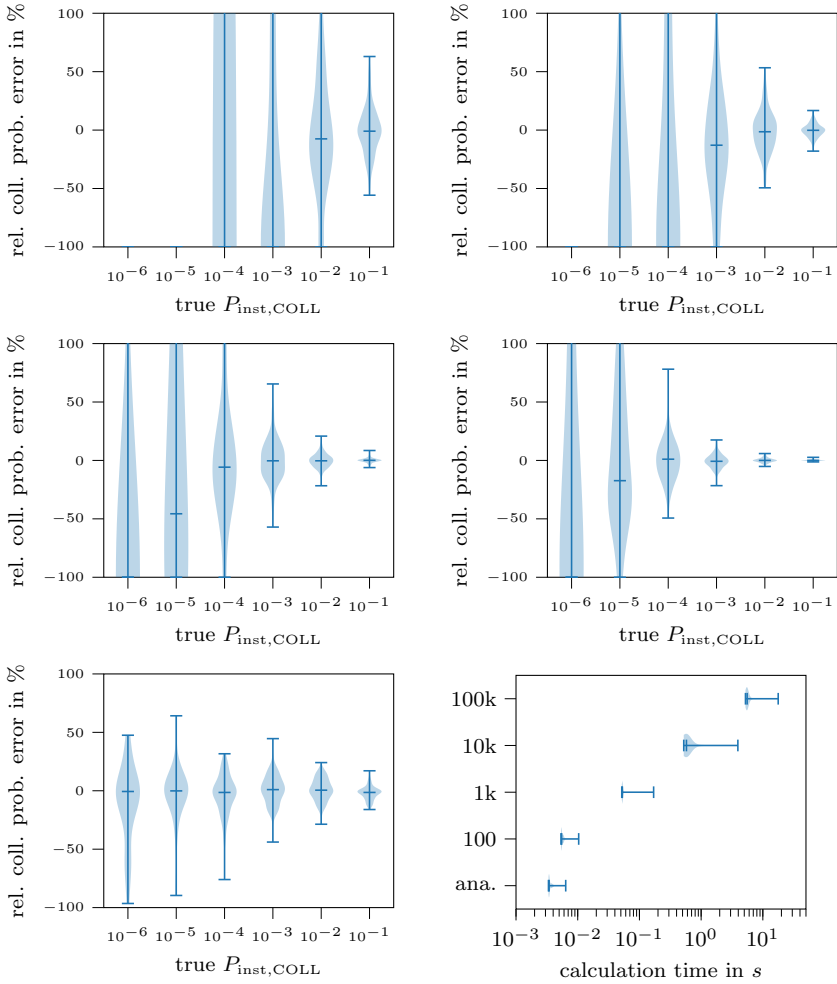


Figure 4.5: Relative signed error of a collision probability calculation with static collision region $M_{\text{COLL}}^{\text{stat}}$ depending on different magnitude intervals with ticks label of lower bin limit: Monte Carlo Simulation with 100 particles (top left), 1k particles (top right), 10k particles (center left), 100k particles (center right) and analytic truncation method (Bottom left). Bottom right: Boxplots of the computational time distribution for Monte Carlo Simulation with different amount of particles and the analytic truncation method.

In contrast to Monte Carlo Simulation, the accuracy of the analytic method is nearly constant in a broad magnitude interval of $P_{\text{inst, COLL}}$ values between 10^{-6} and 1.0. Furthermore, it is not neglecting any collisions up to 10^{-6} . In case of probability values lower than 10^{-6} , numerical difficulties appears. The analytic method is more accurate in intervals with high collision probabilities (0.1 – 1.0) than the Monte Carlo Simulation with 100 particles and similarly accurate than a Monte Carlo Simulation with 10 times more particles .

The plot in the right, bottom corner of Fig. 4.5 shows boxplots of computational time for all Monte Carlo Simulations and the analytic method. The computational effort of Monte Carlo Simulation increases linearly with the amount of particles used for this stochastic integration method, where a Monte Carlo Simulation with 100 particles needs around 6 *ms* in average. The analytic method takes only 4 *ms* per evaluation and is more accurate than the Monte Carlo Simulation with 100 particles over a broad range of magnitudes.

Calculation Time vs. Accuracy for Dynamic Collision Region

The second investigation is similar to the evaluations of the previous section but with dynamic collision regions instead of static regions. To obtain 1000 constellations, also the velocity in polar coordinates is uniformly sampled. The reference value is given by a numerical flux integration. The time interval between two subsequent time points is set to 0.2 *s*. The relative error and the computational time for Monte Carlo Simulations and the analytic truncation technique are depicted in Fig. 4.6.

The results are very comparable to those of static regions. The computational time for Monte Carlo Simulation has nearly doubled comparing to the calculations for static regions and the analytic calculations has more than tripled to 13 *ms* due to the increasing number of PDF truncations and merges. Also for dynamic considerations, the analytic approach outperforms the Monte Carlo Sampling technique in computational time and accuracy over a broad range.

Velocity Dependency

To show the difference in collision event detection between static and dynamic collision region considerations, a constellation with very low instantaneous collision probability was set as an initial time point and the Gaussian is predicted into a subsequent time point according to a constant

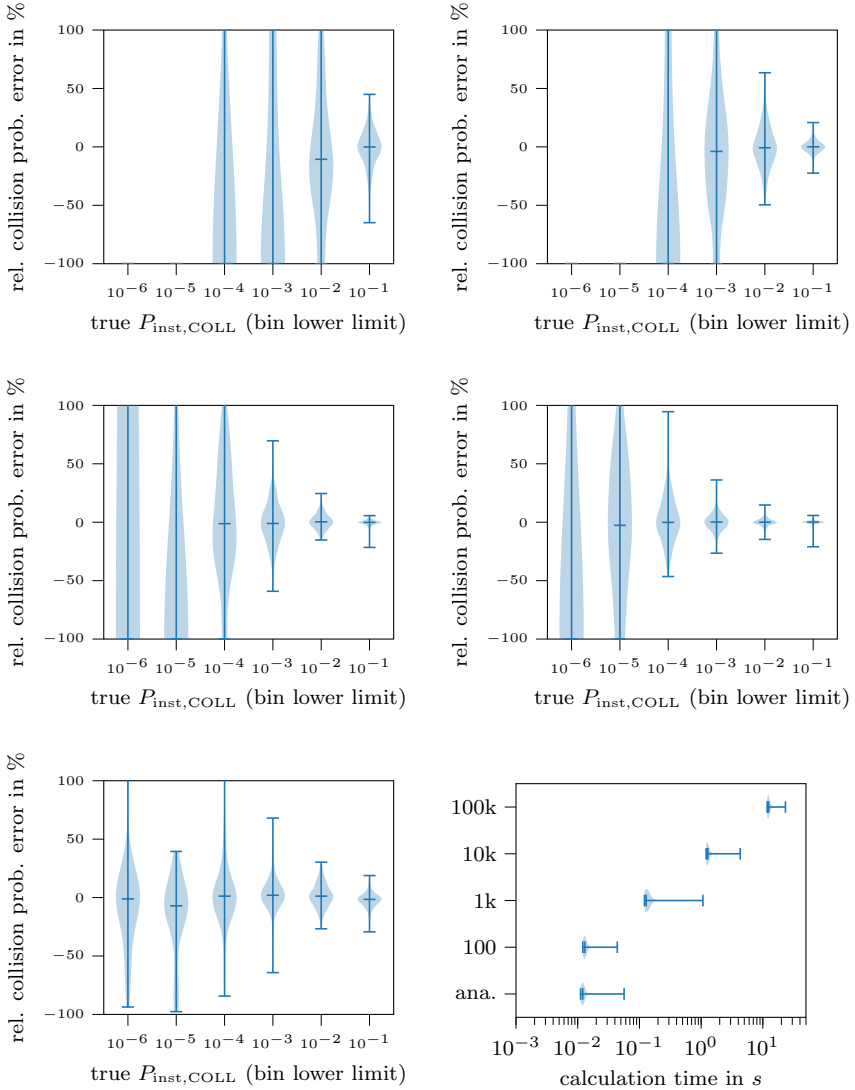


Figure 4.6: Relative signed error of collision probability depending on reference magnitude for calculation methods using dynamic state regions \mathbb{M}_{COLL}^{dyn} : Monte Carlo Simulation with 100 particles (top left), 1k particles (top right), 10k particles (center left) and analytic truncation method (Bottom left). Bottom Right: Boxplots of the computational time distribution for Monte Carlo Simulation with different amount of particles and the analytic truncation method.

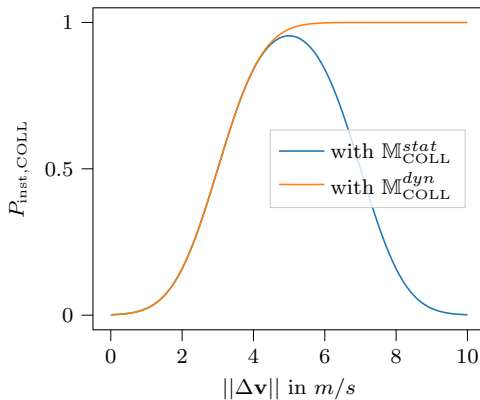


Figure 4.7: Analytic truncation calculation depending on relative velocity size for static $M_{\text{COLL}}^{\text{stat}}$ and dynamic $M_{\text{COLL}}^{\text{dyn}}$ collision region, where the initial state has a small collision probability and the trajectories point into the direction of an object which will be penetrated for high speeds before ending at time step k .

velocity motion model, where the connecting trajectory would penetrate an object. Different moving velocity norms $\|\Delta\mathbf{v}\|$ show similarities and difference in collision probability calculation for static or dynamic collision regions in Fig. 4.7.

One can see that calculations with both collision regions, the static and the dynamic, leads to similar results for low transition velocities. This reflects cases 1 and 2 of Fig. 4.1, where collisions can be detected through the end point of the transition in time step k . Case 3 of Fig. 4.1 becomes dominant for higher velocities, where the static region probability calculation drops down to zero. This is due to the fact, that after the transition into the next time point, the Gaussian PDF is far away from the collision region so that the overlap is small like at the previous time step. In contrast to the static region calculation, the dynamic region detects the penetration of the collision region also for high velocities and converges to its maximum value. This example shows that the dynamic collision region comparing to the static collision region consideration prevents errors at high relative velocities.

4.6 Non-Collided States

After the determination of the collision event PDF and the instantaneous collision probability, which are needed for the severity calculation and the instantaneous collision risk, the quantities to determine time-course sensitive (tcs) values like the time-course sensitive survival probability, risk and utilities, the non-collided PDF parts and the instantaneous non-collision probability are needed. The instantaneous non-collision probability is equal to the instantaneous survival probability in case of only one predicted event at the current time step. Also these quantities have to be as accurate as possible to properly predict future costs.

Given the instantaneous collision probability $P_{\text{inst,COLL},k}$ and in case of one event type, the instantaneous survival probability $P_{\text{inst,surv},k}$ is given by the counter probability like in Eq. (3.4):

$$P_{\text{inst,surv},k} = 1 - P_{\text{inst,COLL},k} \quad . \quad (4.17)$$

The survived or non-collided state PDF $p_{\text{x,surv},k}(\mathbf{x}_k)$ can be calculated by reformulating Eq. (3.5):

$$p_{\text{x,surv},k}(\mathbf{x}_k) = \frac{p(\mathbf{x}_k | I_{k-1} = I_{\text{ctrl}}) - P_{\text{inst,COLL},k} \cdot p_{\text{x,COLL},k}(\mathbf{x}_k)}{P_{\text{inst,surv},k}} \quad . \quad (4.18)$$

Note, that this equation can only determine a survived state PDF with $p_{\text{x,surv},k}(\mathbf{x}_k) \geq 0$ for all \mathbf{x}_k , if the density values of the weighted collided state PDF $p_{\text{x,COLL},k}(\mathbf{x}_k)$ are smaller than the non-truncated PDF: $P_{\text{inst,COLL},k} \cdot p_{\text{x,COLL},k}(\mathbf{x}_k) \leq p(\mathbf{x}_k | I_{k-1} = I_{\text{ctrl}})$. This cannot be guaranteed by applying the analytic truncation method of the previous sections for the collided PDF, because it is producing an approximated Gaussian PDF. As a consequence, for some \mathbf{x}_k , the condition for non-negativity is not fulfilled and the simple fraction with subtraction of Eq. (4.18) cannot be applied, without causing inconsistent values. That is why another way is needed to infer $p_{\text{x,surv},k}(\mathbf{x}_k)$.

In the following subsections, two methods are presented, which differ in the amount of Gaussian PDF's to approximate $p_{\text{x,surv},k}(\mathbf{x}_k)$.

4.6.1 Unimodal Gaussian

In the first approach the survived state PDF $p_{\text{x,surv},k}(\mathbf{x}_k)$ is assumed to be one Gaussian PDF:

$$p_{\text{x,surv},k}(\mathbf{x}_k) \approx \mathcal{N}(\mathbf{x}_k; \hat{\mathbf{x}}_k^{nc}, \Sigma_{\mathbf{x},k}^{nc}) \quad ,$$

where $\hat{\mathbf{x}}_k^{nc}$ is the mean vector and $\Sigma_{x,k}^{nc}$ is the covariance matrix of the approximating Gaussian. The choice of a Gaussian PDF is motivated by reusing transition formulas of the prediction step as well as its simple representation by a small set of parameters. But, instead of using the simple subtraction method of Eq. (4.18) and fit it into the PDF, the Gaussian parameters are determined with the help of the **conservation of stochastic momentum** (see A.6.2 for definition). This method can directly calculate the missing Gaussian parameter by taking the Gaussian parameters of the collided $p_{x,\text{COLL},k}(\mathbf{x}_k) = \mathcal{N}(\mathbf{x}_k; \hat{\mathbf{x}}_k^c, \Sigma_{x,k}^c)$ and initial/non-truncated state PDF $p(\mathbf{x}_k | I_{k-1} = I_{\text{ctrl}}) = \mathcal{N}(\mathbf{x}_k; \hat{\mathbf{x}}_k, \Sigma_{x,k})$. The following equations are gained by the conservation of stochastic momentums for the first and second order:

$$\begin{aligned} \hat{\mathbf{x}}_k &= P_{\text{inst,COLL},k}^{ana} \cdot \hat{\mathbf{x}}_k^c + (1 - P_{\text{inst,COLL},k}^{ana}) \cdot \hat{\mathbf{x}}_k^{nc} \\ \Sigma_{x,k} &= P_{\text{inst,COLL},k}^{ana} \left(\Sigma_{x,k}^c + (\hat{\mathbf{x}}_k^c - \hat{\mathbf{x}}_k)(\hat{\mathbf{x}}_k^c - \hat{\mathbf{x}}_k)^T \right) + \dots \\ &\quad \dots + (1 - P_{\text{inst,COLL},k}^{ana}) \left(\Sigma_{x,k}^{nc} + (\hat{\mathbf{x}}_k^{nc} - \hat{\mathbf{x}}_k)(\hat{\mathbf{x}}_k^{nc} - \hat{\mathbf{x}}_k)^T \right) . \end{aligned}$$

Solving these equations for the wanted parameters, provides the following set of formulas:

$$\begin{aligned} \hat{\mathbf{x}}_k^{nc} &= \frac{1}{1 - P_{\text{inst,COLL},k}^{ana}} \left(\hat{\mathbf{x}}_k - P_{\text{inst,COLL},k}^{ana} \cdot \hat{\mathbf{x}}_k^c \right) \\ \Sigma_{x,k}^{nc} &= \frac{1}{1 - P_{\text{inst,COLL},k}^{ana}} \Sigma_{x,k} - (\hat{\mathbf{x}}_k^{nc} - \hat{\mathbf{x}}_k)(\hat{\mathbf{x}}_k^{nc} - \hat{\mathbf{x}}_k)^T - \dots \\ &\quad \dots - \frac{P_{\text{inst,COLL},k}^{ana}}{1 - P_{\text{inst,COLL},k}^{ana}} \left(\Sigma_{x,k}^c + (\hat{\mathbf{x}}_k^c - \hat{\mathbf{x}}_k)(\hat{\mathbf{x}}_k^c - \hat{\mathbf{x}}_k)^T \right) . \end{aligned}$$

To validate the performance of the instantaneous survival probability magnitude, in A.4 an evaluation regarding the accuracy is done similarly to the validation shown in Sec. 4.5.2. The results are that the accuracy for small survival probabilities is in between a Monte Carlo Simulation with 100 and $1k$ particles. In case of high survival probabilities, the relative errors are negligible small. In the next section, the accuracies of the collided and non-collided PDF's are validated.

4.6.2 Evaluation of Using Unimodal Gaussians for Survived State Probability Density Function

Next to the magnitudes of the instantaneous collision or survival probability, the shapes of the truncated PDF's have to be assessed. The PDF

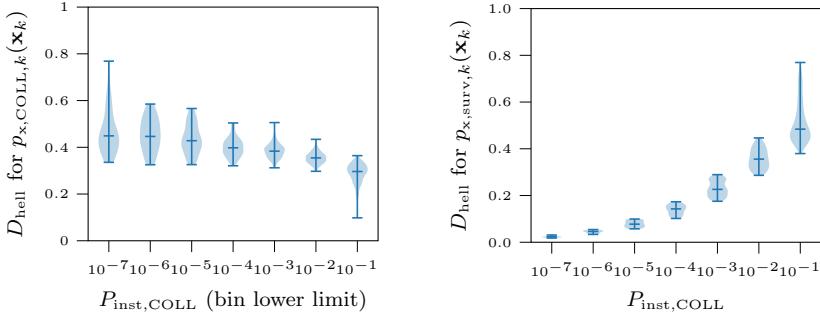


Figure 4.8: Hellinger Distance D_{hell} of original and approximated PDF for collision state PDF $p_{x, COLL, k}(\mathbf{x}_k)$ (left) and for survived state PDF $p_{x, surv, k}(\mathbf{x}_k)$ (right). The accuracy for shapes of the collided state PDF is nearly constant over collision probabilities, whereas the accuracy for survived state PDF decrease by higher collision probabilities.

shapes determine the magnitudes and survival probabilities of subsequent time steps e.g. if the truncation process removes area, which would collide in the next time step, the collision probability will be estimated as too small. On the other hand, if within the truncation process parts are not being removed, the collision probability of subsequent time steps could be overestimated and cause multiple detections. The PDF accuracy is determined by using the Hellinger Distance, outlined in Sec. A.6.4. It determines the similarity of two distributions by either integrating over the collision regions \mathbb{M}_{COLL} to obtain the collided PDF shape accuracy or over the region outside the collision region $\mathbb{R}^n \setminus \mathbb{M}_{COLL}$ for the non-collided PDF accuracy. Both distance measures are depicted in Fig. 4.8 depending on the collision probability magnitude value. A Hellinger Distance D_{hell} of zero means that the reference and the approximated PDF are equal. If there are no overlaps between both PDF's, the Hellinger Distance will become one.

One can see on the left side of Fig. 4.8 that for the collided state PDF, the distance is nearly constant around $D_{hell} = 0.4$ over an interval from 10^{-7} to 1.0. In contrast, the shape accuracy for the survived part increases with higher collision probability, so that the calculated PDF which was obtained by applying the conservation of momentum differs from the true survived PDF. The reasons for higher dissimilarities in case of high collision probabilities lays in the unimodal approximation with Gaussian

PDF's, which cannot represent the discontinuous shape of the true state distribution.

In Fig. 4.9, two cases with Gaussian potential ellipses of initial (black), collided (red) and non-collided PDF (orange) are shown. In the left figure, the collided region is big compared to the initial Gaussian and occupies the main part of the initial PDF. The survived Gaussian PDF overlaps only with a small part into the old collision region (blue), the outer part is represented well. Now, considering the case on the right plot, the collision region is big compared to the extent of the initial Gaussian and is located very near to the distribution center. Like in the first case, the collided PDF is represented well after the truncation process, but after the implementation of the conservation of momentum, the non-collided Gaussian still overlaps with the collision region. It keeps its center with high density values in the proximity of the collision region center and widens its extent or variance. The survived Gaussian PDF only blows up and the distribution inside and outside of the collision region is represented inaccurately. The consequences are that these remaining overlaps of the survived part with the initial PDF do not lead to vanishing collision probabilities at subsequent time steps like it is desired for non-multiple collision detection. The method with an unimodal PDF representation via one Gaussian PDF is not suitable for these cases.

To overcome this issue, instead of using one Gaussian to approximate the non-collided part, one can use more than one Gaussians, approximating the main PDF parts outside the collision region (see Fig. 4.10).

4.6.3 Gaussian Mixture

The idea of using a Gaussian Mixture can also be explained with the following example: One vehicle follows the middle lane of a three-lane highway. A slower vehicle at the front appears, so that the vehicle has two options: either it tailgates the frontal vehicle or it overtakes. If the oncoming vehicle will not change its velocity or if the relative speed to the frontal vehicle is too high, the tailgating maneuver would lead to a crash and it can only avoid the a collision by executing an additional steering maneuver. The question is into which direction the vehicle should move, left or right? If the approaching vehicle does not care about the obligation of overtaking on the left side, it has two optional scenarios depending on the frontal vehicle. The occurrence of two motion opportunities gets more obvious for an intersection scenario, where a vehicle could either yield or not yield in case of an approaching other vehicle. These two arising motion

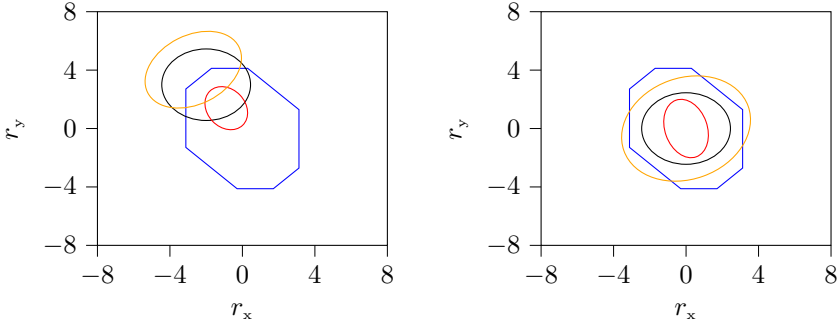


Figure 4.9: Examples for PDF shapes after analytic truncation and after applying conservation of stochastic momentum for two constellations with static collision region (blue). Left: Slighed or touching initial Gaussian PDF (black), where the sigma ellipses of the collided PDF (red) and the non-collided PDF (yellow) do not overlap. Right: Collided and non-collided PDF's are overlapping after truncation process, when the initial PDF largely overlaps with the collision region.

options could be represented by taking two Gaussian PDF's, each Gaussian representing one motion option e.g., left or right overtaking. To create two Gaussians out of one Gaussian, the initial PDF with one Gaussian has to be split.

This idea should be integrated into the prediction process, to let the ego vehicle being aware of this phenomenon. For that, the survived state PDF $p_{x,\text{surv},k}(\mathbf{x}_k)$ is now assumed to be a bimodal Gaussian Mixture distribution:

$$\mathcal{N}(\mathbf{x}_k; \hat{\mathbf{x}}_k, \Sigma_{x,k}) \rightarrow w^1 \mathcal{N}(\mathbf{x}_k; \hat{\mathbf{x}}_k^1, \Sigma_{x,k}^1) + w^2 \mathcal{N}(\mathbf{x}_k; \hat{\mathbf{x}}_k^2, \Sigma_{x,k}^2) \quad (4.19)$$

$$w^1 + w^2 = 1$$

with weights w^1 and w^2 , scene state means $\hat{\mathbf{x}}_k^1$ and $\hat{\mathbf{x}}_k^2$ and the covariance matrices $\Sigma_{x,k}^1, \Sigma_{x,k}^2$ of two clustered state PDF parts at one predicted time point k .

Furthermore, not in each scene with more than one traffic participants, two options are similarly likely, meaning that it is hard to distinguish between both intentions. Take the example with the oncoming vehicle on a highway: if the oncoming vehicle drives on the left lane and the frontal vehicle on the right lane, there will be less benefit to split the Gaussian

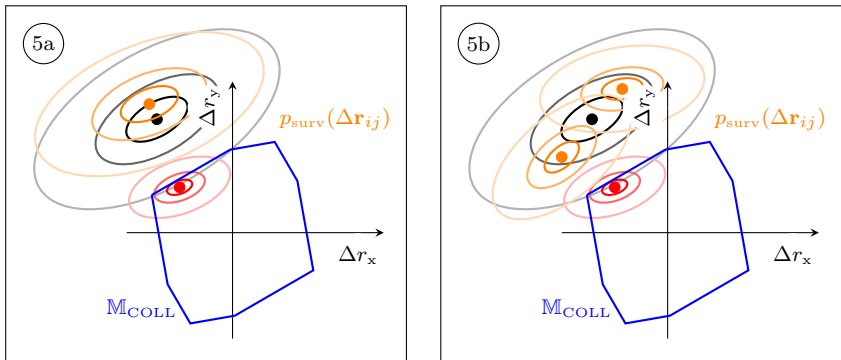


Figure 4.10: Extension of truncation approach by considering multimodal Gaussian Mixture Models. Left: Truncation of previous approach with unimodal Gaussian. Right: Approximation of survived probability with two Gaussian PDF's to improve accuracy.

into two for representing PDF parts far away on the right side of the right lane. This would bind computational resources for very unlikely motion patterns and would not increase the accuracy much. In this case, the distribution can stay unimodal. The other reason for taking a unimodal representation is when the Gaussian's of a Gaussian Mixture Model would be very similar to each other e.g. if the oncoming vehicle is far away from the frontal vehicle, the Gaussian components for left or right overtaking are still equal. Both examples show that there is a transition from unimodal to multimodal depending on the scene and its predicted evolution.

Because of this, two important question arise:

- At which predicted time point k of the scene evolution should the Gaussian's be split?
- How is the split executed?

For the first question of when to split, two heuristic criteria are formulated, based on the positional relation of the collision region and the initial PDF. These criteria consider on the one hand the proximity of the collision region to the PDF and on the other hand the allocation of the probabilities between both possible scenarios. If both criteria are fulfilled, the split will be executed. The second question contains the question, how can one Gaussian be allocated into two Gaussian PDF by considering the collision region.

In the following, both conditions for splitting and the splitting procedure are introduced.

Proximity Criterion

The first criterion regards the proximity of the collision region to the initial Gaussian PDF. If the initial distribution is far away from the collision region, the survived state PDF will be very similar to the initial, non-truncated PDF. Because the non-truncated PDF is an unimodal Gaussian, the survived state PDF can stay as one unimodal Gaussian, too.

The proximity criterion is a transformed Mahalanobis distance, where the mean $\hat{\mathbf{x}}_k$ and the covariance matrix $\Sigma_{x,k}$ of the initial PDF are taken to evaluate distance to the mean state $\hat{\mathbf{x}}_k^c$ of the collided state PDF in the relative positional space:

$$\begin{aligned} D_{\text{prox}} &= \exp\left(-\frac{1}{2}\Delta\hat{\mathbf{r}}_k^T\Sigma_{r,k}^{-1}\Delta\hat{\mathbf{r}}_k\right) \\ \Delta\hat{\mathbf{r}}_k &= \mathbf{C}^{ij}(\hat{\mathbf{x}}_k - \hat{\mathbf{x}}_k^c) \\ \Sigma_{r,k} &= \mathbf{C}^{ij}\Sigma_{x,k}(\mathbf{C}^{ij})^T, \end{aligned}$$

where \mathbf{C}^{ij} is the transformation matrix into the relative positional space of two vehicles i and j , introduced in Eq. (4.4). The idea is also depicted in Fig. 4.11 on the left side.

The condition, whether the proximity criteria is fulfilled, is given by:

$$D_{\text{prox}} > D_{\text{prox}}^{\text{lim}},$$

where $D_{\text{prox}}^{\text{lim}} \in]0, 1]$ is the preset proximity parameter. Small proximity parameters $D_{\text{prox}}^{\text{lim}}$ mean that the condition is also true for far distant vehicles. This causes early splits and unnecessarily redundant calculations in the prediction process. In contrast, high proximity parameters $D_{\text{prox}}^{\text{lim}} \approx 1$ lead to delayed splits, so that the Gaussian is widened through the penetration of the collision region into the initial PDF like it is was shown in the right hand picture of Fig. 4.9. Therefore, the golden mean is in between.

Allocation Criterion

Some scene evolutions are more likely than others. A vehicle on a left lane of a highway road would not consider to move to the right most lane to overtake a vehicle on the middle lane from the right. Although there is

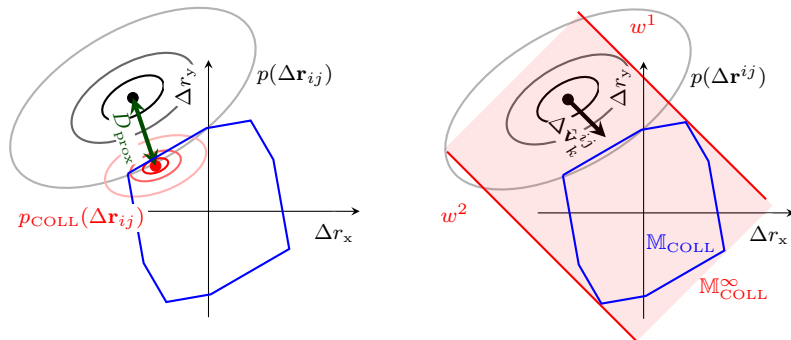


Figure 4.11: Splitting Criteria. Left: The proximity criterion checks whether the Mahalanobis Distance D_{prox} between the non-truncated PDF $p(\Delta\mathbf{r}_{ij})$ and the collided state PDF $p_{\text{COLL}}(\Delta\mathbf{r}_{ij})$ whether states are close enough. Right: According to the current relative motion direction $\Delta\mathbf{v}_{ij}$, the allocation criterion determines the volumes under $p(\Delta\mathbf{r}_{ij})$ above (w^1) and below (w^2) at the predicted collision region $\mathbb{M}_{\text{COLL}}^{\infty}$ (red opaque valley). The ratio of both volumes is compared to a preset value, where a raise of the ratio leading to a split. Both criteria ensures that the shapes of the non-truncated PDF and the collision region are both taken into account for a split decision.

a chance to do so but, if there is no need to consider this scenario in the scene evolution, it can be neglected. Concentrating on the most probable scenarios helps to reduce the number of splits in a complex multiple vehicle scenarios. This is achieved with the aid of the ‘‘allocation criterion’’.

The allocation criterion focuses on the ratio between the future weights w^1 and w^2 of the GMM. If one weight compared to the other is much greater $w^{1/2} \gg w^{2/1}$, it would not cause a split. If both weights will be very similar, two very indifferent alternatives arise like yielding or not yielding at an intersection. In that case, a split is forced.

To predict the future weights without having them predicted at a specific time point k is a catch-22. To avoid going back into the prediction process and making double calculations, a simplified forecast of these future weights is implemented to calculate them approximatively. This forecast is based on the view, how the initial state PDF would look like if the collision region fully penetrates the state PDF according to a constant velocity direction. The collision region would create a swath with lateral width $b^+ - b^-$ into the initial state PDF during an infinite time horizon. The predicted swath region $\mathbb{M}_{\text{COLL}}^{\infty}$ (red) in relative positional space is

presented in Fig. 4.11 and is given by:

$$\mathbb{M}_{\text{COLL}}^{\infty} = \{\mathbf{r} \in \mathbb{R}^2 | b^+ \geq \mathbf{a}_{\text{orth}}^T \mathbf{r} \geq b^-\} .$$

Note, that this region is only exact, if the Gaussian is not diverging by motion uncertainties, the motion direction is constant and the collision region is being located far away from the state PDF, so that volumes in the shadow of the collision region can be neglected. For other constellations it is providing a rough approximation of the future evolution. The line normal vector \mathbf{a}_{orth} is calculated by a 90 degree rotation of the mean relative velocity $\Delta \hat{\mathbf{v}}_k^{ij}$ like in the following

$$\begin{aligned} \mathbf{a}_{\text{orth}} &= \frac{1}{\|\hat{\mathbf{v}}_k\|} \mathbf{R}_{\text{rot}}^{90} \Delta \hat{\mathbf{v}}_k^{ij} \\ \Delta \hat{\mathbf{v}}_k^{ij} &= \hat{\mathbf{v}}_k^i - \hat{\mathbf{v}}_k^j . \end{aligned}$$

In case of missing relative motions or increasing distances $\hat{\mathbf{v}}_k^T \hat{\mathbf{r}}_k \geq 0$ between the state PDF and the collision region, the allocation criterion is unsatisfied, so that a split won't happen.

For noticeable relative motions, the collision region produces a swath $\mathbb{M}_{\text{COLL}}^{\infty}$. Its boundary shifts b^+ and b^- are the distances from the coordinate center according to the normal vector \mathbf{a}_{orth} . They mark the projected boundary of the original collision region $\mathbb{M}_{\text{OCC}}^{ij}(\gamma_k^i, \gamma_k^j)$, which was introduced in Eq. (4.5):

$$\begin{aligned} b^- &= \min_{\mathbf{r} \in \mathbb{M}_{\text{OCC}}^{ij}(\gamma_k^i, \gamma_k^j)} (\mathbf{a}_{\text{orth}}^T \hat{\mathbf{r}}_k) \\ b^+ &= \max_{\mathbf{r} \in \mathbb{M}_{\text{OCC}}^{ij}(\gamma_k^i, \gamma_k^j)} (\mathbf{a}_{\text{orth}}^T \hat{\mathbf{r}}_k) . \end{aligned}$$

A simple check of all corners or a simplex algorithm produces solutions for both shifts.

The weights w^1 and w^2 represent the remaining volume of the survived PDF at infinite time horizon which are separated by the collided swath region $\mathbb{M}_{\text{COLL}}^{\infty}$. The weights representing the non-collided PDF volumes can be determined as follows:

$$\begin{aligned} w^1 &= \int_{\mathbb{R}^2} \sigma(b^+ + \mathbf{a}_{\text{orth}}^T \mathbf{r}_k) \mathcal{N}(\mathbf{r}_k; \hat{\mathbf{r}}_k, \boldsymbol{\Sigma}_{\mathbf{r},k}) d\mathbf{r}_k \\ w^2 &= \int_{\mathbb{R}^2} \sigma(b^- - \mathbf{a}_{\text{orth}}^T \mathbf{r}_k) \mathcal{N}(\mathbf{r}_k; \hat{\mathbf{r}}_k, \boldsymbol{\Sigma}_{\mathbf{r},k}) d\mathbf{r}_k \end{aligned}$$

with an analytic solution that is given by the algorithm shown in Eq. (A.6.3).

The allocation criteria is then fulfilled if the following check holds:

$$D_{\text{alloc}} = \frac{\min(w^1, w^2)}{w^1 + w^2} > D_{\text{alloc}}^{\text{lim}} ,$$

where $D_{\text{alloc}}^{\text{lim}} \in [0, 1]$ is a preset allocation threshold parameter. If this value is too small, the Gaussian PDF is split also in cases if there is a very unlikely option. If this value is too high, this could neglect very likely scenarios and lead to drastic misinterpretations. Then, the survived PDF is widened like in case of unimodality (right hand picture of Fig. 4.9).

In contrast to the proximity criterion, the allocation criterion takes the collision region with its shape into account and not only its location. It completes the consideration when to split the one Gaussian PDF depending on a collision region.

Splitting Procedure

If the proximity and the allocation criteria are satisfied, the state PDF will be allocated according to the two possible scenarios like yielding and not yielding or overtaking on the right and left side. And this allocation happens at a time point, when it is needed to reduce computational effort as much as possible.

The remaining task is to determine the Gaussian parameters of the bimodal Gaussian Mixture Model of Eq. (4.19).

In the previous section, introducing the allocation criteria, two survived PDF weights were determined, each representing the survived volume for one scenario after the collision region has fully penetrated the initial PDF. Or in other words, the collision region was stretched along the velocity direction into infinity. In contrast, the split in the current predicted time point is depending on the current prediction horizon (not stretched) collision region \mathbb{M}_{COLL} . For that, the non-truncated Gaussian PDF $p(\mathbf{x}_k | -\mathbf{e}_{0:k-1}) = \mathcal{N}(\mathbf{x}_k; \hat{\mathbf{x}}_k, \Sigma_{x,k})$ is simply split by a hyperplane $(\mathbf{a}_{\text{split}}, b_{\text{split}})$ into two separate PDF's, where each PDF represents one of the two possible scenarios:

$$\begin{aligned} w^1 \mathcal{N}(\mathbf{x}_k; \hat{\mathbf{x}}_k^1, \Sigma_{x,k}^1) &\stackrel{\text{(A.10)}}{\approx} \sigma(\mathbf{a}_{\text{split}}^T \mathbf{x}_k - b_{\text{split}}) \mathcal{N}(\mathbf{x}_k; \hat{\mathbf{x}}_k, \Sigma_{x,k}) \\ w^2 \mathcal{N}(\mathbf{x}_k; \hat{\mathbf{x}}_k^2, \Sigma_{x,k}^2) &\stackrel{\text{(A.10)}}{\approx} \sigma(-\mathbf{a}_{\text{split}}^T \mathbf{x}_k + b_{\text{split}}) \mathcal{N}(\mathbf{x}_k; \hat{\mathbf{x}}_k, \Sigma_{x,k}) . \end{aligned}$$

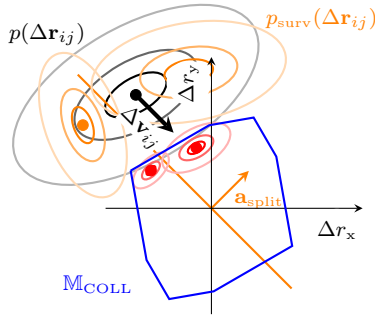


Figure 4.12: Splitting Procedure with quantities. According to the relative motion direction, a truncation line (orange) through origin is determined, which split the initial PDF $p(\Delta\mathbf{r}_{ij})$ in two Gaussian parts, which subsequently are truncated by the collision region \mathbb{M}_{COLL} like for the unimodal case.

The hyperplane with normal vector $\mathbf{a}_{\text{split}}$ and shift b_{split} represents a plane into the direction of the mean relative velocity $\hat{\mathbf{v}}_k$ going through the center of the positional space, where the collision region has its center, too. So the hyperplane parameter in the scene state space are chosen as:

$$\begin{aligned}\mathbf{a}_{\text{split}} &= \mathbf{a}_{\text{orth}}(\mathbf{C}^{ij})^T \\ b_{\text{split}} &= 0 \quad .\end{aligned}$$

The two Gaussians $\mathcal{N}(\mathbf{x}_k; \hat{\mathbf{x}}_k^1, \Sigma_{\mathbf{x},k}^1)$ and $\mathcal{N}(\mathbf{x}_k; \hat{\mathbf{x}}_k^2, \Sigma_{\mathbf{x},k}^2)$ are not adapted by the collision region yet. To gain the six parameters consisting of the weights $w^{nc,1}$, $w^{nc,2}$, the mean vectors $\hat{\mathbf{x}}_k^{nc,1}$, $\hat{\mathbf{x}}_k^{nc,2}$ and the covariance matrices $\Sigma_{\mathbf{x},k}^{nc,1}$, $\Sigma_{\mathbf{x},k}^{nc,2}$ of the survived PDF $p_{\mathbf{x},\text{surv},k}(\mathbf{x}_k)$, each of the Gaussians in the bimodal Gaussian Mixture Model will be adapted like it was presented for the unimodal case, described in Sec. 4.6.1. If no split happens, the algorithm is identical to the aforementioned truncation and conservation of momentum approach.

Setting Design Parameters

The decision when to split is based on the allocation parameter $D_{\text{alloc}}^{\text{lim}}$ and proximity parameter $D_{\text{prox}}^{\text{lim}}$, as it was already discussed. They consider the extent of the initial PDF given by its covariance matrix, the extent of the collided state PDF and a small forecast into the future. If both parameters are over their thresholds, a split is executed. To find out the optimal set

of threshold values, the following points should be considered, which are trade-offs between computational speed, accuracy and smoothness:

1. Avoid splits, which have resulting Gaussians representing only small survived distribution parts.
2. Avoid splits, when the collision probability for one Gaussian of a split PDF is predicted to be small compared to the case of keeping one Gaussian.
3. Avoid splits after a previous split to keep a small amount of prediction tree branches or Gaussian Mixture Model components, respectively.
4. Produce high accuracy in collision probability magnitude and shape over predicted time.
5. Smooth transition in total collision probabilities from scenarios which have got executed splits and those which have not.

Especially the three last points show a high interplay between the decision variables and the splitting procedure. Conservative approximations show that the threshold values should be set to $D_{\text{prox}}^{\text{lim}} = 0.6$ and $D_{\text{alloc}}^{\text{lim}} = 0.2$ to avoid multiple splitting (list point 3). This set of parameters lead to bad accuracies and non-continuous transitions. Higher accuracies in magnitude and smoother transitions can be reached by decreasing thresholds, which will on the other hand increase the computational time, because of more scenarios with splits. A good compromise between all mentioned considerations have the following parameters $D_{\text{prox}}^{\text{lim}} = 0.1$ and $D_{\text{alloc}}^{\text{lim}} = 0.2$.

Until here, the collision event with static and dynamic collision regions as well as the determination of collided and non-collided state PDF's and magnitudes with truncation, conservation of momentum and splitting procedures were introduced. In the following section an alternative approach based on rates is outlined, which do not use any PDF shape truncation or adaptation techniques to calculate collision probabilities. In Sec. 4.8, the differences between the aforementioned and following model are outlined, to find out which model leads to satisfying results and works best as a foundation for investigations with a severity model.

4.7 Collision Event Rate

The collision event rate approach is an alternative approach next to the shape adapted survived state prediction process, introduced in the previous sections, to calculate the total collision probability. In contrast, this approach is heuristically determining the collision probability and bases on the rate formulation presented in Sec. 3.6. The simplification of this continuous time approach is that the shape adaptation of the survived state PDF over the predicted time horizon is not explicitly modeled. Therefore, only a heuristic rate function identifies instantaneously scene states of high criticality and provides a collision probability, which only holds for the current predicted time step without past PDF shape adaptations. Like in case of the truncating probability models, the magnitude will also be reduced by the survival probability.

The idea of a rate function for collision events was originally outlined in [129], where an overlap of the vehicle's Gaussian representation was implemented. Each Gaussian in the framework consists heuristically of a set of parameters describing motion uncertainties, sensor uncertainties and the shapes of two colliding vehicles. The strengths of this framework are its analytic-based calculations and its consideration of multiple other events in an additive way. Both aspects guarantee fast calculability and a foundation for incorporating further event types.

In contrast to [129], this approach uses the collision region formulation of Sec. 4.4 to disband the mixture of uncertainties and shape, so that now the Gaussian PDF is only used as a representation of the distributed vehicle centers.

As aforementioned, the rate formulation neglects the influence of a shape adaption due to events, so that the survived state PDF $p_{x,\text{surv}}(\mathbf{x})$ is similar to the predicted state PDF $p(\mathbf{x}(t+s))$ without any event occurrences:

$$p_{x,\text{surv}}(\mathbf{x}(t+s)) = p(\mathbf{x}(t+s)) \quad .$$

Furthermore, according to Sec. 3.6, the total collision probability is determined by a collision rate $\tau_{\text{COLL}}^{-1}(t+s)$, evaluating each time step separately. This rate takes a transformed overlap probability $P_{\text{ov}} \in [0, 1]$ representing the instantaneous collision probability in relative positional state space:

$$\tau_{\text{COLL}}^{-1}(t+s) = \tau_{\text{max}}^{-1} \cdot \frac{1 - \exp(\beta_0 \cdot P_{\text{ov}}(t+s))}{1 - \exp(\beta_0)} \quad ,$$

where the maximum rate τ_{max}^{-1} and dimensionless slope β_0 are design parameters. The maximum rate τ_{max}^{-1} expands the co-domain of the overlap

probability to higher rates, which can better depict high collision probabilities and limits them to a maximum value for numerical reasons. The slope β_0 balances the errors created by a non-adapted survived state PDF and the progressive behavior of the "time-discrete event probability to event rate transformation" given in Eq. (3.26).

The overlap probability P_{ov} is similarly calculated like the instantaneous collision probability in Sec. 4.5 for a predicted time point $t + s$, where $t = 0$ without loss of generality. It takes the Minkowski region $\mathbb{M}_{\text{OCC}}^{ij}(\gamma^i(s), \gamma^j(s))$, representing the area of collided points in the relative positional space, and the positional PDF $p(\mathbf{r}(s)) = \mathcal{N}(\mathbf{r}; \hat{\mathbf{r}}(s), \Sigma_r(s))$ gained by marginalize over hidden variables or using $\mathbf{r} = \mathbf{C}^{ij} \mathbf{x}$ according to Eq. (4.4):

$$P_{ov}(s) = \int_{\mathbb{M}_{\text{OCC}}^{ij}} p(\mathbf{r}) d\mathbf{r} .$$

This equation can be rewritten into an analytic expression by making a decomposition along the positional axes. Additionally, assuming parallel oriented shapes with a rectangular-shaped Minkowski region $\mathbb{M}_{\text{OCC}}^{ij} = [r_x^{\min}, r_x^{\max}] \times [r_y^{\min}, r_y^{\max}]$ and diagonal covariance matrices:

$$\begin{aligned} P_{ov}(s) &= \int_{r_x^{\min}}^{r_x^{\max}} \int_{r_y^{\min}}^{r_y^{\max}} \mathcal{N}(\mathbf{r}; \hat{\mathbf{r}}(s), \Sigma_r(s)) d\mathbf{r} \\ &= \int_{r_x^{\min}}^{r_x^{\max}} \mathcal{N}(r_x; \hat{r}_x(s), \sigma_{r,x}^2(s)) dr_x \cdot \int_{r_y^{\min}}^{r_y^{\max}} \mathcal{N}(r_y; \hat{r}_y(s), \sigma_{r,y}^2(s)) dr_y \\ &= \left(\Phi \left(\frac{r_x^{\max} - \hat{r}_x}{\sigma_{r,x}} \right) - \Phi \left(\frac{r_x^{\min} - \hat{r}_x}{\sigma_{r,x}} \right) \right) \cdot \dots \\ &\quad \dots \left(\Phi \left(\frac{r_y^{\max} - \hat{r}_y}{\sigma_{r,y}} \right) - \Phi \left(\frac{r_y^{\min} - \hat{r}_y}{\sigma_{r,y}} \right) \right) . \end{aligned}$$

Now, the collision rate can be calculated analytically and can be used to determine the total probability according to Eq. (3.24) of Sec. 3.6.

One can see that this approach is much shorter than the previous approach, but it is neglecting the PDF shape adaptation by already collided states. Therefore, the collision rate τ_{COLL}^{-1} is only an indicator and behaves more like a distance measure between the vehicles with consideration of

their geometrical shapes. This model was implemented in the motion planner published in [47].

4.8 Evaluation of Collision Probability Models

In the previous section different approaches were presented regarding the collision event between two vehicles. They distinguish especially in terms of the representation of the non-collided PDF part like one Gaussian, a Gaussian Mixture Model and without any adaption. Furthermore, they differ in terms of taking static and dynamic collision regions. These different alternatives are combined to three probability models chosen to compare their prediction behavior to a **Monte Carlo Simulation** with 10.000 particles and **dynamic** collision checks (dyn. MCS). The three probability models are as follows:

- Analytic truncation method for static collision region (Sec. 4.4.1) and **event rate**-based approach according to Sec. 4.7 **without** adapting the state PDF shape (ER - non adapt.).
- Analytic truncation method for **static collision** region (Sec. 4.4.1) and unimodal survival state PDF adaptation **without** split according to Sec. 4.6.1 (SC - unimodal).
- Analytic truncation method for **dynamic collision** region (Sec. 4.4.2) and multi-modal survival state PDF adaptation **with** splitting procedure according to Sec. 4.6.3 (DC - multi-modal).

The comparison of these models and their individual properties are highlighted in four different experiments considering overtaking scenarios with multiple models and different shapes, yield and not-yielding at an intersection scenario, velocity and lateral distance dependencies while overtaking and the influence of sampling times on the probability calculation.

4.8.1 Multi-Vehicle Overtaking Scenario

In the first scenario, the ego vehicle is behind a queue of two other standing vehicles on a neighbor lane and predicts an overtaking scenario on its own lane from left to right. The two other vehicles are a passenger car and a long truck standing on the right lane. All vehicles have a noisy

current state and are predicted with motion uncertainties. In Fig. 4.13, the predicted scenarios are shown depending on the collision probability model with their positional Gaussian 2σ -ellipse.

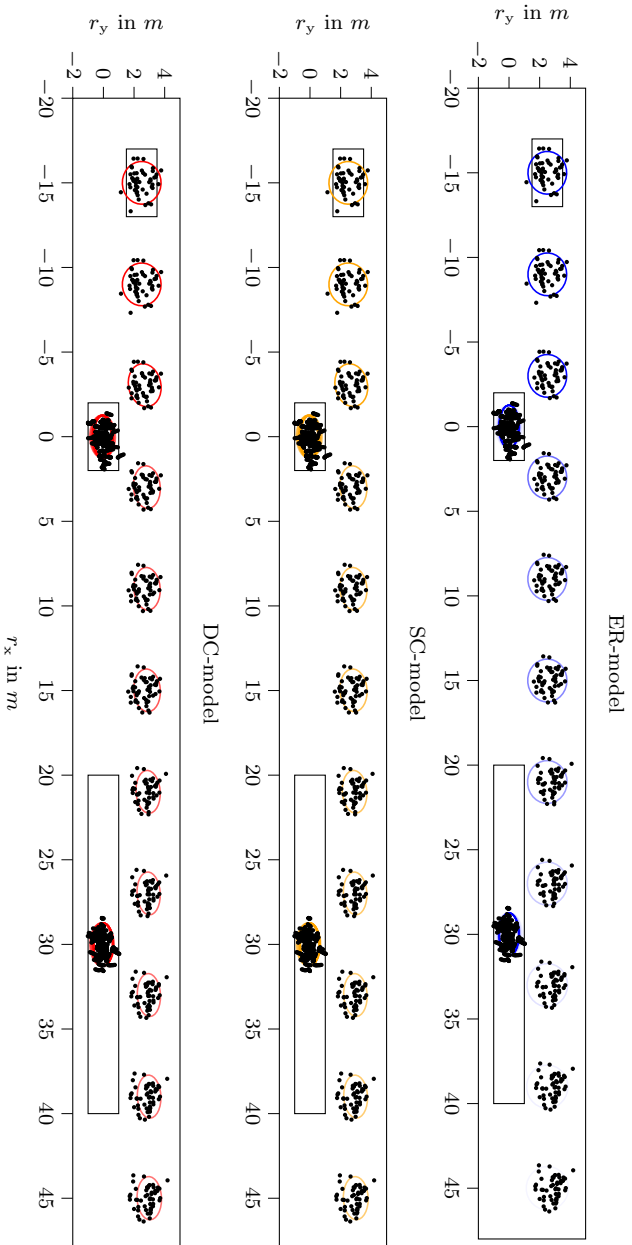


Figure 4.13: Predicted overtaking scenario with ego vehicle from left to right on the left lane and a passenger car and a truck on the right lane. All scenarios have been initialized identically. The Monte Carlo particles (black dots) and predicted Gaussian 2σ -ellipse of the ER-model (blue, top), the SC-model (orange, middle) and the DC-model (red, bottom) are depicted for several time steps.

The non-adapted Gaussians of the event rate model (ER) enlarge slightly over time cause of the initial velocity distribution and an input acceleration noise in longitudinal and lateral direction. One can see that the Gaussian ellipses are adapted according to the foreseen collision in case of the static collision region (SC) and dynamic collision (DC) probability models, so that the drawn particles of the Monte Carlo Simulation (MCS) are well enclosed by the Gaussian ellipses. The nearly equal shapes of SC and DC models of the unimodal Gaussians are a consequence of the low relative velocities, so that the static and dynamic regions become very similar.

In Fig. 4.14, the top plots and the bottom left plot show the instantaneous collision, the time-course sensitive survival and the time-course sensitive collision probabilities for the overtaking scenario prediction. One can see that the ER-model is consequently overestimating the instantaneous collision probability and has a postponed time step of the maximum collision probability with one vehicle compared to the MCS reference. The ER-model overestimates the second crash probability with the long truck due to the multiple counting of Gaussian overlaps. Furthermore, its corresponding time-course sensitive survival probability curve has sharper decay and a deformed curve. This is the consequence of the non-shape-adapting ER model which is not considering shadowing effects produced by the first passenger vehicle - meaning, that a crash with the long truck in the scene would become less likely, because it is protected by the first vehicle in the row. Instead, the ER model's collision probability increases due to the enlarging overlaps as a consequence of enlarging non-truncated Gaussians. On the other hand, the calculation of the survival probability contradicts the shadow effects with its harder decreases so that this phenomenon is partly seen in the time-course sensitive event probability.

The collision probabilities for SC and DC provide a better fit to the MCS. The instantaneous collision, the survival and the time-course sensitive probabilities curves are very similar. In the plot at the bottom right corner, the evolution of the Hellinger Distance is depicted to quantify the similarity of the PDF given by the MC particles and the Gaussian approximations. Here, it is obvious that at the time steps when the biggest amount of particles are going to be removed, the Gaussian approximations fit less accurately. Nevertheless, the distance of SC- and DC-model with their adapting Gaussians have smaller Hellinger distance, which gives the highest similarity to the reference PDF. The ER model fits worst, because of the missing adaptation. The offset of the Hellinger Distance for small time steps is due to approximation issues of MC particles histograms.

This experiment shows that a removal of already collided PDF parts

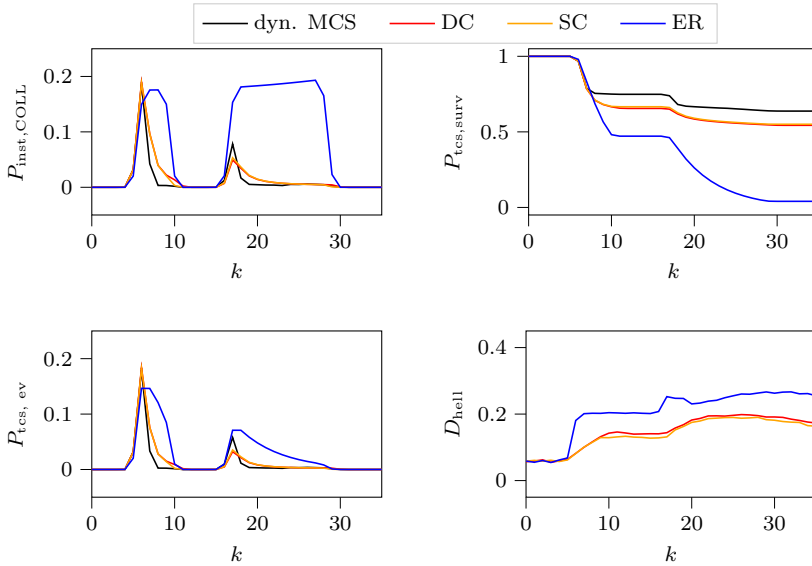


Figure 4.14: Probability curves of overtaking scenario shown in Fig. 4.13 for dynamic Monte Carlo Simulation (dyn. MCS), event-rate based (ER), static collision region based (SC) and dynamic collision region based (DC) model. Top left: Instantaneous collision probability. Top right: time-course sensitive survival probability Probability. Bottom left: time-course sensitive collision probability. Bottom right: Hellinger Distance between the MCS particles and the respective Gaussian distributions. The quantity curves of the SC- and the DC-model approximate best the MCS baseline.

by the Gaussian truncation process leads to a better fit of probability curves and PDF shapes compared to MCS. With the shape adaptation it is possible to represent shadowing effects and to avoid overestimations of bigger dimensioned vehicles, which both increases the prediction accuracy.

4.8.2 Two-Vehicle Intersection Scenario

The second experiment is a prediction of two oncoming vehicles at an intersection. The probability curves and the corresponding scenario prediction are depicted in Fig. 4.15 and in Fig. 4.16 for the ER-, SC- and

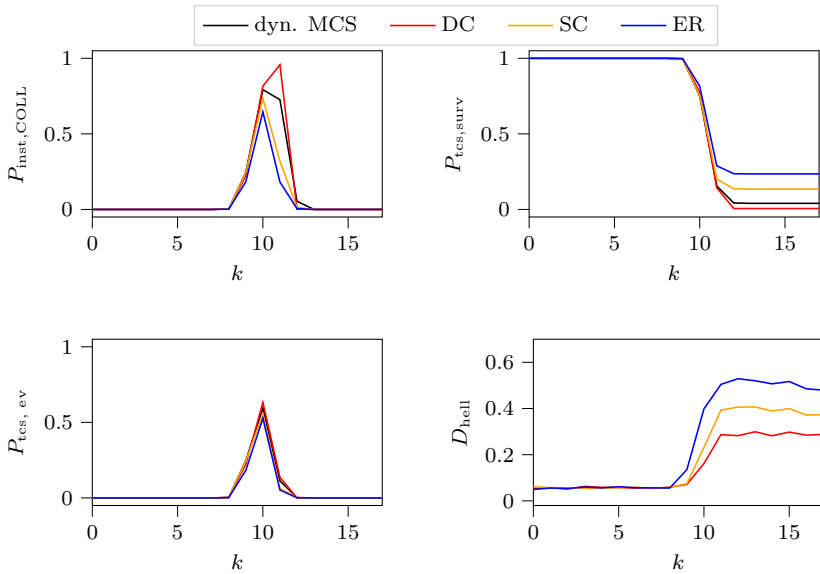


Figure 4.15: Probability curves of overtaking scenario shown in Fig. 4.16 for dynamic Monte Carlo Simulation (dyn. MCS), event-rate based (ER), static collision region based (SC) and dynamic collision region based (DC) model. Top left: Instantaneous collision probability. Top right: time-course sensitive survival probability. Bottom left: time-course sensitive collision probability. Bottom right: Hellinger Distance between the MCS particles and the respective Gaussian distribution. The DC model fits best in shape and magnitude for this scenario because of the splitting of its PDF into two Gaussians.

DC-model. In contrast to the aforementioned experiment, the DC-model splits the Gaussian into two Gaussian evolutions, each representing one single scenario either yielding or not yielding. The multi-modality of the DC model shows significant better performance in terms of PDF shape accuracy with a smaller Hellinger Distance D_{hell} to the MCS than the ER- or SC- model without splits. Also the DC-model magnitudes for instantaneous, time-course sensitive survival and time-course sensitive event probability curves show overestimation of the predicted probability but it fits best to MCS than the other models.

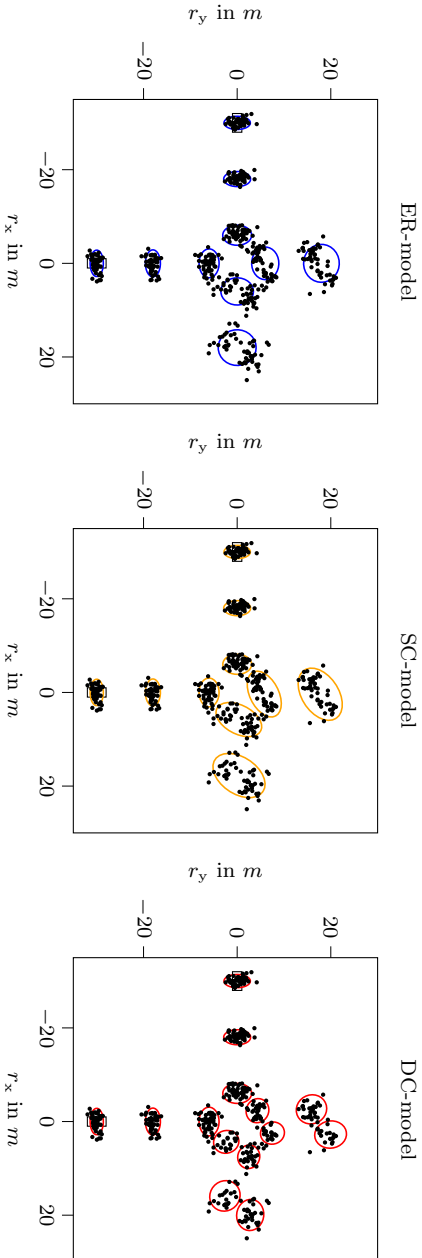


Figure 4.16: Predicted intersection scenario with two vehicles approaching the crossing point at the same time. The Monte Carlo particles (black dots) and predicted Gaussian 2σ -ellipses of the ER-model (blue, left), the SC-model (orange, middle) and the DC-model (red, right) are depicted for several time steps.

4.8.3 Two-Vehicle Overtaking Scenario

The scene of the two-vehicle overtaking scenario is similar to the first experiment with an oncoming ego vehicle on the left lane and another standing vehicle on the right lane, but without the long truck. In this experiment, the total collision probability, the sum of the time-course sensitive probability of each time step, is calculated depending on the relative velocity and the lateral distance of both vehicle centers. The potential fields produced by all models are shown in Fig. 4.17.

The total collision probability potential field on the top left corresponds to the Monte Carlo Simulation with dynamic collision region as reference. This plot shows, that the collision probability increases with the relative velocity, if the vehicle has small lateral distances to the other vehicle. For small relative velocities, there is more time left to leave the lane or move apart from each other to avoid a collision. If the lateral distance between the vehicles is high enough, the phenomenon will turn around: the total collision probability decreases with higher relative speed. This can be explained by the fact that two vehicles driving next to each other with similar speed, have more time to make a critical maneuver to the side towards the other vehicle comparing to a scenario where one vehicle overtakes the other during a short predicted time interval.

The top right picture of Fig. 4.17 shows the potential field of the non-truncating ER model. This model shows the property that the total collision probability decreases with higher velocity for all lateral distances. This is due to the multiple counting of collision overlaps for low relative velocities and could lead to fatal mis-interpretation of vehicles in a following-like scene, where a risk-based planner could be forced to drive faster and to collide instead of slowing down. As a consequence, the ER-model cannot ensure safety in following scenarios.

In contrast to the ER-model, the SC-model with truncation shows better performance in the car-following scene (bottom left of Fig. 4.17). In case of small lateral distances, the total probability is nearly constant over a wide range of relative velocities. Only for small relative velocities it overestimates significantly the total collision probability compared to the MCS reference. This overestimation is a result of the remaining part of the survived PDF inside the collision region, which becomes even worse in cases, where the unimodal Gaussian PDS center is located into the collision region and widened (compared to Fig. 4.9).

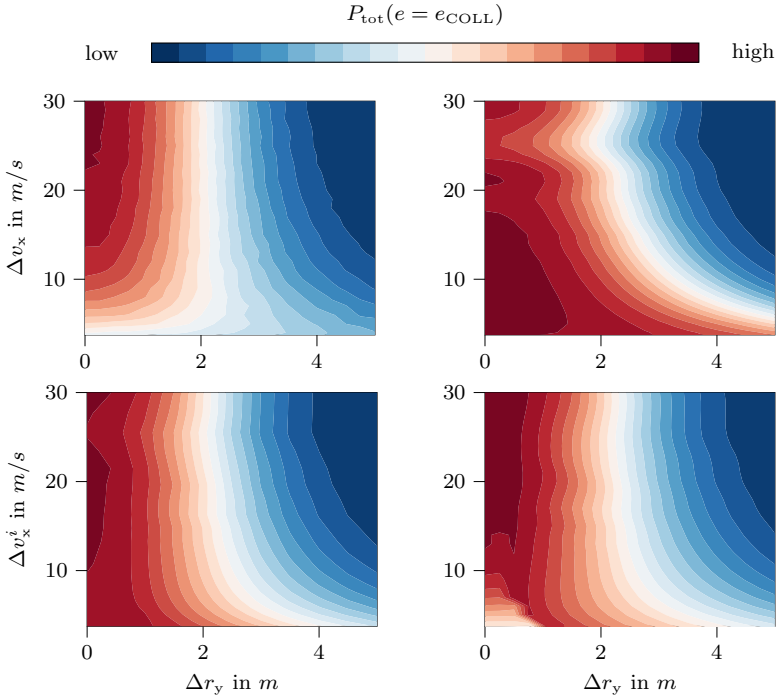


Figure 4.17: Total collision probability depending on relative lateral distance and relative velocity for Monte Carlo Simulation/MCS (top left), event-rate/ER (top right), static collision region/SC (bottom left) and dynamic collision region (DC) based models (bottom right). One can see that the potential field of the DC-model with its splitting procedure and dynamic collision region fits best to the MCS.

In the bottom right corner of Fig. 4.17, the DC-model with split has similar behavior like the dynamic MCS. The only disadvantage is the discontinuous transition from split to non-split probability estimations. Nevertheless, the DC-model with split shows the best fit like in the two experiments before.

4.8.4 Sampling Time Dependency

In the last experiment, the influence of the time interval Δt between two subsequent prediction steps is shown exemplarily for one predicted overtaking scenario, where the DC-model does not split the Gaussian PDF. In Fig. 4.18 on the left side, the magnitudes for all four models are shown. One can see that the Monte Carlo Simulation (MCS) has a nearly constant total probability over the sampling time. The event rate model (ER) without truncation has a strong dependency on the sampling time, beginning at a high total collision probability of one, so that a crash is certain and falling down to zero for very high sampling times, where the prediction "jumps" from collision detection to missed detections. The same sampling issues are also the reason for the wavy character around $\Delta t = 1$ s. The DC-model with dynamic collision region is slightly decreasing for sampling time intervals up to 1 s and raises for higher sampling times. It does not fall down to zero like the ER- and SC-model with its static collision region. For small time steps, the magnitudes of DC and SC model are very similar, because there dynamic collision regions converges to the static collision region. For higher sampling time steps, the static region approximation leads to underestimations like the ER model.

The right plot of Fig. 4.18 shows the maximum appearing Hellinger Distance over the full prediction horizon, i.e., the highest shape dissimilarities of predicted survived state PDF's. The ER-model has the highest Hellinger Distance, which is like aforementioned a problem of missing truncations. With the SC- and DC- model, the PDF has similar distances, with exception of the cases where the collisions are not detected.

All in all, the DC-model is most robust in magnitude and shape against sampling time interval changes due to the usage of the dynamic collision region. The ER-model shows some very good constant collision probability values for small sampling times but can lead to very big differences or even missed detections.

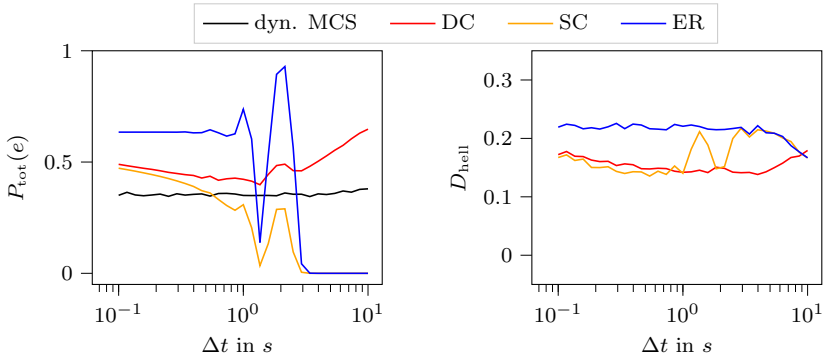


Figure 4.18: Influence on probability calculation and shape similarity by changing sampling time Δt in a narrow overtaking scenario without any PDF splits for dynamic Monte Carlo Simulation (MCS), event rate based (ER), dynamic collision region (DC) and static collision region (SC) models. Left: Total probability over the predicted horizon. Right: Maximal Hellinger distance of the survived Gaussian state PDF's to the survived particle distribution of the MCS. Probability models with static collision regions have detection lacks which becomes stronger for high sampling times. The DC model is more robust against sampling times than the ER and SC model.

4.9 Conclusion

This chapter presents many alternatives to calculate a collision probability for a risk-based motion planning framework. It started by a general consideration for time discrete systems to detect collisions during a prediction process and ended by a comparison between all derived models. The contributions of this chapter are as follows:

- A dynamic collision region in state space for two polygonal vehicles imitating continuous time collision detection in a time-discrete framework.
- Gaussian analytic truncation techniques in state space for static and dynamic collision regions, which outperform stochastic integration techniques like the Monte Carlo simulation in time and accuracy. They can detect collisions sufficiently well over a wide range of magnitudes and velocities in case of the dynamic collision region.
- An analytic method to determine the survived Gaussian state PDF

based on the conservation of stochastic momentum, which has a high accuracy in cases where the moderate distance between collision regions and PDF's. This method is published in [110].

- An extension of the analytic method to determine the survived Gaussian PDF which transforms the unimodal Gaussian PDF into a bimodal Gaussian Mixture Model according to an allocation forecast variable and a proximity variable to represent cases like the yielding and not yielding at an intersection or left and right overtaking along a highway.
- A rate-based model with simple heuristic probability calculations for a risk-ware driver model in parallel lane scenarios.

The findings of different collision probability models in the experiments are summarized as follows:

- Probability models with dynamic collision regions, instead of static region are more robust against sampling time issues.
- Adaptations of the survived state PDF by removing already collided parts can represent shadowing effects e.g. vehicles in a row. They are robust against overestimation for big-sized objects and avoid overestimations in case of small relative velocities of two vehicles. Further investigations have been published in [110].
- Splitting Gaussian procedures increase the accuracy of total collision probability and PDF shapes in a wide range of scenes and can represent simultaneously different predicted scenarios along one prediction like yielding or not yielding.
- For high lateral distances in an overtaking scenario, the total collision probability decreases with the increase of the relative velocity, because of smaller likelihood of steering to the occupied lane.
- The dynamic region based model with splitting technique for the survived state PDF can best approximate the probability of a Monte Carlo Simulation in scenarios with multiple objects of different size, at intersections or with overtaking maneuvers.

The collision event itself is complemented by the severity model in Ch. 6 to obtain the full risk evaluation for the motion planner. Behavior with only constant severity, where the collision probability model guides the behavior is shown in Ch. 7.

5 Other Events

5.1 Distributed Events

The second type of events outlined in this thesis is strongly related to the collision event. For determining the probability of a collision event, a binary indicator was used, which detects whether a scene state has a shape overlap or not: true or false. In contrast, the event detection model for distributed collision changes its binary character to a real probability with values between zero and one. So a collision event e_{OCC} in a single scene state has a likelihood of taking place. This is useful to predict possible events with partially known information or with many uncountable objects in the scene. Some examples are given here:

- Crashes with unknown existence of objects e.g. in covered regions behind curves or house corners where traffic participants could appear.
- Crashes of non-detected objects due to weather conditions like raining or fog like it is depicted in Fig. 5.1
- Quasi-distributed dynamical objects e.g. for crisscross walking pedestrian groups, where each pedestrians location seems to be very fuzzy.
- Crashes with quasi-distributed static objects in case of highly dynamical ego behavior e.g. for after crash scenarios, where the ego vehicle loses control and could crash with surrounding objects.

In the following, the approach and a short evaluation is outlined.

5.1.1 Approach

For one vehicle in such a quasi homogeneous distributed object area, an event rate $\tau_{\text{OCC}}^{-1}(\mathbf{x}_k^i)$ is defined, which depends on the current state \mathbf{x}_k^i and a constant factor ρ_{DISTR} representing the distributed object area. The

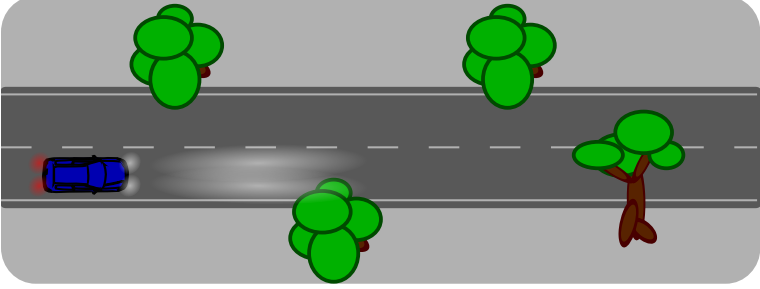


Figure 5.1: Ego vehicle scene under bad-view conditions with fallen tree on the road. Ego vehicle assumes homogeneously distributed objects on the road.

factor ρ_{DISTR} is similar to a liquid density, so that an object flow rate \mathbf{s}^i through the frontal vehicle side with width w_{veh} , represented by the moving direction $\mathbf{s}^i = [\cos(\gamma^i), \sin(\gamma^i)]^T$, determines the event rate $\tau_{\text{OCC}}^{-1}(\mathbf{x}_k^i)$:

$$\begin{aligned} \tau_{\text{OCC}}^{-1}(\mathbf{x}_k) &= \lim_{\Delta t \rightarrow 0} \frac{\Delta N_{\text{COLL}}}{\Delta t} = w_{\text{veh}} \rho_{\text{DISTR}} (\mathbf{s}^i)^T \mathbf{v}_k^i \quad (5.1) \\ &= \mathbf{n}_{\text{flow}}^T \mathbf{x}_k \quad , \end{aligned}$$

where the flow vector $\mathbf{n}_{\text{flow}} \in \mathbb{R}^n$ simplifies the first row of Eq. (5.1).

The distributed event rate $\tau_{\text{OCC}}^{-1}(\mathbf{x}_k^i)$ provides the desired instantaneous distributed event probability $p(e_{\text{OCC}}|\mathbf{x}_k)$ according to Eq. 3.25:

$$p(e_k = e_{\text{OCC}}|\mathbf{x}_k) = 1 - \exp(-\tau_{\text{OCC}}^{-1}(\mathbf{x}_k)\Delta t) = 1 - p(e_k = \neg e_{\text{OCC}}) \quad .$$

Here, a constant velocity \mathbf{v}_k^i which is positive oriented according to the vehicle orientation, so that $\mathbf{n}_{\text{flow}}^T \mathbf{x}_k > 0$.

For a given normal distributed a priori state with probability density function (PDF) written as $p(\mathbf{x}_k) = \mathcal{N}(\mathbf{x}_k; \hat{\mathbf{x}}_k, \Sigma_k)$, the collided state PDF $p(\mathbf{x}_k|e_k = e_{\text{OCC}})$ is determined according to:

$$\begin{aligned} p(e_k = e_{\text{OCC}}) &= \int_{\mathbb{R}^n} p(e_k = e_{\text{OCC}}|\mathbf{x}_k) p(\mathbf{x}_k) d\mathbf{x}_k \\ &= 1 - \int_{\mathbb{R}^n} \exp(-\tau_{\text{OCC}}^{-1}(\mathbf{x}_k)\Delta t) \mathcal{N}(\mathbf{x}_k; \hat{\mathbf{x}}_k, \Sigma_k) d\mathbf{x}_k \\ &= 1 - \exp\left(-\mathbf{n}_{\text{flow}}^T \hat{\mathbf{x}}_k + \frac{1}{2} \mathbf{n}_{\text{flow}}^T \Sigma_k \mathbf{n}_{\text{flow}}\right) \quad . \end{aligned}$$

Taking the event detection model for distributed states provides the collided state PDF:

$$\begin{aligned}
 p(\mathbf{x}_k | e_k = e_{\text{OCC}}) &= \frac{p(e_k = e_{\text{OCC}} | \mathbf{x}_k) p(\mathbf{x}_k)}{p(e_k = e_{\text{OCC}})} \\
 &\propto (1 - \exp(-\mathbf{n}_{\text{flow}}^T \mathbf{x}_k)) \mathcal{N}(\mathbf{x}_k; \hat{\mathbf{x}}_k, \Sigma_k) \\
 &= \mathcal{N}(\mathbf{x}_k; \hat{\mathbf{x}}_k, \Sigma_k) - \mathcal{N}(\mathbf{x}_k; \hat{\mathbf{x}}_k - \Sigma_k \mathbf{n}_{\text{flow}}, \Sigma_k) .
 \end{aligned} \tag{5.2}$$

The last line of Eq. (5.2) can be calculated by taking the equations for conservation of stochastic momentum according to Eq. (A.8) to obtain non-negative PDF values, which ends up in the following formulas for the collided state PDF $p(\mathbf{x}_k | e_k = e_{\text{OCC}}) = \mathcal{N}(\mathbf{x}_k; \hat{\mathbf{x}}_{\text{DISTR},k}, \Sigma_{\text{DISTR},k})$:

$$\begin{aligned}
 \hat{\mathbf{x}}_{\text{DISTR},k} &= \hat{\mathbf{x}}_k + \frac{p(e_k = \neg e_{\text{OCC}})}{p(e_k = e_{\text{OCC}})} \Sigma_k \mathbf{n}_{\text{flow}} \\
 \Sigma_{\text{DISTR},k} &= \frac{1}{p(e_k = e_{\text{OCC}})} (\Sigma_{\mathbf{x},k} + \hat{\mathbf{x}}_k \hat{\mathbf{x}}_k^T) - \hat{\mathbf{x}}_{\text{DISTR},k} \hat{\mathbf{x}}_{\text{DISTR},k}^T - \dots \\
 &\quad \dots - \frac{p(e_k = \neg e_{\text{OCC}})}{p(e_k = e_{\text{OCC}})} (\Sigma_{\mathbf{x},k} + (\Sigma_k \mathbf{n}_{\text{flow}})(\Sigma_k \mathbf{n}_{\text{flow}})^T) .
 \end{aligned}$$

The non-collided PDF is a Gaussian distribution with $p(\mathbf{x}_k | \neg e_{\text{OCC}}) = \mathcal{N}(\mathbf{x}_k; \hat{\mathbf{x}}_k - \Sigma_k \mathbf{n}_{\text{flow}}, \Sigma_k)$. Compared to the initial PDF $\mathcal{N}(\mathbf{x}_k; \hat{\mathbf{x}}_k, \Sigma_k)$, there is only a shift in the mean due to the fact that higher velocities have a higher flow rate and therefore the associated PDF parts are more flattened compared to those with slower velocity states.

Anyway, the intentions after a crash changes to:

$$p(I_{k+1} | \mathbf{I}_k, e_k = e_{\text{OCC}}) = \delta(I_{k+1}^i - I_{\text{nonctrl}}^i) \quad \forall i \in \{1, \dots, N_o\} .$$

The severity of these distributed events $c_{\text{OCC}}(\mathbf{x}_k)$ depends on the assumed distribution partners in the crowd. A corresponding severity model is shown in the next chapter (Ch. 6). The impact of an appropriate severity model on the behavior of a motion planner is shown in Sec. 7.5.

5.1.2 Evaluation

For validating the analytic calculation of the Gaussian approximation method, the Monte Carlo Simulation (MCS) with 10k particles is taken as reference. At the top of Fig. 5.2 the r_x, v_x -diagram is shown with particles and 2σ -ellipses of the Gaussian PDF's. One can see that the Gaussian ellipses are perfectly fitting the MCS particles. The similarity of both PDF's

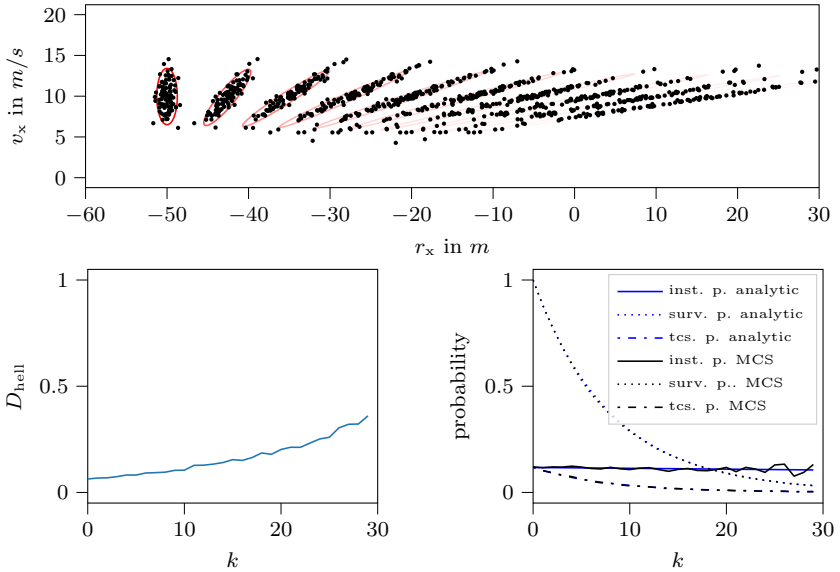


Figure 5.2: Prediction of Gaussian PDF in a homogeneous distributed collision area with $\rho_{\text{DISTR}} = 0.05 \text{ m}^{-2}$ and $w_{\text{veh}} = 2 \text{ m}$. Top: Monte Carlo particles and Gaussian ellipses in r_x, v_x -space over multiple prediction steps. Bottom left: Hellinger distance over predicted time index k . Bottom right: Curves of instantaneous (inst.), time-course sensitive (tcs.) event and survival (surv.) probability for analytic Gaussian adaptation and Monte Carlo Simulation.

is also visible in the diagram for the Hellinger Distance (bottom left), where the similarity is nearly constant at a very low level. The difference from a perfect fit with zero Hellinger Distance is due to the approximating histograms for MCS particles. In the right bottom corner of Fig. 5.2, one can see that also the curves for instantaneous, time-course-sensitive survival and event probabilities are fitting perfectly.

5.2 Dynamical State Restriction

The events which are discussed in the previous sections and chapters represent state changes which occur during interacting with others like in a collision and which are producing damage and harms. Another type of events is given by dynamical state restrictions e_{SR} which do not involve any costs but which provoke an adaptation of the predicted states. An example is a speed limitation to maximum or minimum speed given by a maximum engine power or a missing reverse gear, respectively. They both exclude some physical states and flag some as unreachable. These examples of a dynamical state restriction are related to intrinsic dynamic limitations in the motion model.

The approach bases on the idea to not implement directly the impossible-achieving states into the motion model, rather to outcast them and treat them separately. The advantage is that simple motion models can be applied without considering these state restrictions, as long as there are representable by hyperplanes. To do so, the states, which raise state restrictions after applying the transition with the motion model are adapted and are projected onto the linear restriction like it is depicted in Fig. 5.3 and outlined in the next sections. For example, in case of a maximum speed limitation through engine power, the motion planner predicts the states according to the applied motion model with a fixed acceleration for all states in the distribution described in the probability density function (PDF). Some parts of the PDF with velocities higher than the maximum possible speed are then adapted in a way, that the velocity of the projected states has got maximum speed.

5.2.1 Adaptation of State Probability Density Function

Assuming a linear state restriction $\mathbf{a}^T \mathbf{x} \geq b$, defined by a hyperplane with normalized normal vector \mathbf{a} showing into the forbidden state region and the hyperplane shift b , a projection onto the border to a new state $\mathbf{x}_{\text{adp},k}$ will be executed only if the state \mathbf{x}_k raises the linear restriction. The probability $p(e_k = e_{\text{SR}} | \mathbf{x}_k)$, whether the raising restriction event e_{SR} happen is similar to an indication on which side of the border the current state \mathbf{x}_k is located:

$$p(e_k = e_{\text{SR}} | \mathbf{x}_k) = \sigma(\mathbf{a}^T \mathbf{x}_k - b) \quad . \quad (5.3)$$

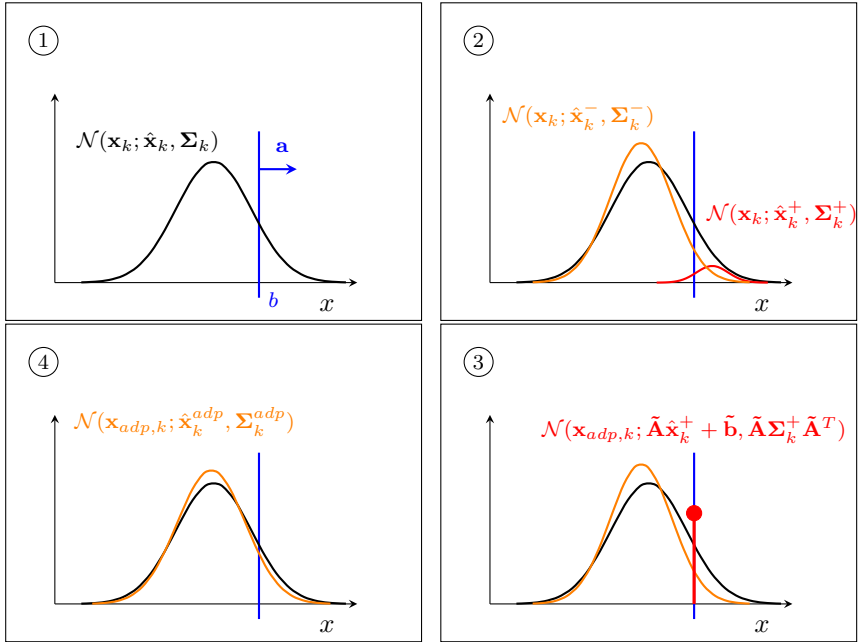


Figure 5.3: State probability truncation approach based on an unimodal Gaussian PDF and a linear restriction boundary showing into the non-allowed state space. The approach starts at the upper left corner (step 1) and continues in clockwise manner. The part of the Gaussian PDF which is on the right side of the boundary will be separated by executing a split of the initial Gaussian (step 2), before the resulting part behind the linear boundary is projected onto the border (step 3) and is finally merged with the non-split PDF (step 4).

The counter probability is $p(e_k = \neg e_{\text{SR}} | \mathbf{x}_k) = 1 - p(e_k = e_{\text{SR}} | \mathbf{x}_k)$. States \mathbf{x}_k behind the restriction hyperplane are projected onto a new adapted state $\mathbf{x}_{\text{adp},k}$ on the linear border. The corresponding state adaptation functions for non-event engaged state PDF is as follows:

$$p(\mathbf{x}_{\text{adp},k} | \mathbf{x}_k, e_k = \neg e_{\text{SR}}) = \delta(\mathbf{x}_{\text{adp},k} - \mathbf{x}_k) \quad . \quad (5.4)$$

The event engaged state PDF $p(\mathbf{x}_{\text{adp},k} | \mathbf{x}_k, e_k = e_{\text{SR}})$ is the projection onto

the restriction plane:

$$\begin{aligned} p(\mathbf{x}_{adp,k} | \mathbf{x}_k, e_k = e_{SR}) &= \delta(\mathbf{x}_{adp,k} - \mathbf{x}_k + \mathbf{a}(\mathbf{a}^T \mathbf{x}_k - b)) \\ &= \delta\left(\mathbf{x}_{adp,k} - \underbrace{(\mathbf{E} - \mathbf{a}\mathbf{a}^T)}_{\tilde{\mathbf{A}}} \mathbf{x}_k - \underbrace{b\mathbf{a}}_{\tilde{\mathbf{b}}}\right), \end{aligned} \quad (5.5)$$

where in the last row it becomes obvious that the transformation associated with the adaptation is affine with a matrix $\tilde{\mathbf{A}}$ and a shifting vector $\tilde{\mathbf{b}}$.

Because these adapted states $\mathbf{x}_{adp,k}$ are only being shifted and are not being removed, the survival probability won't be reduced by this event. The overall adapted distribution $p(\mathbf{x}_{adp,k})$ is calculated by marginalizing over the state restriction event e_{SR} and the initial state \mathbf{x}_k :

$$\begin{aligned} p(\mathbf{x}_{adp,k}) &= \int_{\mathbb{R}^n} p(\mathbf{x}_{adp,k} | \mathbf{x}_k, e_k = e_{SR}) p(e_k = e_{SR} | \mathbf{x}_k) p(\mathbf{x}_k) d\mathbf{x}_k + \dots \\ &\quad \dots + \int_{\mathbb{R}^n} p(\mathbf{x}_{adp,k} | \mathbf{x}_k, e_k = \neg e_{SR}) p(e_k = \neg e_{SR} | \mathbf{x}_k) p(\mathbf{x}_k) d\mathbf{x}_k. \end{aligned} \quad (5.6)$$

Taking the adaptation model in Eq. (5.4), the counter probability $p(e_k = e_{SR} | \mathbf{x}_k)$ and assuming a Gaussian state PDF $p(\mathbf{x}_k) = \mathcal{N}(\mathbf{x}; \hat{\mathbf{x}}_k, \Sigma_{x,k})$, the first term of the overall adapted states $p(\mathbf{x}_{adp,k})$ can be approximated by using the truncation formulas given in Eq. (A.10):

$$\begin{aligned} \int_{\mathbb{R}^n} p(\mathbf{x}_{adp,k} | \mathbf{x}_k, e_k = \neg e_{SR}) p(e_k = \neg e_{SR} | \mathbf{x}_k) p(\mathbf{x}_k) d\mathbf{x}_k &= \dots \\ &\dots = \sigma(b - \mathbf{a}^T \mathbf{x}_{adp,k}) \mathcal{N}(\mathbf{x}_{adp,k}; \hat{\mathbf{x}}_k, \Sigma_k) \\ &\stackrel{(A.10)}{\approx} \pi_k^- \mathcal{N}(\mathbf{x}_{adp,k}; \hat{\mathbf{x}}_k^-, \Sigma_k^-), \end{aligned} \quad (5.7)$$

where π_k^- is equal to the counter event probability $p(e_k = \neg e_{SR})$, $\hat{\mathbf{x}}_k^-$ is the mean state vector and Σ_k^- is the state covariance matrix of the approximated Gaussian PDF within the free space. Note, that comparing to Eq. (5.3) the signs of the hyperplane parameters within the step function have changed.

The second term of Eq. (5.6) is calculated in a similar way but with a different calculation order. In the first algorithm step, the Gaussian

PDF $p(\mathbf{x}_k)$ is truncated by the step function of the probability model of Eq. (5.3) and in the second step, the adaptation model of Eq. (5.5) is applied:

$$\begin{aligned}
& \int_{\mathbb{R}^n} p(\mathbf{x}_{adp,k} | \mathbf{x}_k, e_{\text{SR}}) p(e_{\text{SR}} | \mathbf{x}_k) p(\mathbf{x}_k) d\mathbf{x}_k = \dots \\
& \dots = \int_{\mathbb{R}^n} p(\mathbf{x}_{adp,k} | \mathbf{x}_k, e_{\text{SR}}) \sigma(\mathbf{a}^T \mathbf{x}_k - b) \mathcal{N}(\mathbf{x}_k; \hat{\mathbf{x}}_k, \Sigma_k) d\mathbf{x}_k \\
& \stackrel{\text{(A.10)}}{\approx} \int_{\mathbb{R}^n} \delta(\mathbf{x}_{adp,k} - \tilde{\mathbf{A}}\mathbf{x}_k - \tilde{\mathbf{b}}) \pi_k^+ \mathcal{N}(\mathbf{x}_k; \hat{\mathbf{x}}_k^+, \Sigma_k^+) d\mathbf{x}_k \\
& = \pi_k^+ \mathcal{N}(\mathbf{x}_{adp,k}; \tilde{\mathbf{A}}\hat{\mathbf{x}}_k^+ + \tilde{\mathbf{b}}, \tilde{\mathbf{A}}\Sigma_k^+ \tilde{\mathbf{A}}^T) . \tag{5.8}
\end{aligned}$$

Substituting the solutions given in the eq.'s (5.7) and (5.8) for the split PDF parts into Eq. (5.6) will provide the distribution of the adaptive states $p(\mathbf{x}_{adp,k})$. Next to the two truncation approximations in Eq. (5.7) and Eq. (5.8), the method conserving the stochastic momentum according to Eq. (A.8) approximate the two Gaussian by merging them into one unimodal Gaussian distribution $\mathcal{N}(\mathbf{x}_{adp,k}; \hat{\mathbf{x}}_k^{adp}, \Sigma_k^{adp})$:

$$\begin{aligned}
p(\mathbf{x}_{adp,k}) &= \pi_k^+ \mathcal{N}(\mathbf{x}_{adp,k}; \tilde{\mathbf{A}}\hat{\mathbf{x}}_k^+ + \tilde{\mathbf{b}}, \tilde{\mathbf{A}}\Sigma_k^+ \tilde{\mathbf{A}}^T) + \pi_k^- \mathcal{N}(\mathbf{x}_{adp,k}; \hat{\mathbf{x}}_k^-, \Sigma_k^-) \\
&\approx \mathcal{N}(\mathbf{x}_{adp,k}; \hat{\mathbf{x}}_k^{adp}, \Sigma_k^{adp}) .
\end{aligned}$$

The parameters of the adapted state Gaussian PDF $p(\mathbf{x}_{adp,k})$ are calculated as follows:

$$\begin{aligned}
\hat{\mathbf{x}}_k^{adp} &= \pi_k^+ \cdot (\tilde{\mathbf{A}}\hat{\mathbf{x}}_k^+ + \tilde{\mathbf{b}}) + \pi_k^- \cdot \hat{\mathbf{x}}_k^- \\
\Sigma_k^{adp} &= \pi_k^+ \left(\tilde{\mathbf{A}}\Sigma_k^+ \tilde{\mathbf{A}}^T + (\tilde{\mathbf{A}}\hat{\mathbf{x}}_k^+ + \tilde{\mathbf{b}} - \hat{\mathbf{x}}_k^{adp})(\tilde{\mathbf{A}}\hat{\mathbf{x}}_k^+ + \tilde{\mathbf{b}} - \hat{\mathbf{x}}_k^{adp})^T \right) + \dots \\
&\dots + \pi_k^- \left(\Sigma_k^- + (\hat{\mathbf{x}}_k^- - \hat{\mathbf{x}}_k^{adp})(\hat{\mathbf{x}}_k^- - \hat{\mathbf{x}}_k^{adp})^T \right) .
\end{aligned}$$

A big advantage of this approach is that the previously described split-adaptation-merge procedure would not let grow the number of Gaussians in a Gaussian Mixture Model, so it keeps the computational effort constantly.

The intentions of the traffic participants are not changing according to this event as shown in the extended Bayesian network of Fig. 5.4 represented by the dynamical state restriction event e_{SR} and the intention vector \mathbf{I}_k .

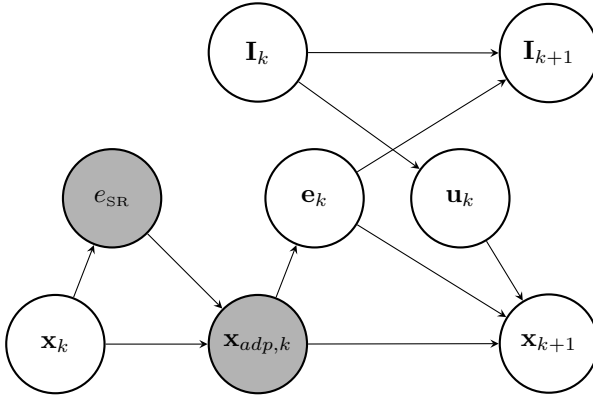


Figure 5.4: Bayesian network in case of a state restriction event e_{SR} . A new variable $x_{adp,k}$ is introduced which post-adapts the predicted states involved in the event before the other events at the predicted time step k are indicated.

5.2.2 Evaluation

In the evaluation of the Gaussian adaptation method for state restrictions a Monte Carlo Simulation (MCS) with 10k particles is applied as the reference. For this a braking trajectory is predicted, which will calculate negative velocities in future time steps. To not forecast states with negative speed, a plane with $v_x \leq 0$ functions as the state restriction is defined. In Fig. 5.5 on the top row, the uncertain state evolution is shown, where the Gaussians 2σ ellipses are adapted in a way, that the main PDF parts stay within the space x of positive velocities. Because this event does not produce any critical outcome, the instantaneous probability stays zero, so that the survival probability is constantly at one (bottom right of fig. 5.5).

The similarity of the Gaussian PDF and the particle representation stays on a high level with low Hellinger Distance over the full prediction horizon (bottom left). The approach leads to high shape similarities also for states which are being highly adapted. All in all, the state restriction adaptation is a very good approximation for a Monte Carlo Simulation.

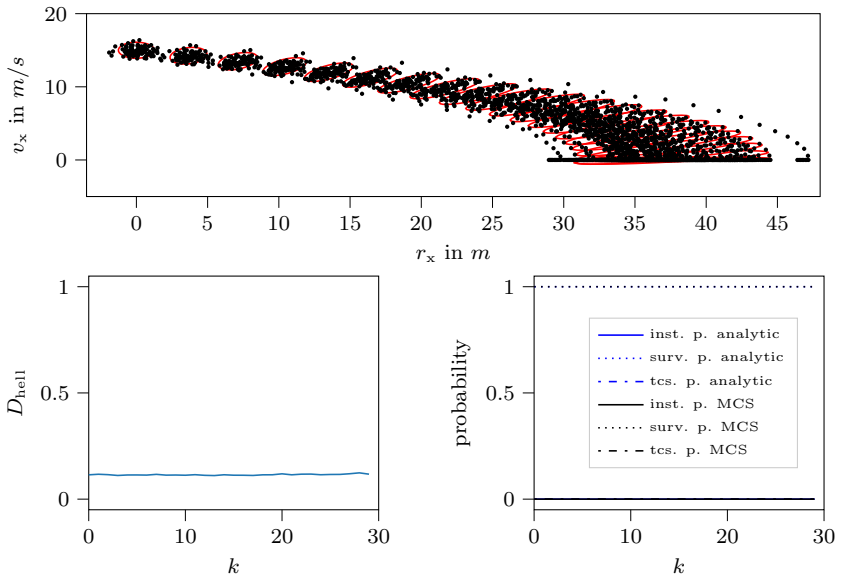


Figure 5.5: Prediction of a braking trajectory with acceleration $a_x = -3 \text{ m/s}^2$, initial mean velocity $v_x(k=0) = 15 \text{ m/s}$ and a state restriction $v_x(k) \leq 0$. Top: Monte Carlo Simulation (MCS) particles and Gaussian 2σ -ellipses in r_x, v_x -space. Bottom left: Hellinger Distance over predicted time step k . Bottom right: Instantaneous (inst.), time-course sensitive (tcs.) and survival (surv.) probability curves for analytic Gaussian adaptation and MCS over time step k , which are not affected by this adaptation.

5.3 Escape Event

A special case of an event type is the escape event e_{ESC} , first mentioned in [129]. It does not really depict a criticality, it is rather a change of future scene evolutions. The escape event models the following three aspects:

- It represents the ego vehicle’s ability to leave the predicted trajectory or scene evolution at any predicted time point and to move into a safe state or into states, which are not producing any costs as one can see in Fig. 5.6.
- It represents a change of scene evolution through random unforeseeable influences like act of nature or abruptly changed driver intentions, which won’t lead to further critical events.

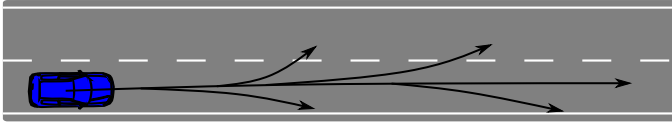


Figure 5.6: Ego vehicle scene with escaping events to the right and left along the predicted trajectory in the middle of the lane.

- It weights earlier predicted time points higher than time points later in future similarly to the decreasing time factor in [171] or for different criticality measures in [48].

The last task of reducing the importance of future time points is a reinforced consequence of the first and second effect. It helps to let the planner focus on the utility and critical events with their costs nearer in future and limits the predicted time horizon in a smooth way.

To ensure that the escape event won't be a counterweight for other critical events in the trajectory evaluation, the escape risk has two properties:

1. The instantaneous probability of an escape event is constant over the predicted time, independent of time, state or input values.
2. The escape risk is always smaller or equal than other critical event risks.

In a scene where no other critical event will happen, the first property of state and input independence guarantees that the planner haven't got ability to change the probability of escaping events. Therefore, trajectories cannot be planned in a way that escaping events are avoided or reinforced. The second condition ensures that in a scene with other threats, the associated event risks are always weighted higher than the escaping event risk, doesn't matter how small their anticipated risks are. Because of that reason, the planner will always focus on avoiding proper critical events or at least weight them against utilities and costs. To not let these risks being weighted out by escaping risk, the risk has to be zero.

The escape event probability is represented by a constant escape event rate τ_{ESC}^{-1} , which is independent of state \mathbf{x}_k , so that the probability for a

prediction time interval Δt is according to Eq. (3.25) as follows:

$$\begin{aligned} p(e_k = e_{\text{ESC}}|\mathbf{x}_k) &= 1 - \exp\left(-\int_0^{\Delta t} \tau_{\text{ESC}}^{-1} dt\right) = 1 - \exp(-\tau_{\text{ESC}}^{-1} \Delta t) \\ &= 1 - p(e_k = \neg e_{\text{ESC}}|\mathbf{x}) . \end{aligned}$$

The non-event state PDF $p(\mathbf{x}_k|e_k = \neg e_{\text{ESC}})$ is similar to the initial state PDF $p(\mathbf{x}_k)$:

$$p(\mathbf{x}_k|e_k = \neg e_{\text{ESC}}) = \frac{p(e_k = \neg e_{\text{ESC}}|\mathbf{x}_k) p(\mathbf{x}_k)}{\int_{\mathbb{R}^n} p(e_k = \neg e_{\text{ESC}}|\mathbf{x}_k) p(\mathbf{x}_k) d\mathbf{x}_k} = p(\mathbf{x}_k) .$$

That's why the state PDF shape does not change when escaping events appear. The influence is depicted in Fig. 5.7.

Because the instantaneous event probability $p(e_k = e_{\text{ESC}}|\mathbf{x}_k) \neq 0$, the severity has to be set to zero to satisfy the above stated zero-risk property:

$$c_{\text{ESC}}(\mathbf{x}_k) = 0 .$$

As a consequence, the instantaneous mean costs \hat{c}_{ESC} are zero.

After leaving the predicted scene evolution, the ego vehicle and all other traffic participants are able to reach a safe state without any further event. The influence of the escape event on the next state \mathbf{x}_{k+1} and intention vector \mathbf{I}_{k+1} is simplified by assuming that all traffic participants immediately stop moving and want to stand still, which is symbolized by the safe mode intention I_{safe} :

$$\begin{aligned} p(\mathbf{x}_{k+1}^i|\mathbf{x}_k, \mathbf{u}_k, e_k = e_{\text{OCC}}) &= \delta(\mathbf{x}_{k+1}^i - [(\mathbf{C}^i)^T \mathbf{0}]^T \mathbf{x}_k) \\ p(I_{k+1}^i|\mathbf{I}_k, e_k = e_{\text{OCC}}) &= \delta(I_{k+1}^i - I_{\text{safe}}^i) \\ &\quad \forall i \in \{1, \dots, N_o\} . \end{aligned}$$

Velocities of all N_o traffic participants are set to zero, while the positions stay constant, so that the scenarios is stopped to a static scene evolution and no events can't happen anymore. Therefore the motion planner does not need to branch trajectories after an escape event has happened and no costs have to be calculated.

All in all, the escape event's technical contribution is the preference of the earlier events compared to events predicted at later time steps. This was achieved by reducing the survival probability by a constant escape event rate τ_{ESC}^{-1} .

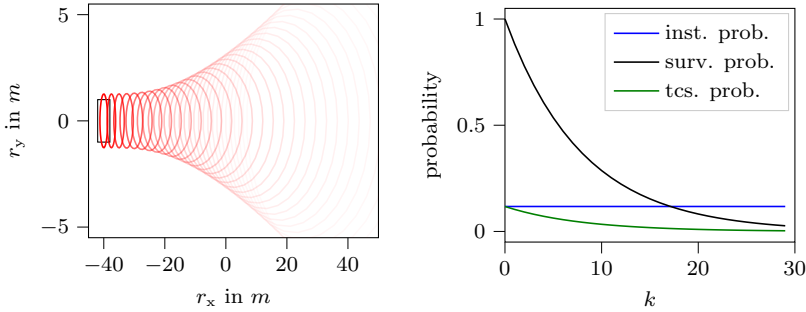


Figure 5.7: Prediction of Gaussian PDF under escape event rate $\tau_{\text{ESC}}^{-1} = 0.25s^{-1}$. Left: Vanishing Gaussian ellipses in r_x, r_y -space show which are only influenced by the motion prediction and not by the event occurrence. Right: Time curves of corresponding instantaneous (inst.), time-course sensitive event (tcs.) and survival (surv.) probability.

5.3.1 Evaluation

The effect of the artificial escape event is shown in Fig. 5.7, where a trajectory with constant velocity is predicted into the future. The vanishing Gaussian PDF's are related to their survival probability, which decreases under the influence of the constant escape rate. The corresponding survival probability is an exponentially decreasing curve, so that other events would become less probable for higher predicted time steps. The time-course sensitive probability indicates the probability that the vehicle escapes in the corresponding time interval from its predicted trajectory and will end in a safe state. Note that the enlarging Gaussian ellipses are due to the uncertain velocity states and the input noise. They are not related to the escape event and do not depict the scene evolution of the after-event states. However, the escape rate enables a limiting prediction horizon because events far away in future can be neglected.

5.4 Conclusion

In this chapter, three other event types were presented which can be added to the motion planner framework in straightforward way like the aforementioned collision events between two vehicles. The contributions of this chapters are:

- An analytic formalism to determine probabilities and shape adaptations for a collision event e_{OCC} in a homogeneous distributed object region.
- An artificial state restriction event e_{SR} for adapting Gaussian PDF's in an analytic way, which can represent hidden state walls like limiting minimum or maximum velocities or other non-reachable areas to separate physical limitations from simple motion models.
- An incorporation of the escape event e_{ESC} [129] into the motion planner framework.

The aforementioned events are part of the motion planner, which is investigated in Ch. 7. The distribution event e_{OCC} and the escape event e_{ESC} are also part of later presented severity model, outlined in the next chapter Ch. 6 to predict in a simple manner collision events and their associated costs after the first contact between two vehicles.

6 Design of Severity Model

The collision severity is the second factor of the collision risk next to the likelihood and represents the costs or harms if a crash or other critical events will happen. These costs can have manifold causes or interpretations, e.g. costs by small intrusions into the car body or even slight crashes with scratches imply repair costs for the vehicles or other property damages. But there are even more important costs, which are hard to monetize like physical or psychological harm of car passengers or pedestrians after they have been hit by interior parts or car bumpers. Comparing different harms and also harms between different participants or victims rises ethical questions. The prediction of these harms, the identification of dependent variables like head accelerations or car intrusions is also not simple and often accompanied by high uncertainty e.g. elderly people are more likely to be injured than young people with better physical constitution and they mostly have a worse starting point to rehabilitate.

Furthermore, in a crowd traffic scene with multiple participants or in cities with multiple static objects like boundaries, cars, street lights, traffic signals and trees, a vehicle out of control can easily hit these objects and causes subsequent crashes. So it can be seen that not only the first hit between two traffic participants influences the severity, but also subsequent events may have an impact on the total consequences. In Sec. 3.4.2, an extended severity also incorporates the scene evolution after the first impact.

In the following sections, the answer to the third and last main question of this thesis is in focus of this and next chapter (see Ch. 7). The foundation of the question how severity models affect motion behavior in risky scenarios is build by clarifying more details about the severity models themselves and by answering the following questions:

1. How can a severity model be designed considering first and subsequent events and which components are needed?
2. How are different traffic participants or vehicle occupants involved into the severity calculation?

3. What is the qualitative difference in output between typical severity models and a multi-event severity model?

First of all, the related work considering severity models for scene criticality assessment and motion planning will be presented in the next section (Sec. 6.1). Afterwards, the severity as part of the survival framework is defined, which will be designed with aid of a modeling scheme including components clarifying different sub-problems like ethical questions. At the end of this chapter, three severity models inspired by models mentioned in the related work are derived using the presented modeling scheme, and another more sophisticated model regarding multiple-events. These models are the foundation of the investigations of the next chapter (see Ch. 7), where the influence of the four severity models on the motion behavior is shown in a wide range of traffic scenarios.

6.1 Related Work

There are many works, which try to predict the severity of a collision. A comprehensive overview is given in [147], where different inputs, models and output quantities are presented depending on their prediction task, e.g. weather conditions for macroscopic traffic considerations or crash constellation on a microscopic level. Investigations in crash outcomes are mostly interested in injuries of the traffic participants and on after-crash states to reconstruct the crash history and origination process for legal reviews [11].

To predict injuries, human harms have to be categorized according to their severeness. An important measure is the abbreviated injury scale (AIS) [72], which decomposes the body into nine body regions and classify their harm between “no injury detected” (0) to “not survivable fatal” (6). Based on this measure, the maximum AIS value (MAIS) [72] takes the maximum AIS value over all body parts and the injury severity score (ISS) aggregates the three highest AIS-values in a quadratic sum [16, 17, 147]. Sometimes it is of interest, whether an accident with a minimum injury occurs. This can be expressed by the measure MAIS n +, where n stands for the minimum AIS injury level. The prediction of serious injuries with MAIS3+ is often modeled by a logistic regression depending on Delta- v , the difference between pre- and post-crash velocity [74, 89, 90, 144, 168]. Fatality rates, which represent the proportion of deaths in specific crashes can be very accurately described by exponential models [55, 56, 87] also using Delta- v considerations. Other injury measures like

the occupant load criterion (OLC) [94] and the head impact criterion (HIC) [118] try to represent the forces on occupants respectively the head injuries as a result of hitting interior parts. They are commonly used for vehicle crash design criteria or if detailed knowledge about the events inside the vehicle is known [113]. In [144], the economic costs of the associated AIS level is aggregated, which results in 3.5 million dollar for fatal accidents in average which are around 1000 times higher than crashes with only property damages. There are different severity measures, but they are mostly for describing harms of occupants.

Next to the aforementioned velocity change Δv [13, 14, 115] further important known input quantities are e.g. the speed level of the involved crash partners [109], which would also increase the fatality rate. The collision direction [109] and the point of impact [13, 14, 56] are further variables, like it was shown in [56]. In [56], four different regions were investigated in the US and it was shown, that the left side impact has the highest severity because of the located drivers seat on the left. A right side impact is around four times more severe than rear or frontal crashes, because of the missing crumple zone. Another very important influence factor is the mass ratio between the involved objects [54]. Vehicles with higher mass better protect their occupants and increase the injury level of the lower-massed vehicle occupants [1]. The last influence factor concerns the number of subsequent crashes. According to National Automotive Sampling System (NASS/CDS)-Data it was shown that 24 % of all crashes has at least one subsequent crash [44], similar results are stated for German and UK databases [57]. Additionally, the authors of [153] showed on the one side that the injury level increases for multi-crashes and on the other side that around 18 % of the maximum injury is not caused by the first crash. To sum up, there are several input variables, which have to be considered while designing a severity model.

For autonomous driving six different severity models types were identified according to their level of detail [80]: relative states like velocity changes [89], conservation of momentums with point masses or expanded objects [79, 155], mass-damper-spring models [27, 28, 51, 123], FEM simulations learned by artificial intelligence [112, 145] for real-time applications and (un-)attractive impact point considerations [64, 74, 162, 163] to mitigate severity levels. As it was stated in the related work for the risk-based motion planner in Sec. 2.4.1, the level of detail depends on the level of collision probability e.g. mitigation systems have often a higher level, whereas motion planner in low risk scenarios have simpler models.

Another categorization is according to the dependency of entity states.

All the works, where only the collision probability is used as risk measure and where the severity is set to a constant value [45, 133, 141] correspond to the first group of state independent severity models. The second group only depends on the ego state and takes the velocity magnitude to calculate a squared quantity like for the iso-risk motion model [99] in a static object traffic environment, for a criticality index function to validate left-lane crossings [35], for mitigation systems based on kinetic energy [91, 97], for motion planning with a kinetic energy transformed into a $[0, 1]$ domain [173] or for a virtual mass depending on fatality statistics [164]. The third group considers the states of both collision partner, the ego vehicle and the other crash partners, to obtain one severity value. Prominent representatives calculate the internal energy of a crash via the conservation of momentum equations [5, 6, 134, 171], which evaluate the crash as one whole event, not considering that one participant can be more harmed than another. Approaches, considering only measures for ego vehicle occupants are Delta-v values derived by either the conservation of momentum [38, 129], the maximum ego vehicle acceleration according to 1D mass-spring systems [28] or a kinetic energy reduction before and after the crash [67]. In mitigation systems for pedestrians, only the pedestrians severity is taken into account, because the unprotected person is the most vulnerable partner in a collision with a vehicle. Examples are given in [79], where a simply Delta-v model is assumed and another example is given in [30], where the severe injury level MAIS 3+ depending on the impact speed is the predictor.

The aforementioned examples show that also masses play an important role in severity outcomes, which first of all produce inequalities between the collision partners. These inequalities are not targeted in common severity calculations and only simplified in pedestrian mitigation techniques. This consideration is an ethical weighting about harms of different collision partners, who are sitting in different vehicle types. The “calculation of the severity function is the most morally difficult component” [70].

Next to an individual consideration of occupants, a further missing point is that the presented frameworks end their prediction process ends at the first contact between collision partners, so only the severity of the first detected collision over the time horizon is considered. But, it was shown that multi-collision increases the severity. Therefore a neglect of a posteriori crash behavior is not appropriate and can underestimate the true severity in a potential crash.

6.2 Problem Definition

In the survival framework, described in Ch. 3, the severity is next to the collision probability the second factor in the risk evaluation and therefore part of the total costs. The collision probability, mentioned in Ch. 4, determines the likelihood of the collision event or first touch event between two vehicles. The severity function represents a surrogate for all crash consequences including the first event and the evolutions caused by the first contact.

In more detail, the mean extended collision severity $\hat{c}_{\text{sev,ext}}(e_k)$ consists of the severity $c_{\text{COLL}}(\mathbf{x}_k, e_k = e_{\text{COLL}})$ of the current predicted collided states probability density function (PDF) written as $p(\mathbf{x}_k | e_k = e_{\text{COLL}}, \mathbf{I}_k = I_{\text{ctrl}})$ of collision and the total costs $C_{\text{tot}}(\mathbf{x}_{k+1}, \mathbf{I}_{k+1} = \mathbf{I}_e)$ caused by subsequent events after the first collision event e_{COLL} (see Eq. (3.10)). The distinction between survived and non-survived scene states was made to separate uncontrolled behavior, signed by intention I_{ctrl} and crash outcomes from trajectories where the planned actions still control the vehicle's behavior. The total costs $C_{\text{tot}}(\mathbf{x}_{k+1}, \mathbf{I}_{k+1} = \mathbf{I}_e)$ after the first event are treated similarly to the original survival framework without an event. So, the survival theory is reused but with a new starting time point k instead of $k = 0$.

In addition, independent of the causer of a collision, all involved participants are influenced by the crash. So another part of the consequence forecast is the consideration of harms and injuries of each traffic participant involved in the collision. For example, if a vehicle is hitting a pedestrian, it becomes clear that the harm of the pedestrian is much higher than the injuries of the vehicle occupants, so the focus of reducing the expected injuries is on the pedestrian, not on the vehicle occupants. The problem gets more tricky, if a crash occurs between two similar weighted vehicles? Where should be the harm avoiding focus or how should severities of different participants be compared? So the inclusion of all traffic participants and their harms is very related to the consideration of multiple events as part in the prediction and evaluation process.

To obtain a representative severity for collision events e_{COLL} , the following models should be identified:

1. The prediction of the next scene state \mathbf{x}_{k+1} impacted by the collision $p(\mathbf{x}_{k+1} | e_k = e_{\text{COLL}}, \mathbf{x}_k, \mathbf{u}_k)$, the next participant's intention $p(\mathbf{I}_{k+1} | e_k = e_{\text{COLL}}, \mathbf{I}_k)$ and behavior model $p(\mathbf{u}_k | \mathbf{I}_k = I_{\text{nonctrl}})$ in case of uncontrolled motion.
2. The harm caused by a collision and predicted total cost $C_{\text{tot}}(\mathbf{x}_{k+1}, \mathbf{I}_e)$

of each traffic participant depending on subsequent events.

3. The severity $c_{\text{COLL}}(\mathbf{x}_k)$ regarding the total costs of one collision event by incorporating all traffic participants with their single costs $C_{\text{tot}}(\mathbf{x}_{k+1}, \mathbf{I}_{k+1} = \mathbf{I}_e)$.

In the next section, it is shown that the determination of the aforementioned quantities and models have some equal underlying sub-models. These sub models can appear multiple times like the physical crash model, which is used to calculate identifiers for injuries and also provide vehicle states after the collision.

6.3 Modeling Scheme for Multiple Events

In the previous chapters, it was stated and shown that events change the states and intentions abruptly. Depending on the intentions, the trajectory evaluation and the behavior will also be adapted according to their intentions. For determining these predictions and evaluations, there are some underlying models, which are identified in this section and discussed in the previous section.

6.3.1 Prediction of Crash Events and A Posteriori Scene Evolutions

Similar to the original motion planning framework, the prediction of future states, intentions and the evaluation of the created evolution is outlined in more detail and is based on the Bayesian Network presented in Fig. 6.1.

State prediction

The collision event itself leads to an immediate change of the vehicle states. Commonly, a contact between two vehicles takes no longer than a collision time interval $\Delta t_{\text{crash}} \ll 0,3 \text{ s}$ [63]. In that time interval one vehicle penetrates into the other vehicle's body and after the impulse is completely transferred the vehicles move apart from the other. It is assumed that in general the prediction time interval is smaller than the crash duration $\Delta t_{\text{crash}} < \Delta t$, so that the process can be represented by an after-crash state $\mathbf{x}_{\text{COLL},k}$. This after-crash state is the outcome of a **physical crash model** $p(\mathbf{x}_{\text{COLL},k} | e_k = e_{\text{COLL}}, \mathbf{x}_k)$. By excluding scratchy contacts between

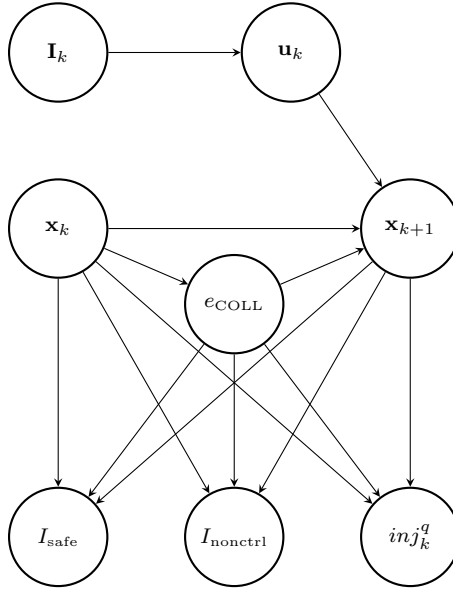


Figure 6.1: Part of the Bayesian network for predicting states, intentions and injuries during the collision at one predicted time step k .

vehicles, the new state will be influenced by a state transition according to the non-event motion model $p(\mathbf{x}_{k+1}|e_{\text{NON}}, \mathbf{x}_k, \mathbf{u}_k)$:

$$\begin{aligned}
 p(\mathbf{x}_{k+1}|e_k = e_{\text{COLL}}, \mathbf{x}_k, \mathbf{u}_k) &= \dots \\
 \dots &= \int_{\mathbb{R}^n} p(\mathbf{x}_{k+1}|e_{\text{NON}}, \mathbf{x}_{\text{COLL},k}, \mathbf{u}_k) p(\mathbf{x}_{\text{COLL},k}|e_k = e_{\text{COLL}}, \mathbf{x}_k) d\mathbf{x}_{\text{COLL},k} .
 \end{aligned}$$

The physical crash model will be introduced later. The motion model is the double integrator, mentioned in Ch. 2.

Intention prediction

The intention I_{ctrl} of the traffic participants before a collision event has happened symbolizes that the traffic participants are able to control their planning freely and are searching for a correct strategy to manage the traffic situation. Another intention was introduced in Ch. 5 in case of escaping behavior, where the intention changes to the target of staying in

safe states: I_{safe} . This was more or less a theoretical construct, because this associated state change happened immediately and guarantees no additional costs but also do not produce any benefits. The associated scene states will correspond to a perfect after crash situation, ending up immediately in a safe state. In case of heavy crashes with a high change of vehicle states like velocities, the driver or automated system has to take back the hold of the vehicle. In this time interval between the crash and the regain of control, the vehicle could move through the whole traffic environment in a criss-cross manner and could hit other traffic participants or surrounding static objects like trees or boundaries. So the intentions \mathbf{I}_{k+1} of the vehicles only depend on the physical crash itself and their capability to cope with the change from a priori \mathbf{x}_k to a posteriori scene state $\mathbf{x}_{\text{COLL},k}$:

$$p(\mathbf{I}_{k+1} = I_{\text{safe}} | e_k = e_{\text{COLL}}, \mathbf{I}_k) = \int_{\mathbb{R}^n} \int_{\mathbb{R}^n} p(\mathbf{I}_{k+1} = I_{\text{safe}} | \mathbf{x}_k, \mathbf{x}_{\text{COLL},k}) \cdot \dots \cdot \dots \cdot p(\mathbf{x}_{\text{COLL},k} | e_k = e_{\text{COLL}}, \mathbf{x}_k) p(\mathbf{x}_k) d\mathbf{x}_{\text{COLL},k} d\mathbf{x}_k \quad ,$$

where $p(\mathbf{I}_{k+1} = I_{\text{safe}} | \mathbf{x}_k, \mathbf{x}_{\text{COLL},k})$ is the **crash coping model** representing the initial probability of not losing control given by the a priori and a posteriori crash states, and will be introduced later.

The likelihood for the non-controlled intention I_{nonctrl} is given by the counter probability:

$$p(\mathbf{I}_{k+1} = I_{\text{nonctrl}} | e_k = e_{\text{COLL}}, \mathbf{I}_k) = 1 - p(\mathbf{I}_{k+1} = I_{\text{safe}} | e_k = e_{\text{COLL}}, \mathbf{I}_k) \quad ,$$

As long as this intention is active, subsequent crashes with surrounding objects can occur.

After-Crash Events and Behavior

If the vehicle reaches the safe intention state I_{safe} after a collision event, no severe event won't happen anymore. The whole traffic scene calms down, traffic participants stop and manage the first crash appropriately by calling the emergency, helping the injured occupants and regulating the oncoming traffic. The same would happen, if the vehicle control system or drivers take hold of their vehicles after a while.

But, if the involved drivers or planning systems lost the control over their vehicle, because of friction loss, additional crashes can occur like aforementioned. The prediction of the after-crash non-controlled behavior has a wide range of possibilities through its instable behavior. The a

posteriori states of a crash with its new velocity direction, is also very uncertain, because of unknown physical vehicle compartment stiffnesses, detailed contact points and intrusion behavior. So, a traffic participant would start with noisy initial directions and could move on in a curvy manner by abrupt steering and braking maneuvers. So the occurrence of collision in an surrounding environment with static boundaries, trees or walls depends on this noisy, hardly predictable after-crash behavior. Nevertheless, to make a rough prediction of what could happen, the a-posteriori crash phase is assumed to have the following properties:

1. A constant escape rate τ_{ESC}^{-1} represents the ability of the driver or vehicle control system to gain back control of its vehicle (Sec. 5.3).
2. A distributed event rate τ_{DISTR}^{-1} represents the possibility to crash into static objects depending on an environment occupancy rate (see Sec. 5.1).
3. A constant braking deceleration a_{brake} along the a posteriori velocity vector depicts the mean velocity reduction of the vehicle during the non-controlled intention state I_{nonctrl} until the vehicle will stop.

This combination helps to deal with very hardly predictable after event consequences in a mathematically simple way and instead of calculating multiple scene evolutions, only one scene prediction has to be evaluated. Dynamic objects are treated as static objects and are incorporated into the occupied area for calculation of the distributed event rate τ_{DISTR}^{-1} . The total event rate for $\tau_{\text{AGG}}^{-1}(t)$ according to Eq. (3.22) is the sum of both single event rates and will be used for the survival probability of Eq. (3.23), which now represents the probability of not being engaged in a **second** collision:

$$\tau_{\text{AGG}}^{-1}(t) = \tau_{\text{ESC}}^{-1} + \tau_{\text{DISTR}}^{-1}(t) \quad .$$

That simplification with the rate based approach does not have the aspiration of representing the after-crash motion and collision behavior in an exact manner, but it describes qualitatively the future evolution and provides a changed motion behavior of the involved vehicles.

6.3.2 Collision Evaluation

After the prediction of states, intentions and behaviors due to the crash and in the a posteriori time phase, the costs with its corresponding parts and structures have to be clarified.

Cost parts

The assessment of crashes has multiple different components. Next to property damage of the car body through scratches or intrusions, there are also costs due to the loss of time and the associated substitution costs of spending time on more relevant things like working at the office than managing the crash. These time costs aggregate over all the traffic participants standing in traffic jams as cause of an accident. Next to these economical lost, there are most notably occupant related costs like treating injuries, rehabilitation or resulting handicaps which e.g. make it impossible to execute a profession. In [19], the main components for economical costs are collected:

- Direct reproduction costs e.g. medical costs and rehabilitation efforts to recreate the victims capabilities
- Indirect reproduction costs e.g. for juristic process, police, public administration and insurance
- Loss of productivity for employer and economy
- External market creation of value like household production
- Humanity costs due to psychological stress through rearranging life plan
- Loss of time in traffic jams or redirections

Depending on the severeness of an injury, the costs increase, where a fatal outcome or death has the maximum loss of economical costs [19, 144]. But next to these costs, also relatives of victims suffer from their loss, which is not depicted by these statistics. Other emotional components like loss of happiness due to restrictions by handicaps are hard to monetize and to compare with other consequences.

In this work, the focus is on the injury of traffic participants, because this strongly correlates with economical costs and emotional harm. With that some questions are still open, like which models provide predictions about the level of severeness and how to compare them between multiple victims? In the following, these questions are answered by looking at the cost structure.

Harm of One Traffic Participant in One Crash Event

The consequences of one crash between two vehicles for the involved occupants depends on the reaction of the body to the accelerations or abrupt changes of the vehicle states. For example, a frontal-to-frontal crash of two vehicles on a country road produces high velocity changes, which also evoke a high probability of fatality. On the other side, a slight scratch on the side of the car body, could only produce uncomfortable sound but does not explicit evoke injuries like broken legs. The change of vehicle states could function as an indicator for severeness. The probability for one occupant q to get an injury inj^q is given by a physical crash model $p(\mathbf{x}_{\text{COLL},k}|e_k = e_{\text{COLL}}, \mathbf{x}_k)$ and an **injury model** $p(inj_k^q|\mathbf{x}_{\text{COLL},k}, \mathbf{x}_k)$:

$$\begin{aligned} p(inj_k^q|e_k = e_{\text{COLL}}, \mathbf{x}_k) &= \dots \\ \dots &= \int_{\mathbb{R}^n} p(inj_k^q|\mathbf{x}_{\text{COLL},k}, \mathbf{x}_k) p(\mathbf{x}_{\text{COLL},k}|e_k = e_{\text{COLL}}, \mathbf{x}_k) d\mathbf{x}_{\text{COLL},k} \quad . \end{aligned}$$

The injury model itself is discussed later in this chapter.

Harm of One Traffic Participant for Multiple Events

For the multi-event severity model, another collision follows after the first collision. We assume that if one occupant is injured during the first collision, one cannot be harmed similarly a second time. This idea equals the concept of time-course sensitivity, as part of the survival theory presented in Ch. 3. The total probability of getting injured $p(inj_{\text{tot}}^q|e_k = e_{\text{COLL}}, \mathbf{x}_k)$ by considering the escape and distributed collision event rates τ_{ESC}^{-1} and τ_{DISTR}^{-1} over an infinite time horizon is given by:

$$\begin{aligned} p(inj_{\text{tot}}^q|e_k = e_{\text{COLL}}, \mathbf{x}_k) &= \dots \tag{6.1} \\ \dots p(inj^q|e_k = e_{\text{COLL}}, \mathbf{x}_k) &+ (1 - p(inj^q|e_k = e_{\text{COLL}}, \mathbf{x}_k)) \cdot \dots \\ \dots \int_{k\Delta t}^{\infty} p(inj^q|e(s) = e_{\text{COLL}}, \mathbf{x}(s)) &\tau_{\text{DISTR}}^{-1}(s) \exp\left(-\int_0^s \tau_{\text{AGG}}^{-1}(t) dt\right) ds \quad . \end{aligned}$$

Here, the time-continuous case like Eq. (3.17) is used, because the events are formulated as rates. Eq. (6.1) considers the full time interval from first contact between the involved vehicles until the occupants vehicle has stopped. The corresponding Bayesian model is depicted in the top row of Fig. 6.2. Now, it is possible to predict the probability of getting an

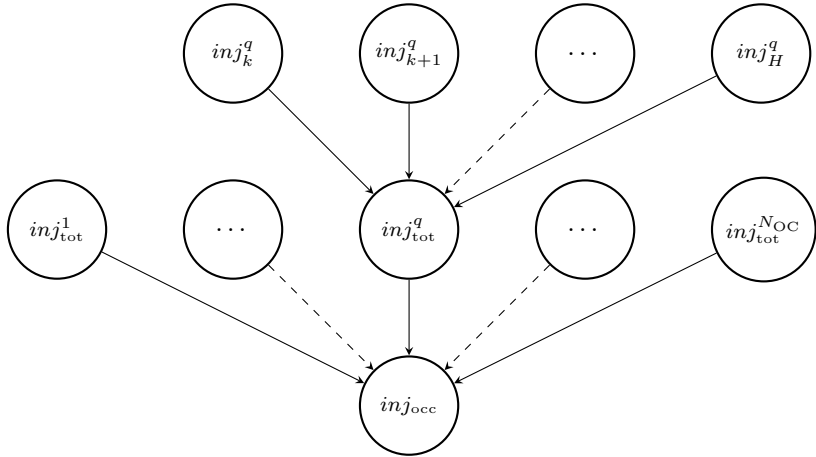


Figure 6.2: Bayesian Model for concatenating injury outcomes of a simple occupant q over predicted time steps after a collision and in case of an uncontrolled intention I_{nonctrl} (first row) and the concatenation of injuries of different multiple occupants or victims.

injury of one potential victim and therefore an approximation of the crash severeness for one victim.

Collision Event Costs for Multiple Traffic Participants

In contrast to crashes with other static objects, dynamic objects mostly have occupants, which can also be harmed during the collision. In crashes, where the colliding objects are very unequal, one traffic participant is often less protected due to different masses, contact points, compartment stiffnesses or is more physically vulnerable than the other one. Therefore the probabilities of injuries are not equal and the question arises, how to concatenate both injury probabilities. In case of a simple addition, the phenomenon during a motion planning arises that the decrease of ones probability is at the expense of the other participant. Therefore, an **ethical model** f_{eth} with an alternative concept is needed to obtain a representative injury value inj_{occ} from different injury probabilities of each

of the N_{OC} -involved occupants:

$$p(\text{inj}_{\text{occ}} | e_k = e_{\text{COLL}}, \mathbf{x}_k) = f_{\text{eth}}(p(\text{inj}_{\text{tot}}^1 | e_k = e_{\text{COLL}}, \mathbf{x}_k), \dots, \dots, p(\text{inj}_{\text{tot}}^q | e_k = e_{\text{COLL}}, \mathbf{x}_k), \dots, p(\text{inj}_{\text{tot}}^{N_{\text{OC}}} | e_k = e_{\text{COLL}}, \mathbf{x}_k)) \ .$$

The corresponding Bayesian model is also represented in Fig. 6.2.

The focus on the injury of occupants instead of property damage can lead to issues of disappearing collisions costs in case of missing predicted injuries. So crashes with slight touches and only some scratches would have zero risk, because of zero predicted injury probability, which stands in contrast to the requirement that a planning system should not produce any crashes at all [79]. So to avoid zero severity prediction, a constant offset c_{CONST} is added to a weighted representative injury inj_{occ} like in the following equation:

$$c_{\text{COLL}}(\mathbf{x}_k) = w_{\text{inj}} p(\text{inj}_{\text{occ}} | e_k = e_{\text{COLL}}, \mathbf{x}_k) + c_{\text{CONST}} \ . \quad (6.2)$$

This constant severity offset c_{CONST} could represent things like administration costs for police, insurance management and so on. The w_{inj} is hard to quantify, because it implicitly weight injury against economical costs. This has to be discussed in more detail e.g. by the whole society or an representative instrument like suggested in [107]. Here, we set $w_{\text{inj}} \gg c_{\text{CONST}}$ to emphasize the importance of harms compared to other costs. Cost parts like comfort, utility or law restrictions are neglected, because they have for sure lower priority in crash scenes (see 2.4.4).

According to Eq. (3.12) the mean severity $\hat{c}_{\text{sev,ext}}(e_k)$ is the expected severity by integrating over the collided state PDF $p_{\mathbf{x},\text{COLL},k}(\mathbf{x}_k)$. For simplicity, it is assumed that the collided state PDF is narrowly distributed so that only the mean collided state scene $\hat{\mathbf{x}}_k^c$ of Eq. (4.16) needs to be evaluated to obtain the mean collision severity $\hat{c}_{\text{sev}}(e_k = e_{\text{COLL}})$:

$$\hat{c}_{\text{sev}}(e_k = e_{\text{COLL}}) = c_{\text{COLL}}(\hat{\mathbf{x}}_k^c) \ .$$

This approximation helps to dispense with the PDF prediction technique for non-linear filtering and to reduce the computational effort.

6.4 Components of Severity

In the previous section, four different sub-models were introduced but not further discussed in more detail: the physical crash model, the coping model, the injury model and the ethical model. Together with the

above-mentioned described prediction and cost structure, these sub-models provide the foundation for the different severity models at the end of this chapter. In the following sections each of these sub-models is outlined.

6.4.1 Physical Crash Model

The physical crash model $p(\mathbf{x}_{\text{COLL},k} | e_k = e_{\text{COLL}}, \mathbf{x}_k)$ predicts the states $\mathbf{x}_{\text{COLL},k}$, right in the moment after a collision event e_{COLL} has happened, depending on the a priori states \mathbf{x}_k . Imagine, there are two vehicles crashing frontally like in overtaking scenarios with opposing traffic. If both vehicles have the same speed but in different directions, their speed were immediately reduced in only a few milliseconds of the crashing contact. To predict this state change requires a modeling of the deceleration behavior during the contact. As shown in the above-mentioned section, this model is not only needed to predict the starting point of the after crash trajectory, it is also determining coping ability after the crash and the harm itself.

Related Work

There are several ways to describe the physical crash. To get detailed time curves of states, the vehicle bodies are modeled by multiple sub-masses connected with different dampers and springs to depict damping and stiffness properties of their physical structure [114, 123]. In [123], the authors use a model with only one mass for each vehicle and a combination of stiffnesses and dampers between both vehicles to imitate the intrusion behavior in frontal crashes. Other works use multiple masses to represent the motor engine and the passenger body, to obtain accelerations on the human body and fatal contacts of the head to interior parts in frontal impacts [51]. A detailed Finite Element Method (FEM) provides best predictions for a known set of parameters, material behavior and human body proportions [11]. These types of model provide dynamic behavior and detailed state changes, but need assumptions about masses, stiffnesses and geometries, which are known for test cases like frontal impacts to barriers, but maybe not for each other vehicle in any other constellation. Furthermore, because of the nonlinearities during the intrusions, the dynamical system has to be simulated, mostly numerically, which takes a lot of computational time and often provides wavy potential fields, where it is hard to find local optima for motion optimizers.

Other approaches are data-driven. In case of using real-world data of crashes a huge database is needed for predicting different crash constel-

lations and vehicle combinations. Databases like the US-American traffic agency named National Highway Traffic Safety Administration (NHTSA) or German In-Depth Accident Study (GIDAS) collect data from vehicle's accidents like contact points, vehicle masses and wearing belts. Implemented event data recorder (EDR)[62] or other "blackboxes" provide speed-time-series during the crash, so that these curves help to reconstruct crashes. These models are often used to predict severities and injuries, but as far as the author knows, they do not predict any after crash states. In [80], the authors use an accident database for obtaining dynamic crash model parameters and model them as normal distributed.

In reconstruction techniques, the a priori velocities are estimated to obtain the a priori traffic situation so that it provides answers to e.g. questions of which driver did a fault [11, 86]. Often, the conservation of momentums techniques and wheel track analysis are executed to obtain a proper a priori crash assumption. The conservation of momentum method provides the advantage to obtain a posteriori crash states without detailed time series or dynamics during the contact. The material and crash properties are represented by only one parameter, a crash restitution coefficient k_{REST} , which depicts the elasticity of the crash, which can be fully elastic with $k_{\text{REST}} = 1$, inelastic with $k_{\text{REST}} =]0, 1[$ or totally plastic $k_{\text{REST}} = 0$. Additional assumptions about the crash constellation like whether the impulse forces showing to the mass center of the vehicles (central and decentralized), the direction of velocity (straight or oblique impact) and the contact conditions (gliding, scratching or getting caught) have to be determined beforehand [11]. E.g. the author of [55] uses point masses in a central, straight impact to obtain the probability of crash fatalities depending on the speed change. In [147] the conservation of momentum for a central, oblique and fully elastic impact and some other crash characteristics were used to predict the kinetic energy. For motion planning, the conservation of mechanical momentum is often used like in [38, 79, 155] to calculate severity measures out of state changes.

Approach

The minimal requirements for a crash model $p(\mathbf{x}_{\text{COLL},k} | e_k = e_{\text{COLL}}, \mathbf{x}_k)$ is to depict differences in

1. crash constellations between slight and full overlapping crashes and
2. vehicle masses to represent trucks, passenger cars and motor cycles.

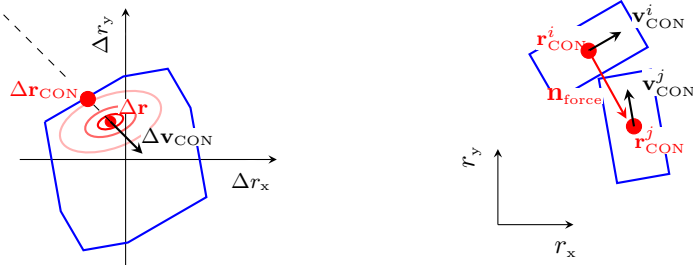


Figure 6.3: Collision region (blue) with collided PDF (red) and projection point Δr_{CON} of contact point Δr in relative positional space (left) and corresponding contact point constellation in world coordinate system with center positions r_{CON}^i , r_{CON}^j , velocities v_{CON}^i , v_{CON}^j and shapes (blue) of crash-involved vehicles (right). The collision force direction n_{force} is on the connection line between both vehicle center positions.

The choice of a proper crash model is on the conservation of momentum, because the model becomes analytically calculable, can incorporate masses and the material specific impact behavior is described by only one crash characteristic parameter k_{REST} , which on the one hand reduces the amount of needed material parameters drastically and is accurate enough for acting sufficiently. For that, a central, oblique and inelastic impact is assumed where the impact force impulse always aligns to the mass/geometric centers of the rectangular-shaped vehicles (see Fig. 6.3). Depending on the constellation between both vehicles, this assumption can depict in a way scratching of the vehicle's surfaces or getting caught on another. Furthermore, forces pointing to the center do not lead to a rotation of vehicles around their axis. In addition, the calculation of a posteriori velocities stays very simple.

Before the velocity change of the vehicles can be calculated, the constellation, where the vehicles touch each other, has to be determined or the point in time when the constellation will take place to infer on the predicted constellation. In the motion-planning framework, the detection of a collision can only state, whether a collision took place in a small time interval instead of a single point in time. So during this time interval the states continue to change and will end somewhere inside the collision region with overlaps, but not tangential shapes. Taking the end point of the corresponding time interval the crash constellation itself will be imprecise in case of highly dynamical motions. That's why the current scene state

\mathbf{x}_k has to be back propagated until the first touch of vehicle's shape where body intrusion is primarily detected.

Assuming a constant velocity during the time interval $\mathbb{T} = [(k-1) \cdot \Delta t, k\Delta t]$, the touching time $\tilde{\Delta t}_{\text{CON}}$ and especially the touching constellation \mathbf{x}_{CON} on the edge of the Minkowski collision region $\partial\mathbb{M}_{\text{COLL,poly}}$ are calculated as follows:

$$\begin{aligned}\tilde{\Delta t}_{\text{CON}} &= \min\{\tilde{\Delta t} \in \mathbb{T} | A_{\tilde{\Delta t}}^{-1} \mathbf{x}_k \in \partial\mathbb{M}_{\text{COLL,poly}}\} \\ \mathbf{x}_{\text{CON},k} &= A_{\tilde{\Delta t}_{\text{CON}}}^{-1} \mathbf{x}_k \quad .\end{aligned}$$

Mind that this is not the position on the surface of the rectangular shaped vehicles, it rather is the position of the vehicles center, when a collision arises. The inverse of the motion matrix $A_{\tilde{\Delta t}}$ is linear in time $\tilde{\Delta t}$ (see Eq. (2.3)), the determination of time candidates for the minimum touching time can be easily executed by checking each Minkowski edge plane for crossing.

After the state of collision was determined, the conservation of linear momentum provides the following set of equations for the a priori state $\mathbf{x}_{\text{CON},k} = [\mathbf{r}_{\text{CON}}^i, \mathbf{v}_{\text{CON}}^i, \mathbf{r}_{\text{CON}}^j, \mathbf{v}_{\text{CON}}^j]^T$ and a posteriori scene state $\mathbf{x}_{\text{COLL},k} = [\mathbf{r}_{\text{COLL}}^i, \mathbf{v}_{\text{COLL}}^i, \mathbf{r}_{\text{COLL}}^j, \mathbf{v}_{\text{COLL}}^j]^T$ with positions and velocities as row vectors:

$$m^i \mathbf{v}_{\text{CON}}^i + m^j \mathbf{v}_{\text{CON}}^j = m^i \mathbf{v}_{\text{COLL}}^i + m^j \mathbf{v}_{\text{COLL}}^j \quad , \quad (6.3)$$

where m^i and m^j are masses of the involved vehicles.

The two contact conditions are depending on the constellation between both vehicles. The force direction $\mathbf{n}_{\text{force}}(\mathbf{r}_{\text{CON}}) = \mathbf{r}_{\text{CON}}^j - \mathbf{r}_{\text{CON}}^i$ determines the orthogonal and tangential direction on the connection line of the involved vehicle center. The resulting equations in the vectorial form are as follows:

$$k_{\text{REST}}(\mathbf{v}_{\text{CON}}^j - \mathbf{v}_{\text{CON}}^i) \mathbf{n}_{\text{force}}^T = -(\mathbf{v}_{\text{COLL}}^j - \mathbf{v}_{\text{COLL}}^i) \mathbf{n}_{\text{force}}^T \quad (6.4)$$

$$\mathbf{v}_{\text{CON}}^i (\mathbf{n}_{\text{force}} \mathbf{R}_{\text{rot}}^{90})^T = \mathbf{v}_{\text{COLL}}^i (\mathbf{n}_{\text{force}} \mathbf{R}_{\text{rot}}^{90})^T \quad . \quad (6.5)$$

The first contact condition according to Eq. (6.4) depicts the velocities the direction where the inelastic impact happens, described by the coefficient of restitution k_{REST} . This coefficient depends on the collision partners, so that the crash into a stiff wall has a different coefficient than a crash with another vehicle. The second condition describes the non-impact-affected orthogonal direction of Eq. (6.5). In combination with the assumption of non-changing positions during the crash $\mathbf{r}_{\text{COLL}}^i = \mathbf{r}_{\text{CON}}^i$ and $\mathbf{r}_{\text{COLL}}^j =$

$\mathbf{r}_{\text{CON}}^j$, the four unknown elements of velocities $\mathbf{v}_{\text{COLL}}^i$ and $\mathbf{v}_{\text{COLL}}^j$ can be determined by taking the conservation of momentum equations according to Eq. (6.3) and both contact conditions Eq. (6.4), Eq. (6.5) to rewrite it into an inhomogeneous linear system:

$$\mathbf{H}(\mathbf{r}_{\text{CON}})[\mathbf{v}_{\text{COLL}}^i, \mathbf{v}_{\text{COLL}}^j]^T = \mathbf{G}(\mathbf{r}_{\text{CON}})[\mathbf{v}_{\text{CON}}^i, \mathbf{v}_{\text{CON}}^j]^T \quad (6.6)$$

$$\mathbf{H}(\mathbf{r}_{\text{CON}}) = \begin{bmatrix} m^i \mathbf{E}_2 & m^j \mathbf{E}_2 \\ \mathbf{n}_{\text{force}}(\mathbf{r}_{\text{CON}}) & -\mathbf{n}_{\text{force}}(\mathbf{r}_{\text{CON}}) \\ \mathbf{n}_{\text{force}}(\mathbf{r}_{\text{CON}}) \mathbf{R}_{\text{rot}}^{90} & \mathbf{0} \end{bmatrix}$$

$$\mathbf{G}(\mathbf{r}_{\text{CON}}) = \begin{bmatrix} m^i \mathbf{E}_2 & m^j \mathbf{E}_2 \\ -k_{\text{REST}} \mathbf{n}_{\text{force}}(\mathbf{r}_{\text{CON}}) & k_{\text{REST}} \mathbf{n}_{\text{force}}(\mathbf{r}_{\text{CON}}) \\ \mathbf{n}_{\text{force}}(\mathbf{r}_{\text{CON}}) \mathbf{R}_{\text{rot}}^{90} & \mathbf{0} \end{bmatrix} .$$

Here, the matrix \mathbf{E}_2 represents the 2×2 - identity matrix. In case of not vanishing masses $m^i, m^j > 0$ and a non-zero force direction $\|\mathbf{n}_{\text{force}}\| > 0$, the linear inhomogeneous system of Eq. (6.6) can simply be solved by calculating the inverse of \mathbf{H} and multiplying it on the left side:

$$[\mathbf{v}_{\text{COLL}}^i, \mathbf{v}_{\text{COLL}}^j]^T = \mathbf{H}(\mathbf{r}_{\text{CON}})^{-1} \mathbf{G}(\mathbf{r}_{\text{CON}})[\mathbf{v}_{\text{CON}}^i, \mathbf{v}_{\text{CON}}^j]^T . \quad (6.7)$$

The Eq. (6.7) provides an analytical equation for predicting velocities after a crash between two vehicles in two dimensional space.

6.4.2 Coping Model

The coping model $p(I_k^i = I_{\text{safe}}^i | \mathbf{x}_k^i, \mathbf{x}_{\text{COLL},k}^i)$ describes the capability to not losing control over the vehicle i after a hit of another vehicle j . Depending on the contact point and the crash constellation, lateral and longitudinal forces deflect the vehicle away from its original a priori states \mathbf{x}_k^i , reducing or increasing its speed. In best case, the vehicles stick together and slow down on their lane until they stop. In worst cases, the vehicles are moving apart, loose friction between wheels and road surfaces, leave their lanes and finally end up in a non-controllable curvy motion patterns, where additional crashes are very likely. Therefore the after crash state $\mathbf{x}_{\text{COLL},k}$ relative to the a priori crash state \mathbf{x}_k is crucial for the probability of losing control.

If the a posteriori velocity vector $\mathbf{v}_{\text{COLL}}^i$ is pointing into the same direction as the a priori velocity vector $\mathbf{v}_{\text{CON}}^i$, the vehicle should keep control after these contacts. Any reduction or increase of speed along the moving direction does not provoke rotation momentums. Therefore, the two following cases have less probability of losing control:

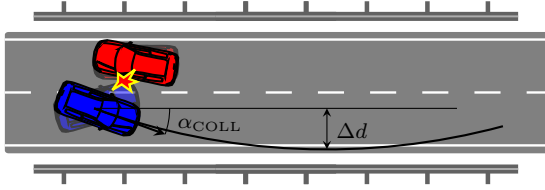


Figure 6.4: After crash evolution for ego vehicle (blue) with circular counter steering trajectory to get back on path.

1. Central and straight crashes, where the force direction and the velocity direction are (anti-)parallel, e.g. in frontal or rear-end crashes.
2. Slight crashes e.g. scratching the vehicle's body side or destroying only the side-view mirror, where only small lateral forces occur, so that the vehicle does not loose road friction.

An after crash situation will become very dangerous, if the vehicle leaves its lane, especially in tree-lined roads. As long as the vehicle stays on its lane, it can brake until stop in a controlled manner. How far, the vehicle will leave its path after a crash is determined by the initial velocity angle after crash α_{COLL} related to the road direction γ^i :

$$\alpha_{\text{COLL}} = \angle(\mathbf{v}_{\text{COLL},k}^i) - \gamma^i .$$

If the vehicle counteracts to its lane leaving movement without losing friction, the minimal lateral distance Δd of the vehicle's current center point can be approximated by:

$$\Delta d = \frac{\|\mathbf{v}_{\text{COLL},k}^i\|^2}{\mu_f g} (1 - |\cos(\alpha_{\text{COLL}})|) ,$$

assuming a motion on a short circular arc, with a radius balancing the friction and centrifugal forces having constant velocity $\|\mathbf{v}_{\text{COLL},k}^i\|$ (see Fig. 6.4). The parameter μ_f describes the friction coefficient between road and wheels and g is the gravity constant. Note, that the after crash velocity norm $\|\mathbf{v}_{\text{COLL},k}^i\|$ is the most influential factor for the radius and therefore the maximum lateral distance Δd .

However, the maximum lateral distance Δd is a predictor for having subsequent crashes. The likelihood of having another crash increases with

growing maximum lateral distance Δd , which is represented by a sigmoid function L (see Eq. A.6.1 in attachment for definition):

$$\begin{aligned} p(I_{k+1}^i = I_{\text{safe}} | \mathbf{x}_k^i, \mathbf{x}_{\text{COLL},k}^i) &= 1 - p(I_{k+1}^i = I_{\text{nonctrl}} | \mathbf{x}_k^i, \mathbf{x}_{\text{COLL},k}^i) \\ &= 1 - L(\Delta d(\mathbf{v}_{\text{COLL},k}^i); \Delta d_{\text{th}}, \Delta d_{\text{sl}}) \quad , \end{aligned}$$

where Δd_{th} represents the lateral distance threshold and Δd_{sl} is the scale parameter for the sigmoid function.

The probability of a second crash depending on the after-crash velocity norm $\|\mathbf{v}_{\text{COLL},k}^i\|$ and after crash angle α_{COLL} according to the presented coping model is depicted in Fig. 6.5 with the coping parameter listed in A.5. Consider a crash with a velocity vector showing into the direction of the road $\angle(\mathbf{v}_{\text{COLL},k}^i) = \gamma^i$ like after a rear-end crash, α_{COLL} and Δd become zero and the likelihood to keep control $p(\mathbf{I}_{k+1} = I_{\text{safe}} | \mathbf{x}_k^i, \mathbf{x}_{\text{COLL},k}^i)$ becomes maximal. Similar consideration holds for scratchy crashes, where the α_{COLL} and the after crash probability becomes zero, too. For high deviation angles α_{COLL} in case of side crashes and high velocities, the probability of losing control is nearly one, and subsequent crashes can occur.

All in all, the presented coping model describes scenarios, where the driver is most likely to regain control of its vehicle within a small surrounding of its lane. In other scenarios, with high crashing angles or after-crash velocities the probability that the vehicle loses control is maximal, so that a subsequent crash is very certain.

Note that the coping model is not depicting the probability of a subsequent crash, it rather determines the likelihood that the vehicle ends up in scenarios, where it is very likely that crashes can occur. The vehicle is able to regain its capability during the braking maneuver, so that the coping probability calculates only the maximum likelihood that something will happen.

6.4.3 Injury Model

There exists much data analysis to predict the injuries of car occupants in case of crashes depending on road infrastructure, weather conditions, vehicle types, crash constellation and speeds. A good review of models with different input and output variables was done in [147]. The output variables are mostly classifiers describing the injury level. These levels are defined by e.g. the Abbreviated Injury Scale (AIS), which splits injuries for one body parts into six different levels, ordered by their severity [72].

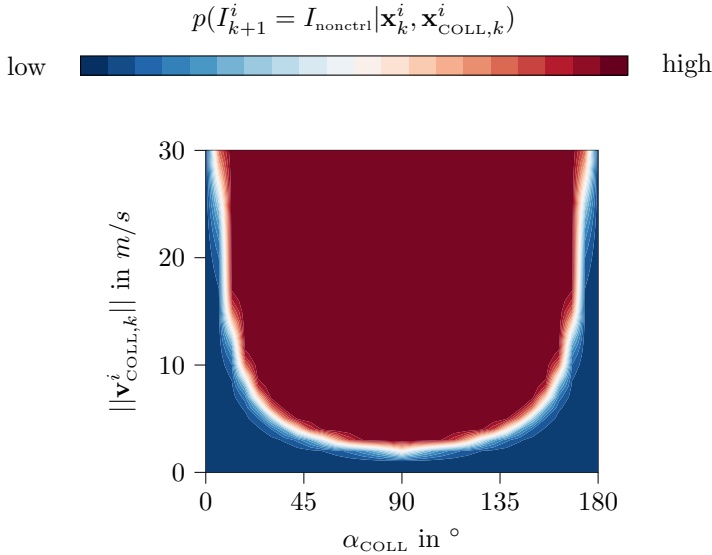


Figure 6.5: Potential plot of probability to loose control after collision depending on angle α_{COLL} between lane and vehicle and the norm of the after crash velocity $\|\mathbf{v}_{\text{COLL},k}^i\|$, where red indicates probability equal to one and blue indicates zero injury likelihood.

Based on this arrangement, measures like the Injury Severity Score (ISS) [16, 17, 147] or the Maximum AIS (MAIS) [72], which tries to represent the general physical constitution of a patient, by either taking the sum of squared AIS-levels of the three highest injured body parts or by taking the maximum AIS-level. In addition, the MAIS $_n$ + with a specific level n or higher is taken to determine the probability of reaching at least an specific injury level [74, 89, 90, 144, 168].

Some model outputs are based on scores like the Head Impact Criterion (HIC) [118], where the acceleration of the head center is taken into account, which needs a detailed analysis of the acceleration time series and is therefore not practical for the used crash model of Sec. 6.4.1.

For predicting the injuries, there are mainly three different kinematic values used: the impact speed of the ego vehicle, the velocity difference between both vehicles, and the velocity difference between the a priori and a posteriori velocity, the Delta-v value. Sometimes, additional information like whether the occupant wore a belt or the constellation like frontal, rear

or side crashes or age is taken into account.

In [61], the authors show that the impact Speed and the Delta- v are good predictors for a logistic regression model for MAIS3+ levels for collisions between vehicles. In [132] and [168], the prediction of different severity levels like severe and fatal are predicted by a logistic regression.

According to the ethic commission [53] and [75], the decision process should not incorporate sex, gender, age, job (or guilty) or other person related characteristics into the decision making process of a motion planner. Furthermore [75] stated that a minimization of injuries or probabilities can be taken into account, which can be satisfied by a planner minimizing injury probabilities.

Based on the related work, the injury model for one occupant q in a vehicle i is given by a sigmoid:

$$p(inj^q | \mathbf{x}_{\text{COLL}}, \mathbf{x}) = L(\|\mathbf{v}_k^i - \mathbf{v}_{\text{COLL},k}^i\|; v_{\text{th}}, v_{\text{sl}}) \quad , \quad (6.8)$$

where v_{th} is the threshold velocity for which the probability becomes 0.5 and v_{sl} describes the slope at $\|\mathbf{v}_k^i - \mathbf{v}_{\text{COLL},k}^i\| = v_{\text{th}}$. For occupants protected by the vehicle compartment, the threshold velocity v_{th} is higher than for pedestrians without a stiff compartment. According to [61], the MAIS3+ parameters for belted occupants are around $v_{\text{th}} = 15.0 \text{ m/s}$ and $v_{\text{sl}} = 2.0 \text{ m/s}$ in case of vehicle crashes. In contrast, a pedestrian will be injured with MAIS level three or higher according to the parameters $v_{\text{th}} = 8.0 \text{ m/s}$ and $v_{\text{sl}} = 3.0 \text{ m/s}$ [132]. The corresponding curves are depicted in Fig. 6.6.

6.4.4 Ethical Model

In contrast to the injury model, determining the probability of only one crash participant, the ethical model considers injuries of multiple traffic participants to obtain one representative value, which can be used as cost indicator for an event. The incorporation of other traffic participants, additionally to the ego vehicles occupants, belongs to the concept of thoughtfulness in traffic environment to protect weaker or less protected traffic participants. In this section, a rough argumentation line about the final ethical model is given.

A naive approach is to sum up all the consequences and human lives. According to the report of German ethic commission, this way of aggregation is strictly forbidden [53]. The authors of [75] have a similar claim to not maximize a utility sum or minimize consequences of an additive function over all injured occupants or pedestrians $q \in \{1, \dots, N_{\text{OC}}\}$ for

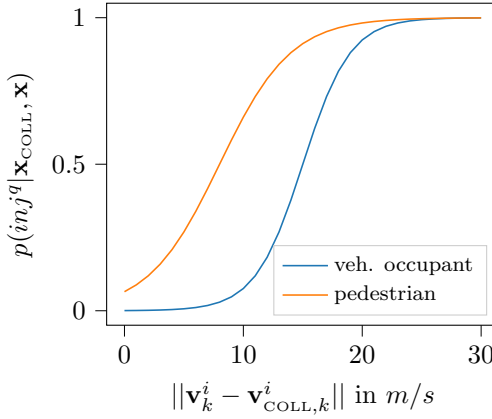


Figure 6.6: Injury probability of MAIS3+ depending on norm of the vectorial velocity change $\|\mathbf{v}_k^i - \mathbf{v}_{\text{COLL},k}^i\|$ for belted vehicle occupants and pedestrians.

inj^q :

$$\begin{aligned}
 f_{\text{eth}}^{\text{agg}}(p(inj_{\text{tot}}^1 | e_k = e_{\text{COLL}}, \mathbf{x}_k), \dots, p(inj_{\text{tot}}^{N_{\text{OC}}} | e_k = e_{\text{COLL}}, \mathbf{x}_k)) &= \dots \\
 \dots &= \sum_{q=1}^{N_{\text{OC}}} p(inj_{\text{tot}}^q | e_k = e_{\text{COLL}}, \mathbf{x}_k) \quad . \quad (6.9)
 \end{aligned}$$

This approach would lead to the phenomenon that different scenarios with big difference in the individual predicted injuries are evaluated identically. For example, one person could be sacrificed to protect others life is similar to the case that all occupants becoming physically disabled (see left picture of Fig. 6.7). The ethic commission goes one step forward and states that there is not an obligation of an individual to save other lives by sacrificing oneself to act in a solidarity manner [53]. Furthermore, the authors also state that each individual is “sacrosanct” and is not “billable” [53]. Therefore, another approach should solve the problem between individual rights and one representative value for different subjects.

Following the guidelines, there are several points, which some authors had recommended. First of all, the risk of all victims should be considered equally [53], so that no preference for any occupant exists. Also in [75], the authors expound that the minimization of risk for each ego vehicle occupant has to be considered in the same manner, that would also be of

ones interest. Additionally, they state that the reduction of the number of victims and of victim's risk at the same time, is a good direction [75] or at least acceptable [53]. This tendency is also confirmed by [160], where probands have to solve a dilemma situation and decide, which people in the scene should kept alive or less harmed. The test was significant for the statement that less people should be hit in an experiment of two choices with different amount of victims for one option.

In the severity calculation, the number of involved or assumed individuals in one vehicle is fixed, so that groups cannot outweigh other smaller groups or single persons, which is in compliance with [75]. To avoid exaggerated self-sacrificing but considering all potential victims, the ethical model takes the maximum injury inj^q of all injured participants N_{OC} :

$$f_{eth}^{max}(p(inj_{tot}^1 | e_k = e_{COLL}, \mathbf{x}_k), \dots, p(inj_{tot}^{N_{OC}} | e_k = e_{COLL}, \mathbf{x}_k)) = \dots \\ \dots = \max(p(inj_{tot}^1 | e_k = e_{COLL}, \mathbf{x}_k), \dots, p(inj_{tot}^{N_{OC}} | e_k = e_{COLL}, \mathbf{x}_k)) \quad .$$

Combined with a motion planner based on cost minimization, this approach focuses on the reduction of predicted harms of the most injured victim. Other victims in the scene have to hazard the consequences or are self-sacrificing until one of them becomes the most harmed occupant (see center picture of Fig. 6.7). During the cost minimization, the maximum level of risk is decreased and the targeted injuries of the affected persons become of comparable size.

The maximum approach has at least one unresolved limitation: In scenes where the maximum injury cannot be reduced, this approach is not able to distinguish between options with different harms for the minor injured participants. This indifference could lead randomly to increasing injuries for all others. According to the injury model of the previous section (Sec. 6.4.3), the severity is a probability approximated by a sigmoid function, so that there is theoretically always a chance to increase the likelihood of staying non-injured or alive by steering and accelerating. Furthermore, experiments presented in [160] show that people would not reject self-sacrificing completely and would consider it, when a high threshold of injuries for others was reached, which is also not represented appropriately by this model. Another ethical decision experiment [29] shows that the number of killed pedestrians is significant for the choice. At this point the model taking only maximum harm, has also to be discarded.

The finally proposed ethical model is derived by the idea that danger is the absence of safety or in other words: **the absence of safety is danger**. Transferred to this model this means that the risk is the counter probability

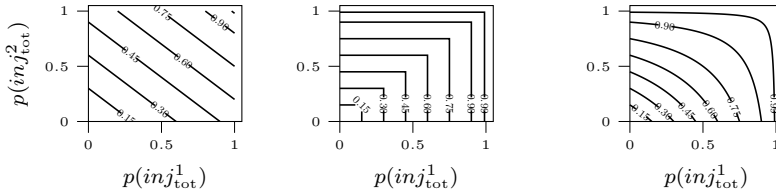


Figure 6.7: Potential lines of different ethical models for concatenating injury probabilities of two occupants 1 and 2. Left: Normalized addition of injury probabilities. Center: Maximum of injury probabilities. Right: Probability of at least one occurring injury of occupant 1, 2 or 1 and 2.

to the case that nobody was injured, which is equal to the probability that at least one occupant is injured. The corresponding ethical model is as follows, where the single injuries are treated as conditionally independent:

$$\begin{aligned}
 f_{\text{eth}}^{\text{as}}(p(\text{inj}_{\text{tot}}^1 | e_k = e_{\text{COLL}}, \mathbf{x}_k), \dots, p(\text{inj}_{\text{tot}}^{N_{\text{OC}}} | e_k = e_{\text{COLL}}, \mathbf{x}_k)) &= \dots \\
 \dots &= 1 - \prod_{q=1}^{N_{\text{OC}}} (1 - p(\text{inj}_{\text{tot}}^q | e_k = e_{\text{COLL}}, \mathbf{x}_k)) \quad . \quad (6.10)
 \end{aligned}$$

The effect of this model is a mixture of both aforementioned approaches (see Fig. 6.7). It approximately aggregates the severity between different victims like the sum model in scenarios with very low severity. Additionally, in scenes with high injury probability for one victim, the focus is mostly fixed on this victim. The behavior in fatal scenes imitates the maximum model but with a smoother adaptation, so that the focus will not completely ignore the less injured victims (see right picture of Fig. 6.7).

The ethical topic around autonomous driving is highly discussed. So note, that the assumed ethical model of Eq. 6.10 and the injury model are proposals by the author. In [107], the report of the German ethic commission was commented by the statement that ethical judgment is inevitably “evil” decisions should not be taken by a programmer. The author of [107] suggests that an independent Non-Governmental Organization keeps track of the implemented ethic principles, which should be discussed by the society to ensure feedback-loops and to relieve pressure on the programmer or car manufacturers. The author of this thesis appreciates that idea to not make decisions for a whole population.

6.5 Severity Models

In the previous sections, sub models for predicting crash, post-crash behavior, consequences and their relationships were introduced. In this section, three severity models for collision evaluation are presented, which are closely related to typical approaches from literature. For this, some of the exhaustively presented sub models are neglected or simplified e.g. taking only the first contact into account or neglecting ethical models because of an ego-centric view. At the end of this section, one severity model is presented, which aggregates the full costs of a crash and its after-crash consequences until the vehicle is standing still like it is proposed in the Ch. 3. In the next chapter, these models are elaborated with regards to their impact on the vehicle motion behavior based on findings from this section.

6.5.1 Constant Severity

The first model is not really a model. It is assuming that the costs of each crash are constant and bigger than zero:

$$c_{\text{COLL}}^{\text{const}}(\mathbf{x}_k) = c_{\text{CONST}} + w_{\text{inj}} > 0 .$$

This constant severity model is the most used model in threat detection or risk assessment monitoring systems like in [141] or for parallel lane scenarios in [133]. Also many Time-To-X (TTX) measures [18, 21, 151, 161] ignore dependencies on input variables and implicitly neglect different crash severities. Here, crash costs will only be of interest in mitigation scenarios but not in normal driving scenarios, that's why they are set as constant. In normal driving, any crash should be avoided or at least monitored, which can be achieved by calculating the collision probability, so that the focus is on the reduction of collision probability. This approach is very conservative and cannot differentiate between highly dynamical crashes with high impact energy and small scratches on a car's body, which is of interest in the transition from normal driving to moderate risk scenes, where future evolutions have multiple risk sources with different crash consequences.

In this thesis, the simple constant severity model is presented to show differences to more sophisticated approaches.

6.5.2 Wall-Impact Severity

The wall-impact model is based on the ideas of risk assessment techniques in highly critical scenarios, where the reduction of the velocity is used to decrease additionally the severity and not only the collision probabilities. In the work of [99], the severity was a quadratic function depending on ego speed. According to a predefined risk level, the vehicle automatically chooses the speed level according to the predicted collision probability and results were shown in a scenario, where the vehicle was slowing down in a narrow tunnel. In [91], the kinematic energy of the ego vehicle was incorporated into a crash mitigation system to force the vehicle to decrease its velocity. In [35], a criticality index for left turnings was introduced, which multiplies the squared ego velocity with the inverse time-to-collision measure, to depict on one side the higher severeness of high velocity crashes and on the other side incorporates time to evade.

As one can see, the previously mentioned models include only states of the ego vehicle and/or harms of the ego vehicle's occupant and nothing or nobody else. This ego-centered view is approximated by representing any collision as a crash into wall (see Fig. 6.8). Here, the ethical model is neglected because of missing other occupants in an ego-centric view. In addition the coping model is not needed, because only the first contact is of interest. Instead of using the kinetic energy or similar squared velocity dependencies like in related works, the injury model of Eq. (6.8) is used to properly predict occupant's harm. The physical crash model of Sec. 6.4.1 between two vehicles is simplified by letting the m^j , representing the mass of the second collision partner j (which is a wall), going to infinity and assuming a straight and central impact. The following model represents the velocity change by an inelastic impact into a wall according to the law of conservation of momentum like in Eq. (6.3) and contact condition for inelastic impacts Eq. (6.4):

$$p^{\text{wall}}(\mathbf{x}_{\text{COLL}}|e_k = e_{\text{COLL}}, \mathbf{x}_k) = \delta(\mathbf{v}_{\text{COLL},k}^i + k_{\text{REST, wall}} \cdot \mathbf{v}_k^i) \quad , \quad (6.11)$$

where \mathbf{v}_k^i is the speed of the ego vehicle j at touching time point, similarly to the touching velocity $\mathbf{v}_{\text{CON},k}^i$, $\mathbf{v}_{\text{COLL},k}^i$ is the velocity after the crash and $k_{\text{REST, wall}}$ is the restitution coefficient between wall and vehicle.

The overall wall-impact severity model can be rewritten into one final equation, using Eq. (6.8) as injury model, Eq. (6.11) as crash model and the cost structure for one crash according to Eq. (6.2):

$$c_{\text{COLL}}^{\text{wall}}(\mathbf{x}_k) = w_{\text{inj}} \cdot L((1 + k_{\text{REST, wall}}) \cdot \|\mathbf{v}_k^i\|, v_{\text{th}}, v_{\text{sl}}) + c_{\text{CONST}} \quad .$$

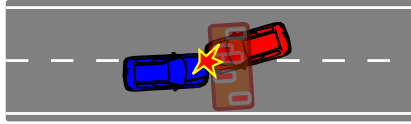


Figure 6.8: Idea of the wall-impact severity model in a two-vehicle crash, where the collision is treated as a frontal crash of the ego vehicle (blue) into an imaginary wall.

It is obvious that the severity is only depending on the ego velocity $\|\mathbf{v}_k^i\|$ at the collision time point.

6.5.3 Vehicle-to-Vehicle Impact Severity

Instead of using the kinetic energy of the ego velocity, the authors of [39], [129] and [171] take the internal energy (heat and plastic deformation) of the collision as a representative quantity in a motion planning system: The higher the internal dissipated energy, the higher the severity. This dissipated energy is derived from a centric, straight impact and results in a formula, which is depended on relative velocities. Furthermore, [39] and [171] take formulas, which are also depending on the vehicle masses. The severity increases for larger masses involved in a crash.

A drawback of this approach is that these equations does not distinguish between the involved vehicles, it only aggregates the full energy without having any information about the single entities with occupant injuries and so on. Therefore, this approach cannot determine, which occupant will be harmed most. So in asymmetric cases e.g. where a truck hits a passenger car, the overall internal energy is not a good predictor for the occupant injuries, because the injury of the car occupants will be much higher than for the truck driver. In this case, the injuries are not equally distributed, so that its underlying ethical model is similar to Eq. (6.9), which was from the ethical point of view not appropriate (see Sec. 6.4.4). Furthermore, the internal energy rises if both vehicles have equal masses, which is in contrast to findings in [56], where the author states a dependency on mass ratio, not on mass sum or product.

However, to adapt the idea of considering both crash participants and

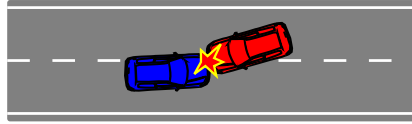


Figure 6.9: Idea of the vehicle-to-vehicle impact severity model in a two-vehicle crash, where the physical crash model based on conservation of momentum is used, but no further events are taken into account.

keeping the character of depending on the relative velocity, the vehicle-to-vehicle severity model $c_{\text{COLL}}^{v_2v}$ is structured as follows: The presented crash model of Sec. 6.4.1 calculates the a posteriori velocities of both vehicles. The injury probabilities of both occupants are determined according to Eq. (6.8). These are inputs for the ethical model according to Eq. (6.10), which based on the calculation of the probability for at least one injury of one of the occupants. The cost from the ethical model is additive to a constant value according to Eq. (6.2). Similar to the wall-impact crash, a subsequent crash is not taken into account, so that a coping model is not needed, like it is seen in Fig. 6.9, where only the first contact plays a role.

6.5.4 Multi-Collision Event Severity

The last model mentioned in this thesis combines the wall-impact severity and the vehicle-to-vehicle impact severity to one severity model and has no origin in the literature. In the previous section it was shown that the wall-impact severity only depends on the ego velocity and the vehicle-to-vehicle impact severity only depends on the relative velocity. The new model takes both inputs, so that the severity of a crash depends on the velocity change through the inter-vehicle crash and the current velocity level. This is realized by assuming multiple events: The first event is an inter-vehicle crash like discussed in the previous section (Sec. 6.5.3) and a second, subsequent event is a crash into a wall according to Sec. 6.5.2.

The probability of the second crash is influenced by multiple variables and parameters. First of all, the coping model determines whether the vehicle will lose control after the first crash event and will end up in a subsequent crash. First, the related probability depends on the angle be-

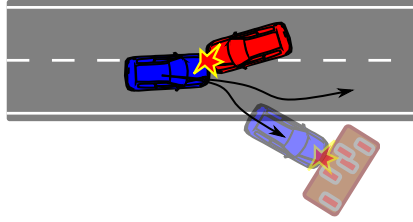


Figure 6.10: Idea of the multi-event impact severity model with a vehicle-to-vehicle crash as the first event and a probable crash into a wall as a potential second event.

tween the contact and the after-crash velocity (see Sec. 6.4.2). Second, the capability to regain control and avoid crashes in case of uncontrolled motion is expressed by a constant escape rate τ_{ESC}^{-1} , explained in Sec. 5.3. It enables the vehicle to not have any further crashes, although it was out of control directly after the first crash. The third component is the crash occurrence with occupied regions in surrounding traffic environment like barriers, walls, standing and driving vehicles. According to Sec. 6.3.1 a collision rate τ_{DISTR}^{-1} depending on the velocity describes the collision probability of one vehicle in an homogeneously distributed static environment. The last component is the time interval when the vehicle is out of control or has the potential to crash into static objects. The time interval length depends the after-first-crash velocity $\mathbf{v}_{\text{COLL},k}^i$ and its deceleration a_{brake} during its after crash braking maneuver: $v^i(t) = \|\mathbf{v}_{\text{COLL},k}^i\| - |a_{\text{brake}}|t$. The collision rate of Eq. (5.1) incorporates the decelerating behavior into a simplified collision rate τ_{DISTR}^{-1} :

$$\tau_{\text{DISTR}}^{-1}(t) = \rho_{\text{DISTR}} \cdot v^i(t),$$

where ρ_{DISTR} is the number of collisions per meter. Taking Eq. (6.1) for total harm, where the harm model of one occupant consists of the injury model according to Eq. (6.8) and the physical crash model according to Eq. (6.11) for impacts with walls. For practical reasons the infinite time horizon in Eq. (6.1) after the first crash is restricted to the moment, where the vehicle is standing still $t_{\text{max}} = |a_{\text{brake}}| / \|\mathbf{v}_{\text{COLL},k}^i\|$.

The crashing evolution of both vehicles is modeled identically. Nevertheless, the velocity change during the first crash and the initial after-first-crash velocities can differ, so that the injury likelihoods may also differ. The combined representative injury is determined by the ethical model

according to Eq. (6.10) calculating the probability of having at least one severe injury. The overall multi-event severity $c_{\text{COLL}}^{\text{multi}}$ is according to the cost structure in Eq. (6.2) like the aforementioned severity models, with a constant severity c_{CONST} offset and the weighted representative injury probability w_{inj} .

6.6 Comparison of Severity Models

In this section a short analysis is given to show the main differences between the state-dependent models like the wall, the inter-vehicle and the multi-event model. The constant model is not discussed here, because of its simplicity it rather serves as a comparative baseline.

In Fig. 6.11 each severity model is shown for different crash constellations, the parameters of all models are listed in Tab. A.5. In the left column the severities are shown for different vehicle speed constellations under a crashing angle of 20° . The wall impact model (top row) has potential lines parallel to the ordinate, meaning that the model is independent of the velocity of the other vehicle j , as a consequence of the ego-centric view and the wall as assumed crashing partner. Furthermore, the logistic injury model provides three different regions: a plateau of low severities for small ego velocities $\|\mathbf{v}^i\|$, an ego speed interval of strong increasing severities and a plateau of high severities in case of high ego speeds. In the right column of Fig. 6.11, the severity is depicted for different crashing angles and ego velocities, where the vehicle speed is set to $\|\mathbf{v}^j\| = 7.5 \text{ m/s}$. One can see that the severity is also independent of the crash constellation and only provides ego speed dependent velocities which are symmetric around $\|\mathbf{v}^i\| = 0 \text{ m/s}$.

In contrast to the wall impact model, the inter-vehicle crash model depends on all mentioned variables. As one can see in the left picture of the center row, the velocities create a valley with minimal values at $\|\mathbf{v}^i\| = \|\mathbf{v}^j\|$, meaning that a crash is evaluated as being of low criticality if their relative velocities are small and is independent of the absolute velocities, so the higher the velocity difference is, the higher the severity. The severity also varies depending on the crashing angle. For low angle crashes like crashes from behind the severity is maximal. For crashes, where the vehicles are scratching the exterior parts, the severity reduces until the fixed constant value for any collision is reached.

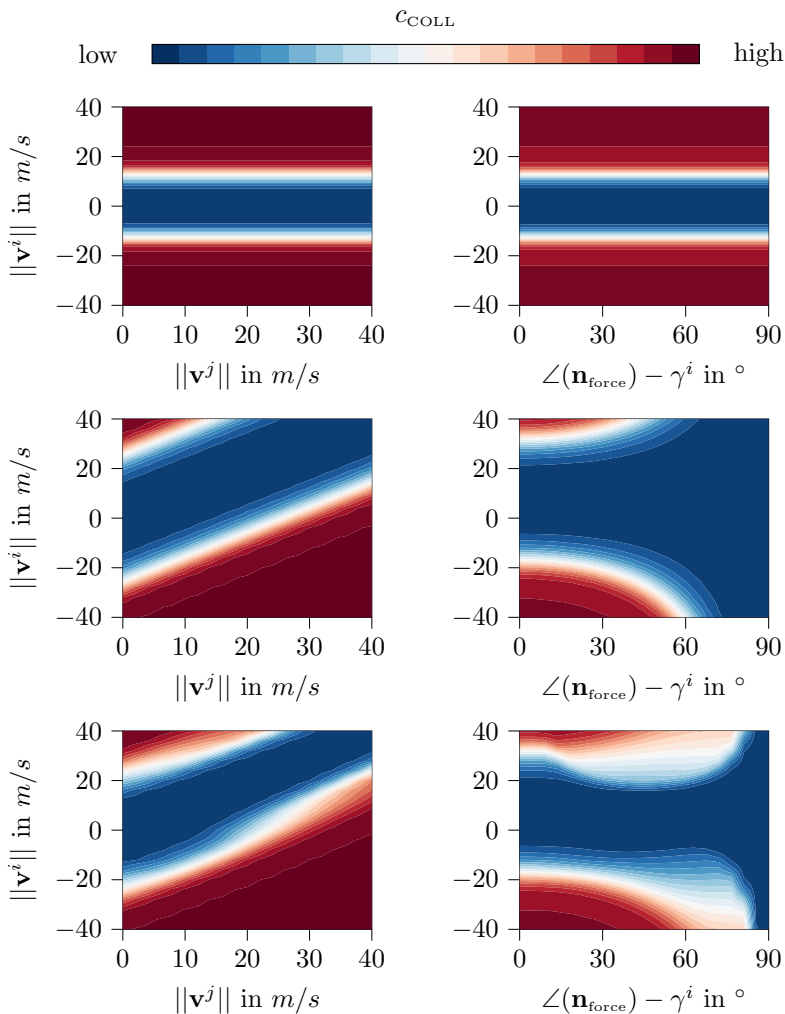


Figure 6.11: Crash severity for wall-impact severity (top row), inter-Vehicle severity (middle row) and multi-event severity (bottom row) depending on the ego velocity $\|\mathbf{v}^i\|$, other velocity $\|\mathbf{v}^j\|$ and crashing angle $\angle(\mathbf{n}_{\text{force}}) - \gamma^i$. Left column: Fixed crashing angle $\angle(\mathbf{n}_{\text{force}}) - \gamma^i = 20^\circ$. Right column: Fixed other velocity $\|\mathbf{v}^j\| = 7.5 \text{ m/s}$.

The multiple-event model (bottom row) which is an extension of the inter-vehicle impact model with another subsequent event shows two main differences. First, the velocity plot inherits the valley of the inter-vehicle impact but this valley is narrowing with higher ego velocity (compare center left with bottom left of Fig. 6.11). This is an effect of the second crash with the wall, because the speed level on which the vehicles have a crash increases the post crash velocity and therefore the probability of a further collision. Second, for small crashing angles, the severity is similar to the severity of the inter-vehicle crash. This is a cause of the neglected probability of subsequent crashes due to small lateral forces during a frontal or rear-end crash. With smaller forces, the vehicle has higher chance to stay on the lane and to not loose control. For higher angles, the influence of the second crash gains importance, because the severity caused by the first inter-vehicle crash becomes small and the lateral forces which push the vehicle out of the lane get higher. For big crashing angles, e.g. where the vehicles have only a slight touch, the lateral forces become small, which let the probability of the second crashes decrease again.

All in all, the wall-impact severity only depends on the ego velocity, the inter-vehicle impact severity depends on the velocity difference and the constellation and the multiple-event model depends on all mentioned inputs and combines qualitatively both severity models.

6.7 Conclusion

In this chapter, the design of severity models for collision event was in focus. The main contributions are as follows:

- A new severity scheme incorporating injury models, ethical considerations between occupants, after-crash coping capabilities and physical crash model, which depends on masses, velocities and crash constellations for a risk-based motion planner with limited computational resources.
- A new coping capability model representing the ability to drive back towards its own lane.
- A new ethical weighting based on the likelihood that at least one occupant gets severely injured.
- A new severity model incorporating ethical considerations and subsequent crashes.

As this chapter shows, not only the probability model depends on the predicted scene states, the presented severity models also include state variables like crashing constellations and velocities. As one can expect that the severity evaluation as part of the risk costs can impact the motion-planning behavior for mitigation like the collision probability evaluation is modeled to produce crash avoiding behavior.

Each of the severity models takes a different set of scene state variables e.g. only ego-states in a wall crash severity model comparing to relative states in a vehicle-to-vehicle severity model, a combined variable set for the new multi-event severity model and an empty set for a constant severity. They all based on different assumptions (partly from literature) about the crash evolution and the consequences. So it is of interest, how will they affect the motion behavior and which differences will occur between them?

7 Severity's Influence on Motion Behavior

In this chapter, the severity models as part of the collision events are investigated to show their impact on the behavior of an vehicle equipped by the motion-planning framework outlined in Ch. 2 and Ch. 3. The collision event has its representation within the framework as a cost-producing risk quantity containing the probability model and the severity model. In the following investigations, the probability model outlined in Ch. 4 is implemented, which imitates the qualitative behavior of Monte Carlo Simulations by adapting the Gaussian probability density function (PDF) shape due to a dynamic collision region and split the non-collided PDF parts according to the constellation of PDF and collision region. Possible corresponding collision severity models are discussed in Ch. 6, where four different models introduced and compared regarding their state dependencies. Next to the collision event, the artificial escaping event (Sec. 5.3) is implemented to the planner to reduce the influence of events far in the future and to emphasize those which will happen in few seconds.

In previous works, collision risk assessments, especially in combination with a severity model, showed effects on the motion planning especially for speed adaptations, e.g. in [99] a maximum risk value was set, which calculates appropriate speed levels for managing scenarios with static objects like tunnels or walls. The speed level was reduced while passing other objects to hold a predefined risk level. Similar behavior is shown in [46], where a Foresighted Driver Model also decreases the speed level while passing another vehicle on the opposite lane. In [64], increasing injury MAIS_n+ levels lead to reducing speed levels in bad weather conditions like fogs.

A detailed investigation of different severity models and their influences on behavior for multiple scenarios has to the best knowledge of the author not been tackled yet. Therefore, a set of different parallel lane scenarios like overtaking and frontal approaching are introduced in Sec. 7.1 so that the four different severity models of Ch. 6 are compared in each of the scenario to show the differences, whether they lead to speed reduction,

how they do it and which safety distances are targeted. To concentrate on the influence of collision risk, desired speeds or other events are not incorporated.

Furthermore, in [54] it was shown that an asymmetric mass distribution between colliding vehicles has a big impact on the harm of occupants, especially for those in the lower weighted vehicle. In Sec. 7.4 this influence of vehicle masses, depicted by different collision partners like trucks, motor cycles or passenger cars, is shown for two severity models. In the end of this chapter, the behavior in case of distributed collision events (see Sec. 5.1) with passengers or static objects on the road is shortly investigated with and without a detailed severity model (see Sec. 7.5).

7.1 Scenario Overview

To limit the amount of different scenarios but to impart an impression of the way how collision severity models influence the motion planning, only scenes with two-vehicles, an ego vehicle i and another vehicle j are presented. Furthermore, scenarios where the ego or other vehicle are exposed to a risk over a long simulation time are same lane scenarios or parallel lane scenarios. By limiting lateral steerings and avoidance maneuvers, the planner's last degree of freedom is to adapt the ego-velocity to a specific level or position itself relatively to the other vehicle like in the following scenario. An overview of scene constellations belonging to same lane scenarios are presented in Fig. 7.1. Here, both vehicles share the same lane so that their lateral offset is around zero. Risky scenarios corresponding to this group are **following** and **being tailgated** in case of vehicles driving in the same direction. If the vehicles are driving into the opposite direction but on the same lane, then this scenario known as "chicken game" is called frontal approaching. In these three scenarios, the initial velocities and positions of the vehicles are in a way that it would come to a collision in finite time, if the vehicles won't intervene.

In Fig. 7.2 those critical scenes are presented, which have a non-zero lateral offset between ego and other lane and are similarly defined like in the case of same lane scenarios: **overtaking**, **being overtaken** and **frontal passing**. In all scenes the vehicle is able to overcome the critical situation by passing each other. These three parallel scenes represent the transition from same lane scenarios to scenarios where both vehicles are far distant from each other so that predicted collision probabilities are vanishing and both can drive and pass freely without interventions.

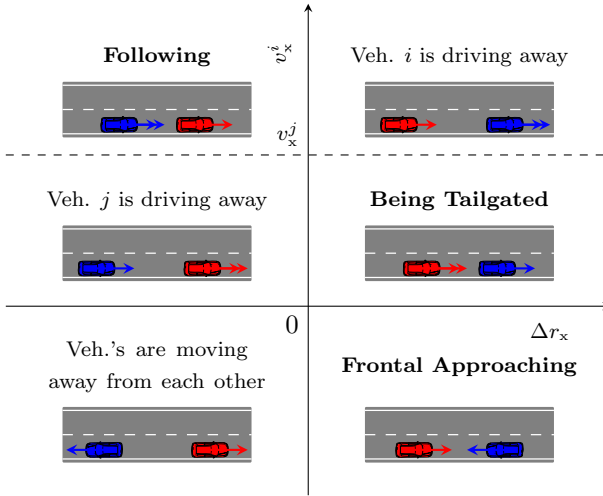


Figure 7.1: Categorization of different same lane scenarios for two vehicles depending on scene states with $\Delta r_y \approx 0$ and from the perspective of vehicle i . The bold written scenarios indicate scenes with high risk potential.

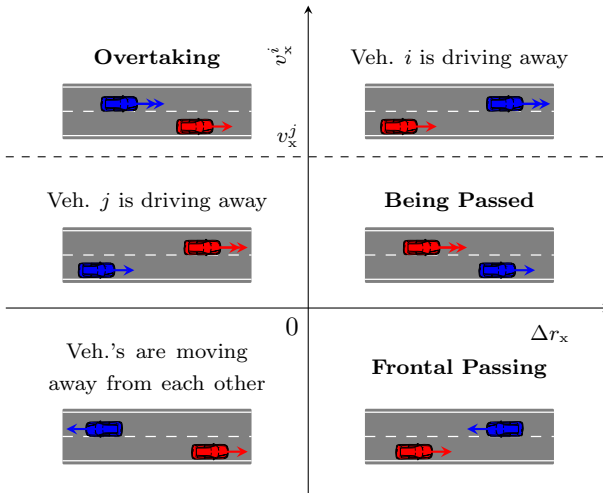


Figure 7.2: Categorization of different parallel or neighbor lane scenarios for two vehicles depending on scene states with $|\Delta r_y| > 0$ from the perspective of vehicle i . The bold written scenarios indicate scenes with high risk potential.

7.2 Same Lane Scenarios

The first category of scenarios deals with those scenarios, where both vehicles are driving on the same lane like the following and frontal approaching scenario.

7.2.1 Following and Being Tailgated

In Fig. 7.3, the integral total costs of the predicted trajectories are shown depending on the initial scene states with ego velocity and relative positions, where the other vehicle is predicted with constant speed $v_x^j = 7.5 \text{ m/s}$. In addition to the total integral cost potential field (color range blue-red), trajectories are drawn into the plot, which are created by letting the planner execute optimal calculated accelerations, i.e., those accelerations which lead to minimal cost. The thick green curves depict a trajectory which brakes with maximum power to avoid a collision.

One can see that for a constant severity (top left) with maximum value, the thick red barrier splits the scene into two regions, where at the left side the ego vehicle is behind the other and on the right side it is vice versa. On the left side, there exists an attractor point in a following scenario representing the headway point at $v^1 = v^2 = 7.5 \text{ m/s}$ and $|\Delta r_x| \approx 50 \text{ m}$ towards which the black trajectories converge. As long as the vehicle is physically able to avoid crashes the real-driven trajectories in a following scenario end up in this stable headway point. On the right side, in a tailgated scene, the ego vehicle has a positive relative distance, the vehicle accelerates according to the comfort, the progress utility and the risk pressure in case of smaller ego velocities relative to the other vehicle's speed.

In comparison to the constant severity, the wall severity in the right upper picture of Fig. 7.3 shows reduced risk zones in scenes, where the ego vehicle drives with small velocity. The MAIS3+ injury saturation for high ego-velocities provides predicted risk potential fields and trajectories which are similar to the planner with constant severity model. For tailgating scenes, there is a region, where trajectories are forced to do a collision. This suck-in is an effect of the higher punishment for high ego velocities. Because the wall-impact severity model is independent of the consequences for the other crash partner, the risk becomes small for low ego speeds, which becomes more attractive for the motion planner.

In this experiment, the inter-vehicle and multiple-event severities in the second row of Fig. 7.3 show similar potential fields and driven trajectories. Although the risk is smaller than for constant severity, the models

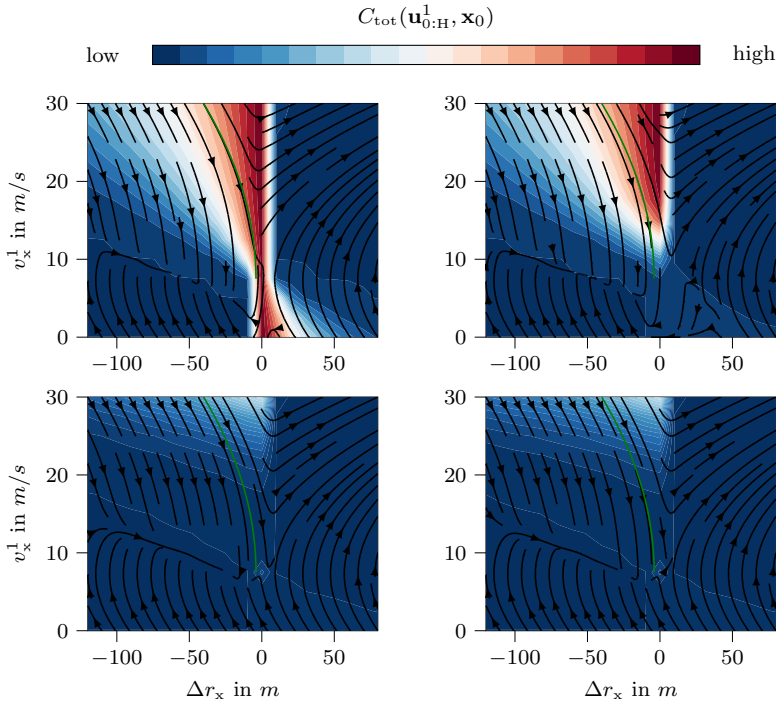


Figure 7.3: Following and Being Tailgating scenarios with total costs potential field and trajectories in $\Delta r_x, v_x$ - state space for different severity models. Red areas indicate high predicted cost regions and the green curves indicate the last braking trajectories to avoid a crash. Top left: constant severity model. Top right: Wall-Impact severity model. Bottom left: Inter-Vehicle impact severity. Bottom right: Multiple-Event impact severity model.

produce crash avoiding and mitigating behavior in following and tailgated scenes. The increasing total costs for higher velocity difference punish scenes, where the speed levels of both traffic participants are dissimilar.

Each severity model shows an attractor region for following scenes, where the ego vehicle velocity becomes equal to the other vehicle speed and converges to a specific headway distance. In Fig. 7.4, the headway distances depending on the velocity level of the other vehicle for the four severity models are depicted. The uncertainties of measurement and behavior are equal for all models and speed levels. One can see, that the

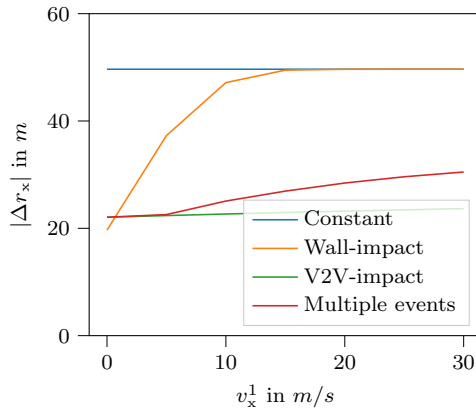


Figure 7.4: Headway distance Δr_x between following and frontal vehicle on the same lane depending on velocity level $v_x = v_x^1 = v_x^2$ and severity models. One can see that the headway distance of the multi-event severity model increases linearly in a similar qualitative manner like the two-seconds headway distance rule.

constant severity model with the always maximal evaluated crash outcome creates the highest distances independent of the other vehicle's speed. The wall-impact severity converges for high velocities to the maximum distance, whereas the inter-vehicle impact model has small headway distances independently of the other speed levels, which only depends on the velocity difference. The multiple-event severity starts also with very low headway distances like the inter-vehicle severity model but has increasing distances because of the additional severity of the second crash, which becomes more serious, when the first inter-vehicle crash is on a higher velocity level. The approximately linear curve reminds qualitatively of the two seconds headway distance rule, but quantitatively this curve is flatter. This driving-school rule regards also long-term braking maneuvers of the ego vehicle in case of frontal stopping vehicles, which is not represented by a constant ego-velocity prediction, where only a deceleration is possible in a short-termed time interval.

7.2.2 Frontal Approaching

In the second group of scenarios, both vehicles approach each other on the same lane while having opposite moving directions. In Fig. 7.5 it is shown that for all severity models, the planner will slow down to a standstill immediately, because it is expecting a crash in future with high severity and probability. In contrast, the planner using the wall-impact severity shows a slightly different behavior, when the ego velocity is around zero (top right). Here, the trajectories converge smoothly to zero compared to the other models, because for small ego velocity in case of wall impacts risk dimension becomes similar to the small dimensions of utility and comfort.

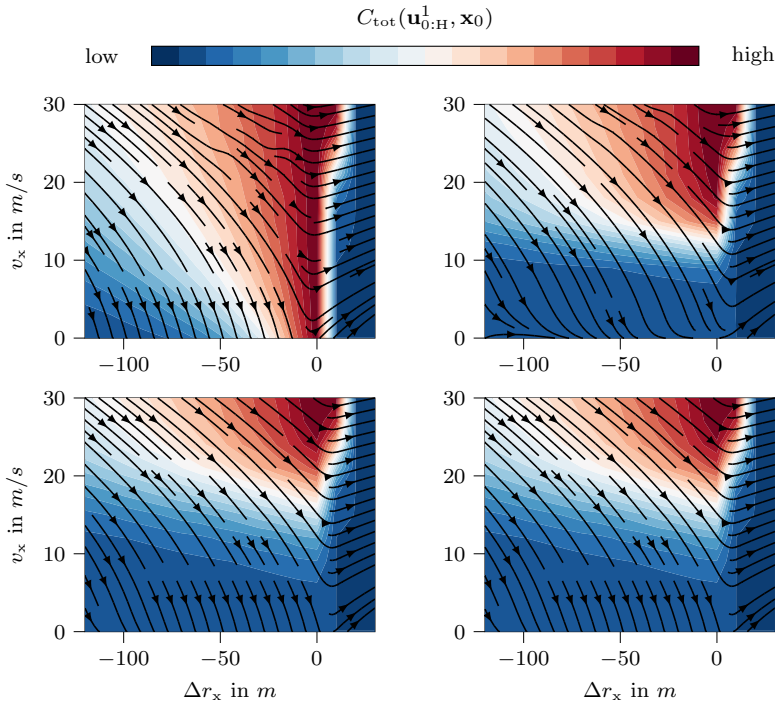


Figure 7.5: Frontal approaching scenarios with total costs potential field and trajectories in $\Delta r_x, v_x$ - state space depending on different severity models. Top left: constant severity model. Top right: wall- impact severity model. Bottom left: inter-vehicle impact severity. Bottom right: multiple-event impact model

7.3 Parallel Lane Scenarios

In the previous section, the same-lane scenarios were discussed, where the ego and the other vehicle drive on an equal lane. In overtaking scenarios, a lateral offset is needed to pass vehicles. The point, where the following behavior switches into an overtaking behavior is depending on the severity model and has different qualitative characteristics. In Fig. 7.6, the predicted total costs are depicted in a potential field depending on the lateral offsets and ego velocities for the constant severity model on the left picture and the multiple-event severity model on the right picture. The black lines represent the relative velocities $\Delta v_{x, \text{opt}}(\Delta r_y)$ with local cost minima for fixed lateral offsets.

One can see, that for the constant severity model the local minimum switches abruptly from negative relative velocities to very high relative velocities, so scenes with overtaking behavior become suddenly attractive in a discrete manner at $\Delta r_y = 3.4 \text{ m}$ (car width $w_{\text{veh}} = 2 \text{ m}$). In contrast, the multiple-event severity model has a two-step transition, starting normally in the following scenario for low lateral offsets, where no overtaking will

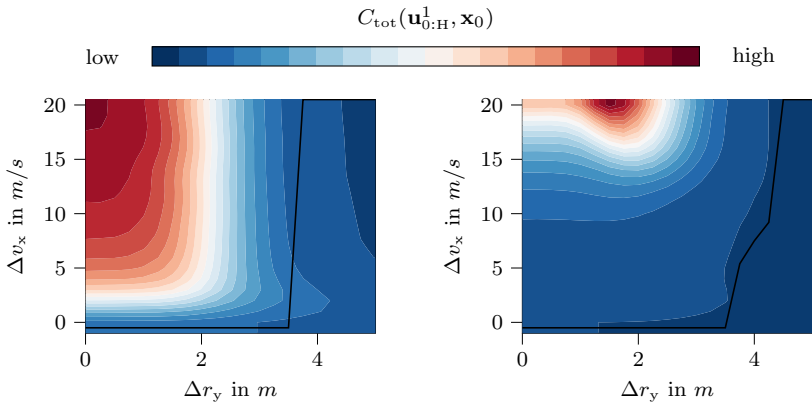


Figure 7.6: Overtaking scenario with total costs potential field and minimum cost curve in $\Delta r_y, \Delta v_x$ - state space for the constant severity model (left) and the multiple-event model (right). One can see that the multiple-event model in contrast to the constant severity model has a lateral offset range $\Delta r_y [3.8 \text{ m}, 4.2 \text{ m}]$, where the velocity differences $\Delta v_{x, \text{opt}}$ smoothly increase with higher lateral offsets. The negative optimal velocity $\Delta v_{x, \text{opt}} < 0$ means that, the ego vehicle will brake in these scenes and will not overtake the frontal vehicle.

take place, until around $\Delta r_y = 3.4 m$. Then, there is a switch to an overtaking behavior with smoothly increasing overtaking velocity differences $\Delta v_{x, \text{opt}}$ with higher lateral offsets until $\Delta r_y = 4.2 m$. For $\Delta r_y > 4.2 m$, the ego vehicle will be not affected anymore and shows similar behavior like the constant severity model. The range of lateral offsets for the smoothly increasing velocity region depends on the model noise like measurements or uncertain behavior assumptions. Nonetheless, both models show qualitatively different behavior in narrow overtaking cases especially in terms of an adaptive velocity in-between range which can be seen as a risk-based explanation for behavior similar to human drivers.

7.3.1 Overtaking

In Fig. 7.7, the velocity difference depending on the longitudinal distances is depicted for a lateral offset of $\Delta r_y = 4.25 m$ between the vehicle. In case of the multiple-event severity model on the right side of Fig. 7.7, the planner produces different behavior depending on its initial states. Trajectories on the left and below the high risk region converge to the headway distance. On trajectories starting at the right of the high risk region, the ego vehicle is braking down to a specific velocity level and passes the other vehicle like it was previously shown from the Δr_y - Δv_x perspective. Trajectories with initial speed difference faster than $25 m/s$ are passing without velocity reduction. In case of a constant severity, depicted on the left side of Fig. 7.7, only two main behaviors appear where the trajectories are either converging to the attractor point defined by the headway distance or are overtaking the other vehicle by accelerating with maximum power. Both starting regions are divided by the high risk diagonal region in red color. The region above the potential hill produces a suck-in behavior, where the ego vehicle is forced to overtake the other vehicle as fast as possible. In this experiment it becomes obvious that depending on the severity model the ego vehicle behaves very differently, and that some severity models provide driver behaviors that are more compatible with the human driving than others.

Both experiments show that there exists a specific relative velocity depending on the lateral offset, which is targeted by the ego vehicle during the overtaking process. Fig. 7.8 shows that these relative velocities depends on the lateral offset and on the other vehicle's speed. In case of higher velocities, the constant severity model (top left) and the wall impact severity model (top right) produce a discrete switch between following and accelerating overtaking behavior. The inter-vehicle impact severity model

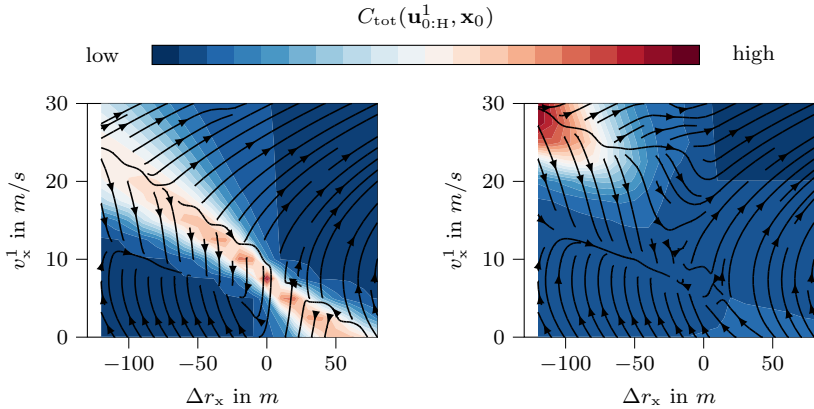


Figure 7.7: Overtaking and overtaken scenario with total costs potential field and trajectories in $\Delta r_x, v_x^1$ - state space depending on different severity models and with fixed lateral offset $\Delta r_y = 4.25 m$. Left: Constant severity model. Right: multiple-event severity model. One can see that not all trajectories lead to overtaking behavior and that in case of taking the multiple-event severity model, the trajectories executes a dip during the overtaking.

(bottom left) has a broad range in lateral offsets, where a limiting relative velocity occur which is independent of the other’s velocity. In contrast, the multiple-event model shows a similar broad range of adapted velocities but the band size is adapted in width and offset depending on the other vehicle’s velocity. This leads to a behavior where the ego vehicle is more cautious in scenarios with small overtaking offsets and where the ego vehicle reduces its velocity differences in case of greater scene speed levels.

7.3.2 Being Passed

In a scene state of “being passed”, the other vehicle is faster than the ego vehicle. For the constant severity model and the wall-impact severity model, the targeted velocities $\Delta v_{x, \text{opt}}$ depends on the lateral offset Δr_y and the other velocity v_x^2 . In Fig. 7.9 one can see that for the wall severity model on the right plot the relative velocity magnitude is similar to the other vehicle’s speed for small offsets, meaning that the ego vehicle is forced to standstill in case of a tailgating scenes. The ego vehicle is reducing its relative velocity with higher offsets. For high lateral offsets, the relative speed is not raising anymore because of an applied speed limitation for the

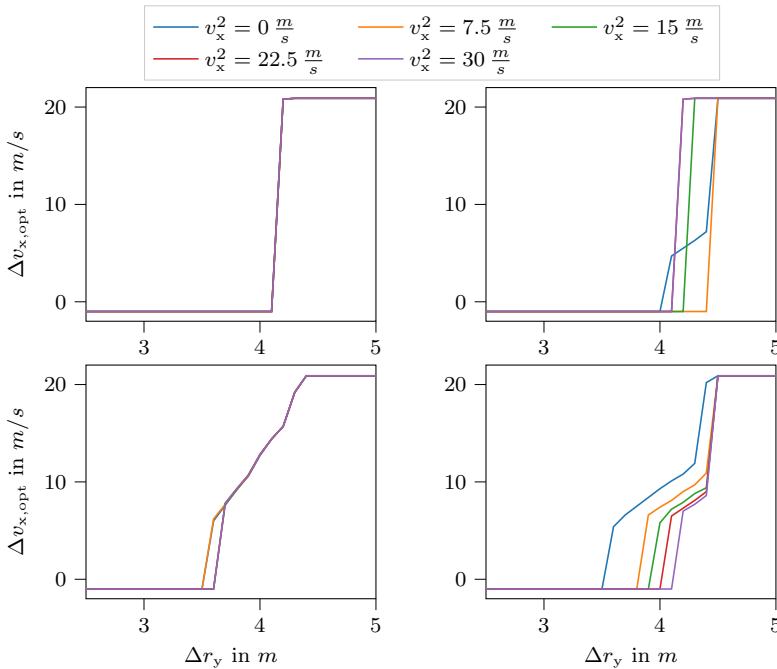


Figure 7.8: Relative overtaking velocities depending on other's velocity level and lateral offset for specific severity models. Top left: constant severity model. Top right: wall- impact severity model. Bottom left: inter-vehicle impact severity. Bottom right: multiple-event impact model

ego vehicle. In contrast, taking the constant severity model on the left of Fig. 7.9 the ego vehicle will only brake to standstill while being overtaken in case moderate lateral offsets. The inter-vehicle and the multiple-event impact severity models do not show any braking behavior while being overtaken (plots not shown): the vehicle will accelerate to avoid any crash similar to the tailgating cases of the shown severity models.

7.3.3 Frontal Passing

The last experiment to evaluate the different severity models in parallel scenes is the frontal passing like on country roads, where another vehicle is driving on a neighboring lane into the opposite direction of the ego

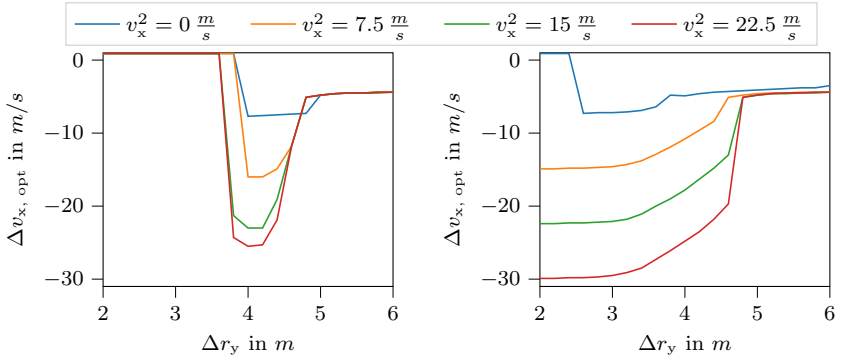


Figure 7.9: Relative targeted velocities while being passed depending on other’s velocity level and lateral offset for specific severity models. Left: constant severity model. Right: wall- impact severity model

vehicle’s motion. In Fig. 7.10, the ego velocity instead of the relative velocity between both vehicles is shown in case of different other vehicle’s passing velocities and lateral offsets. The constant severity (top left) shows a hard switch between stopping and passing with acceleration like in the overtaking case. As expected, the wall-impact severity (top right) shows an independence of the other vehicle’s velocity by choosing the optimal passing velocity. The inter-vehicle (bottom left) and multi event severity model (bottom right) influences the cost calculation in a way, that the ego velocities are reduced for larger other vehicle’s velocities. That behavior remains up to a specific velocity v_x^j , where the severity saturates because of the injury sigmoid function, behaving like the constant severity model with one discrete switch. The three state-dependent models show more cautious behavior by having smaller driving velocities in case of narrower frontal passings.

7.3.4 Behavior Overview

An overview of same lane and parallel lane scenarios, discussed in the previous sections, for all severity models is given by the following table:

Tab. 7.1 summarizes that the motion planner with constant severity model shows only discrete switches between same lane and parallel lane scenarios. In contrast, the state-depending severity models overcome this problem and adapt their velocities according to the lateral offset. In these

Scenario	Sev. Mod.	Constant	Wall-impact	Vehicle-to-Vehicle	Multiple events
Following		Braking to constant headway distance	Braking to velocity dependent headway distance	Braking to constant headway distance	Braking to velocity dependent headway distance
Being Tailgated		Accelerating	Braking to force low crash outcome	Accelerating	Accelerating
Frontal Approaching		Braking to standstill	Braking smoothly to standstill	Braking to standstill	Braking to standstill
Overtaking		Discrete switch	Depending on velocity level: Discrete switch or smooth transition	Smooth transition with fixed difference velocity	Smooth transition and increasing difference velocity
Being Overtaken		Braking to target velocity	Braking to target velocity	Accelerating	Accelerating
Frontal Passing		Discrete switch from standstill to passing	Smooth transition and fixed passing ego velocity	Smooth transition and increasing ego velocity	Smooth transition and increasing ego velocity

Table 7.1: Motion planner behavior overview depending on implemented severity model and initial scenes. The top half scenes are same lane scenario, where the behavior inside the lane is described. The scenarios on the bottom half contain parallel lane scenarios, where the transition over the lateral distance (discrete or smooth) and the target velocity while passing is listed.

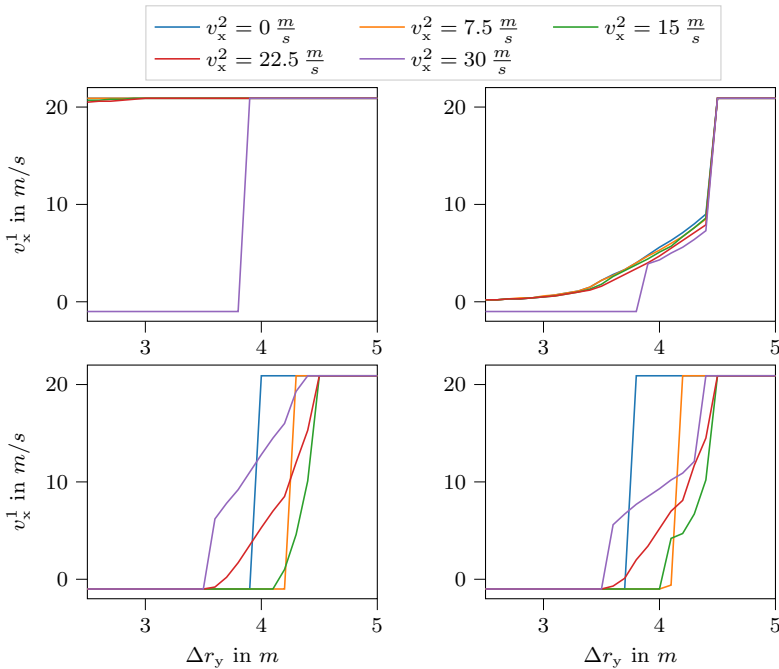


Figure 7.10: Ego velocities while frontal passing depending on other’s velocity level and lateral offset for specific severity models. Top left: constant severity model. Top right: wall-impact severity model. Bottom left: inter-vehicle impact severity. Bottom right: multiple-event impact model.

moderate risk scenarios, the severity and the probability work against each other. The severity increases with higher velocities, whereas the probability declines. Therefore the risk, the product of both, leads to a minimum at specific velocities.

In general, the constant severity and wall-impact model show special behavior in tailgating scenes, where they force the motion planner to zero velocity and therefore evoking critical scenarios. The wall-impact model shows ego-state dependent behavior for low ego-velocities, and similar behavior to the constant severity for high ego-velocities. The vehicle-to-vehicle severity model provides collision avoiding behavior in all shown scenarios and creates a relative velocity adaptivity for lateral offset in moderate risk scenarios e.g. overtaking and frontal passing. The multiple-

event severity keeps the collision avoidance behavior in all scenarios of the vehicle-to-vehicle severity model, as well as its relative velocity adaptivity. Furthermore, it has an ego velocity dependent behavior similar to the wall-impact model.

7.4 Influence of Vehicles Mass-Ratio

In the previous sections, the differences of the four different severity models and their general behavior in different initial scenes are discussed. In these settings, the ego and other vehicle have similar masses and geometry. The derivation of the physical model of the inter-vehicle crash (see Sec. 6.4.1) with conservation of momentum shows a dependency of the after-crash states of both vehicles on the vehicle masses.

In Fig. 7.11, the influence of the mass ratio $\tilde{m} = m^i/m^j$ on the overtaking velocity difference for the inter-vehicle impact and the multiple-event impact severity is shown, where $v^j = 7.5 \text{ m/s}$. Both models show that the overtaking velocity get reduced for higher mass ratios. This is caused by the raising injuries for the weakest collision partner, because higher relative masses increase the crash-related accelerations within the smaller weighted partner, which leads to higher occupant injuries and raises the probability

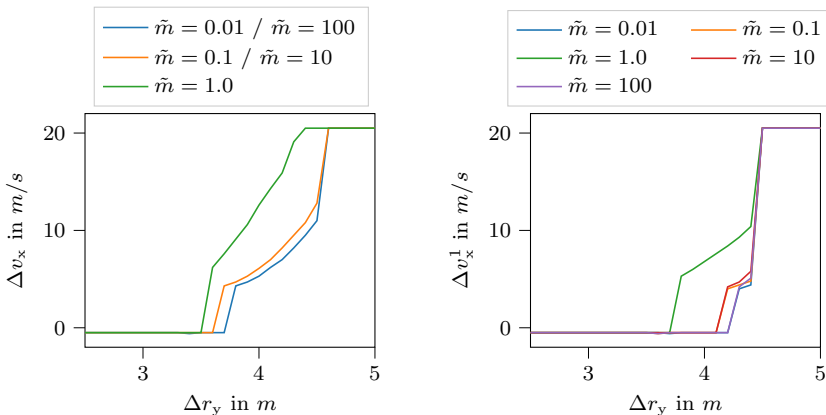


Figure 7.11: Relative overtaking velocities depending on mass ratio \tilde{m} and severity model. Left: inter-vehicle impact severity. Right: multiple-event impact model.

of a subsequent crash. This feature is also in compliant with the findings of [54, 56]. The models enable the effect that the collision partner with the lower mass is more protected, because additional information about the mass distribution between the vehicles is considered appropriately.

7.5 Distributed Collision Areas

As introduced in Sec. 5.1, a collision event does not have to be necessarily deterministic. For these distributed collision events, a severity model can also be implemented to model state dependent outcomes. Fig. 7.12 shows the dependency of the obstacle density parameter ρ_{DISTR} on the targeted driving speed in case of a crash with wall-like objects or pedestrians. One can see that with increasing object density the ego speed is reduced. Furthermore higher injury probabilities like for hitting pedestrians in comparison to the harm likelihood of the ego vehicle's occupants into a wall, reduces also the targeted velocity. Depending on the expected harm of the traffic participants, the behavior will be more cautious in terms of lower velocities if the traffic participant is less protected.

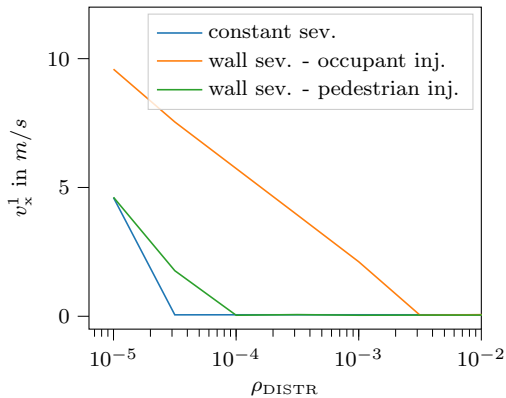


Figure 7.12: Optimal driving velocity in an area of distributed events for constant severity and different injury parameter settings of the wall-impact severity.

7.6 Conclusion

To sum up the chapter of the influence of severity model on the vehicle's behavior, the following findings are:

- Motion planners with state-dependent severity models show a smoother transition from same lane to parallel lane scenes by targeting specific passing velocities.
- Severity models including masses are more cautious in scenarios where the collision partners are unequal.
- The simple constant severity model and the wall-impact model can accelerate the entrance into critical scenes through braking maneuvers in tailgating scenarios.
- The multiple-event severity model shows the best critical scene avoidance behavior by creating speed adaptations depending on collision speeds and relative velocities in parallel lane scenarios, whereas other state-dependent models can only produce either-or behavior. It can best simulate behaviors known from human drivers like speed adaptivity in narrow streets.
- The four severity models have different dependencies of driving velocity on the headway distance in the following scenario. The vehicle-to-vehicle severity model and the constant severity model shows independence of the driving velocity, whereas the other models have increasing headway distances for higher speed levels.
- For distributed collision events, the wall-impact severity model produces behavior, where the motion planner drives through the collision region on specific velocity levels, which decrease by more fragile collision partners and higher obstacle density.

All in all, one can state that the severity models introduced in the previous Ch. 6 keep their state dependency according to their derivations and show in a different manner their influence on the motion behavior.

8 Summary and Outlook

8.1 Summary

The main hypothesis that a severity calculation affects the motion planner can be confirmed. Each of the designed severity models are used as a component of risk assessment and show different behavior in comparison to each other and to the naive constant severity model. Especially in terms of headway distances in following scenarios and speed levels in narrow passing scenarios, where the relative speed is adaptive in a range of lateral offsets and do not switch binary between following and free driving. Furthermore, parameters like masses, only used by a subset of the presented severity models, provokes smaller relative speeds to achieve similar risk levels between dissimilar collision partners. Another fact is that ego-centered severity models, e.g. the wall-impact model, or simple constant models show criticality increasing behavior, which could end up in collisions. Only the vehicle-to-vehicle severity model and the multi-event model can guarantee collision avoidance in the investigated scenarios, because they will not brake during a tailgating scenario.

These results show that the limited view only on probability models is not sufficient to produce safe behavior and thus more sophisticated severity models are necessary to decrease criticality in a scene. Furthermore, with sophisticated severity models it is possible to depict known human behavior like the speed adaptivity, increasing headway distances and mass dependent cautious behavior to protect vulnerable traffic participants.

In the following, the other questions in the introduction of this thesis are answered in more detail:

The first questions of this thesis regard the incorporation of different types of events into a behavior planning framework. It was necessary to build a foundation for investigating collision event-forced severities as one part of different behavior determining factors next to utility and comfort in a broad range of scenarios from free driving to collision mitigation. In Ch. 2 a general structure of the behavior planning including the prediction, evaluation and decision is introduced, which calculates optimized acceler-

ation outputs for an ego vehicle based on objects in the environment. To add events into the stochastic-based prediction framework, event detection models are incorporated to identify critical events dependent on their relative states and enable the determination of event probabilities by a given state distribution. Events mostly have influence on the goals of the drivers that is why a long-term intention variable was introduced. This driver intention impacts the evaluation of considered events by weighting factor according to their importance in the current scene e.g. utility is neglected after a collision was predicted. The evaluation of events is done by determining their risk, the product of probability and severity, so that severity reducing crash mitigation strategies and probability reducing collision avoidance strategies and their combined strategy can be incorporated into one framework. Different events are evaluated according to a hierarchy of importance to not outweigh e.g. comfort against severe injuries. To simplify the behavior investigation impacted by severity models, the planner is limited to a ramped velocity prediction which chooses the first-step acceleration input to minimize the total predicted costs.

The complexity of the prediction process with its multiple scene evolutions addresses the need to simplify the scene prediction part. For that, in Ch. 3 an approach was introduced to determine recursively the probability magnitude and the distribution shape dependent on the initial states distribution and a predicted behavior. This approach focuses on the non-collided trajectory distribution and truncates those parts engaged in a collision and keeps the conditional dependence between events and between discrete time points.

Examples for different event types are given in Ch. 4 and Ch. 5. Both tackle the question of how different event probabilities can be determined. The main focus of this thesis was related to collision events between two vehicles, discussed in Ch. 4. Typical Monte Carlo simulations needs a lot of computational effort and other approaches in the literature cannot depict crash forced PDF adaptations in all geometrical constellations and with multiple objects. To tackle these drawbacks, a new technique was derived based on multiple analytic truncations of the predicted PDF according to the representation of the geometrical overlap of two vehicles. To increase the prediction and detection accuracy of future events, this approach was extended on the one hand by a PDF splitting procedure to depict several evolution scenarios like yielding and not yielding and on the other hand by a dynamic collision region to tackle sampling issues in scenarios with high relative velocities and high sampling time intervals to not miss collisions. Furthermore, this new truncation model for probability calculation and

prediction confirmed the split from shape and magnitude and shows better performance to produce safe behavior than shape-neglecting approaches like rate-based approaches.

In Ch. 5, three more types of events are introduced: 1. for physically not reachable states like in case of limited engine power or internal speed limitations, 2. for distributed collision events for quasi-homogeneous distributed objects like in case of occluded objects through fog or darkness and 3. for escaping events representing an immediate opportunity to move into a safe state. The escaping event is already known in the literature but is adapted into the used motion planning framework. All events show high accuracy in shape and magnitude compared to Monte Carlo simulations.

The last and main question was how severity models affect the motion behavior, which is already answered in the first two paragraphs of this summary section. Thus, a preliminary question of how severity models are designed and what should their incorporate was addressed in Ch. 6, where a scheme was introduced consisting of all necessary components to predict and evaluate the crash itself and the after-crash evolution. For the physical crash a decentralized crash impact model from a conservation of momentum approach was used. A coping model was designed to depict the ability to regain control after a collision and coming back to its own lane. Lastly, a prediction model for severe occupant injuries during the collision and an ethical concatenation of injuries of different traffic participants were introduced. Based on these sub models, three severity models are derived, partly according to ideas given in literature: 1. a wall-impact model, assuming that a crash into a wall is similar to a crash between vehicles, 2. an inter-vehicle crash model regarding only the first event and 3. a multiple-event model with an inter-vehicle crash at the first event and a possible second crash into a wall. As already mentioned above, these severity models show significant behavior differences comparing to the simple constant severity model.

All in all, an event-prediction framework is implemented, which is open to add different types of events and to concatenate them into an overall cost evaluation regarding probability and severity for maneuver planning in moderate risk scenarios, reaching from free driving to collision mitigation.

8.2 Published Contributions

The author of this thesis has published three papers as first and second author. These papers only cover a part of the content outlined in this

thesis:

1. In [111], a risk-based planner according to Ch. 2 was introduced based on event rate considerations for calculating event probabilities according to Sec. 3.6 with a collision model described in Sec. 4.7. The severity was an one-dimensional version of the more sophisticated multi-event severity model of Sec. 6.5.4 with similar sub models like the physical crash model but without ethical considerations. The behavior investigation shows human-imitating behavior like the speed level increase dependent of higher lateral offsets to an overtaken vehicle. It also shows influences on the headway positions, which decreases for larger lateral offsets and tailgating vehicles. Not mentioned there, was the later finding that only a small magnitudes of relative velocities for oncoming shows an converging behavior to the attractor headway position. Higher magnitudes lead to accelerating behavior and as a consequence of that to a crash. This paper has reached a price for best-paper candidate at the 5th International Symposium on Future Active Safety Technology of toward Zero Accidents at 2019.
2. In the work of [47], the survival theory framework of Sec. 3.6 for cost and event probability calculations was introduced in a similar manner like it was presented in Sec. 3.4 of this thesis, but without consideration of PDF shape adaptations. It systematizes the motion planner of the first paper [111]. The models for collision probability and severity calculation were chosen similarly to the first paper [111]. Three different statements were claimed to show the power of the rate-based risk assessment comparing to the very limited, but well-known Intelligent Driver Model [156]. First: the similar behavior between the Intelligent Driver Model and the presented model in a two-car following scenario was highlighted. Second, the rate-based framework was able to handle multiple risk sources in the scene like a frontal vehicle and a tailgating vehicle. Third, the rate-based framework produces velocity adapting behavior while overtaking which cannot be represented by the Intelligent Driver Model.
3. The last paper [110] introduces the analytic truncation method (Sec. 4.5) with static collision region, formulated in Sec. 4.4.1 for calculating collision event probabilities over the full prediction horizon. It shows in different experiments that the analytic model calculates similar collision probability quantities but with higher computational

speed than a Monte Carlo Simulation. Furthermore, the shapes of the Gaussian PDF's can well represent the particle distribution like it was investigated in Sec. 4.8.1. Because of the broad range of similarities, it highlights the necessity of a time-course sensitive PDF shape consideration in addition to the time-course sensitive magnitude in the survival theory.

8.3 Outlook

Until here, the advantages of the introduced framework were discussed and presented, but there are multiple ways to connect further research and extend this work.

The system for risk prediction with different events is only being evaluated off-line via simulated environments for a limited set of scenarios, mostly consisting of only two vehicles in parallel lane scenarios, but the models are designed to be also applicable for more complex scenarios like intersection scenarios with two oncoming vehicles, in-between scenarios, merge-ins or scenarios with multiple different event types like traffic rule restrictions. They all can be investigated and analyzed on top of these thesis.

Further investigations should also consider the acceptance by humans. This includes on one side the vehicle's behavior in traffic with its interaction with other vehicles and the risk-averse strategy. On the other side the approaches made by designing the collision severity with its injury assessment and ethical weighting between different injured occupants are also open for discussion and further improvements in terms of ethical decision making.

The analytic collision probability is faster than the MC algorithm with 100 particles, but is not real-time capable for motion planning methods, because the optimization procedure needs a lot of prediction-evaluation cycles to find a local or at best the global minimum. The author suggests that two strategies with the analytic probability calculation to find a fast initial parameter sets for optimal behavior strategies are 1. using higher sampling time intervals for faster risk calculation in lane segments with low curvatures and 2. using high motion noises and taking the predicted (split) GMM to take the mean states of the highest weighted component as an initial trajectory for the optimization process.

As an advancement for the motion planning framework, the prediction process, which has very simple constant velocity assumptions for other

participants, should include scene-state dependent actions to mimic interactions for a more accurate predictions process. In addition, more events can be incorporated according to the scheme like lane departure events, traffic light events, loss of control in curvatures or also triggering events for changing intentions to avoidance strategy or the detection of inevitable collision scene-states to follow predefined mitigation strategies.

To plan the ego behavior in traffic scenes with multiple objects or events, a more advanced behavior planner with more than a single short-termed velocity ramp is needed as prediction like double-ramps [129] or Rapidly Random Trees (RRT's) [39] and also for lateral motions. Furthermore, after a collision with one other vehicle is predicted, the other vehicles in the traffic scene won't disappear. If it is very crowded, one inter-vehicle-crash can lead to subsequent inter-vehicle crashes which are not addressed by the severity model in this thesis. Not including these additional crashes can lead to drastic underestimations with false escaping behaviors and therefore to more critical evolutions than expected.

Next to the risk, utility and comfort evaluation, also costs for fuel consumption can be taken into account within the evaluation step of the risk-base motion planner to reduce the impact on the environment.

A Attachment

A.1 Hyperplanes Simplification over Time

In this section, a detailed derivation of the simplification in Eq. (4.12) is provided:

$$\begin{aligned} \widehat{\mathbb{M}}_{\text{COLL},k}^{\text{dyn}} &= \bigcap_{l=1}^8 (\mathbb{H}_k^l(-\Delta t) \cup \mathbb{H}_k^l(0)) \\ &\approx \bigcup_{\tilde{\Delta}t \in \mathbb{T}^h} \bigcap_{l=1}^8 \mathbb{H}_k^l(\tilde{\Delta}t) = \mathbb{M}_{\text{COLL},k}^{\text{dyn}} . \end{aligned} \quad (\text{A.1})$$

The first step to transform the right side of Eq. (A.1) to the left side with its approximated collision region $\widehat{\mathbb{M}}_{\text{COLL},k}^{\text{dyn}}$ is to twist the order of union and intersection, which results in the following relationship:

$$\bigcup_{\tilde{\Delta}t \in \mathbb{T}^h} \bigcap_{l=1}^8 \mathbb{H}_k^l(\tilde{\Delta}t) \subseteq \bigcap_{l=1}^8 \bigcup_{\tilde{\Delta}t \in \mathbb{T}^h} \mathbb{H}_k^l(\tilde{\Delta}t) . \quad (\text{A.2})$$

The right side of Eq. (A.2) is similar to the left side of Eq. (A.1), so that only the following relationship has to be checked:

$$\mathbb{H}^l(-\Delta t) \cup \mathbb{H}^l(0) = \bigcup_{\tilde{\Delta}t \in \mathbb{T}^h} \mathbb{H}^l(\tilde{\Delta}t) ,$$

which can be proved by checking the two following conditions:

1. $\mathbb{H}^l(-\Delta t) \cup \mathbb{H}^l(0) \subseteq \bigcup_{\tilde{\Delta}t \in \mathbb{T}^h} \mathbb{H}^l(\tilde{\Delta}t)$
2. $\bigcup_{\tilde{\Delta}t \in \mathbb{T}^h} \mathbb{H}^l(\tilde{\Delta}t) \subseteq \mathbb{H}^l(-\Delta t) \cup \mathbb{H}^l(0)$.

The first condition is simply proved by reformulate it by an equivalent transformation:

$$\begin{aligned} \mathbb{H}^l(-\Delta t) \cup \mathbb{H}^l(0) &\subseteq \bigcup_{\tilde{\Delta}t \in \mathbb{T}^h} \mathbb{H}^l(\tilde{\Delta}t) \\ \Leftrightarrow \mathbb{H}^l(-\Delta t) \cup \mathbb{H}^l(0) \cup \bigcup_{\tilde{\Delta}t \in \mathbb{T}^h} \mathbb{H}^l(\tilde{\Delta}t) &= \bigcup_{\tilde{\Delta}t \in \mathbb{T}^h} \mathbb{H}^l(\tilde{\Delta}t) \quad , \end{aligned}$$

which is obviously true, because the borders are part of the index set $\Delta t, 0 \in \mathbb{T}^h$.

The second condition is reformulated in another way:

$$\begin{aligned} \bigcup_{\tilde{\Delta}t \in \mathbb{T}^h} \mathbb{H}^l(\tilde{\Delta}t) &\subseteq \mathbb{H}^l(-\Delta t) \cup \mathbb{H}^l(0) \\ \Leftrightarrow \bigcup_{\tilde{\Delta}t \in \mathbb{T}^h} \mathbb{H}^l(\tilde{\Delta}t) \setminus (\mathbb{H}^l(\Delta t) \cup \mathbb{H}^l(0)) &= \emptyset \\ \Leftrightarrow \bigcup_{\tilde{\Delta}t \in \mathbb{T}^h} \mathbb{H}^l(\tilde{\Delta}t) \cap (\mathbb{H}^l(\Delta t) \cup \mathbb{H}^l(0))^C &= \emptyset \\ \Leftrightarrow \bigcup_{\tilde{\Delta}t \in \mathbb{T}^h} \mathbb{H}^l(\tilde{\Delta}t) \cap (\mathbb{H}^l(\Delta t))^C \cap (\mathbb{H}^l(0))^C &= \emptyset \quad , \end{aligned}$$

where $(\mathbb{H}^l(-\Delta t))^C$ and $(\mathbb{H}^l(0))^C$ are the complements of the related sets. The following set of inequalities has to be checked for contradiction to show that there don't exist any constellation which is inconsistent:

$$\begin{aligned} \Leftrightarrow \neg \exists \tilde{\Delta}t \in \mathbb{T}^h, \mathbf{x} \in \mathbb{R}^n : \quad &\mathbf{v}^l(\tilde{\Delta}t)^T \mathbf{x} \geq w^l(\tilde{\Delta}t) \\ &\wedge \mathbf{v}^l(-\Delta t)^T \mathbf{x} < w^l(-\Delta t) \\ &\wedge \mathbf{v}^l(0)^T \mathbf{x} < w^l(0) \quad . \end{aligned}$$

One can show that the inequalities in Eq. A.1 with the definitions of the vectors $\mathbf{v}^l(\tilde{\Delta}t)$ and shifts $w^l(0)$ according to Eq. (4.11) provide solutions $\tilde{\Delta}t \in \mathbb{T}^h$ for $\mathbf{u} \neq \mathbf{0}$. So that this condition do not hold in general. So the approximated collision region is really an approximation for the true collision region $\mathbb{M}_{\text{COLL},k}^{\text{dyn}}$.

A.2 Simplifying Dynamic Collision Region

In this attachment, the derivation of the following equality of the following terms for determining the approximated collision region $\widehat{\mathbb{M}}_{\text{COLL},k}^{\text{dyn}}$ is shown:

$$\begin{aligned}\widehat{\mathbb{M}}_{\text{COLL},k}^{\text{dyn}} &= \bigcap_{l=1}^8 (\mathbb{H}_k^l(-\Delta t) \cup \mathbb{H}_k^l(0)) \\ &= \bigcap_{l=1}^4 [\mathbb{H}_{\text{sp},k}^l \cap \mathbb{H}_k^l(-\Delta t) \cap \mathbb{H}_k^{l+4}(0)] \cup [\mathbb{H}_{\text{sp},k}^{l,c} \cap \mathbb{H}_k^l(0) \cap \mathbb{H}_k^{l+4}(-\Delta t)]\end{aligned}$$

The left side is extended by the splitting set and its complement $\mathbb{H}_{\text{sp},k}^l \cup \mathbb{H}_{\text{sp},k}^{l,c} = \mathbb{R}$ as follows:

$$\begin{aligned}\bigcap_{l=1}^8 \left(\left[(\mathbb{H}_{\text{sp},k}^l \cup \mathbb{H}_{\text{sp},k}^{l,c}) \cap \mathbb{H}_k^l(-\Delta t) \right] \cup \left[(\mathbb{H}_{\text{sp},k}^l \cup \mathbb{H}_{\text{sp},k}^{l,c}) \cap \mathbb{H}_k^l(0) \right] \right) &= \dots \\ \dots &= \bigcap_{l=1}^8 \left(\left[\mathbb{H}_{\text{sp},k}^l \cap \mathbb{H}_k^l(-\Delta t) \right] \cup \left[\mathbb{H}_{\text{sp},k}^{l,c} \cap \mathbb{H}_k^l(-\Delta t) \right] \cup \dots \right. \\ &\quad \left. \dots \cup \left[\mathbb{H}_{\text{sp},k}^l \cap \mathbb{H}_k^l(0) \right] \cup \left[\mathbb{H}_{\text{sp},k}^{l,c} \cap \mathbb{H}_k^l(0) \right] \right).\end{aligned}$$

One can show that the following equations hold in case of hyperplanes defined by parameters according to Eq. (4.11):

$$\begin{aligned}\mathbb{H}_{\text{sp},k}^l \cap \mathbb{H}_k^l(0) &\subseteq \mathbb{H}_{\text{sp},k}^l \cap \mathbb{H}_k^l(-\Delta t) \\ \mathbb{H}_{\text{sp},k}^{l,c} \cap \mathbb{H}_k^l(-\Delta t) &\subseteq \mathbb{H}_{\text{sp},k}^{l,c} \cap \mathbb{H}_k^l(0),\end{aligned}$$

which results into the following formulation:

$$\widehat{\mathbb{M}}_{\text{COLL},k}^{\text{dyn}} = \bigcap_{l=1}^4 \left(\left[\mathbb{H}_{\text{sp},k}^l \cap \mathbb{H}_k^l(-\Delta t) \right] \cup \left[\mathbb{H}_{\text{sp},k}^{l,c} \cap \mathbb{H}_k^l(0) \right] \right).$$

In case of point-symmetric collision regions, the edges are parallel so that $\mathbb{H}_{\text{sp},k}^l = \mathbb{H}_{\text{sp},k}^{l+4,c}$ and $\mathbb{H}_{\text{sp},k}^{l,c} = \mathbb{H}_{\text{sp},k}^{l+4}$ holds. By rewriting the iterating intersect with the maximum parameter $l = 8$ to $l = 4$ creates the following

formulation:

$$\widehat{\mathbb{M}}_{\text{COLL},k}^{\text{dyn}} = \bigcap_{l=1}^4 \left(\left[\mathbb{H}_{\text{sp},k}^l \cap \mathbb{H}_k^l(-\Delta t) \right] \cup \left[\mathbb{H}_{\text{sp},k}^{l,c} \cap \mathbb{H}_k^l(0) \right] \right) \cap \dots \\ \dots \cap \left(\left[\mathbb{H}_{\text{sp},k}^{l,c} \cap \mathbb{H}_k^{l+4}(-\Delta t) \right] \cup \left[\mathbb{H}_{\text{sp},k}^l \cap \mathbb{H}_k^{l+4}(0) \right] \right) .$$

Dissolving parentheses for the intersection between the hyperplane sets l and $l+4$ and using $\mathbb{H}_{\text{sp},k}^l \cap \mathbb{H}_{\text{sp},k}^{l+4} = \emptyset$, the final equation arises:

$$\widehat{\mathbb{M}}_{\text{COLL},k}^{\text{dyn}} = \dots \\ \dots = \bigcap_{l=1}^4 \left(\left[\mathbb{H}_{\text{sp},k}^l \cap \mathbb{H}_k^l(-\Delta t) \cap \mathbb{H}_k^{l+4}(0) \right] \cup \left[\mathbb{H}_{\text{sp},k}^{l,c} \cap \mathbb{H}_k^l(0) \cap \mathbb{H}_k^{l+4}(-\Delta t) \right] \right) .$$

To sum up, the statement for the approximated collision region $\widehat{\mathbb{M}}_{\text{COLL},k}^{\text{dyn}}$ reformulates to an union of convex regions for a parallel edge pair.

A.3 Transition of Dynamic Collision Region to Flux Calculation

The flux approach is often a starting point in the literature to derive the collision probability of two agents [125]. This approach counts the volume of a weighted vector field which is colliding into a boundary. In the following, it is shown, how a probability calculation with state space collision region can simply be transformed into a flux approach.

The flux approach only considers new collided states instead of having new collided states and those, which already started in a collision region $\mathbb{M}_{\text{COLL},k-1}^{\text{stat}}$. So that the region $\mathbb{M}_{\text{COLL},k}^{\text{new}}$, depicting only the new collided states is as follows:

$$\mathbb{M}_{\text{COLL},k}^{\text{new}} = \mathbb{M}_{\text{COLL},k}^{\text{dyn}} \setminus \mathbb{M}_{\text{COLL},k-1}^{\text{stat}} . \quad (\text{A.3})$$

Assuming an one coordinate example with r as position, v as velocity, and u as input of the previous time step $k-1$, so the state vector is $\mathbf{x}_k = [r, v]^T$.

The boundary of a collision region with $r \geq r_0$ is according to Eq. (A.3):

$$\begin{aligned} \mathbb{M}_{\text{COLL},k}^{\text{new}} &= \{\mathbf{x}_k \in \mathbb{R}^2 \mid [1 \quad \Delta t] \mathbf{x}_k \geq r_0 - \frac{\Delta t^2}{2}u\} \setminus \{\mathbf{x}_k \in \mathbb{R}^2 \mid [1 \quad 0] \mathbf{x}_k \geq r_0\} \\ &= \{\mathbf{x}_k \in \mathbb{R}^2 \mid [-1 \quad 0] \mathbf{x}_k > -r_0\} \cap \\ &\quad \{\mathbf{x}_k \in \mathbb{R}^2 \mid [1 \quad \Delta t] \mathbf{x}_k \geq r_0 - \frac{\Delta t^2}{2}u\} . \end{aligned}$$

From these subsets follow that $v \geq -\frac{\Delta t}{2}u$, if $\Delta t > 0$.

Furthermore, the intersect itself can be parametrized by calculating those states which will collide with the boundary $r = r_0$ for each point in the time interval $t \in [0, \Delta t]$:

$$[1 \quad t] \mathbf{x}_k = r_0 - \frac{t^2}{2}u \quad \Rightarrow \quad r(t, v) = r_0 - tv - \frac{t^2}{2}u .$$

The overall transformation function with t as a new coordinate changes the collision probability calculation for an arbitrary PDF $p(\mathbf{x}_k)$:

$$\begin{aligned} p^{\text{flow}}(e_k = e_{\text{COLL}}) &= \iint_{\mathbb{M}_{\text{COLL},k}^{\text{new}}} p(\mathbf{x}_k) d\mathbf{x}_k \\ &= \int_{-\frac{t}{2}u}^{\infty} \int_0^{\Delta t} \frac{\partial r(t, v)}{\partial t} p(r(t, v), v) dt dv \\ &= \int_{-\frac{t}{2}u}^{\infty} \int_0^{\Delta t} -v p(r(t, v), v) dt dv . \end{aligned}$$

The transition from line 1 to line 2 was possible by using the transformation theorem. Setting $u = 0$, this formula equals the flux approach introduced in [125], where only flux with negative velocity through the boundary is part of the collision probability, so that flux from inside to outside is not taking into account.

For the collision probability gained by state collision regions, Eq. (A.3) is applied, where the PDF volume under the collided state region $\mathbb{M}_{\text{COLL},k-1}^{\text{stat}}$ of the previous time step has to be subtracted from the overall collision

region $\mathbb{M}_{\text{COLL},k}^{\text{dyn}}$ of the current time step k .

$$\begin{aligned} p^{\text{dyn}}(e_k = e_{\text{COLL}}) &= \iint_{\mathbb{M}_{\text{COLL},k}^{\text{dyn}}} p(\mathbf{x}_k) d\mathbf{x}_k \\ &= \iint_{\mathbb{M}_{\text{COLL},k}^{\text{new}}} p(\mathbf{x}_k) d\mathbf{x}_k - \iint_{\mathbb{M}_{\text{COLL},k-1}^{\text{stat}}} p(\mathbf{x}_k) d\mathbf{x}_k . \end{aligned}$$

To guarantee that the probability of the current dynamic collision region $\mathbb{M}_{\text{COLL},k}^{\text{dyn}}$ provides the proper results, the volume under the collision region of the previous time step has to be zero:

$$\iint_{\mathbb{M}_{\text{COLL},k-1}^{\text{stat}}} p(\mathbf{x}_k) d\mathbf{x}_k \approx 0$$

so that the following holds:

$$p^{\text{dyn}}(e_k = e_{\text{COLL}}) \approx \iint_{\mathbb{M}_{\text{COLL},k}^{\text{new}}} p(\mathbf{x}_k) d\mathbf{x}_k = p^{\text{flow}}(e_k = e_{\text{COLL}}) .$$

It is shown that the collision calculation with the dynamic collision regions $\mathbb{M}_{\text{COLL},k}^{\text{dyn}}$ equals the flow approach, if the PDF volume under the static collision region $\mathbb{M}_{\text{COLL},k-1}^{\text{stat}}$ is zero.

A.4 Accuracy of Instantaneous Survival Probability

The instantaneous survival probability magnitude according to Eq. (4.17) is also investigated exemplary for static collision regions and with the same constellations like in Sec. 4.5.2 and Sec. 4.5.2. The plots in Fig. A.4 shows boxplots of different collision probability magnitudes intervals. For very small collision probabilities, the survival probability becomes similar to one, so that the relative error of the survival probability is similar to the absolute error of the collision probability magnitude, which again is very small. For higher collision probabilities, the accuracy of the analytic method (last row) equals the Monte Carlo Simulation (MCS) with 1000 particles (top right).

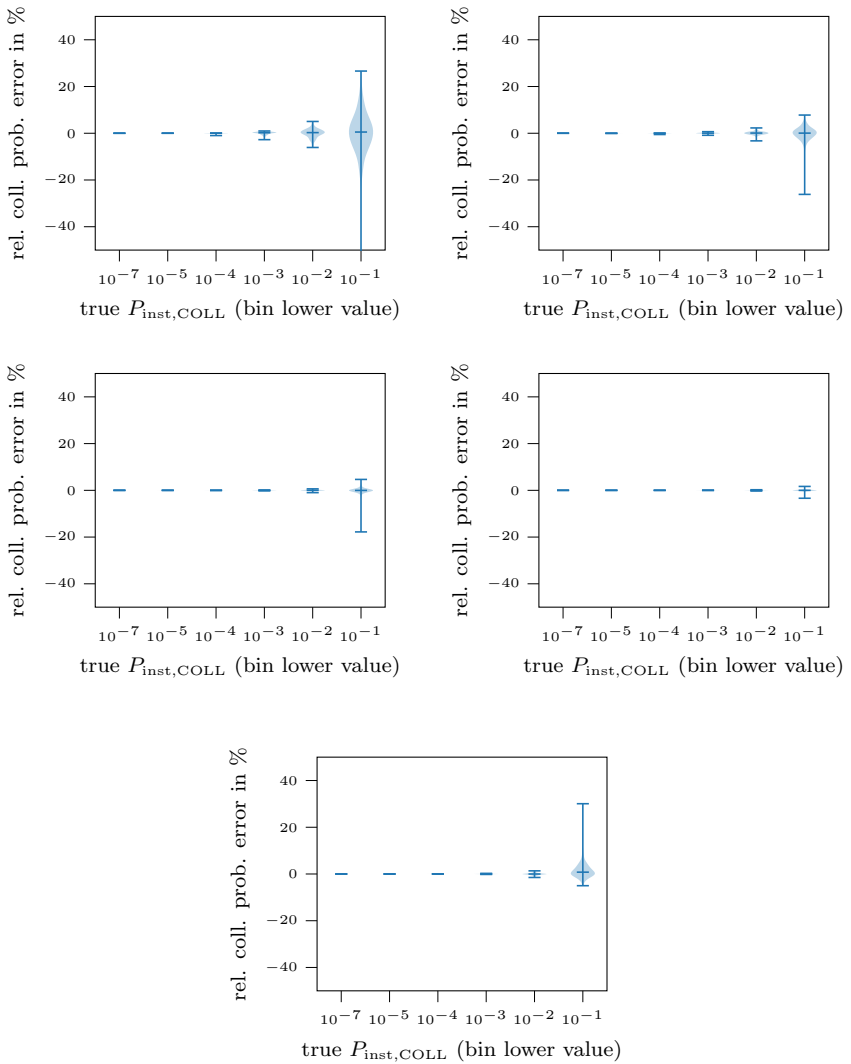


Figure A.1: Relative error of survival probability depending on reference collision probability magnitude for static collision region: Monte Carlo Simulation with 100 particles (top left), 1k particles (top right), 10k particles (center left), 100k particles (center right) and analytic truncation method (Bottom left).

A.5 Simulation Parameters

A.5.1 Time vs. Accuracy

Variable	Symbol	Min. value	Max. value
Vehicle width	w_{veh}	2 m	-
Vehicle length	l_{veh}	4 m	-
Distance to center	$\ \Delta\mathbf{r}\ $	0 m	100 m
Polar position angle	$\angle(\Delta\mathbf{r})$	0	$\frac{\pi}{2}$
Vehicle orientations	γ^i, γ^j	0°	90°
Variance in y-direction	σ_y^2	1 m ²	10 m ²
Relative Variance	$\frac{\sigma_x^2}{\sigma_y^2}$	1	10
Velocity norm	$\ \Delta\mathbf{v}\ $	0 m/s	30 m/s
Polar velocity angle	$\angle(\Delta\mathbf{v})$	0°	360°
Time interval	Δt	0.2 s	-

Table A.1: Range of scene states and parameters for validating accuracy and computational time between Monte Carlo Simulation and analytic truncation approach.

A.5.2 Parameters of Collision Probability Models

Variable	Symbol	Value
Time interval	Δt	0.2 s
Slope rate	β_0	-2.0
Maximum collision rate	τ_{max}^{-1}	10.0 s ⁻¹

Table A.2: Parameters for collision event-rate model.

Variable	Symbol	Value
Time interval	Δt	0.2 s
Proximity parameter	$D_{\text{prox}}^{\text{lim}}$	0.1
Allocation parameter	$D_{\text{alloc}}^{\text{lim}}$	0.2

Table A.3: Parameters for analytic collision event model with PDF shape split.

Variable	Symbol	Value
Time interval	Δt	0.2 s
Initial amount of particles	-	10000

Table A.4: Parameters for Monte Carlo Simulation.

A.5.3 Parameters of Severity Models

Variable	Symbol	Value
Severity offset	c_{CONST}	0.001
Restitution coefficient vehicle to wall	k_{REST}^{v2w}	0.2
Restitution coefficient vehicle to vehicle	k_{REST}^{v2v}	0.1
MAIS3+ vehicle occupant threshold	$v_{\text{th}}^{\text{occ}}$	15.0 m/s
MAIS3+ vehicle occupant slope	$v_{\text{sl}}^{\text{occ}}$	2.0 m/s
MAIS3+ pedestrian threshold	$v_{\text{th}}^{\text{ped}}$	8.0 m/s
MAIS3+ pedestrian slope	$v_{\text{sl}}^{\text{ped}}$	3.0 m/s
Barrier distance threshold	Δd_{th}	0.5 m
Barrier distance slope	Δd_{sl}	0.1 m
Friction coefficient	μ_{f}	0.8
Gravity constant	g	9.81 m/s ²
Collision distribution parameter	ρ_{DISTR}	0.01
After collision deceleration	a_{brake}	-5.0 m/s ²

Table A.5: Parameters for severity models.

A.5.4 Parameters of Behavior Planner

Variable	Symbol	Value
Maximal acceleration	-	2.0 m/s ²
Maximal deceleration		-7.0 m/s ²
Escape event rate	τ_{ESC}^{-1}	0.25 s ⁻¹
Progress utility weight	w_{prog}	0.00001
Progress limiting velocity weight	w_{prog}	0.00002
Comfort weight	w_{comf}	0.00001

Table A.6: Parameters for behavior planner.

A.5.5 Multi-Object Overtaking Scenarios

Variable(s)	Symbol(s)	Value(s)
Vehicle widths	$w_{\text{veh}}^{1/2/3}$	2 m
Vehicle lengths	$l_{\text{veh}}^{1/2}, l_{\text{veh}}^{2/3}$	4 m, 20 m
Initial ego positions	r_x^1, r_y^1	-15 m, 2.5 m
Initial veh. 2 positions	r_x^2, r_y^2	0 m, 0 m
Initial veh. 3 positions	r_x^3, r_y^3	30 m, 0 m
Ego velocity	v_x^1, v_y^1	10 m/s, 0 m/s, 0 m/s
Vehicle 2/3 velocities	$v_x^{2/3}, v_y^{2/3}$	0 m/s
Vehicle accelerations	$\mathbf{u}^{1/2/3}$	$[0 \text{ m/s}^2, 0 \text{ m/s}^2]^T$
Predicted input noise	$\sigma_{u,x}^2, \sigma_{u,y}^2$	$0.0001 \text{ m}^2/\text{s}^2, 0.001 \text{ m}^2/\text{s}^2$
Initial variance matrix (ego vehicle)	$\Sigma_{x,0}^0$	$\text{diag}(0.4, 0.4, 10^{-4} \text{ s}^{-2}, 10^{-4} \text{ s}^{-2}) \text{ m}^2$
Initial variance matrix (vehicle 2/3)	$\Sigma_{x,0}^{2/3}$	$\text{diag}(0.4, 0.1, 10^{-4} \text{ s}^{-2}, 10^{-4} \text{ s}^{-2}) \text{ m}^2$
Vehicle orientations	$\gamma^{1/2/3}$	0°
Time interval	Δt	0.2 s
Time step horizon	H	35
Initial amount of MC particles	-	10000
Amount of shown MC particles per time step	-	50
Time step interval between PDF representations in figure	-	4

Table A.7: Scene states and parameter settings for multi-object prediction scenario shown in Fig. 4.13.

A.5.6 Intersection Scenario

Variable(s)	Symbol(s)	Value(s)
Vehicle widths	$w_{\text{veh}}^{1/2}$	2 m
Vehicle lengths	$l_{\text{veh}}^{1/2}$	4 m
Initial ego positions	r_x^1, r_y^1	$-30\text{ m}, 0\text{ m}$
Initial vehicle 2 positions	r_x^2, r_y^2	$0\text{ m}, -30\text{ m}$
Initial Ego velocity	v_x^1, v_y^1	$15\text{ m/s}, 0\text{ m/s}$
Initial vehicle 2 velocities	v_x^2, v_y^2	$0\text{ m/s}, 15\text{ m/s}$
Vehicle accelerations	$\mathbf{u}^{1/2}$	$[0\text{ m/s}^2, 0\text{ m/s}^2]^T$
Predicted input noise	$\sigma_{u,x}^2, \sigma_{u,y}^2$	$0.1\text{ m}^2/\text{s}^2, 0.1\text{ m}^2/\text{s}^2$
Initial variance matrix (veh. ego)	$\Sigma_{x,0}^1$	$\text{diag}(0.5, 2.0, 0.2\text{ s}^{-2}, 0.1\text{ s}^{-2})\text{ m}^2$
Initial variance matrix (veh. 2)	$\Sigma_{x,0}^2$	$\text{diag}(2.0, 0.5, 0.1\text{ s}^{-2}, 0.2\text{ s}^{-2})\text{ m}^2$
Ego vehicle orientation	γ^1	0°
Vehicle 2 orientation	γ^2	0°
Amount of drawn MC particles per time step	-	50
Time step interval between drawn PDF representations	-	4

Table A.8: Scene states and parameter settings for intersection prediction scenario shown in Fig. 4.16.

A.5.7 Overtaking Scenario

Variable(s)	Symbol(s)	Value(s)
Vehicle widths	$w_{\text{veh}}^{1/2}$	$2 m$
Vehicle lengths	$l_{\text{veh}}^{1/2}$	$4 m$
Initial ego position	r_x^1	$-15 m$
Initial vehicle 2 position	r_x^2	$0 m$
Lateral ego velocity	v_y^1	$0 m/s$
Vehicle 2 velocity	v_x^2, v_y^2	$0 m/s, 0 m/s$
Vehicle accelerations	$\mathbf{u}^{1/2}$	$[0 m/s^2, 0 m/s^2]^T$
Predicted input noise	$\sigma_{u,x}^2, \sigma_{u,y}^2$	$0.1 m^2/s^2, 0.01 m^2/s^2$
Initial variance matrices	$\Sigma_{x,0}^{1,2}$	$\text{diag}(0.4, 0.4, 0.2 s^{-2}, 0.5 s^{-2}) m^2$
Vehicle orientations	$\gamma^{1/2}$	0°
Time interval	Δt	$0.2 s$

Table A.9: Scene states and parameter settings for overtaking scenario analysis shown in Fig. 4.17.

A.5.8 Overtaking Scenario with variable Sampling Time

Variable(s)	Symbol(s)	Value(s)
Vehicle widths	$w_{\text{veh}}^{1/2}$	2 m
Vehicle lengths	$l_{\text{veh}}^{1/2}$	4 m
Initial ego vehicle positions	r_x^1, r_y^1	-20 m, 3 m
Initial vehicle 2 positions	r_x^2, r_y^2	0 m, 0 m
Ego velocity	v_x^1, v_y^1	10 m/s, 0 m/s
Vehicle 2 velocity	v_x^2, v_y^2	0 m/s, 0 m/s
Vehicle accelerations	$\mathbf{u}^{1/2}$	$[0 \text{ m/s}^2, 0 \text{ m/s}^2]^T$
Predicted input noise	$\sigma_{u,x}^2, \sigma_{u,y}^2$	$0.1 \text{ m}^2/\text{s}^2, 0.01 \text{ m}^2/\text{s}^2$
Initial variance matrices	$\Sigma_{x,0}^{1,2}$	$\text{diag}(0.4, 0.4, 0.2 \text{ s}^{-2}, 0.5 \text{ s}^{-2}) \text{ m}^2$
Vehicle orientations	$\gamma^{1/2}$	0°

Table A.10: Scene states and parameter settings for overtaking scenario with different sampling time Δt shown in Fig. 4.18.

A.5.9 Scenario with distributed Events

Variable(s)	Symbol(s)	Value(s)
Vehicle widths	w_{veh}^1	$2 m$
Vehicle lengths	l_{veh}^1	$4 m$
Initial ego positions	r_x^1, r_y^1	$-50 m, 0 m$
Ego velocity	v_x^1, v_y^1	$10 m/s, 0 m/s$
Vehicle accelerations	\mathbf{u}^1	$[0 m/s^2, 0 m/s^2]^T$
Predicted input noise	$\sigma_{u,x}^2, \sigma_{u,y}^2$	$10^{-3} m^2/s^2, 10^{-3} m^2/s^2$
Initial variance matrices	$\Sigma_{x,0}^1$	$\text{diag}(0.4, 0.4, 3.0 s^{-2}, 10^{-4} s^{-2}) m^2$
Vehicle orientations	γ^1	0°
Occupation density	ρ_{DISTR}	$0.05 m^{-2}$

Table A.11: Scene states and parameter settings for prediction scenario with distributed events shown in Fig. 5.2 and Fig. 7.12.

A.5.10 Scenario with Restriction Event

Variable(s)	Symbol(s)	Value(s)
Vehicle widths	w_{veh}^1	$2 m$
Vehicle lengths	l_{veh}^1	$4 m$
Initial ego positions	r_x^1, r_y^1	$0 m, 0 m$
Ego velocity	v_x^1, v_y^1	$10 m/s, 0 m/s$
Vehicle accelerations	\mathbf{u}^1	$[-3 m/s^2, 0 m/s^2]^T$
Predicted input noise	$\sigma_{u,x}^2, \sigma_{u,y}^2$	$0.1 m^2/s^2, 0.01 m^2/s^2$
Initial variance matrices	$\Sigma_{x,0}^1$	$\text{diag}(0.4, 0.4, 0.3 s^{-2}, 10^{-4} s^{-2}) m^2$
Vehicle orientations	γ^1	0°

Table A.12: Scene states and parameter settings for prediction scenario with restriction shown in Fig. 5.5.

Variable(s)	Symbol(s)	Value(s)
Vehicle widths	w_{veh}^1	2 m
Vehicle lengths	l_{veh}^1	4 m
Initial ego positions	r_x^1, r_y^1	-40 m, 0 m
Ego velocity	v_x^1, v_y^1	10 m/s, 0 m/s
Vehicle accelerations	\mathbf{u}^1	$[0 \text{ m/s}^2, 0 \text{ m/s}^2]^T$
Predicted input noise	$\sigma_{u,x}^2, \sigma_{u,y}^2$	$0.1 \text{ m}^2/\text{s}^2, 0.01 \text{ m}^2/\text{s}^2$
Initial variance matrices	$\Sigma_{x,0}^1$	$\text{diag}(0.4, 0.4, 0.3 \text{ s}^{-2}, 10^{-4} \text{ s}^{-2}) \text{ m}^2$
Vehicle orientations	γ^1	0°

Table A.13: Scene states and parameter settings for prediction scenario with escape events shown in Fig. 5.7.

A.5.11 Scenario with Escaping Event

Variable(s)	Symbol(s)	Value(s)
Vehicle widths	w_{veh}^1	2 m
Vehicle lengths	l_{veh}^1	4 m
Initial ego positions	r_x^1, r_y^1	-40 m, 0 m
Ego velocity	v_x^1, v_y^1	10 m/s, 0 m/s
Vehicle accelerations	\mathbf{u}^1	$[0 \text{ m/s}^2, 0 \text{ m/s}^2]^T$
Predicted input noise	$\sigma_{u,x}^2, \sigma_{u,y}^2$	$0.1 \text{ m}^2/\text{s}^2, 0.01 \text{ m}^2/\text{s}^2$
Initial variance matrices	$\Sigma_{x,0}^1$	$\text{diag}(0.4, 0.4, 0.3 \text{ s}^{-2}, 10^{-4} \text{ s}^{-2}) \text{ m}^2$
Vehicle orientations	γ^1	0°

Table A.14: Scene states and parameter settings for prediction scenario with escape events shown in Fig. 6.5.

Variable(s)	Symbol(s)	Value(s)
Vehicle widths	$w_{\text{veh}}^{1/2}$	$2 m$
Vehicle lengths	$l_{\text{veh}}^{1/2}$	$4 m$
Initial vehicle 2 positions	r_x^2, r_y^2	$0 m, 0 m$
Initial vehicle 2 velocities	v_x^2, v_y^2	$7.5 m/s, 0 m/s$
Vehicle accelerations	$\mathbf{u}^{1/2}$	$[0 m/s^2, 0 m/s^2]^T$
Predicted input noise	$\sigma_{u,x}^2, \sigma_{u,y}^2$	$0.1 m^2/s^2, 0.01 m^2/s^2$
Initial variance matrix (veh. ego)	$\Sigma_{x,0}^1$	$\text{diag}(0.4, 0.4, 0.01 s^{-2}, 0.01 s^{-2}) m^2$
Initial variance matrix (veh. 2)	$\Sigma_{x,0}^2$	$\text{diag}(0.1, 0.1, 0.01 s^{-2}, 0.01 s^{-2}) m^2$
Ego vehicle orientation	γ^1	0°
Ego's lateral position	r_y^1	$4.25 m$
Ego's longitudinal position	r_x^1	$-10 m$

Table A.15: Scene states and parameter settings for behavior analysis.

A.6 Probability Distributions

This attachment section provides an introduction of probability density distributions (PDF) in general regarding their properties and different types for those readers who are not familiar with this topic or want to refresh their knowledge. Furthermore, this section provides some basic concatenation tools for two or more PDF's and presents similarity measures, which both are essential parts of this thesis to either create algorithms or validate the results.

System and models with noises often have to deal with uncertainties. So variables in the system are not deterministic anymore, not having one fixed resulting value. The variables can have different values with different probability of occurrence. The description of a random variable \mathcal{X} is the starting point from where further mathematical fundamentals are presented.

A.6.1 Probability Density Function

The probability of a continuous distributed variable $x \in \mathbb{R}$ can be expressed by a probability density function (PDF) $p(x)$ which must be positive and which integral over its domain is equal to one [24, 152]:

$$p(x) \geq 0 \tag{A.4}$$

$$\int_{\mathbb{R}} p(x) dx = 1 .$$

The indefinite integral of a PDF is called cumulative density function (CDF) $P(x)$ and is defined as:

$$P(x) = \int_{-\infty}^x p(\tilde{x}) d\tilde{x} .$$

There is an infinite number of possible candidate functions fulfilling the conditions for a PDF $p(x)$ according to Eq. (A.4). Some of them, which are used in this thesis, are presented in the following.

The most simplest one is the **delta-function** $\delta(x)$:

$$\delta(x) = \begin{cases} 1 & \text{if } x = 0 \\ 0 & \text{else.} \end{cases}$$

$$\sigma(x) = \begin{cases} 1 & \text{if } x \geq 0 \\ 0 & \text{else.} \end{cases} ,$$

where its CDF is equivalent to the step function σ . Both functions are depicted in Fig. A.2.

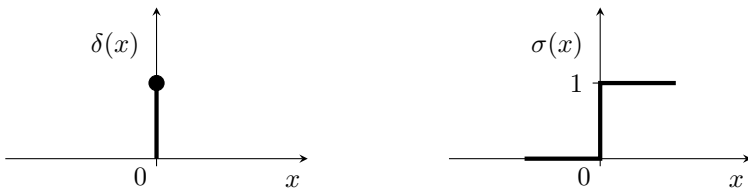


Figure A.2: Dirac distribution with PDF $\delta(x)$ (left) and CDF $\sigma(x)$ (right)

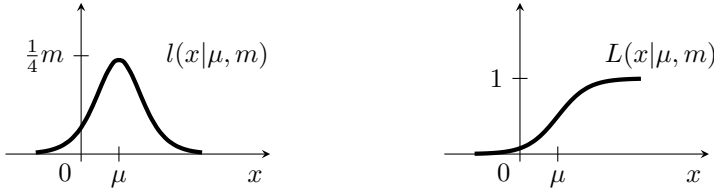


Figure A.3: Logistic distribution with its PDF $l(x|\mu, m)$ (left) and CDF $L(x|\mu, m)$ (right)

One additional property of the dirac distribution $\delta(x)$ is that a convolution with another PDF $p(y)$ of a second variable y gives the probability density value at x :

$$\int_{\mathbb{R}} \delta(x - y) p(y) dy = p(x) .$$

The second type of PDF's is the **logistic PDF** $l(x)$, which is symmetric around μ with a maximum height at $l(x = \mu|\mu, m) = \frac{1}{4}m$ depending on the scale parameter m :

$$l(x; \mu, m) = \frac{\exp\left(\frac{x-\mu}{m}\right)}{m \left(1 + \exp\left(\frac{x-\mu}{m}\right)\right)^2} .$$

The corresponding CDF $L(x; \mu, m)$ is given by:

$$L(x; \mu, m) = \frac{\exp\left(\frac{x-\mu}{m}\right)}{1 + \exp\left(\frac{x-\mu}{m}\right)}$$

and is often used for a binomial logistic regression to categorize a variable x into two sets, where $L(x; \mu, m)$ provides the probability that the value x belongs to a predefined class or not. The point $x = \mu$, where $L(x; \mu, m) = \frac{1}{2}$ expresses that the regression models output is indifferent. The logistic PDF and its CDF are depicted in Fig. A.3.

The last presented type of PDF's is the normal distribution or **Gaussian distribution** $\mathcal{N}(x; \mu_x, \sigma_x^2)$ with mean μ_x and standard deviation σ_x :

$$\phi(x) = \mathcal{N}(x; \mu_x, \sigma_x^2) = \frac{1}{\sqrt{2\pi\sigma_x^2}} \exp\left(-\frac{(x - \mu_x)^2}{2\sigma_x^2}\right) . \quad (\text{A.5})$$

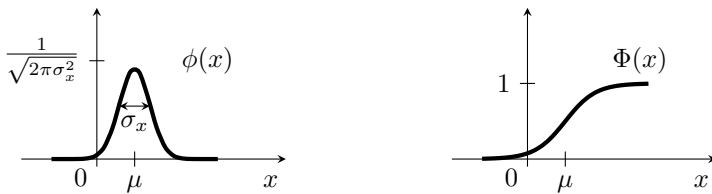


Figure A.4: Gaussian distribution with its PDF $\phi(x) = \mathcal{N}(\mathbf{x}; \mu, \sigma_x)$ (left) and CDF $\Phi(x)$ (right)

With the help of the error function erf the CDF $\Phi(x)$ can be written as:

$$\Phi(x) = \frac{1}{2} \left[1 + erf \left(\frac{x - \mu_x}{\sqrt{2}\sigma_x} \right) \right] \quad (\text{A.6})$$

$$erf(x) = \frac{2}{\sqrt{\pi}} \int_0^x \exp(-\tilde{x}^2) d\tilde{x} .$$

In Fig. A.4, the Gaussian PDF and CDF are shown.

Sometimes, distributions depend on multiple variables $\mathcal{X}_1, \dots, \mathcal{X}_n$. In case of the normal distribution, the multivariate Gaussian $\phi(\mathbf{x})$ arises out of the univariate Gaussian, defined in Eq. (A.5):

$$\phi(\mathbf{x}) = \mathcal{N}(\mathbf{x}; \mu, \Sigma_x) = \frac{1}{(2\pi^{|\Sigma_x|})^{n/2}} \exp(-(\mathbf{x} - \mu)^T \Sigma_x^{-1} (\mathbf{x} - \mu)) \quad (\text{A.7})$$

Note, as long as the covariance matrix Σ_x is not diagonal, the CDF cannot be determined analytically. In case of a diagonal covariance matrix, Eq. (A.7) can be separated as a product of univariate Gaussian, where the multivariate CDF is the product of each individual variable according to Eq. (A.6).

The aforementioned PDF's are all unimodal functions, meaning that they have only one value x or vector \mathbf{x} where the PDF has a local maximum. Distributions with more than one extrema can be created by superpose different placed unimodal functions. An often used distribution is a Gaussian Mixture Model (GMM) $\mathcal{G}(\mathbf{x})$, where $D > 1$ weighted Gaussian functions $\mathcal{N}(\mathbf{x}; \mu^d, \Sigma_x^d)$ are summed up:

$$\mathcal{G}(\mathbf{x}) = \sum_{d=1}^D w_d \mathcal{N}(\mathbf{x}; \mu^d, \Sigma_x^d) \quad \text{with} \quad \sum_{d=1}^D w_d = 1 .$$

The GMM can also be used as a regression model for other complex multimodal distributions.

A.6.2 Stochastic Moments

A stochastic moment m with order r of a distributed random variable \mathcal{X} is defined as [124]:

$$m_k := \mathbb{E}[\mathcal{X}^r] \ .$$

With stochastic moments m , properties like location and shape of the distributions can be described. With help of the first and second moment m_1 , m_2 , quantities like mean value $\hat{\mathbf{x}}$ ($r = 1$) and covariances $\Sigma_{\mathbf{x}}$ ($r = 2$) can be derived. Using the linearity of the expectation operator \mathbb{E} these quantities can be expressed as follows:

$$\begin{aligned} \hat{\mathbf{x}} &= \mathbb{E}[\mathcal{X}] = \int_{\mathbb{R}^n} \mathbf{x} p(\mathbf{x}) d\mathbf{x} = m_1 \\ \Sigma_{\mathbf{x}} &= \mathbb{E}[(\mathcal{X} - \hat{\mathbf{x}})^2] = \mathbb{E}[\mathcal{X}^2] - 2\mathbb{E}[\mathcal{X}]\hat{\mathbf{x}}^T + \hat{\mathbf{x}}\hat{\mathbf{x}}^T \\ &= m_2 - m_1 m_1^T \ . \end{aligned}$$

This shows that the second moment m_2 is a sum of the covariance matrix and another matrix shift given by the dyadic product of the mean vectors $\hat{\mathbf{x}}$.

Assume a distribution $p(\mathbf{x})$ of a multivariate random variable which is a weighted sum of sub-functions $p^d(\mathbf{x})$, where the mean $\hat{\mathbf{x}}^d$ and the variance $\Sigma_{\mathbf{x}}^d$ of each component are known.

$$p(\mathbf{x}) = \sum_{d=1}^D w_d p^d(\mathbf{x}) \quad \text{with} \quad \sum_{d=1}^D w_d = 1 \ .$$

To conserve the first two stochastic moments, the overall mean value $\hat{\mathbf{x}}$ and covariance matrix $\Sigma_{\mathbf{x}}$ are as follows:

$$\begin{aligned} \hat{\mathbf{x}} &= \sum_{d=1}^D w_d \hat{\mathbf{x}}^d & (\text{A.8}) \\ \Sigma_{\mathbf{x}} &= \sum_{d=1}^D w_d (\Sigma_{\mathbf{x}}^d + \hat{\mathbf{x}}^d (\hat{\mathbf{x}}^d)^T) - \hat{\mathbf{x}}\hat{\mathbf{x}}^T \ . \end{aligned}$$

A.6.3 Truncated Gaussian Probability Density Functions

In Sec. A.6.1, the univariate Gaussian PDF was introduced, where the distribution is non-zero for all $x \in \mathbb{R}$. In case of a restricted domain $x \in [b^-, b^+]$ with $-\infty < b^- < b^+ < \infty$, the truncated Gaussian PDF $\phi^t(x)$ is set to zero outside the new interval and normalized to one:

$$\begin{aligned}\phi^t(x) &= \frac{\mathcal{N}(\mathbf{x}; \mu, \Sigma_x)}{\Phi(b^+) - \Phi(b^-)} \quad \text{with } x \in [b^-, b^+] \\ &= \sigma(x - b^-) \sigma(b^+ - x) \frac{\mathcal{N}(x; \mu, \Sigma_x)}{\Phi(b^+) - \Phi(b^-)} \quad \text{with } x \in \mathbb{R} .\end{aligned}$$

Here, $\phi(x)$ and $\Phi(x)$ are the parameterized PDF and CDF according to Eq. (A.5) and Eq. (A.6), respectively.

Through the two-sided truncation boundaries with b^- and b^+ , the mean \hat{x}^t and standard deviation σ_x^t are given by [68, 152]:

$$\begin{aligned}\hat{x}^t &= \hat{x} - \sigma_x \frac{\phi(b^+) - \phi(b^-)}{\Phi(b^+) - \Phi(b^-)} \\ (\sigma_s^t)^2 &= \sigma_x^2 \left(1 - \frac{\alpha^+ \phi(b^+) - \alpha^- \phi(b^-)}{\Phi(b^+) - \Phi(b^-)} - \left[\frac{\phi(b^+) - \phi(b^-)}{\Phi(b^+) - \Phi(b^-)} \right]^2 \right) ,\end{aligned}\tag{A.9}$$

where $\alpha^+ = (b^+ - \mu)/\sigma_x$ and $\alpha^- = (b^- - \mu)/\sigma_x$. For an one-side truncated Gaussian the parameters has to adapted in case of only having a lower limitation $[b^-, \infty[$ with $\phi(b^+ \rightarrow \infty) = 0$ and $\Phi(b^+ \rightarrow \infty) = 1$ or only having an upper limitation $]-\infty, b^+]$ with $\phi(b^- \rightarrow -\infty) = 0$ and $\Phi(b^- \rightarrow -\infty) = 0$. Taking the mean μ^t and the variance σ_x^t , a Gaussian distribution ϕ^t can be formulated, which approximates $\phi(x)^t$ (see Fig. A.5).

In case of a multivariate Gaussian with a two-sided truncation the boundaries can be represented as two parallel linear planes with $\mathbf{a}^T \mathbf{x} \geq b^-$ and $\mathbf{a}^T \mathbf{x} \leq b^+$, where the normal vector \mathbf{a} pointing into the direction of the non-truncated part of the first plane and the shifts $b^- < b^+$ represent the lower and upper limitation like for the univariate case.

The two-sided truncated multivariate distribution $\phi^t(\mathbf{x})$ can be expressed with the help of two step functions $\sigma(x)$:

$$\phi^t(\mathbf{x}) = \sigma(\mathbf{a}^T \mathbf{x} - b^-) \sigma(b^+ - \mathbf{a}^T \mathbf{x}) K^t \mathcal{N}(\mathbf{x}; \mu^d, \Sigma_x^d) \quad \text{with } \mathbf{x} \in \mathbb{R}^n ,$$

where K^t is the normalizing factor. To obtain the normalizing factor, the mean vector $\hat{\mathbf{x}}^t$ and covariance matrix Σ_x^t of the truncated Gaussian $\phi^t(\mathbf{x})$,

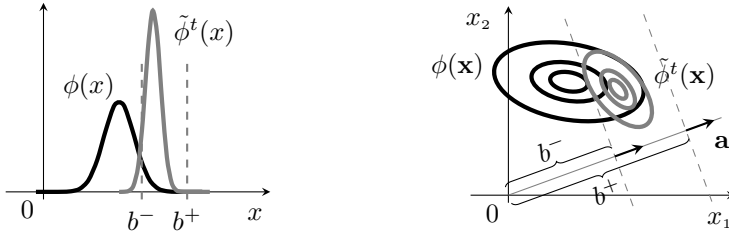


Figure A.5: Gaussian distribution as an approximation of a truncation by linear boundaries for univariate (left) and multivariate case (right).

one has to project the axis \mathbf{x} according to the normal vector \mathbf{a} , so that the Gaussian PDF is represented as an univariate instead of an multivariate Gaussian PDF. Afterwards, the univariate Gaussian PDF can be truncated according to the univariate case like in Eq. (A.9). The resulting mean and variances are used to manipulate the non-truncated, multivariate Gaussian to obtain the truncated case.

However, the projection $x^p = \mathbf{a}^T \mathbf{x}$ results in the following projected mean \hat{x}^p , projected variance Σ_x^p and a normalization factor K^p :

$$\begin{aligned}\hat{x}^p &= \mathbf{a}^T \hat{\mathbf{x}} \\ \sigma_x^p &= \mathbf{a}^T \Sigma_x \mathbf{a} \\ K^p &= \frac{1}{\Phi^p(b^+) - \Phi^p(b^-)}\end{aligned}$$

where $\Phi^p(x)$ is the CDF of the projected Gaussian. The truncated, projected mean $\hat{x}^{p,t}$ and variance $\sigma_x^{p,t}$ are calculated according to the univariate case given in Eq. (A.9). The effect on the multivariate, non-truncated Gaussian is a back transformation into the n -dimensional space [122] and determines the desired mean vector $\hat{\mathbf{x}}^t$ and Σ_x^t of the multivariate, truncated Gaussian PDF:

$$\begin{aligned}\hat{\mathbf{x}}^t &= \hat{\mathbf{x}} - \frac{\Sigma_x \mathbf{a}}{\sigma_x^p} (\hat{x}^p - \hat{x}^{p,t}) \\ \Sigma_x^t &= \Sigma_x - \frac{\Sigma_x \mathbf{a}}{\sigma_x^p} (\sigma_x^p - \sigma_x^{p,t}) \frac{\mathbf{a}^T \Sigma_x}{\sigma_x^p} \\ K^t &= K^p .\end{aligned}\tag{A.10}$$

In case of only a one-sided truncation line, the shifts b^- and b^+ has to be set appropriately like described for the univariate case.

A.6.4 Distance Measures

In some applications it is necessary to evaluate, how distant a data point is to a reference distribution given by a random variable \mathcal{X} . The Mahalanobis-Distance D_{meha} describes the distance of a vector \mathbf{y} to the center $\hat{\mathbf{x}}$ of a Gaussian PDF by skewing the state space according to the covariance matrix $\Sigma_{\mathbf{x}}$ [24]:

$$D_{\text{meha}} = (\mathbf{y} - \hat{\mathbf{x}})^T \Sigma_{\mathbf{x}}^{-1} (\mathbf{y} - \hat{\mathbf{x}}) .$$

As one can see, this distance bases on the exponent of a multivariate Gaussian PDF like in Eq. (A.7).

Instead of determining the distance of only one point to another distribution, it is also sometimes necessary to determine the distance of a full distribution to a reference distribution. For this, different similarity measures are developed, which mostly integrates over the state space of the random variable. To handle also sampled distributions without a given parametrized $p(x)$, the measure should handle cases where $dp = dP(x)/dx = 0$ holds, which means that in specific sub areas \mathbb{R}^n samples do not exist. A known measure solving this issue is the Hellinger Distance [24] which co-domain is $[0, 1]$, where one represents the case that the PDF's are totally different and zero indicates an equivalence of both PDF's.

The Hellinger Distance D_{hell} for two PDF's $p(\mathbf{x})$ and $q(\mathbf{x})$ is calculated according to:

$$D_{\text{hell}}^2(P, Q) = \frac{1}{2} \int_{\mathbb{R}^n} \left(\sqrt{dp} - \sqrt{dq} \right) .$$

For two samples with K discrete bins with dP^k and dQ^k , the Hellinger Distance is calculated as follows:

$$D_{\text{hell}} = 1 - \sum_{k=1}^K \sqrt{dP^k \cdot dQ^k} .$$

Note, that for creating a histogram from samples drawn from a PDF, the number of samples must be high enough and the bins small enough to obtain a good approximation of dp . For a high dimensional space, this becomes a highly computational task.

A.7 Bayesian Theory

In Sec. A.6, the distribution of a random variable was presented. In the following part, the decomposition of numerous random variables is discussed. Different rules for reformulating PDF's like the sum and product rule are presented in the first part. Afterwards, the terms independence and conditional independence are repeated. At the end, this section closes with the Bayes theorem and Bayesian Network as a graphical representation of relationships between variables. The formulas are extracted from [24].

A.7.1 Sum and Product Rule

Consider a multivariate random variable \mathcal{X} , which can be described by a PDF $p(\mathbf{x})$. If one is interested only in the distribution of the first element x_1 of the vector \mathbf{x} , the distribution has to be marginalized over all the other elements x_2, \dots, x_n :

$$p(x_1) = \int_{\mathbb{R}^{n-1}} p(x_1, x_2, \dots, x_n) dx_2 \cdots dx_n . \quad (\text{A.11})$$

This is called the **sum rule** for continuous distributed variables. For discrete element in \mathcal{X} , the sum instead of the integral is used to marginalize over the corresponding element. For a multivariate Gaussian PDF with \hat{x} and $\Sigma_{\mathbf{x}}$, the univariate distribution $p(x_1)$ can be determined by using the first basis vector $\mathbf{e}_1 = [1, 0, \dots, 0]^T$:

$$p(x_1) = \mathcal{N}(x_1; \mathbf{e}_1^T \hat{\mathbf{x}}, \mathbf{e}_1^T \Sigma_{\mathbf{x}} \mathbf{e}_1) .$$

For cases where a PDF is extracted with more than one element of \mathbf{x} , one can use a multi-column matrix consisting of the corresponding basis vector instead of one single basis vector.

Another important rule is the **product rule**, which states that a joint distribution $p(\mathbf{x})$ can be decomposed into a product of conditional probabilities:

$$\begin{aligned} p(\mathbf{x}) &= p(x_1|x_2, \dots, x_n) \cdot p(x_2|x_3, \dots, x_n) \cdots p(x_n) \quad (\text{A.12}) \\ &= p(x_n) \cdot \prod_{i=1}^{n-1} p(x_i|x_{i+1}, \dots, x_n) . \end{aligned}$$

The order of variables can be chosen freely, but the conditional probabilities remain in general. The number of combination is $n!$.

A.7.2 Bayesian Theorem

The Bayesian theorem describes an explicit change of a cause-effect-dependency of two variables. Given an independent variable \mathcal{X}_1 and a dependent variable \mathcal{X}_2 , representing the cause and effect, respectively, their conditional probability $p(x_2|x_1)$ can be used to infer on the effect-cause probability:

$$p(x_1|x_2) = \frac{p(x_2|x_1)p(x_1)}{p(x_2)} = \frac{p(x_2|x_1)p(x_1)}{\int_{\mathbb{R}} p(x_2|x_1)p(x_1)dx_1} \quad , \quad (\text{A.13})$$

where $p(x_1)$ is the distribution of the independent variable. The Bayesian theorem is a direct consequence of the different ways to decompose a PDF by the product rule of Eq. (A.12).

A.7.3 Statistical Independence

The independence of two variables \mathcal{X}_1 and \mathcal{X}_2 means that both distributions can be treated individually, so one random variable is not depending on the other one. There is no correlation between the variables. In this case the following equations hold:

$$\begin{aligned} p(x_1, x_2) &\stackrel{(\text{A.12})}{=} p(x_1|x_2) \cdot p(x_2) = p(x_2|x_1) \cdot p(x_1) \\ &= p(x_1) \cdot p(x_2) \quad . \end{aligned}$$

For a Gaussian PDF, the covariance matrix becomes diagonal if Eq. (A.14) is satisfied.

The term **conditional independence** means that two variables become independent if another independent variable \mathcal{X}_3 is observed.

$$\begin{aligned} p(x_1, x_2|x_3) &\stackrel{(\text{A.12})}{=} p(x_1|x_2, x_3) \cdot p(x_2|x_3) = p(x_2|x_1, x_3) \cdot p(x_1|x_3) \\ &= p(x_1|x_3) \cdot p(x_2|x_3) \quad . \end{aligned} \quad (\text{A.14})$$

The independence criteria is a special case with strong underlying assumptions. In multivariate models there are often mixed, where one variable is only depending on a subset of other variables. A decomposition according to Eq. (A.12) with the correct order and dependencies can drastically reduce the complexity.

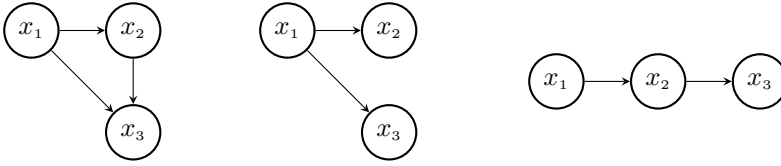


Figure A.6: Bayesian networks representing $p^1(x_1, x_2, x_3)$ (left), $p^2(x_1, x_2, x_3)$ (center) and $p^3(x_1, x_2, x_3)$ (right), which are mathematically formulated in this section.

A.7.4 Bayesian Network

As it already discussed, probability models can have different representations depending on the order, how this model is decomposed. An often used way is to illustrate the modeled dependencies in a Bayesian network. This network is a directed, non-cycled graphs with random variables as nodes and edges with arrows showing the cause-effect dependencies between the variables. Typical examples are shown in Fig. A.6.

With this representation, the joint distribution model can easily being extracted as follows:

$$\begin{aligned}
 p^1(x_1, x_2, x_3) &= p(x_3|x_1, x_2) p(x_2|x_1) p(x_1) \\
 p^2(x_1, x_2, x_3) &= p(x_3|x_1) p(x_2|x_1) p(x_1) \\
 p^3(x_1, x_2, x_3) &= p(x_3|x_2) p(x_2|x_1) p(x_1) .
 \end{aligned}$$

Here, the joint probability of $p^1(x_1, x_2, x_3)$ was decomposed according to the product rule of Eq. (A.12). The model $p^2(x_1, x_2, x_3)$ shows a case if one variable \mathcal{X}_1 influences two other variables. If \mathcal{X}_1 is observed, $\mathcal{X}_2, \mathcal{X}_3$ becomes conditionally independent according to Eq. (A.14). The model $p^3(x_1, x_2, x_3)$ has a structure similar to a Dynamic Bayesian Network, where each node represents a variable at a specific point in time and one time point is only depending on the previous time point.

Index

- Bayesian
 - network, 30, 214
 - product rule, 212
 - sum rule, 212
 - theorem, 53, 213
- behavior, 42, 139, 177
 - planner, 3, 27
- collision
 - avoidance, 15, 22, 40
 - mitigation, 15, 20–40
- collision region
 - dynamic, 72, 78, 89, 100, 106, 189, 191, 192
 - static, 72, 77–78, 87, 89, 105, 106, 192
- costs
 - comfort, 38, 40, 55, 59
 - event, 39, 56, 59, 141
 - instantaneous, 41, 55–57, 59
 - progress, 40, 55, 59
 - time-course sensitive, 59–61
 - total, 42, 43, 61, 63
- delta-function, 205
- distance measure
 - Hellinger, 94, 109, 111, 115, 121, 126, 211
 - Mahalanobis, 98, 211
- distribution, 204
 - Gaussian, 82, 92, 96, 107, 119, 124, 206
 - Gaussian Mixture, 96, 125, 207
 - logistic, 151, 153, 206
 - shape, 81
 - truncated Gaussian, 82–87, 124–125, 209
- environment
 - uncertain, 26
- error-function, 207
- event, 28
 - collision, 29, 31, 32, 40, 68, 160
 - detection model, 31, 53, 73
 - distributed collision, 29, 118–121, 140, 161, 181
 - dynamic restrictions, 29, 122
 - escape, 29, 31, 127–130, 140, 161
 - multiple, 61, 108
 - non-reachable sets, 31
 - priorities, 39
 - rate, 64–66, 104–106, 129, 140, 142, 161
 - speed limitation, 31
- event rate, 119
- intention, 11, 29, 54
 - controlled, 29, 33, 51, 54, 138

- non-controlled, 30, 33, 51, 54, 120, 139, 140
 - safe, 30, 33, 51, 54, 129, 139, 149
 - transition model, 31, 129
- model
 - behavior, 13, 24, 32, 42–44, 161
 - event detection, 31, 71, 78, 80, 119, 122, 129
 - intention transition, 31, 120
 - motion, 9, 13, 33
- momentum
 - mechanical, 148
 - stochastic, 93, 120, 208
- probability
 - collision event, 23, 25, 70, 81
 - event, 18, 52, 54, 62
 - instantaneous, 55, 64–66, 81, 92, 109, 110, 120, 126, 130
 - survival, 55, 57–59, 62, 64–66, 71, 92, 109, 110, 120, 126, 130, 194
 - time-course sensitive, 57, 59–142
 - total, 60, 113
- risk, 14, 24, 39, 56, 70, 132
- scenario, 10
 - being passed, 167, 175
 - following, 167, 169
 - frontal approaching, 167, 172
 - frontal passing, 167, 176
 - intersection, 110
 - overtaking, 106, 113, 167, 174
 - tailgated, 167, 169
- scene, 9
- severity, 25, 56, 61, 129
 - collision, 21–22, 70, 132, 144
 - event, 18
- severity model, 169, 172
 - constant, 157, 162, 169, 172, 174–177, 181
 - inter-vehicle impact, 169, 176, 177
 - inter-vehicles, 159–160, 164, 169, 172, 174, 180
 - multiple events, 160–169
 - multiple-events, 169, 172, 174, 176, 177, 180
 - wall impact, 162, 169, 172, 174–177, 181
 - wall-impact, 158–159
- situation, 11
- step-function, 205
- threat, 15, 16
- traffic environment, 8
- utility, *see* costs

Bibliography

- [1] S. Acierno, R. Kaufman, F.P. Rivara, D.C. Grossman, and C. Mock. Vehicle mismatch: injury patterns and severity. *Accident Analysis & Prevention*, 36:761–772, September 2004.
- [2] J.S. Albus and W.G. Rippey. Rcs: a reference model architecture for intelligent control. In *Proceedings of PerAc '94. From Perception to Action*, pages 218–229. IEEE Comput. Soc. Press, 1994.
- [3] Salvatore Alfano. Addressing nonlinear relative motion for spacecraft collision probability. *AIAA/AAS Astrodynamics Specialist Conference and Exhibit*, 3, August 2006.
- [4] Salvatore Alfano. Review of conjunction probability methods for short-term encounters. *Advances in the Astronautical Sciences*, 127:719–746, January 2007.
- [5] Daniel Althoff. *Safety assessment for motion planning in uncertain and dynamic environments*. PhD thesis, Technische Universität München, 2014.
- [6] Daniel Althoff, James J. Kuffner, Dirk Wollherr, and Martin Buss. Safety assessment of robot trajectories for navigation in uncertain and dynamic environments. *Autonomous Robots*, 32:285–302, 2012.
- [7] Matthias Althoff and Alexander Mergel. Comparison of markov chain abstraction and monte carlo simulation for the safety assessment of autonomous cars. *IEEE Transactions on Intelligent Transportation Systems*, 12:1237–1247, December 2011.
- [8] Matthias Althoff, Olaf Stursberg, and Martin Buss. Model-based probabilistic collision detection in autonomous driving. *IEEE Transactions on Intelligent Transportation Systems*, 10:299–310, June 2009.
- [9] Samer Ammoun and Fawzi Nashashibi. Real time trajectory prediction for collision risk estimation between vehicles. In *Proceedings*

- 2009 IEEE 5th International Conference on Intelligent Computer Communication and Processing, ICCP 2009, 2009.
- [10] Stefan Annell, Alexander Gratner, and Lars Svensson. Probabilistic collision estimation system for autonomous vehicles. In *IEEE Conference on Intelligent Transportation Systems, Proceedings, ITSC*, 2016.
- [11] Hermann Appel, Gerald Krabbel, and Dirk Vetter. *Unfallforschung, Unfallmechanik und Unfallrekonstruktion*. Vieweg+Teubner Verlag, 2002.
- [12] Alexandre Armand. *Situation Understanding and Risk Assessment Framework for Preventive Driver Assistance*. PhD thesis, July 2016.
- [13] J. Augenstein, E. Perdeck, J. Stratton, K. Digges, G. Bahouth, N. Borchers, and P. Baur. Methodology for the development and validation of injury predicting algorithms. 2003.
- [14] Jeffrey Augenstein, Elana Perdeck, James Stratton, Kennerly Digges, and George Bahouth. Characteristics of crashes that increase the risk of serious injuries. *Annual proceedings / Association for the Advancement of Automotive Medicine. Association for the Advancement of Automotive Medicine*, 47:561–576, February 2003.
- [15] Edmond Awad, Sohan Dsouza, Azim Shariff, Iyad Rahwan, and Jean-François Bonnefon. Universals and variations in moral decisions made in 42 countries by 70,000 participants. *Proceedings of the National Academy of Sciences*, 117:2332–2337, February 2020.
- [16] Susan P. Baker and Brian O’Neill. The injury severity score: an update. *Journal of Trauma and Acute Care Surgery*, 16:882–885, 1976.
- [17] Susan P. Baker, Brian O’Neill, William Haddon Jr., and William B. Long. The injury severity score: a method for describing patients with multiple injuries and evaluating emergency care. *Journal of Trauma and Acute Care Surgery*, 14:187–196, 1974.
- [18] Thomas Batz, Kym Watson, and Jurgen Beyerer. Recognition of dangerous situations within a cooperative group of vehicles. In *2009 IEEE Intelligent Vehicles Symposium*, pages 907–912. IEEE, June 2009.

-
- [19] Herbert Baum, Thomas Kranz, and Ulrich Westerkamp. Volkswirtschaftliche kosten durch straßenverkehrsunfälle in deutschland. 2010.
- [20] Antoine Bautin, Luis Martinez-Gomez, and Thierry Fraichard. Inevitable collision states: A probabilistic perspective. In *2010 IEEE International Conference on Robotics and Automation*, pages 4022–4027. IEEE, May 2010.
- [21] Adam Berthelot, Andreas Tamke, Thao Dang, and Gabi Breuel. Handling uncertainties in criticality assessment. In *IEEE Intelligent Vehicles Symposium, Proceedings*, 2011.
- [22] Adam Berthelot, Andreas Tamke, Thao Dang, and Gabi Breuel. A novel approach for the probabilistic computation of time-to-collision. In *IEEE Intelligent Vehicles Symposium, Proceedings*, 2012.
- [23] Adam Berthelot, Andreas Tamke, Thao Dang, and Gabi Breuel. Stochastic situation assessment in advanced driver assistance system for complex multi-objects traffic situations. In *IEEE International Conference on Intelligent Robots and Systems*, 2012.
- [24] Christopher M Bishop. *Pattern recognition and machine learning Solutions to exercis*, volume 4. 2006.
- [25] L. Blackmore, Hui Li, and B. Williams. A probabilistic approach to optimal robust path planning with obstacles. In *2006 American Control Conference*. IEEE, 2006.
- [26] Andrew Blake, Alejandro Bordallo, Kamen Brestnichki, Majd Hawasly, Svetlin Valentinov Penkov, Subramanian Ramamoorthy, and Alexandre Silva. Fpr-fast path risk algorithm to evaluate collision probability. *IEEE Robotics and Automation Letters*, 5:1–7, January 2020.
- [27] Dennis Böhmländer, Tobias Dirndorfer, Ali H. Al-Bayatti, and Thomas Brandmeier. Context-aware system for pre-triggering irreversible vehicle safety actuators. *Accident Analysis and Prevention*, 103:72–84, June 2017.
- [28] Dennis Böhmländer, Vitor Yano, Thomas Brandmeier, Alessandro Zimmer, Lee Luan Ling, Chi-Biu Wong, and Tobias Dirndorfer. A novel approach for intelligent pre-crash threat assessment systems.

- In *17th International IEEE Conference on Intelligent Transportation Systems (ITSC)*, pages 954–961. IEEE, October 2014.
- [29] Jean Francois Bonnefon, Azim Shariff, and Iyad Rahwan. The social dilemma of autonomous vehicles. *Science*, 352, 2016.
- [30] Christian Braeuchle, Folko Flehmig, Wolfgang Rosenstiel, and Thomas Kropf. Maneuver decision for active pedestrian protection under uncertainty. In *16th International IEEE Conference on Intelligent Transportation Systems (ITSC 2013)*, pages 646–651. IEEE, October 2013.
- [31] Mattias Brännström, Erik Coelingh, and Jonas Sjöberg. Threat assessment for avoiding collisions with turning vehicles. In *2009 IEEE Intelligent Vehicles Symposium*, pages 663–668. IEEE, June 2009.
- [32] Mattias Brännström, Erik Coelingh, and Jonas Sjöberg. Model-based threat assessment for avoiding arbitrary vehicle collisions. *IEEE Transactions on Intelligent Transportation Systems*, 11(3):658–669, 2010.
- [33] Adrian Broadhurst, Simon Baker, and Takeo Kanade. Monte carlo road safety reasoning. In *IEEE Intelligent Vehicles Symposium, Proceedings*, volume 2005, 2005.
- [34] Gaoya Cao, Florian Damerow, Benedict Flade, Markus Helmling, and Julian Eggert. Camera to map alignment for accurate low-cost lane-level scene interpretation. In *2016 IEEE 19th International Conference on Intelligent Transportation Systems (ITSC)*. IEEE, November 2016.
- [35] Ching-Yao Chan. Defining safety performance measures of driver-assistance systems for intersection left-turn conflicts. In *2006 IEEE Intelligent Vehicles Symposium*, pages 25–30. IEEE, 2006.
- [36] Tay C. Tay Christopher. *Analysis of Dynamic Scenes: Application to Driving Assistance*. Theses, Institut National Polytechnique de Grenoble - INPG, September 2009.
- [37] Florian Damerow and Julian Eggert. Predictive risk maps. In *17th International IEEE Conference on Intelligent Transportation Systems (ITSC)*, pages 703–710. IEEE, October 2014.

- [38] Florian Damerow and Julian Eggert. Balancing risk against utility: Behavior planning using predictive risk maps. In *2015 IEEE Intelligent Vehicles Symposium (IV)*, volume 2015-August, pages 857–864. IEEE, June 2015.
- [39] Florian Damerow and Julian Eggert. Risk-averse behavior planning under multiple situations with uncertainty. In *2015 IEEE 18th International Conference on Intelligent Transportation Systems*, volume 2015-October, pages 656–663. IEEE, September 2015.
- [40] Philip J Davis and Philip Rabinowitz. *Methods of numerical integration*. Courier Corporation, 2007.
- [41] Mark de Berg, Otfried Cheong, Marc van Kreveld, and Mark Overmars. *Computational Geometry*. Springer Berlin Heidelberg, 2008.
- [42] Statistisches Bundesamt (Destatis). Unfallentwicklung auf deutschen straßen 2015. *Statistisches Bundesamt*, July 2016.
- [43] Statistisches Bundesamt (Destatis). Todesursachen in deutschland-fachserie 12 reihe 4. *Statistisches Bundesamt*, January 2017.
- [44] K Digges and G Bahouth. Frequency of injuries in multiple impact crashes. *Annual proceedings. Association for the Advancement of Automotive Medicine*, 47:417–423, 2003.
- [45] Julian Eggert. Predictive risk estimation for intelligent ADAS functions. In *17th International IEEE Conference on Intelligent Transportation Systems (ITSC)*, pages 711–718. IEEE, October 2014.
- [46] Julian Eggert, Florian Damerow, and Stefan Klingelschmitt. The foresighted driver model. In *2015 IEEE Intelligent Vehicles Symposium (IV)*, pages 322–329. IEEE, June 2015.
- [47] Julian Eggert and Fabian Müller. A foresighted driver model derived from integral expected risk. In *2019 IEEE Intelligent Transportation Systems Conference (ITSC)*, pages 1223–1230. IEEE, October 2019.
- [48] Julian Eggert and Tim Pupal. Continuous risk measures for ADAS and AD. May 2017.
- [49] Andreas Eidehall and Lars Petersson. Statistical threat assessment for general road scenes using monte carlo sampling. *IEEE Transactions on Intelligent Transportation Systems*, 9:137–147, March 2008.

- [50] Andreas Eidehall, Jochen Pohl, Fredrik Gustafsson, and Jonas Ekmark. Toward autonomous collision avoidance by steering. *IEEE Transactions on Intelligent Transportation Systems*, 8:84–94, March 2007.
- [51] Mustafa Elkady, Ahmed Elmarakbi, John MacIntyre, and Mohammed Alhariri. Collision mitigation and vehicle transportation safety using integrated vehicle dynamics control systems. *Journal of Traffic and Transportation Engineering (English Edition)*, 4:41–60, February 2017.
- [52] Christer Ericson. *Real-time collision detection*. Morgan Kaufmann series in interactive 3D technology. Elsevier, Amsterdam [u.a.], 2005.
- [53] Ethik-Kommission. Automatisiertes und vernetztes Fahren. June 2017.
- [54] L. Evans and M. C. Frick. Car size or car mass: Which has greater influence on fatality risk? *American Journal of Public Health*, 82:1105–1112, 1992.
- [55] Leonard Evans. Driver injury and fatality risk in two-car crashes versus mass ratio inferred using newtonian mechanics. *Accident Analysis and Prevention*, 26:609–616, 1994.
- [56] Leonard Evans and Michael C. Frick. Mass ratio and relative driver fatality risk in two-vehicle crashes. *Accident Analysis and Prevention*, 25:213–224, 1993.
- [57] Paul Fay, Raimondo Sferco, and Richard Frampton. Multiple impact crashes-consequences for occupant protection measures. *Proceedings of the 2001 IRCOBI Conference on the Biomechanics of Impact*, October 2001.
- [58] Dave Ferguson, Michael Darms, Chris Urmson, and Sascha Kolski. Detection, prediction, and avoidance of dynamic obstacles in urban environments. In *2008 IEEE Intelligent Vehicles Symposium*, pages 1149–1154. IEEE, June 2008.
- [59] Thierry Fraichard. A short report about motion safety. In *IEEE International Conference on Robotics and Automation (ICRA)*, pages 10–14, 2007.

- [60] Thierry Fraichard and Hajime Asama. Inevitable collision states - a step towards safer robots. *Advanced Robotics*, 18, 2004.
- [61] Douglas J Gabauer and Hampton Clay Gabler. Comparison of delta-v and occupant impact velocity crash severity metrics using event data recorders. In *Annual Proceedings/Association for the Advancement of Automotive Medicine*, volume 50, page 57, 2006.
- [62] Hampton C. Gabler, Douglas J. Gabauer, Heidi L. Newell, and Michael E. O'Neill. Use of event data recorder (EDR) technology for highway crash data analysis. *NCHRP Project*, pages 17–24, 2004.
- [63] Hampton C. Gabler, Carolyn E. Hampton, and John Hinch. Crash severity: A comparison of event data recorder measurements with accident reconstruction estimates. March 2004.
- [64] Romain Gallen, Nicolas Hautiere, Aurelien Cord, and Sebastien Glaser. Supporting drivers in keeping safe speed in adverse weather conditions by mitigating the risk level. *IEEE Transactions on Intelligent Transportation Systems*, 14:1558–1571, December 2013.
- [65] Konstantin Garidis, Leon Ulbricht, Alexander Rossmann, and Marco Schmäh. Toward a user acceptance model of autonomous driving. 2020.
- [66] Anderas Georgi, Marc Zimmermann, Thomas Lich, Lisa Blank, Nils Kickler, and Reiner Marchthaler. New approach of accident benefit analysis for rear end collision avoidance and mitigation systems. In *Proceeding of the 21st International Technical Conference on the Enhanced Safety of Vehicles (ESV)*, pages 1–8, 2009.
- [67] Alex Gilbert, Dobrila Petrovic, Kevin Warwick, and Vasilis Serghi. Autonomous vehicle simulation model to assess potential collisions to reduce severity of impacts. In *Proceedings of the 4th International Conference on Vehicle Technology and Intelligent Transport Systems*, volume 2018-March, pages 243–250. SCITEPRESS - Science and Technology Publications, 2018.
- [68] Giovanni Girone, Antonella Massari, Fabio Manca, and Claudia Marin. Mean difference of truncated normal distribution. *Applied Mathematics*, 11:1162–1166, November 2020.

- [69] David Gonzalez, Joshue Perez, Vicente Milanés, and Fawzi Nashashibi. A review of motion planning techniques for automated vehicles. *IEEE Transactions on Intelligent Transportation Systems*, 17:1135–1145, April 2016.
- [70] Noah J. Goodall. Ethical decision making during automated vehicle crashes. *Transportation Research Record: Journal of the Transportation Research Board*, 2424:58–65, January 2014.
- [71] Daniel Greene, Juan Liu, Jim Reich, Yukio Hirokawa, Akio Shinagawa, Hayuru Ito, and Tatsuo Mikami. An efficient computational architecture for a collision early-warning system for vehicles, pedestrians, and bicyclists. *IEEE Transactions on Intelligent Transportation Systems*, 12, 2011.
- [72] Carl Haasper, Mirko Junge, Antonio Ernstberger, H. Brehme, Lars Hannawald, C. Langer, Joachim Nehmzow, Dietmar Otte, Ulrich Sander, Christian Krettek, and Hans Zwipp. The abbreviated injury scale (AIS). options and problems in application. *Der Unfallchirurg*, 113:366–372, May 2010.
- [73] Jason Hardy and Mark Campbell. Contingency planning over probabilistic obstacle predictions for autonomous road vehicles. *IEEE Transactions on Robotics*, 29, 2013.
- [74] Philip Heck, Jan Bellin, Martin Matousek, Stefan Wonneberger, Ondrej Sychrovsky, Radim Sara, and Markus Maurer. Collision mitigation for crossing traffic in urban scenarios. In *IEEE Intelligent Vehicles Symposium, Proceedings*, pages 559–566, 2013.
- [75] Alexander Hevelke and Julian Nida-Rümelin. Responsibility for crashes of autonomous vehicles: An ethical analysis. *Science and Engineering Ethics*, 21:619–630, June 2015.
- [76] Jörg Hillenbrand, Andreas M. Spieker, and Kristian Kroschel. A multilevel collision mitigation approach - its situation assessment, decision making, and performance tradeoffs. *IEEE Transactions on Intelligent Transportation Systems*, 7, 2006.
- [77] Adam Houenou, Philippe Bonnifait, and Veronique Cherfaoui. Risk assessment for collision avoidance systems. In *17th International IEEE Conference on Intelligent Transportation Systems (ITSC)*. IEEE, October 2014.

- [78] Jonathan P. How. Ethically aligned design [from the editor]. *IEEE Control Systems*, 38:3–4, June 2018.
- [79] Clemens Markus Hruschka, Michael Schmidt, Daniel Topfer, and Sebastian Zug. Uncertainty-adaptive, risk based motion planning in automated driving. In *2019 IEEE International Conference on Vehicular Electronics and Safety (ICVES)*, 2019.
- [80] Clemens Markus Hruschka, Daniel Topfer, and Sebastian Zug. Risk assessment for integral safety in automated driving. In *2019 2nd International Conference on Intelligent Autonomous Systems (ICoIAS)*, pages 102–109. IEEE, February 2019.
- [81] Jinwook Huh and Daniel D. Lee. Learning high-dimensional mixture models for fast collision detection in rapidly-exploring random trees. In *2016 IEEE International Conference on Robotics and Automation (ICRA)*, pages 63–69. IEEE, May 2016.
- [82] Gregory Hutchins. *ISO 31000: 2018 Enterprise Risk Management. Quality + Engineering/* CERM Academy, 2018.
- [83] Inseok Hwang and Chze Eng Seah. Intent-based probabilistic conflict detection for the next generation air transportation system. In *Proceedings of the IEEE*, volume 96, pages 2040–2059, December 2008.
- [84] Jonas Jansson and Jonas Jansson. *Collision Avoidance Theory with Application to Automotive Collision Mitigation Department of Electrical Engineering*. 2005.
- [85] Jie Ji, Amir Khajepour, Wael William Melek, and Yanjun Huang. Path planning and tracking for vehicle collision avoidance based on model predictive control with multiconstraints. *IEEE Transactions on Vehicular Technology*, 66:952–964, February 2017.
- [86] Heiko Johannsen. *Unfallmechanik und Unfallrekonstruktion: Grundlagen der Unfallaufklärung*. Springer, 2013.
- [87] Hans C. Joks. Velocity change and fatality risk in a crash—a rule of thumb. *Accident Analysis & Prevention*, 25, February 1993.
- [88] Philipp Junietz, Jan Schneider, and Hermann Winner. Metrik zur bewertung der kritikalität von verkehrssituationen und -szenarien.

11. *Workshop Fahrerassistenzsysteme und automatisiertes Fahren*, 2017.
- [89] Chris Jurewicz, Amir Sobhani, Jeremy Woolley, Jeff Dutschke, and Bruce Corben. Exploration of vehicle impact speed – injury severity relationships for application in safer road design. *Transportation Research Procedia*, 14:4247–4256, 2016.
- [90] Chris Jurewicz, Stephen Tofter, and Tario Makwasha. Improving the performance of safe system infrastructure. November 2015.
- [91] Nico Kaempchen, Bruno Schiele, and Klaus Dietmayer. Situation assessment of an autonomous emergency brake for arbitrary vehicle-to-vehicle collision scenarios. *IEEE Transactions on Intelligent Transportation Systems*, 10:678–687, 2009.
- [92] Rickard Karlsson, Jonas Jansson, and Fredrik Gustafsson. Model-based statistical tracking and decision making for collision avoidance application. In *Proceedings of the American Control Conference*, volume 4, 2004.
- [93] Christos Katrakazas, Mohammed Quddus, Wen-Hua Chen, and Lipika Deka. Real-time motion planning methods for autonomous on-road driving: State-of-the-art and future research directions. *Transportation Research Part C: Emerging Technologies*, 60:416–442, November 2015.
- [94] Lars Kübler, Simon Gargallo, and Konrad Elsässer. Frontal crash pulse assessment with application to occupant safety. *ATZ worldwide*, 111, June 2009.
- [95] Beomjun Kim, Kwanwoo Park, and Kyongsu Yi. Probabilistic threat assessment with environment description and rule-based multi-traffic prediction for integrated risk management system. *IEEE Intelligent Transportation Systems Magazine*, 9:8–22, 2017.
- [96] Jaehwan Kim and Dongsuk Kum. Collision risk assessment algorithm via lane-based probabilistic motion prediction of surrounding vehicles. *IEEE Transactions on Intelligent Transportation Systems*, 19:2965–2976, September 2018.
- [97] Raphael Labayrade, Cyril Royere, and Didier Aubert. A collision mitigation system using laser scanner and stereovision fusion and its

- assessment. In *IEEE Intelligent Vehicles Symposium, Proceedings*, volume 2005, 2005.
- [98] Alain Lambert, Dominique Gruyer, and Guillaume Saint Pierre. A fast monte carlo algorithm for collision probability estimation. In *10th International Conference on Control, Automation, Robotics and Vision, ICARCV 2008*, 2008.
- [99] Alain Lambert, Dominique Gruyer, Guillaume Saint Pierre, and Alexandre Ndjeng Ndjeng. Collision probability assessment for speed control. In *2008 11th International IEEE Conference on Intelligent Transportation Systems*, pages 1043–1048. IEEE, October 2008.
- [100] Andreas Lawitzky, Dirk Wollherr, and Martin Buss. Maneuver-based risk assessment for high-speed automotive scenarios. In *2012 IEEE/RSJ International Conference on Intelligent Robots and Systems*, pages 1186–1191. IEEE, October 2012.
- [101] Alex Lee, Yan Duan, Sachin Patil, John Schulman, Zoe McCarthy, Jur van den Berg, Ken Goldberg, and Pieter Abbeel. Sigma hulls for gaussian belief space planning for imprecise articulated robots amid obstacles. In *2013 IEEE/RSJ International Conference on Intelligent Robots and Systems*, pages 5660–5667. IEEE, November 2013.
- [102] Kibeom Lee and Dongsuk Kum. Collision avoidance/mitigation system: Motion planning of autonomous vehicle via predictive occupancy map. *IEEE Access*, 7:52846–52857, 2019.
- [103] Stéphanie Lefèvre, Dizan Vasquez, and Christian Laugier. A survey on motion prediction and risk assessment for intelligent vehicles. *ROBOMECH Journal*, 1:1, December 2014.
- [104] Martin Liebner and Felix Klanner. *Driver Intent Inference and Risk Assessment*. Springer International Publishing, 2016.
- [105] Miaomiao Liu, Yongsheng Chen, Guangquan Lu, and Yunpeng Wang. Modeling crossing behavior of drivers at unsignalized intersections with consideration of risk perception. *Transportation Research Part F: Traffic Psychology and Behaviour*, 45:14–26, 2017.
- [106] Jianbo Lu, Hassen Hammoud, Todd Clark, Otto Hofmann, Mohsen Lakehal-ayat, Shweta Farmer, Jason Shomsky, and Roland Schaefer.

- A system for autonomous braking of a vehicle following collision. March 2017.
- [107] Christoph Luetge. The german ethics code for automated and connected driving. *Philosophy and Technology*, 30:547–558, December 2017.
- [108] Stephen N. Luko. Risk management principles and guidelines. *Quality Engineering*, 25:451–454, October 2013.
- [109] E. Miltner and H.-J. Salwender. Influencing factors on the injury severity of restrained front seat occupants in car-to-car head-on collisions. *Accident Analysis & Prevention*, 27:143–150, April 1995.
- [110] Fabian Müller and Julian Eggert. Time-course sensitive collision probability model for risk estimation. In *2020 IEEE 23rd International Conference on Intelligent Transportation Systems (ITSC)*, pages 1–8, 2020.
- [111] Fabian Müller and Julian Eggert. Behaviour investigation of a risk-aware driving model for trajectory prediction. In *Proceedings of the 5th International Symposium on Future Active Safety Technology toward Zero Accidents (FAST-zero '19)*, page 8, Darmstadt, December 2021.
- [112] Marcus Müller, Michael Botsch, Dennis Böhmmländer, and Wolfgang Utschick. Machine learning based prediction of crash severity distributions for mitigation strategies. *Journal of Advances in Information Technology*, 9:15–24, 2018.
- [113] Marcus Müller, Xing Long, Michael Botsch, Dennis Böhmmländer, and Wolfgang Utschick. Real-time crash severity estimation with machine learning and 2D mass-spring-damper model. In *2018 21st International Conference on Intelligent Transportation Systems (ITSC)*, volume 2018-Novem, pages 2036–2043. IEEE, November 2018.
- [114] Marcus Müller, Parthasarathy Nadarajan, Michael Botsch, Wolfgang Utschick, Dennis Böhmmländer, and Stefan Katzenbogen. A statistical learning approach for estimating the reliability of crash severity predictions. In *2016 IEEE 19th International Conference on Intelligent Transportation Systems (ITSC)*, pages 2199–2206. IEEE, November 2016.

-
- [115] Sean O'Brien. Measurement and assessment of passenger vehicle compatibility in front and side collisions. *Faculty of Engineering, RMIT University, Melbourne/Australia*, 2010.
- [116] World Health Organization. Global health observatory data repository, road traffic deaths data by who region. July 2021.
- [117] World Health Organization et al. Global status report on road safety 2018: summary, 2018.
- [118] Tia Orton, Shane Richardson, Anna Magennis, Nikola Josevski, Tandy Pok, Andreas Sandvik, Chris Jones, Tom Emmett, Tony Clinigin, and Shuang Li. Evaluation of vehicle interior head impacts for the forensic analysis of mais head injury risk. *2012 IEEE-EMBS Conference on Biomedical Engineering and Sciences*, pages 469–474, December 2012.
- [119] Russell A. Paielli and Heinz Erzberger. Conflict probability estimation for free flight. *Journal of Guidance, Control, and Dynamics*, 20:588–596, May 1997.
- [120] Chonhyon Park, Jae Sung Park, and Dinesh Manocha. Fast and bounded probabilistic collision detection in dynamic environments for high-DOF trajectory planning. July 2016.
- [121] Jae Sung Park, Chonhyon Park, and Dinesh Manocha. Efficient probabilistic collision detection for non-convex shapes. In *Proceedings - IEEE International Conference on Robotics and Automation*, pages 1944–1951, May 2017.
- [122] Sachin Patil, Jur van den Berg, and Ron Alterovitz. Estimating probability of collision for safe motion planning under gaussian motion and sensing uncertainty. In *2012 IEEE International Conference on Robotics and Automation*, pages 3238–3244. IEEE, May 2012.
- [123] Witold Pawlus, Hamid Reza Karimi, and Kjell Gunnar Robbersmyr. Development of lumped-parameter mathematical models for a vehicle localized impact. *Journal of Mechanical Science and Technology*, 25:1737–1747, July 2011.
- [124] Nicola Cufaro Petroni. *Probability and Stochastic Processes for Physicists*. Springer, 2020.

- [125] Andreas Philipp and Daniel Goehring. Analytic collision risk calculation for autonomous vehicle navigation. In *2019 International Conference on Robotics and Automation (ICRA)*, pages 1744–1750. IEEE, May 2019.
- [126] A. Polychronopoulos, M. Tsogas, A. Amditis, U. Scheunert, L. Andreone, and F. Tango. Dynamic situation and threat assessment for collision warning systems: The euclidean approach. In *IEEE Intelligent Vehicles Symposium, Proceedings*, 2004.
- [127] Tim Puphal, Malte Probst, and Julian Eggert. Probabilistic uncertainty-aware risk spot detector for naturalistic driving. *IEEE Transactions on Intelligent Vehicles*, 4(3):406–415, 2019.
- [128] Tim Puphal, Malte Probst, Misa Komuro, Yiyang Li, and Julian Eggert. Comfortable priority handling with predictive velocity optimization for intersection crossings. In *2019 IEEE Intelligent Transportation Systems Conference (ITSC)*, pages 2435–2442. IEEE, October 2019.
- [129] Tim Puphal, Malte Probst, Yiyang Li, Yosuke Sakamoto, and Julian Eggert. Optimization of velocity ramps with survival analysis for intersection merge-ins. In *2018 IEEE Intelligent Vehicles Symposium (IV)*, pages 1704–1710, 2018.
- [130] Weiwei Qi, Wei Wang, Bin Shen, and Jiabin Wu. A modified post encroachment time model of urban road merging area based on lane-change characteristics. *IEEE Access*, 8, 2020.
- [131] Yadollah Rasekhipour, Amir Khajepour, Shih-Ken Chen, and Bakhtiar Litkouhi. A potential field-based model predictive path-planning controller for autonomous road vehicles. *IEEE Transactions on Intelligent Transportation Systems*, 18:1255–1267, May 2017.
- [132] D. Richards and R. Cuerden. The relationship between speed and car driver injury severity. *Road Safety Web Publication*, page 16, 2009.
- [133] Claas Rodemerk, Stefan Habenicht, Alexander Weitzel, Hermann Winner, and Thomas Schmitt. Development of a general criticality

- criterion for the risk estimation of driving situations and its application to a maneuver-based lane change assistance system. In *IEEE Intelligent Vehicles Symposium, Proceedings*, pages 264–269, 2012.
- [134] M. Ruf, J. Ziehn, B. Rosenhahn, J. Beyerer, D. Willersinn, and H. Gotzig. Situation prediction and reaction control SPARC. *9. Workshop Fahrerassistenzsysteme (FAS 2014)*, pages 55–66, 2014.
- [135] M. Ruf, J. R. Ziehn, D. Willersinn, B. Rosenhahn, Jürgen Beyerer, and Heinrich Gotzig. A continuous approach to autonomous driving. In *Proceedings of the Conference on Vehicle and Infrastructure Safety Improvement in Adverse Conditions and Night Driving (VISION 2014)*, 2014.
- [136] Lukas Rummelhard, Amaury Nègre, Mathias Perrollaz, and Christian Laugier. Probabilistic Grid-based Collision Risk Prediction for Driving Application. June 2014.
- [137] Jayant P. Sangole and Gopal R. Patil. Adaptive neuro-fuzzy interface system for gap acceptance behavior of right-turning vehicles at partially controlled T-intersections. *Journal of Modern Transportation*, 22, 2014.
- [138] Simo Särkkä. *Bayesian filtering and smoothing*. Number 3. Cambridge University Press, 2013.
- [139] Christian Schmidt. *Fahrstrategien zur Unfallvermeidung im Straßenverkehr für Einzel- und Mehrobjektszenarien*. PhD thesis, Karlsruher Institut für Technologie, 2013.
- [140] Susanne Schönebeck, Andreas Schepers, Martin Pöppel-Decker, Nadja Färber, and Arnd Fitschen. *Voraussichtliche Entwicklung von Unfallzahlen und Jahresfahrleistungen in Deutschland*. Bundesanstalt für Straßenwesen (BASt), December 2020.
- [141] Matthias Schreier. *Bayesian Environment Representation, Prediction, and Criticality Assessment for Driver Assistance Systems in Schweinfurt*. PhD thesis, 2015.
- [142] Robin Schubert, Eric Richter, and Gerd Wanielik. Comparison and evaluation of advanced motion models for vehicle tracking. In *2008 11th International Conference on Information Fusion*, pages 1–6, 2008.

-
- [143] Shai Shalev-Shwartz, Shaked Shammah, and Amnon Shashua. On a formal model of safe and scalable self-driving cars. pages 1–37, 2017.
- [144] Steven G. Shelby. Delta- v as a measure of traffic conflict severity. *Traffic Safety*, 2011.
- [145] Bruno Simon, Florian Franke, Peter Riegl, and Andreas Gaull. Motion planning for collision mitigation via FEM – based crash severity maps. In *Intelligent Vehicles Symposium*, pages 1924–1931, 2019.
- [146] Oscar S. Siordia, Isaac Martin de Diego, Cristina Conde, Gerardo Reyes, and Enrique Cabello. Driving risk classification based on experts evaluation. In *2010 IEEE Intelligent Vehicles Symposium*, pages 1098–1103. IEEE, June 2010.
- [147] Amir Sobhani, William Young, David Logan, and Sareh Bahrololoom. A kinetic energy model of two-vehicle crash injury severity. *Accident; analysis and prevention*, 43:741–54, May 2011.
- [148] Jan Erik Stellet, Jan Schumacher, Wolfgang Branz, and J. Marius Zollner. Uncertainty propagation in criticality measures for driver assistance. In *2015 IEEE Intelligent Vehicles Symposium (IV)*, volume 2015-August, pages 1187–1194. IEEE, June 2015.
- [149] Daniel Svensson. Derivation of the discrete-time constant turn rate and acceleration motion model. pages 1–5, 2019.
- [150] Andreas Tamke, Thao Dang, and Gabi Breuel. A flexible method for criticality assessment in driver assistance systems. In *2011 IEEE Intelligent Vehicles Symposium (IV)*, pages 697–702. IEEE, June 2011.
- [151] Han Shue Tan and Jihua Huang. DGPS-based vehicle-to-vehicle cooperative collision warning: Engineering feasibility viewpoints. *IEEE Transactions on Intelligent Transportation Systems*, 7, 2006.
- [152] Nick T. Thomopoulos. *Statistical distributions: Applications and Parameter Estimates*. Springer, 2017.
- [153] Atsushi Togawa, Daisuke Murakami, Hidetsugu Saeki, Chinmoy Pal, and Tomosaburo Okabe. An insight into multiple impact crash statistics to search for future directions of counter-approaches. In *22th International Technical Conference on the Enhanced Safety of Vehicles (ESV)*, 2011.

- [154] Noel E. Du Toit and J. W. Burdick. Probabilistic collision checking with chance constraints. *IEEE Transactions on Robotics*, 27:809–815, August 2011.
- [155] Reza Tolouei, Mike Maher, and Helena Titheridge. Vehicle mass and injury risk in two-car crashes: A novel methodology. *Accident Analysis & Prevention*, 50:155–166, January 2013.
- [156] Martin Treiber, Ansgar Hennecke, and Dirk Helbing. Congested traffic states in empirical observations and microscopic simulations. *Physical Review E*, 62:1805–1824, August 2000.
- [157] Heinz Unbehauen. *Regelungstechnik II*, volume 9. Springer, 2007.
- [158] Pauli Virtanen, Ralf Gommers, Travis E. Oliphant, Matt Haberland, Tyler Reddy, David Cournapeau, Evgeni Burovski, Pearu Peterson, Warren Weckesser, Jonathan Bright, Stéfan J. van der Walt, Matthew Brett, Joshua Wilson, K. Jarrod Millman, Nikolay Mayorov, Andrew R. J. Nelson, Eric Jones, Robert Kern, Eric Larson, C J Carey, İlhan Polat, Yu Feng, Eric W. Moore, Jake VanderPlas, Denis Laxalde, Josef Perktold, Robert Cimrman, Ian Henriksen, E. A. Quintero, Charles R. Harris, Anne M. Archibald, Antônio H. Ribeiro, Fabian Pedregosa, Paul van Mulbregt, and SciPy 1.0 Contributors. SciPy 1.0: Fundamental Algorithms for Scientific Computing in Python. *Nature Methods*, 17:261–272, 2020.
- [159] Walther Wachenfeld, Philipp Junietz, Raphael Wenzel, and Hermann Winner. The worst-time-to-collision metric for situation identification. In *IEEE Intelligent Vehicles Symposium, Proceedings*, volume 2016-August, 2016.
- [160] Maximilian Alexander Wächter, Anja Faulhaber, Felix Blind, Silja Timm, Anke Dittmer, Leon René Sütfeld, Achim Stephan, Gordon Pipa, and Peter König. Human decisions in moral dilemmas are largely described by utilitarianism: virtual car driving study provides guidelines for ADVs. 2017.
- [161] Sebastian Wagner, Korbinian Groh, Thomas Kuhbeck, Michael Dörfel, and Alois Knoll. Using time-to-react based on naturalistic traffic object behavior for scenario-based risk assessment of automated driving. In *IEEE Intelligent Vehicles Symposium, Proceedings*, June 2018.

- [162] Hong Wang, Yanjun Huang, Amir Khajepour, Teng Liu, Yechen Qin, and Yubiao Zhang. Local path planning for autonomous vehicles: Crash mitigation. In *2018 IEEE Intelligent Vehicles Symposium (IV)*, volume 2018-June, pages 1602–1606. IEEE, June 2018.
- [163] Hong Wang, Yanjun Huang, Amir Khajepour, Yubiao Zhang, Yadollah Rasekhipour, and Dongpu Cao. Crash mitigation in motion planning for autonomous vehicles. *IEEE Transactions on Intelligent Transportation Systems*, 20:3313–3323, September 2019.
- [164] Jianqiang Wang, Jian Wu, Xunjia Zheng, Daiheng Ni, and Keqiang Li. Driving safety field theory modeling and its application in pre-collision warning system. *Transportation Research Part C: Emerging Technologies*, 72:306–324, November 2016.
- [165] James Ward, Gabriel Agamennoni, Stewart Worrall, and Eduardo Nebot. Vehicle collision probability calculation for general traffic scenarios under uncertainty. In *2014 IEEE Intelligent Vehicles Symposium Proceedings*, pages 986–992. IEEE, June 2014.
- [166] Andrzej Wardzinski. Dynamic risk assessment in autonomous vehicles motion planning. In *2008 1st International Conference on Information Technology*, pages 1–4. IEEE, May 2008.
- [167] Moritz Werling, Julius Ziegler, Sören Kammel, and Sebastian Thrun. Optimal trajectory generation for dynamic street scenarios in a Frenét Frame. In *2010 IEEE International Conference on Robotics and Automation*, pages 987–993, 2010.
- [168] Per Wramborg. A new approach to a safe and sustainable road structure and street design for urban areas. *Proceedings of the Road Safety on Four Continents Conference*, 13:12–12, 2005.
- [169] Chaozhong Wu, Liqun Peng, Zhen Huang, Ming Zhong, and Duanfeng Chu. A method of vehicle motion prediction and collision risk assessment with a simulated vehicular cyber physical system. *Transportation Research Part C: Emerging Technologies*, 47:179–191, October 2014.
- [170] Qun Wu, Qiao jun Xiang, Chuan Lu, and Jian Lu. Traffic safety evaluation of highway intersection with the use of conflict severity

- concept. In *2008 International Conference on Intelligent Computation Technology and Automation (ICICTA)*, volume 2, pages 574–578. IEEE, October 2008.
- [171] Guotao Xie, Xinyu Zhang, Hongbo Gao, Lijun Qian, Jianqiang Wang, and Umit Ozguner. Situational assessments based on uncertainty-risk awareness in complex traffic scenarios. *Sustainability (Switzerland)*, 9:1582, 2017.
- [172] Boliang Yi, Stefan Gottschling, Jens Ferdinand, Norbert Simm, Frank Bonarens, and Christoph Stiller. Real time integrated vehicle dynamics control and trajectory planning with MPC for critical maneuvers. In *IEEE Intelligent Vehicles Symposium, Proceedings*, volume 2016-August, 2016.
- [173] Lijun Zhang, Wei Xiao, Zhuang Zhang, and Dejian Meng. Surrounding vehicles motion prediction for risk assessment and motion planning of autonomous vehicle in highway scenarios. *IEEE Access*, 8:209356–209376, 2020.
- [174] Adam Ziebinski, Rafal Cupek, Damian Grzechca, and Lukas Chruszczyk. Review of advanced driver assistance systems (ADAS). volume 1906, page 120002, 11 2017.

Curriculum Vitae

Personal Data

Name	Fabian Müller
Year of Birth	1989
Place of Birth	Berlin, Germany

Career

2017 – 2021	Research Associate at Technische Universität Darmstadt/ Institute for Automatic Control and Mechatronics/ Department Control Methods and Robotics in cooperation with Honda Research Institute Europe in Offenbach
2013 – 2017	Master of Science in Mechatronics, Technische Universität Darmstadt, Major field of studies: Simulation and Control of Mechatronic Systems
2009 – 2013	Bachelor of Science in Mechanical Engineering, Technische Universität Berlin
2009	Abitur, Hermann-von-Helmholtz Gymnasium in Potsdam
